Distribution Agreement

In presenting this thesis or dissertation as a partial fulfillment of the requirements for an advanced degree from Emory University, I hereby grant to Emory University and its agents the non-exclusive license to archive, make accessible, and display my thesis or dissertation in whole or in part in all forms of media, now or hereafter known, including display on the world wide web. I understand that I may select some access restrictions as part of the online submission of this thesis or dissertation. I retain all ownership rights to the copyright of the thesis or dissertation. I also retain the right to use in future works (such as articles or books) all or part of this thesis or dissertation.

Signature:

_____ _____

Elise Viox Date

Characterizing and targeting inflammation in COVID-19 using a rhesus macaque model of SARS-CoV-2 infection

By

Elise Viox
Doctor of Philosophy

Graduate Division of Biological and Biomedical Science
Immunology and Molecular Pathogenesis

_____
Mirko Paiardini, Ph.D.
Advisor

_____
Eric Hunter, Ph.D.
Committee Member

_____
Joshy Jacob, Ph.D.
Committee Member

_____
Steven Bosinger, Ph.D.
Committee Member

_____
Matthew Parsons, Ph.D.
Committee Member

Accepted:

_____
Kimberly J. Arriola, Ph.D.
Dean of the James T. Laney School of Graduate Studies

_____
Date

Characterizing and targeting inflammation in COVID-19 using a rhesus macaque model of SARS-CoV-2 infection

By

Elise Viox

B.S., B.A., Emory Univeristy, 2015

Advisor: Mirko Paiardini, Ph.D.

An abstract of
A dissertation submitted to the Faculty of the
James T. Laney School of Graduate Studies at Emory University
In partial fulfillment of the requirements for the degree of
Doctor of Philosophy

Program in Immunology and Molecular Pathogenesis
Graduate Division of Biological and Biomedical Sciences

2023

Abstract

Characterizing and targeting inflammation in COVID-19 using a rhesus macaque model of SARS-CoV-2 infection

By Elise Viox

The Coronavirus disease 2019 (COVID-19) pandemic, caused by severe acute respiratory syndrome coronavirus 2 (SARS-CoV-2), has resulted in over 6.9 million deaths and continues to pose a significant threat to global health. Although several therapeutics have been approved or granted emergency use authorization for COVID-19, these drugs have limited therapeutic indications. Therefore, it is essential that SARS-CoV-2 viral pathogenesis and COVID-19 immune responses are fully characterized to inform the design of additional, effective therapeutics that can be used across the full spectrum of disease.

Inflammation following SARS-CoV-2 infection is a hallmark of COVID-19 severity, but the inflammatory pathways contributing to host defense vs. immune-mediated pathology have not been fully elucidated. To investigate the early inflammatory events in COVID-19, we utilized a rhesus macaque model of SARS-CoV-2 which recapitulates key features of mild-to-moderate disease. In this model, we found that SARS-CoV-2 infection resulted in a robust, but transient, upregulation of the type I interferon (IFN-I) response and a significant enrichment of several inflammatory cytokine signaling pathways in the lower airways. To characterize the cell subsets that were contributing towards the production of these inflammatory cytokines in the lower airways, we performed longitudinal single cell RNA sequencing (scRNAseq) of Bronchoalveolar Lavage (BAL) fluid in infected RMs. We found that SARS-CoV-2 infection induced an influx of two subsets of infiltrating myeloid cells, CD163+MRC1- and TREM2+ macrophages, into the alveolar space and that these infiltrating macrophages produced the majority of inflammatory cytokines in the lower airway during acute SARS-CoV-2 infection.

Type I interferons (IFN-I) are essential for defense against viral infections but also drive recruitment of inflammatory cells to sites of infection, a key feature of severe COVID-19. To dissect the roles of antiviral and pro-inflammatory IFN-I responses in early SARS-CoV-2 infection, we modulated IFN-I signaling in rhesus macaques (RMs) prior to and during the first few days of SARS-CoV-2 infection using a mutated IFNα2 called IFN modulator (IFNmod). IFNmod binds with high affinity to IFNAR2, but markedly lower affinity to IFNAR1, blocking the binding and signaling of all forms of endogenous IFN-I. Administration of IFNmod in SARS-CoV-2-infected RMs not only resulted in an attenuation of antiviral interferon-stimulated genes (ISGs) and inflammatory genes, but also led to a profound decrease in SARS-CoV-2 viral loads, with 1-3-log reductions in both the upper and lower airways of treated animals. Additionally, a reduction in the influx of CD163+MRC1- and TREM2+ macrophages to the lung as well as lower levels of inflammatory chemokines and cytokines and lung pathology was observed with IFNmod treatment.

Collectively, the results of these studies are consistent with a model where an early and controlled IFN-I response is beneficial following SARS-CoV-2 infection, whereas excess IFN-I signaling leads to an influx of inflammatory macrophages in the lower airways and immunopathology.

Characterizing and targeting inflammation in COVID-19 using a rhesus macaque model of SARS-CoV-2 infection

By

Elise Viox

B.S., B.A., Emory University, 2015

Advisor: Mirko Paiardini, Ph.D.

A dissertation submitted to the Faculty of the
James T. Laney School of Graduate Studies at Emory University
In partial fulfillment of the requirements for the degree of
Doctor of Philosophy

Program in Immunology and Molecular Pathogenesis
Graduate Division of Biological and Biomedical Sciences

2023

Acknowledgements:

This work is dedicated in loving memory to my mother, Janet Knobbe, who instilled in me a love for science and provided me with endless love and encouragement during this journey.

I want to thank my dad, Mark Viox, for always believing in me- your support means the world to me. To my brothers Daniel, Jeff, and David: you inspire me every day and I am so proud to be your sister.

To my partner, Hirsh, I would not have gotten through grad school without you. I cannot thank you enough for being so selfless and taking care of me these past five years.

I want to also thank my friends, especially Chrissy and Vidisha, who kept me laughing through the good times and the bad and made grad school infinitely more fun.

I would also like to thank all of the Paiardini lab members past and present for their support and friendship over the years, especially Tim, Zach, Maria, Kevin, Justin, James, Amberly, Tomas, Laurence, Hong, and Sadia. Tim and Maria, this work would not have been possible without you. Tim, thank you for taking me under your wing at Emory and being a great friend, you are greatly missed. Zach, thank you for your friendship and for saving me during every crisis I encountered in lab, I would not have gotten through them without you.

Last but not least, I would like to thank my advisor. Mirko, your guidance and mentorship have been invaluable to me. Thank you for always going to bat for your students and for your patience and understanding. And thank you for the bravery you demonstrated in pursuing these COVID projects in a time when there was so much fear and uncertainty. I am so proud of what we accomplished here.

Table of Contents

Figure Index:

Figure 2.S10. Expression of CCR2 in monocytes in rhesus macaque BAL (Cohort 2 n = 6)

Figure 2.S11. Comparison of human lung macrophage/monocytes subsets with that of rhesus macaque

Figure 2.S12. Expression of pro-inflammatory mediators in human BAL samples.

Figure 2.S13. Annotation of pDC in BAL from untreated Cohort 1 (n=3) and baricitinib treated (n=2) rhesus macaques.

Figure 3.1. Administration of IFNmod in uninfected RMs resulted in modest upregulation of ISGs without changes to inflammatory genes or inflammatory cytokines and chemokines.

Figure 3.2. Administration of IFNmod in Calu-3 human lung cells modulated type I IFN responses and inhibited SARS-CoV-2 replication to levels comparable to Nirmatrelvir.

Figure 3.3. IFNmod administration reduced viral loads of SARS-CoV-2 infected RMs.

Figure 3.4. IFNmod administration resulted in lower levels of lung pathology and inflammatory cytokines and chemokines in SARS-CoV-2-infected RMs.

Figure 3.5. IFNmod-treated RMs had lower frequencies of CD14+CD16+ monocytes and expression of Siglec-1 compared to untreated RMs.

Figure 3.6. IFNmod treatment suppresses gene expression of ISGs, inflammation, and neutrophil degranulation in the BAL of SARS-CoV-2 infected NHPs.

Figure 3.7. Effect of IFNmod treatment on gene expression of BAL single-cells using 10X.

Figure 3.8. Effect of IFNmod treatment on lung cells.

Figure 3.S1. IFNmod treatment initiated post-SARS-CoV-2 infection leads to reduction in viral RNA loads and inflammatory gene expression.

Figure 3.S2. Administration of IFNmod was safe and well-tolerated in SARS-CoV-2-infected RMs.

Figure 3.S3. IFNmod reduced nasopharyngeal, BAL, and lung viral loads in SARS-CoV-2-infected RMs.

Figure 3.S4. Mx1 is more highly localized to viral foci in untreated SARS-CoV-2-infected RMs and IFNmod treatment decreases lung pathology.

Figure 3.S5. Flow gating strategy and expression of Siglec1+ in BAL.

Figure 3.S6. IFNmod treatment does not impact SARS-CoV-2-specific T cell or neutralizing antibody responses.

Figure 3.S7. Gene expression in BAL in rhesus macaques infected with SARS-CoV-2 after treatment with IFNmod.

Figure 3.S8. Gene expression in PBMCs and whole blood in rhesus macaques infected with SARS-CoV-2 after treatment with IFNmod.

Figure 3.S9. Expression of marker genes in BAL single-cells.

Figure 3.S10. Effect of IFNmod treatment on different BAL cell types.

Figure 3.S11. Cell annotation of lung samples.

Figure 3.S12. Effect of IFNmod treatment on gene expression of lung cells.

Table Index

Chapter 1: Introduction- SARS-CoV-2

A. Origin and Initial Spread of SARS-CoV-2

In December of 2019, a cluster of patients with pneumonia of unknown etiology was first reported in in Wuhan, a city in the Hubei Province of China [1, 2]. These patients experienced symptoms of fever, difficulty breathing, and bilateral, pulmony infiltrates consistent with viral pneumonia and tested negative for common respiratory pathogens as well as SARS-CoV-1 and MERS-CoV. Additionally, these initial patients were found to have had direct contact with the Wuhan Huanan Seafood Wholesale Market shortly before developing symptoms [1-3].

A novel coronavirus referred to as 2019 novel coronavirus (2019-nCoV) was isolated from the bronchoalveolar-lavage fluid of several of these patients in early January, 2020 and was later identified as the causative agent of the Wuhan outbreak [4, 5]. 2019-nCoV was later renamed as Severe acute respiratory syndrome coronavirus 2 (SARS-CoV-2) by The International Committee on Taxonomy of Viruses and the disease caused by infection with SARS-CoV-2 was termed Coronavirus Disease 2019 (COVID-19) [6].

Following the report of the initial cases, SARS-CoV-2 spread rapidly throughout China and several travel-related SARS-CoV-2 cases were detected in Thailand, Japan, the Republic of Korea, and the United States. SARS-CoV-2 was later confirmed to be spread through human-to-human transmission via respiratory droplets [7-9]. On January 31, 2020, the outbreak was declared a public health emergency by The U.S. Secretary of the Department of Health and Human Services (HHS) and a few months later on March 11, 2020, after more than 118,000 COVID cases were reported in 114 countries and 4,291

individuals were recorded to have died from COVID-related causes, the WHO declared COVID-19 a global pandemic[10-12]. To date, there have been a total of more than 770 million confirmed cases of COVID-19 during the pandemic, including greater than 6.9 million deaths [13].

In addition to SARS-CoV-2, only six other coronaviruses are known to infect humans: the common human coronaviruses (HCoV)-229E, HCoV-NL63, HCoV-OC43, and HCoV-HKU1 which cause mild respiratory symptoms and the highly pathogenic Severe acute respiratory syndrome coronavirus 1 (SARS-CoV-1) and Middle East respiratory syndrome coronavirus (MERS-CoV). All six of these coronaviruses are believed to have zoonotic origins, with phylogenetic analyses indicating that SARS-CoV-1, MERS-CoV, HCoV-NL63, and HCoV-229E originated from bat coronaviruses, while HCoV-OC43 and HCoV-HKU1 originated from rodent coronaviruses [14-17]. The origins of SARS-CoV-2 are hotly debated, with theories spanning from a laboratory leak to zoonosis [18]. SARS-CoV-2 has been shown to possess 96.2% nucleotide homology with RaTG13, a coronavirus that was isolated from *Rhinolophus affinis* bats, indicating probable bat origin. However, given that the receptor binding domain (RBD) of the spike protein from RaTG13 is significantly different than the RBD of SARS-CoV-2, it is likely that there was an intermediate host[19]. Since wild and exotic animals including palm civets and racoon dogs, which were previously implicated as intermediate hosts for SARS-CoV-1, were known to have been traded in the Wuhan Huanan Market, it is probable that the first animal-to-human transmission event occurred in this setting [20]. However, since the live animals that were being sold at the Huanan Market were removed when it was closed

and decontaminated on January 1st, 2020, the exact circumstances surrounding the initial emergence of SARS-CoV-2 will likely not be fully resolved [21].

B. Clinical Features of COVID-19:

The clinical presentation of COVID-19 varies widely, ranging from asymptomatic to respiratory failure and death. Patients with SARS-CoV-2 infection are generally grouped into the following categories based on the severity of illness: asymptomatic, mild illness, moderate illness, severe illness, and critical illness. Individuals with asymptomatic SARS-CoV-2 infection, by definition, do not present with COVID-19 symptoms. However, chest CT imaging abnormalities have been described in some asymptomatic patients [22]. Individuals with mild illness generally experience one of more of the following: fever, headaches, fatigue, cough, sore throat, loss of taste and smell, nausea, vomiting, or diarrhea. Moderate COVID-19 illness is further defined by shortness of breath or dyspnea with pulse oximetry readings equal to or exceeding 94% SpO_2. Individuals are classified as having severe COVID-19 if they meet one or more of the following criteria: SpO_2 below 94%, respiratory rate greater than 30 breaths per minute, greater than 50% lung infiltrates, or a PaO_2/FiO_2 less than <300 mm Hg. Finally, COVID-19 patients experiencing respiratory failure, multiple organ failure, and/or septic shock are considered to have critical COVID-19 illness [23].

Estimates of the percentage of SARS-CoV-2-infected individuals that are asymptomatic differ considerably between studies and between SARS-CoV-2 variants. A meta-analysis of data collected from early in the pandemic indicated that 13.34% of individuals infected with SARS-CoV-2 were asymptomatic [24]. However, later in the

pandemic when Omicron was the dominant variant, the pooled percentage of asymptomatic infections amongst individuals with confirmed Omicron infections was estimated to be much higher at 32.40% [25]. In the first few months of the pandemic, it was reported by the Chinese Center for Disease Control and Prevention that of 44,672 confirmed, symptomatic COVID-19 cases, 81% were mild, 14% were severe and 5% were critical [26]. Additionally, the case fatality rate of COVID-19 was reported to be 2.3% in this study, which is substantially lower than that of SARS-CoV-1 (9.5%) and MERS-CoV (34.4%) [27]. Risk of progressing to severe COVID-19 has been found to be increased in individuals over the age of 50, particularly in people age 65 and older [28, 29]. Additionally, underlying medical conditions including but not limited to chronic kidney disease, chronic respiratory disease, obesity, diabetes, hypertension, cardiovascular disease, and cancer were shown to be risk factors for severe COVID-19, with the risk increasing with higher numbers of comorbidities [30-34].

Individuals infected with SARS-CoV-2 variants pre-dating Omicron generally reached peak viral loads around the same time as symptom onset, approximately 2-5 days post infection [35-37]. In Omicron-infected individuals, however, peak viral loads were typically not achieved until around 3 days after symptom onset [38]. Symptoms are usually resolved within 7-10 days of symptom onset in individuals with mild to moderate COVID [39]. Individuals who progress to severe COVID-19 typically do so around 8 days after symptom onset and individuals who develop critical disease do so approximately 16 days after symptom onset [26]. Severe and critical COVID-19 patients that recover typically take 3-6 weeks to resolve symptoms [39].

Although COVID-19 symptoms are resolved in the majority of individuals within a few weeks, some individuals with COVID-19 have symptoms that persist, recur, or arise multiple months after SARS-CoV-2 infection. The WHO refers to this phenomena as long COVID (also known as post COVID-19 Condition or PASC (post-acute sequelae of COVID-19)) [40]. Long COVID symptoms include but are not limited to fatigue, chest pain, heart palpitations, cough, dyspnea, abdominal pain, nausea, cognitive impairment, fatigue, disordered sleep, memory loss, tinnitus, erectile dysfunction, and irregular menstruation [41, 42]. Some individuals with long COVID also report new-onset conditions including dysautonomia, postural orthostatic tachycardia syndrome (POTS), cardiovascular disease, thrombotic disease, type 2 diabetes, and chronic fatigue syndrome [43-47]. It is estimated that approximately 10% of individuals infected with SARS-CoV-2 have developed long COVID. The incidence of long COVID is believed to be highest in individuals that were originally hospitalized with COVID (50-70%) and estimated at 10-30% for non-hospitalized individuals [48]. Females have been shown to be more at risk than males for developing long COVID and hispanics and LatinX are disproportionately affected [49]. Individuals who had type 2 diabetes, Epstein-Barr virus viremia, or specific auto-antibodies at the time of original COVID-19 diagnosis also have been found to be at increased risk of long COVID [49]. Importantly, vaccination has been shown to significantly decrease risk of developing long COVID, with an estimated incidence of only 10-12% in vaccinated individuals [50, 51].

C. Viral Properties of SARS-CoV-2

SARS-CoV-2 is an enveloped, single-stranded, positive-sense (+ssRNA) virus belonging to the Betacoronavirus genus of the Coronaviridae family [52]. Other members within Betacoronavirus genus include the common human coronaviruses (HCoV)-OC43 and HCoV-HKU1 as well as Severe Acute Respiratory Syndrome Coronavirus 1 (SARS-CoV-1) and Middle East Respiratory Syndrome Coronavirus (MERS-CoV) [53]. The genome of SARS-CoV-2 is approximately 30kb in length and was found to exhibit approximately 79% sequence identity with SARS-CoV-1 and 50% identity with MERS-CoV [52]. SARS-CoV-2 is arranged in 14 open reading frames (ORFs) that encode for a total of 29 proteins [54]. Of these 29 proteins, 16 are nonstructural proteins (NSP1-16) and make up the SARS-CoV-2 replication-transcription complex (RTC) and nine are accessory proteins (ORF3a, ORF3b, ORF6, ORF7a, ORF7b, ORF8, ORF9b, ORF9c, and ORF10) whose main known functions are to suppress the host innate immune response. The remaining four proteins are structural and include the nucleocapsid (N), membrane (M), envelope (E), and spike (S) proteins[55].

The SARS-CoV-2 N protein is a RNA-binding protein that shares 91% sequence homology with the SARS-CoV-1 N protein [56]. The primary function of the N protein is to package the viral RNA genome into a ribonucleocapsid (RNP) complex [57]. Additionally, the N protein also plays a role in regulating the host immune response, having been shown to both antagonize RNAi and inhibit IFN-I signaling [58, 59]. The M protein is the most abundant structural protein in coronaviruses and plays a critical role in the assembly of the SARS-CoV-2 virion [60]. 90% homology is shared between the M proteins of SARS-CoV-2 and SARS-CoV-1 [61]. The E protein interacts with the M protein and also plays an essential part in SARS-CoV-2 viral assembly. Additionally, the E protein has been

implicated in functioning as a viporin and facilitating viral release [62]. The S protein is a homotrimeric transmembrane glycoprotein that projects from and surrounds the surface of SARS-CoV-2 virions, forming the characteristic “crown-like” appearance associated with coronaviruses. The main function of the S protein is to bind to the host cellular entry receptor ACE2 (angiotensin converting enzyme 2) and mediate viral-cell membrane fusion [63]. The S protein of SARS-CoV-2 is highly similar to the S protein of SARS-CoV-1, with 76% amino acid identity between the S proteins of both viruses [64]. The S protein is composed of two subunits, S1 and S2, which mediate binding and viral fusion to the host cell respectively. S1 contains a receptor binding domain (RBD) which directly binds to the SARS-CoV-2 cellular entry receptor (ACE2) [21, 65]. ACE2 is a negative regulator of the renin–angiotensin–aldosterone system (RAAS) and is widely expressed in different human tissues including the lower respiratory tract, lung, heart, thyroid, small intestine, and kidneys among others [66]. Within the lung, ACE2 is primarily expressed by type II alveolar (AT2) and type I alveolar (AT1) epithelial cells [67].

D. SARS-CoV-2 Viral Entry and Life Cycle

Binding of SARS-CoV-2 RBD to ACE2 induces conformational changes in the spike protein that expose a cleavage site in the S2 subunit. Following ACE2 binding, the SARS-CoV-2 virion can enter the host cell via two different pathways: 1) cell surface entry or 2) endosomal entry. In the first pathway, the S2 subunit is cleaved by the host transmembrane protease serine 2 (TMPRSS2), triggering rearrangement and release of the fusion peptide into the cell membrane [68]. TMPRSS2 has previously been shown to also cleave the spike protein of other coronaviruses including HCoV-229E, SARS-CoV-

1, and MERS-CoV and is co-expressed with ACE2 in lung type II pneumocytes and nasal goblet secretory cells [69-72]. If the host cell does not express sufficient levels of TMPRSS2, SARS-CoV-2 can enter the cell via clathrin-mediated endocytosis. Following endosomal acidification, S2 is then cleaved by the host cysteine protease cathepsin L (CTSL) in the endolysosome, resulting in conformational changes in the fusion peptide and its insertion into the endosomal membrane [73, 74].

Following fusion of viral and host cell membranes, SARS-CoV-2 viral RNA is released and uncoated. The ORFs ORF1a and ORF1b are then directly translated by host machinery to produce polyproteins pp1a and pp1ab which are proteolytically cleaved into NSP1-16. NSP1-16 then assemble to form the RTC which drives the production of full length negative-sense genomic RNA (gRNA) that is used as a template for full length positive-sense gRNA. Additionally, through discontinuous transcription, a subset of negative-sense subgenomic RNAs (sgRNAs) are produced that, following transcription into positive-sense subgenomic mRNAs, are translated into structural and accessory proteins. The structural proteins and viral genomic RNA are then assembled into SARS-CoV-2 virions in the ER-Golgi intermediate compartment where they undergo budding [75]. In the Golgi apparatus, the S protein is cleaved by furin-like proteases into the aforementioned S1 and S2 subunits [76, 77]. The newly minted SARS-CoV-2 virions then are then transported to the plasma membrane via the secretory pathway and released via exocytosis [75].

In addition to being transmitted via cell-free virus, SARS-CoV-2 engages in a process called trans-infection where cells that are non-permissive to SARS-CoV-2 infection capture virions and present them to permissive cells. These permissive cells are

then able to undergo ACE2-mediated infection. In the case of SARS-CoV-2, trans-infection has been shown to be facilitated via lectin receptors such as DC-SIGN (Dendritic Cell-Specific Intercellular adhesion molecule-Grabbing Non-integrin), L-SIGN (liver/lymph node-specific Intercellular adhesion molecule-Grabbing Non-integrin), and Siglec-1 (Sialic acid-binding Ig-like lectin 1) that are primarily expressed on the surface of antigen presenting cells (APCs)[78]. These receptors interact with sialylated gangliosides such as GM1 on the SARS-CoV-2 membrane, leading to the internalization of the SARS-CoV-2 virion within a viral containing compartment (VCC) and the transfer of the virion to SARS-CoV-2-susceptible ACE2- and TMPRSS2-expressing cells [78, 79].

Non-productive SARS-CoV-2 infection has also been shown to take place in monocytes and macrophages through the phagocytosis of antibody-opsonized SARS-CoV-2 via FCγRs. SARS-CoV-2 is able to replicate inside of blood monocytes and lung macrophages but these cells do not produce infectious virions because they undergo a form of inflammatory cell death called pyroptosis [80].

E. Innate Immune Sensing of SARS-CoV-2

The innate immune system of the host serves as the first line of defense against SARS-CoV-2. A multitude of innate immune cells including monocytes, macrophages, dendritic cells, neutrophils, and natural killer cells as well as non-immune cells such as epithelial cells express pattern recognition receptors (PRRs) that can recognize pathogen-associate molecular patterns (PAMPs) or damage-associated molecular patterns (DAMPs). These PRRs include toll-like receptors (TLRs), RIG-I-like receptors (RLR), and NOD-like receptors (NLRs). During SARS-CoV-2 viral entry and replication,

SARS-CoV-2 viral components can be sensed by PRRs located on the cell surface, in endosomes, and in the cytoplasm of host cells. Several studies have suggested that the SARS-CoV-2 E protein may be sensed by the cell surface toll-like receptor (TLR) TLR2 and that the SARS-CoV-2 S protein binds to TLR1, TLR4, and TLR6 on the cell surface [81-85]. Additionally, SARS-CoV-2 infection has been shown to activate the endosomal PRRs TLR3 which recognizes dsRNA and TLR7 which recognizes ssRNA [86]. In the cytosol, the RLRs RIG-I and MDA5 which sense 5′-triphosphate RNA and dsRNA respectively and the cytosolic DNA sensing pathway involving cyclic GMP-AMP synthase (cGAS)-stimulator of interferon genes (STING) have been shown to be activated by SARS-CoV-2 [86-89]. It is believed that SARS-CoV-2 may activate the cGAS-STING pathway through promoting the release of mitochondrial DNA in infected endothelial cells, which is then sensed by cGAS [89, 90]. Finally, the NLR inflammasome sensor NLRP3 has also been suggested to sense infection with coronaviruses [91-93].

Following sensing of SARS-CoV-2 viral components, PRR signaling results in the activation of IRF3 and IRF7 and subsequent induction of type I and type III interferons. Additionally, PRR signaling downstream of SARS-CoV-2 recognition also leads to the NF-κB-mediated induction of pro-inflammatory cytokines such as IL-1β, IL-6, TNF, IL-12, IFN-β, IFN-γ, and IL-17[20]. Additionally, pro-inflammatory chemokines such as CXCL8, CXCL10, MIP1alpha, and CCL2 are produced and recruit innate and adaptive immune cells from the periphery to the site of infection, in this case the lung, in an effort to contain and eliminate the pathogen [20].

In severe COVID-19, a dysregulated release of these pro-inflammatory cytokines and chemokines has been observed and can progress to cytokine storm. Cytokine storm

can then lead to respiratory distress syndrome (ARDS), multi-organ failure, and death [20, 94, 95]. With the overexuberant proinflammatory cytokine response seen in severe COVID-19, an increase of serum markers associated with severe inflammation including C-reactive protein and ferritin which are induced by IL-6 as well as D-dimer have been observed [96-99]. Additionally, severe COVID-19 patients also experience an influx of proinflammatory monocyte-derived macrophages, neutrophils, and lymphocytes to the lung[100].

F. Type I IFN:

Interferons (IFNs) are a group of multifaceted cytokines that can be classified into three different families: Type I IFN (IFN-I), Type II IFN (IFN-II), and Type III IFN (IFN-III).

Type I IFNs were first described by Alick Isaacs and Jean Lindenmann in 1957 while studying the phenomena of viral interference and play critical roles in antiviral immunity [101-105]. In humans, the Type I IFN family is made up of 13 different IFNα subtypes (IFN-α1, -α2, -α4, -α5, -α6, -α7, -α8, -α10, -α13, -α14, -α16, -α17 and -α21), and one subtype each of IFNβ, IFNε, IFNτ, IFNκ, IFNω, IFNδ and IFNζ [106]. As was described previously, IFN-I are produced following the sensing of PAMPs or DAMPs via PRRs which are located on the plasma membrane, in the endosomes, or in the cytosol [107]. PAMPs binding to their respective PRRs results in the downstream activation of the transcription factors IRF3/IRF7 which translocate to the nucleus and promote the expression of IFN-I. While the majority of cells are capable of producing IFN-I, plasmacytoid DCs (pDCs) are known to rapidly produce large quantities of IFN-I in response to viral infections, accounting for 95% of type I IFN production by mononuclear cells [108].

IFN-I binds to a heterodimeric receptor composed of two subunits, Interferon Alpha and Beta Receptor Subunit 1 (IFNAR1) and Interferon Alpha and Beta Receptor Subunit 2 (IFNAR2), to form a ternary complex. IFNAR1 and IFNAR2 are ubiquitously expressed on the surface of all nucleated cells and are associated with the Janus activated kinases (JAKs) tyrosine kinase 2 (TYK2) and JAK1 respectively. Following ligand binding to the IFN-I receptor, IFNAR1 and IFNAR2 are dimerized and their associated Janus activated kinases are autophosphorylated and activated. Next, signal transducer and activator of transcription (STATs) are recruited and phosphorylated and form complexes that are translocated to the nucleus. One of these complexes is composed of STAT1, STAT2, and IFN-regulatory factor 9 (IRF9) and is called IFN-stimulated gene (ISG) factor 3 (ISGF3). Additionally, complexes made up of STAT2 homodimers and IRF9 as well as complexes made up of STAT1 homodimers are formed. After translocating to the nucleus, both the ISGF3 and STAT2/IRF2 complexes bind to IFN-stimulated response elements (ISREs) on the promoters of ISGs, resulting in ISG transcription and the STAT1 homodimers bind to gamma-activated sequences (GASs), inducing the transcription of pro-inflammatory genes [109].

ISGs encode a variety of proteins whose activities can be broadly categorized as antiviral or antiproliferative/immunomodulatory. Antiviral ISGs inhibit viral replication through multiple mechanisms including blocking viral transcription, blocking viral mRNA translation, and degrading viral RNA. ISGs with antiviral activity include 2′,5′-oligoadenylate (OAS), Protein kinase R (PKR), and MX1 [110]. Antiviral ISGs are classified as “robust” ISGs as their expression requires small amounts of IFN-I signaling and is largely not influenced by IFN-I binding affinity. Conversely,

antiproliferative/immunomodulatory ISGs such as CXCL11, IL-8, and IRF1 require much higher amounts of IFN-I signaling and are more strongly activated by high affinity IFN-I and are therefore classified as being "tunable" ISGs [111].

G. IFN-I Responses in Severe COVID-19 Patients:

Although high levels of type I IFN are often observed in individuals infected with common cold coronaviruses including HCoV-229E, infection with the highly pathogenic coronaviruses SARS-CoV-1 or MERS-CoV has typically been shown to result in more dampened IFN-I responses [112, 113]. Similar to what was observed in SARS-CoV-1 and MERS-CoV, there were multiple reports of impaired IFN-I responses in patients with severe COVID-19 early in the pandemic. Enrichment for rare inborn errors of IFN-I immunity (TLR3, IRF7, TICAM1, TBK1, or IFNAR1) and neutralizing autoantibodies against IFN-I were observed in patients with life-threatening COVID-19 in multiple studies [114-118]. Additionally, Hadjadj et al. observed an absence of IFN-β and impaired IFN-α production in the blood of severe and critical COVID-19 patients [119]. Conversely, Kwon et al. found that high levels of blood IFN-α were associated with COVID-19 severity and Broggi *et al.* observed that the morbidity of individuals hospitalized with COVID-19 correlated with a high expression of both IFN-I and IFN-III in BAL fluid [120, 121].

While the results of these studies were largely considered to be contradictory, it is likely that both too little and too much IFN-I can have detrimental impacts in SARS-CoV-2 infection. For example, insufficient levels of IFN-I signaling have the potential to lead to uncontrolled virus replication and sustained levels of IFN-I can drive immunopathology. Additionally, timing also likely plays a major role in whether IFN-I is protective or

detrimental, with early IFN-I responses being beneficial and later or sustained IFN-I responses being detrimental.

H. Inhibition of IFN-I by SARS-CoV-2:

Previously, multiple SARS-CoV-1 proteins that antagonize IFN-I production and signaling have been identified including but not limited to nsp1, papain-like protease (PLpro), nsp7, nsp15, orf3b, M protein, orf6 and N protein [122-135]. Given the high amino acid sequence homology between SARS-CoV-2 and SARS-CoV-1 proteins, it is unsurprising that many of SARS-CoV-2 proteins have been found to also inhibit IFN-I production and signaling [136].

As described previously, IFN-I are produced following sensing of PAMPs via PRRs and downstream signaling. SARS-CoV-2 is capable of evading recognition by PRRs and thus, blocking the downstream production of interferon, through multiple mechanisms. For example, SARS-CoV-2 replicates its genome inside of double membrane vesicles which allows it evade detection of its dsRNA intermediates by RIG-I and MDA-5 [137]. Additionally, SARS-CoV-2 non-structural proteins nsp14 and nsp16 also help SARS-CoV-2 evade detection by RIG-I and MDA-5 by modifying the cap-like structure of SARS-CoV-2 viral RNA to mimic that of host mRNA [138]. Multiple SARS-CoV-2 proteins have also been shown to block the downstream signaling of RIG-I and MDA-5, therefore also interfering with IFN-I production. SARS-CoV-2 nsp5, for example, was found to promote the proteasome-mediated destruction of MAVS, a signaling adaptor protein of RIG-I and MDA5. Additionally, SARS-CoV-2 nsp13 has also been shown to blocks TBK1 phosphorylation and SARS-CoV-2 nsp6 to bind to TBK1 and suppress phosphorylation

of IRF3 [139, 140]. Proteins encoded by SARS-CoV-2 also have been shown to inhibit IFN-I signaling. For example, Nsp14 has been shown to target IFNAR1 for degradation, ORF3a induces Suppressor of Cytokine Signaling 1 (SOCS1) thus preventing activation of JAKs, and ORF7a and ORF7b block STAT2 phosphorylation [140-142].

I. Animal Models of COVID-19:

In order to more thoroughly characterize the pathogenesis of SARS-CoV-2 and evaluate the efficacy of candidate COVID-19 therapeutics and vaccines, considerable efforts have been made to identify appropriate animal models for COVID-19 that recapitulate the spectrum of human disease.

Early modeling studies predicted that the RBD of SARS-CoV-2 would likely recognize ACE2 orthologues from bats, civets, ferrets, non-human primates, cats, and pigs but would likely not recognize ACE2 from mice and rats [21]. Notably, it was shown that ACE2 in apes, African monkeys, and Asian monkeys possessed the same twelve amino acid residues as human ACE2 that were determined to be critical for virus recognition [143].The ability of SARS-CoV-2 to infect HeLa cells expressing ACE2 from Chinese horseshoe bats, civets, pigs and mice was then evaluated and showed that SARS-CoV-2 was able to use ACE2 from all of these species save for mouse as an entry receptor to infect host cells [19]. Animal SARS-CoV-2 challenge studies later confirmed that bats, ferrets, non-human primates, cats, dogs, and golden Syrian hamsters were susceptible to SARS-CoV-2 infection but showed that both pigs and mice were not [144-149].

Although wild type mice were shown to not be susceptible to SARS-CoV-2 infection, multiple different approaches have been taken to establish mouse models of

SARS-CoV-2. One such method has been to generate mouse-adapted SARS-CoV-2 strains such as MASCp6, HRB26M, MA10, and WBP-1 to increase the binding affinity of the SARS-CoV-2 Spike RBD to wild type mouse ACE2; these strains have been shown to not only establish infection in wild type mice but also result in mild to lethal disease [150-152]. An additional strategy has been to use transgenic, CRISPR/Cas9 knockin-in, or viral-vector transduction approaches to express human ACE2 (hACE2) in mice, thereby sensitizing them to wild type SARS-CoV-2 infection [146, 153-155]. hACE2 mice develop mild to severe lung pathology and K18-hACE2 and HFH4-hACE2 mice in particular have been shown to progress to lethal disease [156, 157].

Another small animal model that has been widely used for SARS-CoV-2 studies is Syrian hamsters (*Mesocricetus auratus*). Syrian hamsters challenged with high-dose, intranasal SARS-CoV-2 inoculum have been shown to recapitulate severe COVID-19, making it an ideal model to both study the pathogenesis of severe COVID-19 and to evaluate candidate therapeutics for severe and critical disease. In particular, Syrian hamsters challenged with high dose SARS-CoV-2 have been shown to have severe pneumonia, high viral loads, upregulation of pro-inflammatory cytokine and chemokine gene expression in the lungs, and partial mortality consistent with what is observed in patients with severe COVID-19 [145, 158].

Non-human primate models of SARS-CoV-2 infection have proven to be essential for the pre-clinical evaluation of candidate therapeutics and vaccines[159-161]. Non-human primate species that have been shown to be susceptible to SARS-CoV-2 infection include African green monkeys (Chlorocebus aethiops), rhesus macaques (*Macaca mulatta*), cynomolgus macaques (*Macaca fascicularis*), common marmosets (*Callithrix jacchus*)

and baboons (*Papio hamadryas*) [162]. African green monkeys (AGMs) infected with SARS-CoV-2 develop a spectrum of disease, with the majority experiencing mild disease and only several animals progressing to moderate or severe disease [163-167]. Importantly, unlike other in SARS-CoV-2 NHP models, acute respiratory distress syndrome (ARDS) has been observed in several AGMs [168]. Lung pathology in infected AGMs has been shown to vary, with several animals having no lung lesions at necropsy and others having evidence of hemorrhage, edema, and lymphadenopathy[165]. Studies of SARS-CoV-2 infection in cynomolgus macaques have shown that only about half of the animals develop clinical symptoms of disease but the majority of animals develop interstitial pneumonia [147, 162, 165, 169-171]. Rhesus macaques have been shown in multiple studies to support high levels of SARS-CoV-2 viral replication in the upper and lower airways, develop SARS-CoV-2-specific antibody and T cell responses similar to humans, and generally experience mild symptomatic disease with the minority of infected animals experiencing viral pneumonia[147, 148, 172]. Additionally, we and others have observed that acute SARS-CoV-2 infection in RMs macaques elicits many of the immunopathological events (including elevated inflammatory cytokines and chemokines, recruitment of monocytes and neutrophils, formation of neutrophil extracellular traps (NETs), induction of IFN-I inflammatory genes) reported in individuals with COVID-19 [173, 174].

J. ***COVID-19 Vaccines***

The development of SARS-CoV-2 vaccines has occurred at an unprecedented rate during the COVID-19 pandemic, owing to recent advancements in vaccine technology and decades of prior research on structure-based vaccine design for other viral

pathogens [175-179]. To date, four COVID-19 vaccines have received emergency use authorization (EUA) by the U.S. Food and Drug Administration (FDA): the Pfizer-BioNTech (BNT162b2) COVID-19 Vaccine, the Moderna (mRNA-1273) COVID-19 Vaccine, the Janssen (JNJ-78436735) COVID-19 Vaccine, and the Novavax (NVX-CoV2373) COVID-19 Vaccine [180].

The four vaccines that were granted EUAs by the FDA utilize a variety of vaccine platforms; the Pfizer-BioNTech (BNT162b2) and Moderna (mRNA-1273) vaccines use an mRNA platform, the Janssen (JNJ-78436735) COVID-19 vaccine uses a recombinant viral vector platform, and the Novavax (NVX-CoV2373) vaccine uses a protein subunit platform. Both the BNT162b2 and mRNA-1273 vaccines consist of a lipid nanoparticle-encapsulated mRNA that encode the full-length, prefusion-stabilized (S-2P) SARS-CoV-2 spike protein. However, the BNT162b2 and mRNA-1273 vaccines vary in their dosing regimen, with BNT162b2 being administered in two 30μg doses 21 days apart and mRNA-1273 being given in in two 100μg doses administered 28 days apart. In Phase 1 trials evaluating BNT162b2 and mRNA-1273 vaccines, both vaccines were found to have a mild reactogenicity profile[181, 182]. Additionally, both vaccines were observed to result in high titers of SARS-CoV-2-neutralizing antibodies that were boosted following administration of the second doses and to elicit antigen-specific CD4 T-cell responses that were Th1-biased [181-183]. Remarkably, both mRNA vaccines showed high efficacy in Phase 2/3 trials, with BNT162b2 conferring 95% protection against confirmed Covid-19 in individuals that had received their second dose at least 7 days prior and mRNA-1273 having 94.1% efficacy at preventing symptomatic Covid-19 in individuals that had received their second dose at least 14 days prior [184, 185]. Based on the highly encouraging

results of these trials, the BNT162b2 and mRNA-1273 vaccines were the first to receive EUA from the FDA on December 11 and December 18, 2020, respectively [186, 187]. The Pfizer-BioNTech and Moderna COVID-19 vaccines were later granted full approval by the FDA on August 23, 2021 and January 31, 2022 respectively and have since been updated to the bivalent formulation with the original and Omicron BA.4/BA.5 strains [188-190].

On February 27, 2021, Janssen's COVID-19 vaccine (JNJ-78436735) became the third to receive emergency use authorization by the FDA [187]. JNJ-78436735 is recombinant vaccine with a replication-incompetent adenovirus serotype 26 (Ad26) vector which encodes the prefusion-stabilized SARS-CoV-2 spike protein [191]. Administered as a single 5×10^{10} viral particle dose, the JNJ-78436735 vaccine was shown to be 66.9% protective against moderate to severe–critical Covid-19 in individuals who had received their vaccine within at least 14 days of onset [191]. Although the JNJ-78436735 vaccine was originally shown to have a mild to moderate reactogenicity profile, cases of individuals that developed thrombosis with thrombocytopenia syndrome (TTS) a few weeks after vaccination with JNJ-78436735 started being reported in April of 2021 [192]. TTS is a rare and potentially-life threatening syndrome characterized by blood clot formation and thrombocytopenia and, prior to being reported in patients who had received the JNJ-78436735 COVID-19 vaccine, had also been reported in several individuals that received the ChAdOx1 nCoV-19 AstraZeneca COVID-19 vaccine which is also an adenovirus-vector-based [193]. These reports resulted in a pause in the administration of the JNJ-78436735 COVID-19 vaccine which was lifted several weeks later after a thorough review. However, after continued monitoring, the FDA later announced on May 5, 2022 that, due to TTS risks, they were limiting the authorized use of the JNJ-78436735

COVID-19 vaccine to only adults that could not receive the other authorized COVID-19 vaccines due to access issues or medical contraindications [194]. JNJ-78436735 later had its emergency use authorization revoked on June 1, 2023 after Janssen Biotech Inc. voluntarily requested its withdrawal [195].

The Novavax (NVX-CoV2373) vaccine was the most recent COVID-19 vaccine to be granted authorization for emergency use on July 13, 2022. A recombinant, full-length, prefusion-stabilized, spike nanoparticle vaccine with a saponin-based adjuvant named Matrix-M, NVX-CoV2373 is administered as a two 5μg protein, 50μg adjuvant doses spaced 21 days apart and was shown to be 90.4% effective at preventing symptomatic COVID-19 [196, 197].

In addition to the four aforementioned vaccines, the WHO has also approved the following vaccines for emergency use: the ChAdOx1-S recombinant COVID-19 vaccines made by AstraZeneca and the Serum Institute of India Pvt. Ltd, the SARS-CoV-2 rS Protein Nanoparticle recombinant vaccine from Serum Institute of India Pvt. Ltd, the Ad5-nCoV-S recombinant vaccine from CanSino Biologics Inc., the recombinant protein subunit vaccine from SK Bioscience Co., Ltd, and inactivated COVID-19 vaccines from the Beijing Institute of Biological Products Co., Ltd. (BIBP) and Sinovac Life Sciences Co., Ltd, and Bharat Biotech International Ltd [198].

Although the initial reported efficacy of these COVID-19 vaccines was highly encouraging, vaccine-induced immunity has been shown to wane over time [199-204]. Additionally, VOCs have emerged that are less susceptible to neutralization by antibodies elicited in vaccinated individuals. Therefore, repeated boosting and updates to the

composition of vaccines to reflect dominant SARS-CoV-2 variants is likely needed to maintain protection [205].

K. SARS-CoV-2 Variants

As an RNA virus with an error-prone RNA-dependent RNA polymerase (RdRp) that has low proofreading capacity, SARS-CoV-2 is prone to mutations during viral replication, with an estimated mutation rate of 1×10^{-6}–2×10^{-6} mutations per nucleotide per replication cycle. Additionally, since SARS-CoV-2 undergoes discontinuous transcription, it is subject to high rates of recombination, further contributing towards genetic diversity [206]. The majority of SARS-CoV-2 mutations are likely deleterious and purged or are neutral and remain silent. However, some mutations can result in phenotypic changes that confer a fitness advantage and drive viral evolution.

Due to the potential for SARS-CoV-2 to evolve to become more transmissible, evade neutralizing antibody responses elicited by vaccines, and/or become resistant to current therapeutics, considerable efforts have been made to track emerging SARS-CoV-2 variants. The SARS-CoV-2 Interagency Group (SIG) was established by the U.S. Department of Health and Human Services (HHS) to classify emerging SARS-CoV-2 variants into one of four classes based on risk to global health: variants of concern (VOCs), variants of interest (VOIs), variants of high consequence (VOHCs), and variants being monitored (VBMs). The SIG defines a VOC as a variant that 1) has increased clinical disease severity, 2) results in a change in COVID-19 epidemiology that requires major public health interventions, and/or 3) results in a significant decrease in the efficacy of current vaccines in preventing severe disease. Since the beginning of the pandemic,

five different SARS-CoV-2 variants have been designated as VOCs: Alpha (B.1.1.7), Beta (B.1.351), Gamma (P.1), Delta (B.1.617.1/2), and, most recently, Omicron (B.1.1.529) [207].

During the first 11 months of the COVID-19 pandemic, little diversifying selection in SARS-CoV-2 took place in humans [208]. However, in October of 2020, a new SARS-CoV-2 variant named Alpha (B.1.1.7) began to emerge in the United Kingdom [209]. The Alpha variant possessed a total of 17 mutations in the viral genome as compared to the ancestral virus, with eight of these mutations being present in the spike protein[210]. As compared to the ancestral Wuhan strain, Alpha was observed to possess significant transmission advantages and quickly became the dominant SARS-CoV-2 variant in the UK before spreading globally [210].

The second VOC, Beta (B.1.351), was first reported in South Africa in October 2020 and was shown to possess nine mutations in the spike protein relative to the ancestral strain, with three of these mutations (K417N, E484K, and N501Y) located in the Spike RBD [211]. Like Alpha, Beta was found to have increased RBD binding affinity to ACE2 as well as enhanced transmissibility [212-214]. Additionally, Beta was more resistant to neutralization by existing monoclonal antibody therapies and sera from vaccinated or previously infected individuals [214]. Gamma (P.1.) was the third SARS-CoV-2 variant to be classified as a VOC and was first identified in December 2020 in Brazil [215]. Containing 11 mutations in the spike protein, three of which were located in the RBD (K417T, E484K, and N501Y), Gamma also was shown to have increased resistance to monoclonal antibody therapies, convalescent sera, and sera from vaccinated individuals [214, 215].

The fourth variant of concern, Delta (B.1.617.1/2), was first identified in December of 2020 in India and was initially only considered a variant of interest (VOI). However,

following the second wave of COVID-19 infections in India that occurred in April of 2021, the WHO re-classified it as a VOC in May of 2021 [216]. Delta contained a total of eight mutations in the spike protein, with L452R and T478K mutations in the RBD, and was less susceptible to neutralization by monoclonal antibody therapies available at the time including bamlanivimab and antibodies from individuals that had been previously infected or vaccinated [217, 218]. Importantly, infection with the Delta variant in unvaccinated individuals resulted in more severe disease than infection with the ancestral strain and breakthrough infections were observed in fully vaccinated individuals, prompting the recommendation of an additional booster dose [219, 220].

The fifth SARS-CoV-2 variant to be classified as a VOC by the WHO was Omicron (B.1.1.529) [221]. First identified in samples collected in South Africa in mid-November of 2021, Omicron spread at an unprecedented rate and was reported to be the dominant global SARS-CoV-2 variant by January 11th, 2022 [222]. With over 30 mutations in the SARS-CoV-2 spike protein, 15 of which are located in the RBD, B.1.1.529 had the largest number of mutations of all of the variants previously categorized as VOCs [223]. Initial modeling studies predicted that Omicron was 2.8 times as infectious as the Delta variant and had an 88% likelihood of escaping neutralizing antibody responses elicited by the vaccines available at the time [224]. Additionally, Omicron was shown to be the most resistant VOC to IFNβ in vitro [225]. Since the first emergence of Omicron, several subvariants of B.1.1.529 have emerged including BA.1, BA.2, BA.3, BA.4, and BA.5. Additionally, recombinant sub-variants of Omicron have also emerged including XD, XE, XF, XBB, XBD, and XBF [226].

At the time of writing, the EG.5 variant has newly been designated as a VOI and BA.2.86 as a VBM. EG.5 or "Eris" is a descendant lineage of XBB.1.9.2 that was first reported on February 17th 2023 and, as of late July 2023, has increased in global prevalence to 17.4%. Given its increased prevalence as well as its observed growth advantage and immune escape characteristics, EG.5 was designated as a VOI by the WHO on August 9th 2023 [227]. BA.2.86 or "Pirola" is believed to be a descendant of the Omicron subvariant BA.2. Although only a total of six cases of BA.2.86 have been reported as of August 21st, 2023, the broad geographic distribution (Israel, Denmark, the United Kingdom and the United States) and lack of a link between cases indicates that this variant is already widespread. Importantly, BA.2.86 is a highly mutated BA.2 variant, carrying a total of 34 amino-acid mutations in the spike protein alone, raising concerns that BA.2.86 will be able to escape neutralizing antibodies elicited by current vaccines and previous natural infections [228, 229].

L. COVID-19 Therapeutics:

COVID-19 therapeutics that have been authorized by the FDA can be broadly categorized into the following classes: antibody-based therapies, anti-inflammatory agents, and antiviral agents.

Early in the pandemic, plasma from patients that had previously recovered from COVID-19 (referred to as convalescent plasma) was used to treat individuals with severe COVID-19 in the hopes that the polyclonal SARS-CoV-2-specific antibodies in the convalescent plasma would neutralize virus in the recipient [230]. However, multiple randomized control trials (RCTs) including the RECOVERY trial later showed that

convalescent plasma treatment in patients hospitalized with COVID-19 had no effect on mortality or progression to ventilation [231-233]. Additionally, a meta-analysis of convalescent plasma treatment in mild-to-moderate COVID-19 patients showed no clinical benefit [234]. A multitude of monoclonal antibodies (mAbs) that neutralize SARS-CoV-2 have also been developed as COVID-19 prophylactics and therapeutics. These mAbs primarily target the RBD of the SARS-CoV-2 spike protein and block the interaction between SARS-CoV-2 spike and host ACE2. Casirivimab/imdevimab was the first mAb therapy to be authorized for emergency use in COVID-19 patients by the FDA. This was followed by the EUA of SARS-CoV-2 neutralizing mAbs Bamlanivimab/etesevimab, Sotrovimab, Tixagevimab/cilgavimab (Evusheld), and Bebtelovimab. With the exception of Evusheld which was used for pre-exposure prophylaxis in high risk individuals, these antibodies were authorized to treat individuals with mild to moderate COVID-19 that had developed symptoms less than seven days prior and were shown to reduce the risk of both hospitalization and death [235-237]. Despite the initially demonstrated efficacy of these SARS-CoV-2 neutralizing mAbs, the emergence of variants resistant to neutralization by these antibodies has rendered them ineffective and necessitated the development of new mAb therapies. Currently, no mAb is authorized for use in COVID-19 patients in the United States owing to the resistance of previous mAbs to Omicron [238].

Anti-inflammatory agents currently authorized for use by the FDA include the JAK1/2 inhibitor baricitinib and the anti-IL-6 receptor monoclonal antibody Tocilizumab [239]. Prior to the pandemic, both of these medications were FDA approved for the treatment of moderate to severe rheumatoid arthritis, with Tocilizumab also having been approved for giant cell arteritis, systemic sclerosis-associated interstitial lung disease, polyarticular

juvenile idiopathic arthritis, systemic juvenile idiopathic arthritis, and cytokine release syndrome [240, 241]. Early in the pandemic, artificial intelligence algorithms predicted baricitinib as a potential COVID-19 therapeutic [242, 243]. Subsequent in vitro studies showed that baricitinib was may not only be capable of inhibiting the signaling of pro-inflammatory cytokines implicated in severe COVID-19 but could potentially inhibit cellular entry of SARS-CoV-2 through blocking clathrin-mediated endocytosis [244]. Baricitinib treatment was also shown to reduce systemic inflammation, lung pathology, and pro-inflammatory cytokine expression in lung macrophages in SARS-CoV-2-infected rhesus macaques, although it did not result in a reduction in viral loads [173]. Importantly, baricitinib was evaluated in patients hospitalized with COVID-19 in the ACTT2 and CoV-BARRIER clinical trials and was shown to reduce mortality and time to recovery when administered in combination with remdesivir compared to remdesivir treatment alone, especially in individuals that required high-flow oxygen or noninvasive ventilation [245, 246]. The FDA originally granted EUA for baricitinib co-administered with remdesivir in patients hospitalized with COVID-19 that required supplemental oxygen, invasive mechanical ventilation, or extracorporeal membrane oxygenation (ECMO) on November 19, 2020. Baricitinib was later FDA approved for the treatment of adults hospitalized with COVID-19 who required supplemental oxygen, non-invasive or invasive mechanical ventilation, or extracorporeal membrane oxygenation (ECMO) on May 11, 2022, making it the first immunomodulatory agent to receive full FDA approval for the treatment of COVID-19 [247, 248].

Early studies of Tocilizumab in patients with severe COVID-19 indicated that Tocilizumab may reduce mortality and risk of invasive mechanical ventilation [249, 250].

Additional, larger clinical trials later showed a clear clinical benefit of Tocilizumab, with critically ill COVID-19 patients that received Tocilizumab in the REMAP-CAP trial and The RECOVERY group trial experiencing lower in-hospital mortality than patients that did not receive Tocilizumab [249, 251]. Based on these results, Tocilizumab was FDA approved on December 21, 2022, for the treatment of adults hospitalized with COVID-19 that were receiving systemic corticosteroids and required one of the following: supplemental oxygen, non-invasive or invasive mechanical ventilation, or extracorporeal membrane oxygenation (ECMO) [252].

Three antiviral agents are currently either FDA approved or authorized for emergency use for the treatment of COVID-19. These include remdesivir, Nirmatrilvir-ritonavir, and Molnupiravir [239]. Remdesivir (GS-5734) is a nucleotide prodrug of an adenosine analog that blocks viral replication through binding to and inhibiting the viral RNA-dependent, RNA polymerase [253]. A broad-spectrum antiviral, remdesivir was previously shown to have antiviral activity against SARS-CoV, MERS-Co-V, Ebola, and respiratory syncytial virus (RSV) [249, 253, 254]. Initial in vitro studies showed that remdesivir was also an effective antiviral against SARS-CoV-2 [255]. However, intravenous remdesivir was shown to have no effect or at most, be marginally beneficial in patients hospitalized with COVID-19 in clinical trials [256-260]. In the interim report of the WHO Solidarity trial, remdesivir-treated inpatients were reported to have similar in-hospital mortality and hospitalization duration to those receiving no trial drug [256]. Additionally, in the Adaptive Covid-19 Treatment Trial (ACTT-1), remdesivir showed little effect on time to recovery in hospitalized patients on high-flow oxygen or ventilation and only a 1-2 day reduction in median time to recovery in hospitalized patients not on high-flow oxygen or ventilation [257].

In spite of this, remdesivir was granted FDA approval on October 22, 2020, making it the first treatment to be FDA approved for COVID-19. Due to the lack of evidence of remdesivir being beneficial at the time of its FDA approval, the WHO issued a conditional recommendation against using remdesivir in hospitalized patients [252]. However, the WHO continued randomization of patients to remdesivir in the ongoing Solidarity trial to further investigate its efficacy and, in an updated report published in May of 2022, showed that remdesivir-treated hospitalized COVID-19 patients that were not ventilated experienced a decrease in-hospital mortality (11.9% vs. 13.5%) and progression to ventilation (14.1% vs. 15.7%) compared to hospitalized COVID-19 patients that were not ventilated and did not receive remdesivir. Consistent with the interim report, however, the full report still concluded that for individuals that were ventilated, remdesivir did not have a beneficial impact [261]. Based on these final Solidarity trial results, the WHO revised their conditional recommendation to include remdesivir as a treatment for severe COVID-19 [262]. Additionally, a placebo-controlled clinical trial of remdesivir in COVID-19 outpatients at high risk of progressing to severe disease showed that early administration of remdesivir resulted in an 87% lower risk of hospitalization [263]. This led to the WHO and FDA to update their respective recommended use and approval of remdesivir to include COVID-19 outpatients with mild to moderate disease at high risk of progressing to severe disease [264].

Nirmatrilvir-ritonavir is packaged and sold together under the brand name Paxlovid and received FDA EUA on December 22, 2021 and FDA approval on May 25, 2023 for use in individuals with mild to moderate COVID-19 at risk of progressing to severe disease [265]. As such, Paxlovid was the first oral antiviral FDA approved for the treatment of

COVID-19. Nirmatrilvir is an inhibitor of 3CL protease, the main protease of SARS-CoV-2 that cleaves the SARS-CoV-2 pp1a and pp1ab polyproteins into multiple nonstructural proteins, while ritonavir is an inhibitor of cytochrome P450 (CYP) 3A4 that functions to boost the oral availability of nirmatrilvir which would otherwise be metabolized by CYP3A4 [266, 267]. In vitro, Nirmatrelvir was shown to inhibit viral replication of multiple coronaviruses, including SARS-CoV-2, SARS-CoV-1, and MERS-CoV as well as common cold-causing coronaviruses HKU1, OC43, 229E, and NL63. In vivo, Nirmatrilvir was shown in a mouse-adapted SARS-CoV-2 model to reduce lung pathology, lung viral loads, and weight loss [268]. Remarkably, Paxlovid was shown in the EPIC-HR trial to reduce the risk of hospitalization or death by 89% as compared to placebo in COVID-19 outpatients that were both unvaccinated and at high risk of progressing to severe COVID-19 and was recently shown in a retrospective cohort study to also reduce the risk of COVID-19 ER-visits, hospitalization, or death in vaccinated individuals [269, 270].

Molnupiravir is a broad-spectrum antiviral with demonstrated antiviral activity against influenza, Ebola, Venezuelan equine encephalitis virus (VEEV), SARS-CoV-1, MERS-CoV, and SARS-CoV-2 [271-274]. A ribonucleoside analog, molnupiravir inhibits RNA-dependent RNA polymerase similar to remdesivir and was shown in the MOVe-OUT trial to modestly reduce the risk of hospitalization and death in unvaccinated COVID-19 outpatients at high risk for progressing to severe COVID-19 from 9.7% in the placebo group to 6.8% in the molnupiravir group [272, 275]. Molnupiravir was authorized for emergency use by the FDA in COVID-19 outpatients at high risk of severe disease on December 23, 2021 but has not received full FDA approval [276].

M. Evaluating IFN as a Therapeutic for COVID-19:

Type I interferons have been approved by the Food and Drug Administration (FDA) to treat a variety of diseases. For example, non-pegylated and pegylated forms of IFNα-2a and IFNα-2b in combination with the antiviral Ribavirin have been used to treat chronic hepatitis B and chronic hepatitis C infections for over thirty years. IFNα-2b is also FDA approved for the treatment of certain cancers including but not limited to hairy cell leukemia, AIDS-related Kaposi sarcoma, and follicular non-Hodgkin lymphoma [277]. More recently, a mono-pegylated interferon (IFN) α-2b isoform called ropeginterferon alfa-2b was also FDA approved for the treatment of adults with the rare blood cancer polycythemia vera (PV) [278, 279]. Additionally, IFNβ-1a, pegylated IFNβ-1a, and IFNβ-1b are approved to treat relapsing forms of multiple-sclerosis [280]. While the efficacy of IFN-I as pre-exposure prophylaxis and as a treatment has also been evaluated against multiple respiratory viral pathogens including common-cold causing rhinoviruses, influenza, SARS-CoV-1, MERS-CoV, and now SARS-CoV-2, IFN-I has never received FDA-approval for use in viral respiratory infections [281].

IFN-I has consistently been shown to have an antiviral effect against SARS-CoV-1 and MERS-CoV in vitro [282-294]. Additionally, SARS-CoV-1 cynomolgus macaques treated with prophylactic pegylated IFN-α and MERS-CoV-infected common marmosets treated with interferon-β1b post-infection were found to have lower viral loads and less lung pathology than untreated controls [295, 296]. However, the therapeutic efficacy of IFN-I in SARS-CoV-1 and MERS-CoV patients has been largely inconclusive. During the SARS-CoV-1 outbreak, multiple clinical studies were performed in which patients received IFN-α with corticosteroids and/or ribavirin [297, 298]. However, these studies either

entirely lacked a control group, were not randomized, or had a high risk of bias, and thus the efficacy of these treatments were determined to be inconclusive in systematic reviews conducted by multiple, independent groups [299, 300]. Similarly, systematic reviews of case reports and retrospective observational studies in which IFN-I was administered with or without antivirals to MERS-CoV patients have reported that the efficacy of IFN treatment for MERS is inconclusive [301, 302]. However, in a more recent randomized, double-blind, placebo-controlled trial conducted in MERS-CoV patients, administration of IFN-I in combination with antivirals has shown promise. The trial, called MIRACLE (MERS-CoV Infection Treated with a Combination of Lopinavir–Ritonavir and Interferon Beta-1b), was conducted in Saudi Arabia between 2016 and 2020. In the MIRACLE trial, a 14-day course of recombinant interferon beta-1b administered subcutaneously in combination with oral lopinavir/ritonavir was shown to reduce 90-day mortality of patients hospitalized with MERS from 44% in the placebo group to 28% in the interferon-treated group, with the greatest effect being observed in patients who initiated treatment within 7 days of symptom onset [303].

Multiple clinical trials have evaluated IFN-I as a candidate COVID-19 therapeutic and, as with both SARS-CoV-1 and MERS-CoV, have yielded varying results. Early on in the pandemic, IFNβ-1a alone and IFNβ-1a administered in combination with lopinavir/ritonavir were evaluated along with remdesivir, hydroxychloroquine, and lopinavir/ritonavir as therapeutics for hospitalized COVID patients in the global WHO Solidarity Trial. Unfortunately, IFNβ-1a with and without lopinavir/ritonavir as well as all of the other tested antivirals were shown to have little to no effect on the overall patient mortality, ventilation requirements, and duration of hospital stay [256]. Similarly, in the

Phase 3 DisCoVeRy trial, an add-on to the WHO Solidarity Trial, interferon IFN-β-1a administered in combination with lopinavir/ritonavir did not improve the clinical status of or accelerate viral clearance in hospitalized COVID-19 patients on oxygen and/or ventilatory support [304]. Furthermore, in the in the Phase 3 Adaptive COVID-19 Treatment Trial (ACTT-3), the combination of IFNβ-1a and remdesivir in hospitalized COVID-19 patients was not only shown to provide no clinical benefit, but resulted in worse outcomes and more adverse events in patients who required high-flow oxygen or non-invasive ventilation at baseline when compared to treatment with placebo plus remdesivir [305].

While no beneficial effects were observed with IFN-β-1a treatment in hospitalized patients in the aforementioned clinical trials, the combination of IFN-β-1b, lopinavir/ritonavir, and ribavirin in hospitalized COVID-19 patients was shown to reduce times to viral clearance, resolution of symptoms, and hospital stay compared to patients treated with lopinavir/ritonavir alone in a Phase 2 clinical trial in Hong Kong [306]. Additionally, it was shown that patients hospitalized with severe COVID-19 that received subcutaneous interferon beta-1a in combination with hydroxychloroquine plus lopinavir/ritonavir or atazanavir/ritonavir had lower 28-day mortality rates when compared to patients receiving hydroxychloroquine plus lopinavir/ritonavir or atazanavir/ritonavir without interferon in an open-label, randomized study in Iran [307, 308]. IFN-I was also shown to have some promise as a therapeutic in individuals with moderate COVID-19, with a phase 3 randomized open label study in India showing that COVID-19 outpatients that received pegylated IFN-α2b and standard of care (SOC) experienced a faster time to viral clearance than outpatients that received SOC alone [309].

Several clinical studies have also evaluated IFN-λ as a candidate COVID-19 therapeutic. Although IFN-λ was shown to inhibit SARS-CoV-2 replication in primary human airway epithelial cell culture and in mice [310, 311], two initial Phase 2 clinicals trials evaluating early administration of IFN-λ in COVID-19 outpatients showed no clinical benefits [312, 313]. These clinical trials were run concurrently in late spring to mid-summer of 2020, with one being conducted in Toronto and enrolling a total of 60 patients and the other being conducted within the Stanford Health Care system and enrolling 120 patients. In both studies, COVID-19 outpatients received a single subcutaneous *180μg* dose of Eiger Biopharmaceutical's Pegylated IFN Lambda-1a or a placebo, with the primary objective of evaluating if Pegylated IFN Lambda-1a had an effect on time to SARS-CoV-2 viral clearance. Enrollment criteria differed between the two trials, with patients in the Toronto study being eligible if they were within seven days of COVID-19 symptom onset or, if asymptomatic, following their first SARS-CoV-2 positive nasopharyngeal swab, and patients in the Stanford study being eligible if they were within 72 hours of a SARS-CoV-2 positive oropharyngeal swab. In spite of these differences in enrollment criteria, the time from symptom onset to randomization was similar in both trials, with a mean time of 4.5 days in the Toronto study and a median of 5 days in the Stanford study. Interestingly, although SARS-CoV-2 viral clearance was accelerated in peginterferon lambda patients as compared to the placebo patients in the Toronto study, no differences in duration of viral shedding were observed between treatment groups in the Stanford study. Given that SARS-CoV-2 viral clearance was found to be most pronounced in the Toronto patients with high viral loads and patients in the Stanford trial had substantially lower viral loads than the Toronto patients (median 4.4 log copies per mL vs. 6.71 log copies per mL), the

authors hypothesized that the difference in viral loads could possibly explain this discrepancy in outcomes between the two trials. Of note, the Toronto trial measured SARS-CoV-2 viral loads in nasopharyngeal swabs. Conversely, the Stanford trial used oropharyngeal swabs for longitudinal SARS-CoV-2 viral loads citing increased patient tolerability. Previous studies comparing paired nasopharyngeal and oropharyngeal swabs in COVID-19 inpatients have shown higher viral loads, detection rates, and sensitivities of nasopharyngeal vs. oropharyngeal swabs [314]. Therefore, this difference in sampling may also help to explain the difference in primary outcomes between the two trials. Regardless of the effects or lack of effects on viral clearance, no differences in either the frequency or the severity of symptoms was observed between treatment groups in both the Toronto and Stanford trials [312, 313].

However, the recent results of the TOGETHER trial have shown great promise for the use of early IFN-λ as a therapeutic for COVID-19. Like the Toronto and Stanford trials, the TOGETHER trial evaluated the effects of administering a single subcutaneous *180μg* dose of Eiger Biopharmaceutical's pegylated interferon lambda vs. a placebo in adult COVID-19 outpatients. However, the TOGETHER trial only enrolled COVID-19 outpatients at high risk of developing severe COVID-19, with the primary objective of evaluating if pegylated interferon lambda reduced hospitalization and emergency room visits. The TOGETHER trial enrolled a total of 1,951 patients in Brazil and Canada that received treatment within 7 days of COVID-19 symptom onset. Of note, the vast majority of enrolled participants in this trial were vaccinated, with 83% of patients having received at least one dose of a COVID-19 vaccine. Strikingly, a 51% decrease in COVID-19-related hospitalizations and emergency department visits was observed in the interferon lambda

group (2.7%) compared to the placebo group (5.6%) in the TOGETHER trial. Furthermore, when only considering patients who received interferon lambda or placebo treatment within 3 days of symptom onset, there was a 65% reduction in COVID-19-related hospitalizations and an 81% reduction in COVID-19 related deaths with interferon lambda treatment. During the course of the clinical trial (June of 2021 to February of 2022), the dominant global SARS-CoV-2 VOC changed multiple times. This allowed for the assessment of IFN lambda treatment efficacy with multiple SARS-CoV-2 strains. For each VOC, treatment with pegylated IFN lambda reduced the relative risk for hospitalization relative to placebo treatment, with Omicron having the greatest effect with a relative risk of 0.17, followed by Delta with a relative risk of 0.54, and Alpha/Gamma having a relative risk of 0.74 [315].

N. Summary

Although the COVID-19 Public Health Emergency was declared to have ended on May 11, 2023, the COVID-19 pandemic continues to result in significant morbidity and mortality[316]. Current COVID-19 vaccines are effective at protecting from severe disease. However, individuals with mild disease are still at risk of developing severe COVID-19. Additionally, the emergence of VOC that are resistant to vaccine-induced immunity remains a significant global concern. Therefore, effective therapeutics spanning the full spectrum of COVID-19 severity are necessary. Although significant progress has been made in characterizing the pathogenesis of SARS-CoV-2 since its emergence, further research is needed to develop targeted, immunomodulatory COVID-19 therapeutics.

Chapter Two: TREM2+ and interstitial-like macrophages orchestrate airway inflammation in SARS-CoV-2 infection in rhesus macaques

Amit A. Upadhyay[1], Elise G. Viox[1], Timothy N. Hoang[1], Arun K. Boddapati[2], Maria Pino[1], Michelle Y.-H. Lee[1], Jacqueline Corry[3], Zachary Strongin[1], David A. Cowan[2], Elizabeth N. Beagle[2], Tristan R. Horton[2], Sydney Hamilton[2], Hadj Aoued[2], Justin L. Harper[1], Christopher T. Edwards[1], Kevin Nguyen[1], Kathryn L. Pellegrini[2], Gregory K. Tharp[2], Anne Piantadosi[4], Rebecca D. Levit[5], Rama R. Amara[1,6], Simon M. Barratt-Boyes[3,7], Susan P. Ribeiro[4], Rafick P. Sekaly[4], Thomas H. Vanderford[1], Raymond F. Schinazi[8], Mirko Paiardini[1,4*], Steven E. Bosinger[1,4*].

[1]Division of Microbiology and Immunology, Emory National Primate Research Center, Emory University, Atlanta, Georgia, USA.

[2]Emory NPRC Genomics Core Laboratory, Emory National Primate Research Center, Emory University, Atlanta, Georgia, USA

[3]Department of Infectious Diseases and Microbiology, University of Pittsburgh, Pittsburgh, Pennsylvania, USA.

[4]Department of Pathology and Laboratory Medicine, School of Medicine, Emory University, Atlanta, Georgia, USA.

[5]Department of Medicine, School of Medicine, Emory University, Atlanta, Georgia, USA.

[6]Department of Microbiology and Immunology, Emory School of Medicine, Emory University, Atlanta, Georgia, USA

[7]Department of Immunology, University of Pittsburgh, Pittsburgh, Pennsylvania, USA.

[8]Department of Pediatrics, School of Medicine, Emory University and Children's Healthcare of Atlanta, Atlanta, Georgia, USA.

These authors contributed equally: Amit A. Upadhyay, Elise G. Viox and Timothy N. Hoang

These authors jointly supervised this work: Mirko Paiardini and Steven E. Bosinger

[*]Correspondence to

Steven E. Bosinger: steven.bosinger@emory.edu;

Mirko Paiardini: mirko.paiardini@emory.edu

Published in *Nature Communications* Volume 14, No. 1 1914, April 6th, 2023, PMID: 37024448

Abstract:

The immunopathological mechanisms driving the development of severe COVID-19 remain poorly defined. Here, we utilize a rhesus macaque model of acute SARS-CoV-2 infection to delineate perturbations in the innate immune system. SARS-CoV-2 initiates a rapid infiltration of plasmacytoid dendritic cells into the lower airway, commensurate with IFNA production, natural killer cell activation, and a significant increase of blood CD14-CD16+ monocytes. To dissect the contribution of lung myeloid subsets to airway inflammation, we generate a longitudinal scRNA-Seq dataset of airway cells, and map these subsets to corresponding populations in the human lung. SARS-CoV-2 infection elicits a rapid recruitment of two macrophage subsets: CD163+MRC1- , and TREM2+ populations that are the predominant source of inflammatory cytokines. Treatment with baricitinib (Olumiant®), a novel JAK1/2 inhibitor is effective in eliminating the influx of non-alveolar macrophages, with a reduction of inflammatory cytokines. This study delineates the major lung macrophage subsets driving airway inflammation during SARS-CoV-2 infection.

Main Text:

INTRODUCTION

The COVID-19 pandemic began with a series of reports of localized outbreaks of pneumonia caused by a novel coronavirus, SARS-CoV-2, in Wuhan, China in December 2019[4, 19]. As of early 2023, there have been over 672 million documented infections, and nearly 7 million fatalities attributed to sequelae of COVID-19. The rapid development and availability of effective vaccines[317-319] against SARS-CoV-2 infection has provided much needed optimism that infection rates will decline and that the containment of the virus at the population level is possible. Despite these landmark achievements, continued research efforts are essential to safeguard against potential breakthrough variants, to develop therapies for those afflicted while the vaccine rollout continues, and to prevent or minimize the impact of future viral outbreaks. In this light, basic research into the innate and adaptive immune responses to SARS-CoV-2 continues to be critical for informing vaccine and therapeutic approaches directed at ending the COVID-19 pandemic or at decreasing mortality.

Since the emergence of the COVID-19 pandemic, research into the virology, immune responses and pathogenesis of SARS-CoV-2 infection has amassed at an unprecedented rate, and numerous hypotheses have arisen to explain the underlying mechanisms of severe COVID-19. Of these, the concepts that have accumulated the most supporting evidence are: (i) evasion or impairment of early Type I interferon (IFN) responses[320], (ii) vascular complications arising from hypercoagulability syndromes[321],

and (iii) perturbations of the granulocyte and myeloid compartments in the lower airway and blood manifesting in inflammatory cytokine production[100, 322]. Immunologically, severe disease in COVID-19 patients has been associated with a widespread increase in levels of inflammatory mediators (e.g. CXCL10, IL-6, and TNF□) in plasma and bronchoalveolar lavage (BAL) fluid in what is commonly referred to as a "cytokine storm"[323], and an expansion of macrophages, neutrophils and lymphocytes in the lower airway[100]. Despite this impressive accruement of data, the precise early immunological events and immune cell infiltration that drive inflammation in the lower airway remain uncharacterized.

Non-human primate (NHP) models of SARS-CoV-2 infection (primarily macaque species and African green monkeys (AGMs)) have proven to be critical tools, primarily due to the ability to examine early events after infection longitudinally and in tissues not available in most human studies[324]. NHPs support high levels of viral replication in the upper and lower airway[147, 148, 172], share tissue distribution of ACE2 and TMPRSS2 with humans[72], and have been invaluable pre-clinical models of vaccines[159, 160, 325] and therapeutics[173, 326]. Additionally, mild to moderate COVID-19 has been shown to be recapitulated in SARS-CoV-2-infected NHPs[324] that typically resolve by 10-15 days post infection (dpi)[173, 324, 327]. Mechanistic studies of SARS-CoV-2 infection in NHPs have utilized a variety of high-throughput techniques and have reported (i) Type I IFN responses are robustly induced in blood and the lower airway very early after infection[173, 174], (ii) elevated pro-inflammatory cytokines consistent with the "cytokine storm" seen in humans are detectable in plasma and BAL[328], (iii) vascular pathology and gene expression consistent

with hypercoagulability are evident in the lower airways[174], and (iv) increased production of inflammatory cytokines by myeloid origin cells[166, 173].

In the current study, we used SARS-CoV-2 infected rhesus macaques (RMs) to investigate the early inflammatory events occurring in the blood and lower airway using high dimensional flow cytometry, multi-analyte cytokine detection, and bulk and single-cell RNA-Seq (scRNA-Seq). To dissect the role of discrete immune subsets within the myeloid fraction in SARS-CoV-2-driven inflammation, we used two different strategies, employing scRNA-Seq and bulk-RNA-Seq reference datasets to classify the macrophage/monocyte populations and to identify analogous populations in human airway datasets. With this approach, we identified the main subsets of pro-inflammatory macrophages that expand after SARS-CoV-2 infection and are the predominant source of inflammatory cytokines in the airway. We also observed an early induction of plasmacytoid dendritic cells (pDCs) in blood and the lower airway that coincided with the peak of the IFN signaling. Finally, we described that treatment of SARS-CoV-2 infected RMs with baricitinib, a JAK1/2 inhibitor recently demonstrated to reduce hospitalization time and mortality for severe COVID-19 patients[245], suppressed airway inflammation by abrogating the infiltration of pro-inflammatory macrophages to the alveolar space. Collectively, this study defines the early kinetics of pDC recruitment and Type I IFN responses, and identifies discrete subsets of infiltrating macrophages as the predominant source of pro-inflammatory cytokine production in SARS-CoV-2 infection.

RESULTS

Study Overview

An overview of the study design is shown in **Fig. 2.1a**. We analyzed three separate cohorts of macaques: Cohort 1, Baricitinib-treated and Cohort 2. For Cohort 1 and Baricitinib-treated, a total of eight RMs (mean age 14 years old; range 11-17 years old) were inoculated intranasally and intratracheally with 1.1×10^6 plaque-forming units (PFU) of SARS-CoV-2 (2019-nCoV/USA-WA1/2020). At 2dpi, four of the eight animals started receiving baricitinib[173]. For this study, pre-infection baseline and hyperacute time points (1-2dpi) include n = 8 RMs, all untreated, and the remaining longitudinal time-points assessed to determine the pathogenesis of SARS-CoV-2 infection are comprised of n = 4 of the RMs that remained untreated. Inoculation with SARS-CoV-2 led to reproducibly high viral titers detectable in the upper and lower airways by genomic and sub-genomic qPCR assays (**Fig. 2.1b**). The peak of viremia in the nasal passage, throat and BAL was at 2-4dpi (**Fig. 2.1b**). To increase the power of our scRNA-Seq and flow cytometry experiments, we analyzed an additional six macaques infected with the same dose and strain of SARS-CoV-2 (2019-nCoV/USA-WA1/2020) (mean age 10.5 years old; range 6-19.5 years old), referred to as Cohort 2. Animals from Cohort 2 served as SARS-CoV-2-infected, untreated controls in part of a larger study testing the impact of interferon blockade[329].

SARS-CoV-2 induces a robust, but transient, expansion of pDCs during hyperacute infection

To characterize the innate immune response following SARS-CoV-2 infection, we analyzed changes in innate populations using multi-parametric flow cytometry in blood and BAL samples in the first 2dpi, or "hyperacute" phase of infection (**Fig. 2.1c-e, Fig. 2.S1**), and over the full course of infection (**Fig. 2.S2**). In blood, we did not observe a significant increase in the proportion of classical monocytes (CD14+CD16-) at 2dpi (**Fig. 2.1c**) nor at extended time-points (**Fig. 2.S2a,d)**. Similar to reports in humans[322], we observed a rapid, but transient, increase in blood CD14-CD16+ and CD14+CD16+ monocytes (**Fig. 2.1c**, **Fig. 2.S2a,d)**. Using these conventional markers for blood monocyte subsets, we did not observe any significant changes in CD14-CD16+, CD14+CD16+, nor CD14-CD16+ within the BAL (**Fig. 2.1c, Fig. 2.S2a)**.

We observed a significantly elevated level of pDCs in blood at 2dpi and similarly, a trend of elevated pDCs in BAL samples (**Fig. 2.1d, Fig. 2.S2c,f**). This expansion was transient, as pDC numbers returned to baseline by 4dpi. While the overall frequencies of natural killer cells (NK) were not changed in blood or BAL (**Fig. 2.S2b,e)**, the fraction and absolute number of Granzyme B+ NK cells increased significantly at 2dpi in blood, from 4% to 25% **(Fig. 2.1e)** and remained elevated throughout the course of infection (**Fig. 2.S2b,e**). Similarly, increases in NK cell activation were also observed in the BAL, rising from 12% to 33% at 2dpi **(Fig. 2.1e)**, and persisting at this level until the study termination at 10/11dpi (**Fig. 2.S2b,e**). Collectively, these data indicate that during the hyperacute

phase of SARS-CoV-2 infection, there is a significant mobilization of innate immune cells capable of initiating and orchestrating effector responses of the Type I IFN system.

SARS-CoV-2 infection drives robust, but transient, upregulation of IFN responses in blood and lower airway

To understand the extent of immunological perturbations induced by SARS-CoV-2 infection, we performed extensive gene expression profiling of PBMC and BAL samples. During the hyperacute phase, the BAL had widespread induction of pathways associated with innate immunity and inflammation (**Fig. 2.2a**). Notably, we observed a rapid and robust induction of interferon-stimulated genes (ISGs) in the PBMC and BAL compartments starting at 1 or 2dpi (**Fig. 2.2b, Fig. 2.S3a**). The ISG response, although widespread, had largely returned to baseline by 10/11dpi (**Fig. 2.2b, Fig. 2.S3a**). We also detected a trend of elevated IFN□□protein in 4/6 and 5/8 animals in BAL and plasma, respectively (**Fig. 2.2c,d)** and a significant increase in RNA-Seq read counts mapping to IFNA genes at 2dpi in BAL (**Fig. 2.2e)**, which coincided with the expansion of pDCs in the airway and blood (**Fig. 2.1d**). A significant enrichment of genes representing NK cell cytotoxicity (**Fig. 2.2a**) was observed at 2dpi in BAL, consistent with our observation of elevated Granzyme B+ NK cells by flow cytometry (**Fig. 2.1e**). Taken together, these data demonstrate the presence of primary cells able to produce Type I IFNs (i.e., pDCs), coincident with detectable IFNA transcripts and protein, and with downstream IFN-induced effector functions (ISGs, NK cell activation) following SAR-CoV-2 infection, and that these responses were transient, having largely subsided by 10/11dpi.

SARS-CoV-2 infection drives a shift in airway macrophage populations

We observed that SARS-CoV-2 infection induced significant enrichment of several inflammatory cytokine signaling pathways, namely IFNA, IL4, IL6, IL10, IL12, IL23 and TNF, and the chemokine pathways CXCR4 and CXCR3, in both PBMCs and BAL of RMs, with higher magnitude in the BAL (**Fig. 2.2a, Supplementary Datas 1-3**). For many of these pathways, we were able to quantify significant increases in the upstream regulator at either the protein, or mRNA level, or both: IL6 protein levels were significantly increased in the BAL fluid (BALF) (**Fig. 2.2c**), as were RNA transcripts in BAL (**Fig. 2.S3b)**. Similarly, the induction of CXCR3 pathways signaling was consistent with detection of increased IP10/CXCL10 protein in BALF and RNA at 2dpi in BAL **(Fig. 2.2c, Fig. 2.S3b)**. The appearance of inflammatory pathways in the blood and airway have been reported in a multitude of human studies (reviewed in[330]). However, we noted that SARS-CoV-2 infection also drove early expression of several immunoregulatory/immunosuppressive pathways in the BAL, namely: PD1 and CTLA4 signaling, and negative regulators of MAP kinase and DDX58/RIG-I signaling (**Fig. 2.2a)**. Previously, we reported that the myeloid fraction in BAL was primarily responsible for the production of pro-inflammatory mediators, however the specific immunophenotypes were not defined. To further investigate the presence of different macrophage subsets within the lower airway after SARS-CoV-2 infection, we performed GSEA on bulk BAL data using AM gene signature (obtained from SingleR[331]) specific for RM pulmonary macrophages. We observed that genes specific for alveolar macrophages (AMs) were significantly enriched at baseline (-5dpi) relative to 4dpi, indicating a downregulation of this gene set after SARS-CoV-2 infection (**Fig. 2.2f**). Collectively, these bulk RNA-Seq data indicate a rapid and significant

shift in the balance of macrophage populations in the lower airway following SARS-CoV-2 infection.

SARS-CoV-2 infection induces an influx of two subsets of infiltrating macrophages into the alveolar space

In our prior work in RMs, we demonstrated that cells of myeloid origin were the predominant subset responsible for production of inflammatory cytokines in the lower airway following SARS-CoV-2 infection[173]. While our prior scRNA-Seq analyses determined the majority of cells in the BAL after infection to be of monocyte/macrophage origin, with relatively few neutrophils or granulocytes, the precise immunophenotypes of the myeloid cells driving inflammation in the lower airway have not been precisely delineated.

Cell classification based on cell-surface marker genes is typically problematic in scRNA-Seq data due to gene dropouts inherent to the technology. Accurate classification is further complicated in the rhesus model system, in which genomic references have incomplete annotation, and markers from other model species may not phenocopy. Several significant advances have been made recently elucidating the resident tissue macrophage subsets in the lung and their function during viral infection and inflammation[332-335]. However, analysis of scRNA-Seq data from RM lung suspensions and BAL during steady state condition indicated that several key markers used to differentiate macrophages in the murine lung (e.g. Lyve1) were not expressed at levels sufficient to distinguish populations in the rhesus pulmonary myeloid populations (**Fig. 2.S7**).

Therefore, we used two overlapping alternative strategies to accurately classify tissue macrophages and monocyte-derived/infiltrating macrophages in the RM airway after SARS-CoV-2 infection in our scRNA-Seq data. The first strategy was based on using existing lung scRNA-Seq data from uninfected RMs as a reference to map and annotate the BAL cells. We processed lung 10X data from three uninfected RMs (NCBI GEO: GSE149758)[336] through the Seurat pipeline[337] and reproduced the four reported macrophage/monocyte subsets: CD163+MRC1+, resembling alveolar macrophages; CD163+MRC1+TREM2+ macrophages, similar to infiltrating monocytes; CD163+MRC1-, similar to interstitial macrophages; and CD16+ non-classical monocytes (**Fig. 2.S4a-d**). We used Seurat to map BAL macrophages/monocytes from SARS-CoV-2 infected RMs and transfer annotations from the lung reference. The second strategy involved using bulk RNA-Seq on sorted AM and IM from the lungs of three uninfected RMs[338], according to the phenotype defined by Cai et al[339], based on expression of CD206/MRC1 and CD163, to annotate cells using SingleR[331] **Fig. 2.S4e,f**). 2069 genes were found to be differentially expressed between IMs and AMs (FDR< 0.05, fold-change>2) (**Fig. 2.S4e**). Of note, CX3CR1 was upregulated in the IMs, consistent with both murine and human definitions of this subset (**Fig. 2.S4f**). APOBEC3A, an RNA-editing cytidine deaminase, was also upregulated in IMs along with PTGS2, a pro-inflammatory COX-2 cyclooxygenase enzyme, TIMP1, which enables migration of cells via the breakdown of connective tissue, VCAN, an immunosuppressive regulator, and PDE4B, which regulates expression of TNF□□(**Fig. 2.S4f**). We annotated the lung macrophage/monocyte subsets using the bulk sorted AM and IM datasets and found that almost all of CD163+MRC1+ cluster and some CD163+MRC1+TREM2+ cells were annotated as AM and the

remaining as IM (**Fig. 2.S4g**). Thus, benchmarking our lung scRNA-Seq based reference against rudimentary bulk transcriptomic signatures demonstrated their accuracy in resolving the AM phenotype from non-AM in steady state conditions.

We next analyzed changes in the myeloid populations within the BAL of RMs after SARS-CoV-2 infection by applying these signatures to two independent scRNA-Seq datasets from rhesus macaques infected intranasally and intratracheally with $1.1x10^6$ PFU of the USA-WA1/2020 strain of SARS-CoV-2: Cohort 1, comprised of a dataset of n = 3 (baseline and 4 dpi)[173] and Cohort 2, comprised of n = 5 (baseline) and n = 6 (4 dpi)[329]. Using the lung/scRNA-Seq reference, we found that most of the BAL macrophages/monocytes belonged to the AM-like CD163+MRC1+ macrophage subset at -5dpi along with some cells from the CD163+MRC1+TREM2+ macrophage subset (**Fig. 2.3a,b and Fig. 2.S5a**). At 4dpi, there was an influx of both CD163+MRC1+TREM2+ macrophages and the IM-like CD163+MRC1- macrophages with few cells annotated as CD16+ non-classical monocytes. The expression of gene markers such as MARCO, FABP4 and CHIT1 further supported the cell subset annotations (**Fig. 2.3c**). We also observed a similar increase in APOBEC3A and decreases in the alveolar macrophage-associated genes MARCO and CHIT1 expression in BAL samples analyzed by bulk RNA-Seq, indicating a loss of CD163+MRC1+ cells (**Fig. 2.3d**). By analyzing the sc-RNA-Seq datasets, the percentage total of CD163+MRC1+ macrophages at baseline compared to 4 d.p.i. reduced from 93.3% to 55%, and 89.3% to 63.1% of all macrophages/monocytes in BAL in Cohorts 1 and 2, respectively (**Fig. 2.3e, f**). Estimates of cellular frequencies in pooled scRNA-Seq datasets can be driven by unbalanced cell

counts from individual samples. To account for this potential bias, we examined the changes in myeloid populations by individual animals. We observed that in Cohort 1, the CD163+MRC+ cells decreased from mean 90.2% (sd = 5.2%) to mean 65.4% (sd = 32%), p = ns, and in Cohort 2, they decreased significantly from mean 92% (sd = 5.1%) to mean 65.7% (sd = 16.4%) p = 0.0087 **(Fig. 2.3g, h)**. Conversely, we saw an overall increase in the percentage of CD163+MRC1+TREM2+ macrophages from 6.5% to 36.8% (Cohort 1) and 10.3% to 19.8% (Cohort 2) (**Fig. 2.3e, f**). At the individual level, we observed that levels of CD163+MRC1+TREM2+ cells increased from mean 9.7% (sd = 5.3%) to mean 28.6% (sd = 25.2%) in Cohort 1 (p = ns), and mean 7.7% (sd = 4.9%) to mean 20.0% (sd = 10.4%) (p = 0.03) **(Fig. 2.3g, h)**. Additionally, we observed increases in the IM-like CD163+MRC1- macrophages: in the pooled scRNA-Seq data from 0.2% to 8% in Cohort 1 and 0.4% to 17% in Cohort 2 (**Fig. 2.3e, f**). Considering individual animals, the CD163+MRC1- cells increased from mean 0.15% (sd = 0.19%) to mean 5.9% (sd = 6.9%) in Cohort 1 and significantly from mean 0.28% (sd = 0.18%) to mean 14.2% (sd = 9.1%) (p = 0.004) **(Fig. 2.3g, h)**. Thus, SARS-CoV-2 infection resulted in an influx of monocyte-derived and IM-like macrophages in BAL at 4dpi.

To further validate our cell classification and support the observation that it is the infiltrating cells that increase in numbers and predominantly produce inflammatory mediators, we used the second strategy of using gene expression of bulk sorted AM and IM cells to classify the BAL macrophages/monocytes. Using this definition, we confirmed that there is an increase in the percentage of non-AM population with a corresponding decrease in the AM population (**Fig. 2.S5b, d**). The non-AM population was also found to show higher expression of pro-inflammatory cytokines (**Fig. 2.S5e**).

Differential expression analysis of 4dpi and -5dpi BAL macrophages/monocytes showed that CHIT1, MARCO and MRC1 were among the top-ranking genes exhibiting downregulation in the BAL, while genes such as ADAMDEC1[340] and S100A8[341] that are associated with monocyte-derived macrophages were among the most upregulated (**Supplementary Data 4**). These data demonstrate that our observation of an influx of infiltrating macrophages into the BAL at 4dpi was consistent across multiple definitions of this phenotype.

Infiltrating macrophages produce the majority of lower airway inflammatory cytokines during acute SARS-CoV-2 infection

Given our observation of the dynamics of pulmonary macrophages within the alveolar space during early SARS-CoV-2 infection, we characterized the transcriptional changes in each macrophage/monocyte population (**Fig. 2.3**), and also in conventional myeloid dendritic cells. Myeloid DCs were present at very low frequencies (< 2%), and not more than 70 total cells were detected to be harbouring mRNA from TNF, IL6 or IL10 after infection. IL1B expression was slightly higher, but accounted for <2.5% of IL1B expressing cells in the BAL at 4 dpi (**Supplementary Fig, 6a-e**). Several chemokines (CCL4L1, CCL3, CXCL3, CCL2), multiple ISGs, NFKB1A, S100A8, and GZMB were among the most upregulated genes at 4 dpi in BAL populations (**Supplementary Data 4**). Elevated expression of multiple inflammatory genes, including IL6, TNF, IL10, and IL1B, were observed in the CD163+MRC1+TREM2 Mac and CD163+MRC1- subsets in both Cohort 1 and 2 (**Fig. 2.3i-l, Fig. 2.S7**) after infection. The infiltrating macrophages

were also observed to upregulate multiple chemokines, including those specific for recruiting neutrophils (CXCL3, CXCL8), macrophages (CCL2, CCL3, CCL5, CCL4L1), and activated T cells (CXCL10) as well as multiple ISGs (**Fig. 2.S7 & 8)**. When we examined CD163+ MRC1+ macrophages, many of the same inflammatory cytokines and gene sets seen in the infiltrating macrophages were elevated at 4dpi, albeit at much lower magnitude (**Fig. 2.S7 & 8**). Having observed a significantly higher average expression of inflammatory cytokines in infiltrating macrophages compared to CD163+MRC1+ macrophages, we compared the fractions of sequencing reads detected from each of the subsets to assess the overall contribution to inflammatory cytokine production (**Fig. 2.3i**). In Cohort 1, at 4 dpi, we observed that the CD163+MRC1+TREM2+ macrophages accounted for 55% of IL6, 57% of TNF, and 86% of IL10 expression while the CD163+MRC1- macrophages accounted for 20% of IL6, 21% of TNF, and 6% of IL10 expression **(Fig. 2.3i)**. In Cohort 2, we also observed that the infiltrating macrophages contributed more to the expression of most inflammatory cytokines than alveolar macrophages: the expression in CD163+MRC1+TREM2+ and CD163+MRC1- cells was 39.2% and 47% for IL10, 17.4% and 74.9%% for IL6, and 22.4% and 46.6% for TNF, respectively (**Fig. 2.3j**). To account for potential bias in cell counts in our pooled data, we also examined the contributions of cytokines to the BAL expression in individual animals **(Fig. 2.3k, l)**. In Cohort 1, the overall trend of higher contribution to inflammatory expression in the infiltrating macrophage populations seen in the pooled data was only observed for IL10 and CCL4L1, largely due to inbalances in cell counts and low statistical power (**Fig. 2.3k**). However, in Cohort 2, we observed consistently elevated levels in the infiltrating CD163+MRC1+TREM2+ and CD163+MRC1- macrophage populations (**Fig.**

2.3l). For IL10, the mean±sd expression in CD163+MRC1+ was 17.3±12.4%, compared to 40.4±12.1% in CD163+MRC1+TREM2+ cells (p = 0.03) and 42.3±21.2% for CD163+MRC1- (ns) **(Fig. 2.3l)**. For IL6, the mean±sd expression in CD163+MRC1+ was 9.4±12.2%, compared to 12.2±24.5% in CD163+MRC1+TREM2+ cells (ns) and 78.4±28.8% for CD163+MRC1- (p = 0.065). Additionally, while our observation for IL6 trended to significance, we found a wide variability in the percentages in CD163+MRC1- cells; to address this, we analyzed another set of data[329] in which we obtained scRNA-Seq expression of BAL macrophage after 2 dpi of SARS-CoV-2 infection – these data also trended to much higher expression of IL6 in the CD163+MRC1- cells (67.1±32.4%) compared to CD163+MRC1+ macrophages (27.7±29.5%)**(Fig. 2.S9)**. For CCL4L1, CD163+MRC1+ contributed 9.6±6.3% of expression, in comparison to 23.7±13.5% in CD163+MRC1+TREM2+ cells (p = 0.03) and 66.7±18.2% in CD163+MRC1- cells(p = 0.03). CXCL10 was observed at 19.2±16.7% in CD163+MRC1+ compared to 15.3±9.3% in the CD163+MRC1+TREM2+ and 65.4±15.2% 71.3%] in the CD163+MRC1- populations. Overall, these data indicate that the infiltrating macrophage populations are responsible for the majority of lower airway inflammatory cytokine production during acute SARS-CoV-2 infection.

To validate the increase in infiltrating myeloid populations, we quantitated by flow cytometry the frequency of CCR2+ myeloid populations in peripheral blood and BAL from an additional six SARS-CoV-2-infected rhesus macaques (**Fig. 2.S10**). CCR2 has been demonstrated to regulate monocyte infiltration into the lung parenchyma of SARS-CoV-2 infected mice[342] and its expression is upregulated in the BAL of infiltrating macrophages

in NHPs infected with influenza virus[338]. Consistent with our observation of elevated infiltrating myeloid cells by scRNA-Seq, we found that there was a concomitant increase in the frequency of CCR2+ CD14-CD16+ and CD14+CD16+ monocytes at 2 dpi. These results further support the infiltration of inflammatory monocytes in BAL after SARS-CoV-2 infection.

Identification of pro-inflammatory subsets in human SARS-CoV-2 infection corresponding to NHP immunophenotypes

To translate our findings in the NHP model to human SARS-CoV-2 infection, we used a similar bioinformatic approach to that employed to define rhesus myeloid subsets (Supplementary Methods). We used macrophages/monocytes from publically available scRNA-Seq dataset of lungs from six healthy human donors (GEO: GSE135893[343]) and classified these based on a recent classification into FABP4hi, SPP1hi, FCN1hi and proliferating macrophages[344] (**Fig. 2.4a**). When the canonical marker genes were compared between the healthy lung macrophages/monocytes of human and rhesus macaque, we found that there were comparable populations between the two (**Fig. 2.4a, 4b and 4c**). Namely the CD163+MRC1+ rhesus subset was highly similar to the FABP4hi human subset; the CD163+MRC1+TREM2+ rhesus subset was congruent with the SPP1hi human subset; and the CD163+MRC1- macrophages and CD16+ monocytes rhesus were transcriptionally similar to the FCN1hi human subset. Next, we combined data from all macrophage/monocyte cells from the six healthy human samples with the three healthy rhesus samples and applied reference based integration in Seurat using the human samples as reference (**Fig. 2.S11a,b**). We looked at the distribution of different

human and rhesus cell types in each cluster and found that the earlier observations regarding the similarity of subsets based on canonical markers was further supported by the global gene expression of these cells (**Fig. 2.S11c**). Finally, to test the robustness of our cellular classifications to identify macrophage subsets between species accurately, we generated gene signatures for each subset/species combination and tested for enrichment in the opposite species; for all comparisons, a signature scored highest with its corresponding opposite subset (**Fig. 2.S11d**).

Using the healthy human dataset as reference, we classified macrophages/monocytes from the myeloid cluster (**Fig. 2.S11e,f**) in a publically available scRNA-Seq dataset of human BAL samples from healthy donors or subjects with moderate or severe COVID-19 infection[100] (**Fig. 2.4d and Fig. 2.S11g)**. As reported in the original study[100], we found that there was a significant increase in the SPP1hi and FCN1hi subsets with COVID-19 infection while the FABP4hi population that is largely representative of the resident alveolar macrophages was found to be significantly reduced in both moderate and severe COVID-19 infection (**Fig. 2.4d and 4e**). In addition, we also looked at the contribution of these different populations towards inflammation and found that the non-resident SPP1hi and FCN1hi subsets were largely responsible for the expression of pro-inflammatory mediators in patients with severe COVID-19 (**Fig. 2.4f, Fig. 2.S12**). Respectively, (FABP4hi, SPP1hi, and FCN1hi) the contribution of each population to overall expression was: IL10 (1.3%, 56.7%, 42%), IL1B (6.6%, 37%, 56%), IL6 (2.4%, 40.8%, 56.7%), TNF (1.6%, 44.1%, 54.1%), CXCL10 (1.8%, 36.5%, 61.7%) and CXCL8 2.6%, 48.1%, 49.1%). **(Fig. 2.4f)** Of note, ISG expression (IFI27,ISG15, ISG20, MX2) was significantly upregulated in the SPP1hi, and FCN1hi populations relative to the FABP4hi in severe

disease but not in moderate cases. Lastly, when we examined the contribution of cytokine expression in by individual patients in these dataset, we noted that for severe COVID-19, we observed that the infiltrating populations had significantly higher expression of IL10 (mean±sd SPP1hi 50.9±8.7%, p = 0.03; FCN1hi 46.9±8.3%, p = 0.03), IL1B (mean±sd SPP1hi 31.7±14.9% , p = 0.03; FCN1hi 63.3±20.1%, p = 0.03), TNF (mean±sd SPP1hi 43.4±9.3% , p = 0.03; FCN1hi 53.7±13.7%, p = 0.03), CXCL10 (mean±sd SPP1hi 27.3±9.5%, p = 0.03; FCN1hi 69.8±11.1%, p = 0.03), CXCL3 (mean±sd SPP1hi 55.9±9.6% , p = 0.03; FCN1hi 37.6±13%, p = 0.06) and CXCL8 (mean±sd SPP1hi 42.7±14% , p = 0.03; FCN1hi 53.4±17.4%, p = 0.03) compared to the FABP4hi population (mean±sd for IL10 2.2±2.8%, IL1B 4.7±8.2%, TNF 2.7±4.5%, CXCL10 2.6±2.9%, CXCL3 6.4±9.5% and CXCL8 3.8±5.9%) (**Fig. 2.4g**). Collectively, these analyses demonstrate that the myeloid subsets defined transcriptionally in RMs have analogous populations in the human lung, and an overall concordance in their expansion and contribution to SARS-CoV-2 induced inflammation in the lower airway.

Baricitinib treatment prevents the influx of inflammatory IM into the lower airway

Baricitinib is a JAK1/2 inhibitor approved for the treatment of active rheumatoid arthritis that was recently approved by FDA for COVID-19 treatment in certain hospitalized adults[345], and reported to reduce mortality when administered as monotherapy[346] or in combination with remdesivir[245]. In our earlier study, using data from the Cohort 1 and baricitinib-treated animals

(Fig. 2.1A), we found that baricitinib was able to suppress the expression of pro-inflammatory cytokines in BAL of RMs infected with SARS-CoV-2[173]. Here, we extended

this study to further characterize the impact of baricitinib on the myeloid populations in the airway from five RMs before infection (-5 dpi) and at 4 dpi, with three RMs that remained untreated and two that received baricitinib). We found that two days of baricitinib administration virtually abrogated the influx of infiltrating macrophages into the alveolar space at 4 dpi, as we did not detect any increase in the CD163+MRC1- or CD163+MRC1+TREM2+ populations in baricitinib treated animals (**Fig. 2.5a-d**). This observation was consistent using classifications of macrophages either based on mapping to 10X lung reference or using bulk sorted AM/IM cells (**Fig. 2.5a-d, Fig. 2.S5a-d**). In addition to preventing the influx of infiltrating macrophages, baricitinib treatment also resulted in significantly lower expression of inflammatory cytokines and chemokines, but the ISG expression remained comparable to untreated animals (**Fig. 2.5e-g, Fig. 2.S5e**). In summary, these data further elucidate the mechanism of action by which baricitinib treatment abrogates airway inflammation in SARS-CoV-2 infection[173], by demonstrating its ability to block infiltration of discrete pro-inflammatory macrophage populations into the alveolar compartment. Similar to our observations using flow cytometry, there was an increase in the abundance of pDC at 4 dpi in the BAL detected by scRNA-Seq data, however this increase was abrogated in baricitinib-treated animals (**Fig. 2.5h,i**).

DISCUSSION

The mechanisms by which SARS-CoV-2 infection establishes severe disease remain largely unknown, but remain a key priority for reducing the toll of the COVID-19 pandemic. As the appearance of symptoms range from 2-14 days after SARS-CoV-2 infection,

characterization of the early immunological events using clinical samples is challenging. Here, we utilized the RM model of SARS-CoV-2 infection and an integrated systems analysis to dissect the immune response during hyper-acute infection. Our findings were: (i) SARS-CoV-2 infection initiated a robust Type I IFN response in the blood and lower airway apparent at 1-2dpi; (ii) SARS-CoV-2 induced a rapid influx of two infiltrating macrophage populations, into the bronchoalveolar space, which produced the majority of inflammatory cytokine production; and (iii) the mechanism of action of baricitinib, a drug recently authorized by FDA for use in the treatment of COVID-19 for certain hospitalized adults[345], is to abrogate infiltration of these inflammatory cells into the airway. Our data present, to date, the most comprehensive analysis of the immunopathological events occurring during hyperacute SARS-CoV-2 infection.

Using our reference datasets of RM lung macrophages, we identified two myeloid cell subsets, both clearly distinct from alveolar macrophages, infiltrating the airway after SARS-CoV-2 infection, that were the main producers of lower airway inflammatory cytokines and chemokines. One population, defined as CD163+MRC1+TREM2+ cells, were highly similar to murine definitions of infiltrating CCR2+ monocytes. The second, CD163+MRC1-, largely resembled interstitial macrophages. Our data are consistent with a recent observation of a rapid (3dpi) increase of IMs in the BAL of RMs using flow cytometry[327]. Similarly, an accumulation of non-AMs (defined as CD16+CD206-HLA-DR+/CD11b+), and reciprocal reduction of AMs, has been observed in the BAL and lungs of infected RMs and AGMs[328]. We found that these myeloid subsets, defined transcriptionally in NHPs, had analogous populations in the human lung. Lastly, our data

are consistent with our recent findings in the murine model, in which SARS-CoV-2 elicited recruitment of circulating monocytes to the lung parenchyma, but was significantly abrogated in CCR2-deficient mice[342]. The CD163+MRC1+ Mac/AM-like subset also contributed to the inflammatory milieu, producing IL6, TNF, and IL10, albeit in significantly lower quantities.

It is important to note that our observations were during hyperacute infection, and that our animals did not develop severe disease, so although our data indicate that these infiltrating populations orchestrate early inflammation and may contribute to airway pathogenesis, we cannot formally make this link. However, this model is consistent with recent data by Ren et al.[347], who observed a significant loss of MARCO expression in BAL-resident myeloid populations of patients with severe COVID-19 relative to those with moderate disease, similar to our observations, in which the appearance of infiltrating macrophages diluted the population of MARCO+ macrophages. Those observations, taken together with our data, suggest that the inflammatory macrophage phenotype we identify here may be preferentially retained in the lower airway of patients with severe COVID-19. Additionally, we demonstrated that *in vivo* treatment with the JAK1/2 inhibitor baricitinib, which has demonstrated efficacy in reducing severe disease, was able to virtually abrogate the recruitment of these inflammatory macrophages into the airway, providing an additional mechanistic link with the development of COVID-19-related pathogenesis.

In addition to inflammatory cytokines, we observed that the infiltrating macrophage subsets produced high levels of IL10, and were enriched in IL10 signaling pathways. Lung IM's are considered to be a "professional IL10-producing cell" producing IL10 at both a steady state and in response to innate stimuli (LPS, unmethylated CpGs)[348]. The majority of data to date has demonstrated an immunoregulatory, protective role for IMs in murine models of asthma, lung fibrosis, and allergen induced inflammation[333]. However, while the pro-inflammatory potential of IMs has been relatively understudied, they have been demonstrated to be efficient at producing IL6 and TNF in response to TLR ligands[349]. Given our observations of high IL10 production in infiltrating macrophages, we cannot exclude a potential immunoregulatory role for this subset, and indeed, it presents an interesting hypothesis in which the balance of infiltrating IM vs TREM2+ macrophages into the bronchoalveolar space determines the pathogenic outcome of SARS-CoV-2 infection. Lastly, recent publications have reported that lung IMs may be comprised of two, or even three, functionally distinct populations, defined by an axis of expression of Lyve1, MHC, CD169, and CD11c[332-335]. We did not observe separate clustering amongst BAL IMs, nor differential expression amongst these markers, and further work is needed to understand the congruency of macaque macrophage subsets with those identified in the murine model.

We observed a very rapid and robust induction of the Type I IFN pathway at 1-2dpi, characterized by elevated pDCs in the airway and blood, IFNA and IFNB transcripts and protein, upregulated ISGs, and increased granzyme B in NK cells. The Type I IFN response in SARS-CoV-2 infection has been intensely studied: in vitro infection of airway

epithelial cells have consistently resulted in a muted ISG response[350], and patients developing severe COVID-19 have been reported to have higher incidence of mutations in IFN response genes, or elevated levels of autoantibodies against IFN-response genes (reviewed in[320,351-358]). Our data, in which the IFN response peaked at 2dpi and had largely abated by 10/11dpi, provides well defined kinetics of the ISG response, and similar observations have been reported in other NHP studies[174, 327]. The rapid and short-lived nature of the IFN response underscores the difficulty in interpreting the IFN response in clinical samples.

Our multiparametric analyses demonstrated an increase of pDCs at 2dpi that coincided with the peak of ISG production, IFNA/B detection, and NK cell activation, thus implicating pDCs as the primary cell orchestrating the IFN response in the lower airway. We had previously observed a reduction in peripheral blood pDCs frequencies and activity in human SARS-CoV-2 infection[359], and other have reported signatures of pDCs apoptosis that predicted lower IFN-I responses[360]. Taken in the context of these clinical findings, our observation of pDC accumulation in the BAL indicates that they undergo rapid mobilization from the blood to the lower airway, and this suggests they likely drive early protective innate immune responses. However, pDCs may also contribute to pathological inflammation; and future interventional studies targeting the pDC/IFN axis in animal models will be necessary to test these hypotheses.

In our prior study, we demonstrated the ability of baricitinib to block airway pro-inflammatory cytokine production in SARS-CoV-2-infected RMs while preserving Type I

IFN responses[173]. The efficacy of baricitinib to treat severe COVID-19 was recently tested in two Phase 3 clinical trials (ACTT-2 and COV-BARRIER) and recently received approval as monotherapy to treat COVID-19 in patients requiring supplemental oxygen or mechanical ventilation[345]. To date, nearly 1 M patients have received baricinitib to treat severe COVID-19 disease, underscoring the importance for understanding its mechanism of action. Here, we extended our original findings to demonstrate that baricitinib blocked the influx of inflammatory macrophages into the bronchoalveolar space. These data add to our mechanistic understanding of the action of baricitinib, and provide a potential explanation for the disparity of baricitinib's impact on IFN vs IL6/TNF signaling when considering the timing of the drug administration. We administered baricitinib at 2 dpi, after the peak influx of pDCs, but before the likely appearance of the inflammatory macrophages at 3-4 dpi. The ongoing ISG response, and suppressed TNF/IL6 response, suggest that the primary mechanism by which baricitinib protects the airway is by blocking recruitment of inflammatory cells to the bronchoalveolar space. Of note, in the presence of baricitinib and concomitant elimination of infiltrating monocytes/macrophages, viral load in the BAL was unchanged compared to controls, suggesting that these populations exert minimal control of virus levels. However, as the rhesus model of SARS-CoV-2 tends to be consistent with mild COVID-19 in the majority of studies, it will be critical to examine the mechanism of baricitinib in a model of severe disease. In regards to guiding future clinical applications of baricitinib, our data suggest that timing is critical, and would favor earlier drug administration. Additionally, given the pervasiveness of SARS-CoV-2, and growing capacity for re-infection, future studies on the application of baricitinib for treatment second infections would be of benefit.

Our study had some limitations; first, while the RM/SARS-CoV-2 model has rapidly been adopted by several groups for pre-clinical testing of anti-COVID drugs and vaccines, no group has demonstrated overt, reproducible symptomatic disease[324]. Thus, linking early immunological events to the development of severe COVID-19 requires validation in human studies, such as the observations of reduced MARCO expression in the airway myeloid populations of severe COVID-19 patients noted above[347]. Additionally, to estimate the overall contribution to inflammatory cytokine production in macrophages, we calculated the fraction of sequencing reads for a given mRNA transcript assigned to a subset, however we did not measure protein quantities on a single-cell level, and instead were limited to assessing overall levels in BALF. Prior studies have attempted to estimate the correlation of cytokine mRNA to secreted protein levels and have reported good agreement for TNF, IL6, CXCL10 and CXCL8, but poorer concordance for IL10 and IL1B[361]. Another drawback was the relatively low power of our study. While our observations at 0, 1, and 2 dpi were n = 8, we were limited to n = 4 for day 4-10 observations. For our scRNA-Seq experiment, we addressed power issues conducting our analysis on two independent cohorts for a total of nine animals. Overall, there was no lack of statistical power for our key observations.

While the global vaccine rollout has made great strides to reduce the transmission and severity of SARS-CoV-2 infection, millions of people remain vulnerable. Understanding the early events of SARS-CoV-2 infection, and the mechanisms by which clinically approved drugs afford protection, remains a global priority. In this study, we have

identified two populations of inflammatory myeloid cells that are responsible for the preponderance of airway inflammation in acute SARS-CoV-2 infection. We also demonstrated that treatment with baricitinib, recommended by the World Health Organization for treatment of severe COVID-19 in January 2022, blocked infiltration of these inflammatory cells into the alveolar space. These data identify both a key druggable target (airway infiltrating macrophages), and an efficacious mechanism by which to lower airway inflammation, and should prove useful for identifying additional drugs to reduce the incidence and mortality of severe COVID-19 disease.

METHODS

Animal and SARS-CoV-2 infections

The animal care facilities at ENPRC are accredited by the Association for Assessment and Accreditation of Laboratory Animal Care (AAALAC) as well as the U.S. Department of Agriculture (USDA). Emory University's Institutional Animal Care and Use Committee (IACUC) reviewed and approved all animal experiments under permit PROTO202000035. All procedures were performed as per the institutional regulations and guidelines set forth by the NIH's Guide for the Care and Use of Laboratory Animals (8^{th} edition) and were conducted under anesthesia and appropriate follow-up pain management to minimize animal suffering. Eight (4 females, 4 males, aged >11 yrs) specific-pathogen-free Indian-origin rhesus macaques were infected via intranasal and intratracheal routes with 1.1×10^6 plaque forming units (PFU) SARS-CoV-2 as previously described[173] and were maintained in the ABSL3 at YNPRC (IACUC permit PROTO202000035). The processing of nasopharyngeal swabs, BAL and mononuclear

cells was performed as described previously[173]. Six (2 females, 4 males, aged >6 yrs) additional specific-pathogen-free Indian-origin rhesus macaques were added to the study (IACUC permit PROTO202100003) and were also infected via intranasal and intratracheal routes with 1.1 x 10^6 plaque forming units (PFU) SARS-CoV-2 for characterization of CCR2 expression in whole blood and BAL.

The 8 animals under IACUC permit PROTO202000035 were age and sex matched between untreated control and baricitinib-treated experimental arms, with 2 females and 2 males assigned to each respective arm. Cohort 2 (IACUC permit PROTO202100003) was comprised of 2 females and 4 males, all of which served as untreated controls. Efforts to include equal numbers of females and males in Cohort 2 were made. However, female macaques were limited at the time of Cohort 2 animal assignment due to breeding demands. In total, between Cohort 1 and 2, 4 female and 6 male untreated controls were included in this study.

Viral Stocks

The viral stocks used for infecting the 8 RMs on IACUC permit PROTO202000035 were previously described[173]. SARS-CoV-2 (NR-52281: BEI Resources, Manassas, VA; USA-WA1/2020, Lot no. 70033175) was passaged on Vero E6 cell line (African Green Monkey Kidney cell line; CRL-1586, ATCC) at a MOI of 0.01. The $TCID_{50}$ method was used to propagate and titrate SARS-CoV-2 followed by storage of aliquots at -80°C. The infectious dose delivered was determined by back titration of viral stocks via plaque assay. The virus stock was sequenced to confirm the presence of furin cleavage motif. The viral stocks used had less than 6% of genomes with a mutation that may abrogate

furin cleavage. The 6 RMs on IACUC permit PROTO202100003 were infected with the viral stock NR-53899: BEI Resources, Manassas, VA; USA-WA1/2020.

Determination of viral load RNA

The SARS-CoV-2 genomic and sub-genomic RNA was quantified in nasopharyngeal swabs, throat swabs, and BAL as previously described[173, 325]. The swabs were kept in 1mL of Viral Transport Medium (VTM-1L, Labscoop, LLC). The viral RNA was extracted from fresh specimens of nasopharyngeal (NP) swabs, throat swabs, and BAL manually using the QiaAmp Viral RNA mini kit as per the manufacturer's protocol. For genomic RNA, CDC designed N2 primer and probe set: CoV2-N2-F: 5'-TTACAAACATTGGCCGCAAA-3', CoV2-N2-R: 5'-GCGCGACATTCCGAAGAA-3', and CoV2- N2-Pr: 5'-FAM-ACAATTTGCCCCCAGCGCTTCAG-BHQ-3'[362] were used for quantitative PCR (qPCR). For sub-genomic RNA, the primer and probe sequences for E gene subgenomic mRNA transcript[363] were used: SGMRNA-E-F: 5'-CGATCTCTTGTAGATCTGTTCTC-3', SGMRNA-E-R: 5'-ATATTGCAGCAGTACGCACACA-3', and SGMRNA-E-Pr: 5'-FAM-ACACTAGCCATCCTTACTGCGCTTCG-3'. The qPCR reactions were performed with the TaqMan Fast Virus 1-step Master Mix using the manufacturer's cycling conditions, 200nM of each primer, and 125nM of the probe in duplicate. 257 copies/mL VTM/plasma/BAL ws the limit of detection for this assay. The CDC RNase P p30 subunit qPCR, modified for rhesus macaque specific polymorphisms, was used to verify sample quality using the following primer and probe sequences: RM-RPP30-F 5'-AGACTTGGACGTGCGAGCG-3', RM-RPP30-R 5'-GAGCCGCTGTCTCCACAAGT-3',

and RPP30-Pr 5'-FAM-TTCTGACCTGAAGGCTCTGCGCG-BHQ1-3'. The RNA integrity and sample quality was verified by running a single well from each extraction.

Tissue processing

NP swabs were collected under anesthesia by using a clean rayon-tipped swab (ThermoFischer Scientific, BactiSwab NPG, R12300) placed approximately 2-3cm into the nares. Oropharyneal swabs were collected under anesthesia using polyester tipped swabs (Puritan Standard Polyester Tipped applicator, polystyrene handle, 25-806 2PD, VWR International) to streak the tonsils and back of throat bilaterally (throat/pharyngeal). The swabs were dipped in 1 mL viral transport media (Viral transport Media, VTM-1L, Labscoop, LLC) and vortexed for 30 sec, and the eluate was collected.

To collect BAL, a fiberoptic bronchoscope (Olympus BF-XP190 EVIS EXERA III ULTRA SLM BRNCH and BF-P190 EVIS EXERA 4.1mm) was manipulated into the trachea, directed into the primary bronchus, and secured into a distal subsegmental bronchus upon which 35-50 mL of normal saline (0.9% NaCl) was administered into the bronchus and re-aspirated to obtain a minimum of 20ml of lavage fluid. BAL was filtered through a 70µm cell strainer and multiple aliquots were collected for viral loads. Next, the remaining BAL was centrifuged at 2200rpm for 5 minutes and the BAL fluid supernatant was collected for mesoscale analysis. Pelleted BAL cells were resuspended in R10 and used for downstream analyses.

Mononuclear cells were counted for viability using a Countess II Automated Cell Counter (Thermo Fisher) with trypan blue stain and were cryo-preserved in aliquots of up to $2x10^7$ cells in 10% DMSO in heat-inactivated FBS. Whole tissue segments (0.5 cm^3) were snap

frozen dry, or stored in RNAlater (Qiagen), or Nuclisens lysis buffer (Biomerieux) for analyses of compound distribution, RNA-seq, and tissue viral quantification, respectively.

Immunophenotyping and flow cytometric purification of RM pulmonary macrophages

23-parameter flow cytometric analysis was perform on fresh EDTA whole blood and BAL mononuclear cells from SARS-CoV-2 infected RMs as described previously[173] using anti-human monoclonal antibodies (mAbs), which we and others[173, 364, 365], including databases maintained by the NHP Reagent Resource (MassBiologics), have shown as being cross-reactive in RMs.

A panel of the following mAbs was used for the longitudinal phenotyping of innate immune cells in whole blood (500 µL), and mononuclear cells (10^6 cells) derived from BAL from Cohort 1 and baricitinib-treated animals: anti-CD20-BB700 (clone 2H7; 2.5uL; cat. # 745889), anti-Ki-67-BV480 (clone B56; 5uL; cat. # 566109), anti-CD14-BV605 (clone M5E2; 2.5uL; cat. # 564054), anti-CD56-BV711 (clone B159; 2.5uL; cat. # 740781), anti-CD115-BV750 (clone 9-4D2-1E4; 2.5uL; cat. # 747093), anti-CD3-BUV395 (clone SP34-2; 2.5uL; cat. # 564117), anti-CD8-BUV496 (clone RPA-T8; 2.5uL; cat. # 612942), anti-CD45-BUV563 (clone D058-1283; 2.5uL; cat. # 741414), anti-CCR2-BUV661 (clone LS132.1D9; 2.5uL; cat. # 750472), anti-CD16-BUV737 (clone 3G8; 2.5uL; cat. # 564434), anti-CD69-BUV805 (clone FN50; 5uL; cat. # 748763), and Fixable Viability Stain 700 (2uL; cat. # 564997) all from BD Biosciences; anti-CD38-FITC (clone AT1; 5uL; cat. # 60131FI) from STEMCELL Technologies; anti-CD161-BV421 (clone HP-3G10; 5uL; cat.

339914), anti-HLA-DR-BV650 (clone L243; 5uL; cat. # 307650), anti-CD11c-BV785 (clone 3.9; 5uL; cat. # 301644), anti-CD11b-PE (clone ICRF44; 2.5uL; cat. # 301306), and anti-CD123-APC-Fire750 (clone 315; 2.5uL; cat. # 306042) all from Biolegend; anti-GranzymeB-PE-TexasRed (clone GB11; 2.5uL; cat. # GRB17) from Thermo Fisher; anti-CD66abce-PE-Vio770 (clone TET2; 1uL; cat. # 130-119-849) from Miltenyi Biotec; and anti-CD27-PE-Cy5 (clone 1A4CD27; 2.5uL; cat. # 6607107) and anti-NKG2A-APC (clone Z199; 5uL; cat. # A60797) from Beckman Coulter (Fig. 2.S4).

For Cohort 2 animals, a different panel of the following mAbs was used for the longitudinal phenotyping of innate immune cells in whole blood (500 µL), as described in (20), and mononuclear cells (2x106 cells) derived from BAL: anti-CD20-BB700 (clone 2H7; 2.5 µL; cat. # 745889), anti-CD11b-BV421 (clone ICRFF44; 2.5 µL; cat. # 562632), anti-Ki-67-BV480 (clone B56; 5 µL; cat. # 566109), anti-CD14-BV605 (clone M5E2; 2.5 µL; cat. # 564054), anti-CD56-BV711 (clone B159; 2.5 µL; cat. # 740781), anti-CD163-BV750 (clone GHI/61; 2.5 µL; cat. # 747185), anti-CD3-BUV395 (clone SP34-2; 2.5 µL; cat. # 564117), anti-CD8-BUV496 (clone RPA-T8; 2.5 µL; cat. # 612942), anti-CD45-BUV563 (clone D058-1283; 2.5 µL; cat. # 741414), anti-CCR2-BUV661 (clone LS132.1D9; 2.5 µL; cat. # 750472), anti-CD16-BUV737 (clone 3G8; 2.5 µL; cat. # 564434), anti-CD101-BUV805 (clone V7.1; 2.5 µL; cat. # 749163), anti-CD169-PE (clone 7-239; 2.5 µL; cat. # 565248), and anti-CD206-PE-Cy5 (clone 19.2; 20 µL; cat. # 551136) and Fixable Viability Stain 700 (2 µL; cat. # 564997) all from BD Biosciences; anti-ACE2-AF488 (clone Polyclonal; 5 µL; cat. # FAB9332G-100UG) from R & D; anti-HLA-DR-BV650 (clone L243; 5 µL; cat. # 307650), anti-CD11c-BV785 (clone 3.9; 5 µL; cat. # 301644), and anti-CD123-APC-Fire750 (clone 315; 2.5 µL; cat. # 306042) all from Biolegend; anti-GranzymeB-PE-

TexasRed (clone GB11; 2.5 µL; cat. # GRB17) from Thermo Fisher; anti-CD66abce-PE-Vio770 (clone TET2; 1 µL; cat. # 130-119-849) from Miltenyi Biotec; anti-NKG2A-APC (clone Z199; 5 µL; cat. # A60797) from Beckman Coulter. mAbs for chemokine receptors (i.e. CCR2) were incubated at 37C° for 15 min, and cells were fixed and permeabilized at room temperature for 15 min with Fixation/Permeabilization Solution Kit (BD Biosciences; cat. #554714). For each sample, a minimum of $1.2x10^5$ stopping gate events (live CD3+ T-cells) were recorded. All samples were fixed with 4% paraformaldehyde and acquired within 24 hours of fixation. Acquisition of data was performed on a FACSymphony A5 (BD Biosciences) driven by FACS DiVa Version 8.0 software and analyzed with FlowJo (version 10.7; Becton, Dickinson, and Company). The gating strategy is show in **Fig. 2.S1**.

Bulk RNA-Seq library & sequencing

The data for -5dpi, 2dpi and 4dpi for bulk BAL samples was obtained from our previous study[173]. Here we expanded our study to include 7dpi and 10dpi/11dpi samples for BAL and -5dpi, 1dpi, 2dpi, 4dpi, 6dpi, 7dpi, 8dpi and 10/11dpi for PBMC. Cell suspensions were prepared in BSL3, for bulk RNA-Seq, 250,000 cells (PBMCs) or 100,000 cells (BAL) were lysed directly into 700 ul of QIAzol reagent. The RNeasy Mini or Micro kits (QIAGEN) with on-column DNase digestion was used to isolate RNA. The quality of RNA was determined using an Agilent Bioanalyzer and the cDNA synthesis was carried out using the total RNA with Clontech SMARTSeq v4 Ultra Low Input RNA kit (Takara Bio) as per the manufacturer's instructions. Dual-indexed bar codes were appended to the amplified cDNA after fragmenting using the NexteraXT DNA Library Preparation kit (Illumina).

Agilent 4200 TapeStation was used to validate the libraries by capillary electrophoresis and the libraries were pooled at equimolar concentrations. The libraries were sequenced on an Illumina NovaSeq6000 at 100SR, yielding 20-25 million reads per sample.

Bulk RNA-Seq analysis

The BCL files were converted to Fastq using bcl2fastq v2.20.0.422 . The genome sequences for Macaca mulatta (Mmul10 Ensembl release 100), SARS-CoV-2 (strain MN985325.1 - NCBI) and ERCC sequences were combined to build a STAR index (v2.7.3a) as described previously and the reads were aligned to this reference[173]. The ReadsPerGene files were converted into the htseq format and were then imported in DESeq2 v1.24.0[366] using the DESeqDataSetFromHTSeqCount function. The design used was: ~ Subject + Group * Timepoint where Group distinguished between samples that were untreated or treated with baricitinib during the time course. Differentially expressed genes for BAL and PBMC were determined using a threshold of padj < 0.05, fold-change > 2 and filtering out lowly expressed genes where all of the samples at a particular timepoint were required to have detectable expression by normalized reads > 0 for that gene.

The input for GSEA v4.1.0[367] was the regularized log expression values obtained from DESeq2. The following gene sets were used for GSEA analysis: Hallmark and Canonical pathways (MsigDB), NHP ISGs[368] and Rheumatoid arthritis (KEGG map05323). Since the gene names are largely consistent between the rhesus monkey and human genome references, they were used unaltered with human MsigDB gene sets. The default parameters were ued to run GSEA with gene_set permutation type. Volcano plots of differential expression at each timepoint were generated with EnhancedVolcano (v1.8.0)

R library[369]. The regularized log expression values from DESeq2 were used to generate heatmaps using the ComplexHeatmap (v2.0.0) R library[370].

scRNA-Seq analysis

The filtered count matrices for BAL were obtained from[173]. For each BAL sample from SARS-CoV-2 infected rhesus macaque, the count matrix was filtered to include only the protein coding genes. Genes encoded on Y chromosome, mitochondrial genes, RPS and RPL genes, B-cell receptor and T-cell receptor genes, and HBB were filtered out. The Seurat library v4.0.4[337] was used to perform the analysis. The following parameters were used to filter cells: (i) nFeature_RNA >=200 & <=4000, (ii) % of HBB gene < 10, (iii) % of mitochondrial genes < 20, (iv) % of RPS/RPL genes < 30 and (v) log10(nFeature_RNA) / log10(nCount_RNA) >= 0.8. The number of cells from each sample that passed QC metrics are included in **Supplementary Data 5**. All the BAL samples from each animal at -5dpi and 4dpi were then integrated as per the Seurat integration pipeline[371] using the default CCA method after normalizing the samples using SCTransform method. The first 30 dimensions were used with RunUMAP and FindNeighbors functions.

For identification of DC, all the BAL samples from -5dpi and 4dpi for both treated and untreated rhesus macaques were integrated using CCA. The clusters were determined using the FindClusters function in Seurat and the cells were annotated using SingleR (v1.4.0) (**Fig. 2.S10 a,b**). The seurat cluster 11 was classified as pDC based on the expression of canonical markers (**Fig. 2.S10c).** The clusters 17 and 22 were classified as mDC and activated mDC based on expression of marker genes reported previously[372].

For getting the subset of macrophages/monocytes, the largest cluster primarily comprised of macrophages/monocytes annotated by SingleR (BluePrintEncode database) was selected. Cells that were annotated as another cell type in this cluster were filtered out. The macrophages/monocytes from all BAL samples were then split into individual samples, normalized using SCTransform method and then integrated again using 30 dimensions. We used the FindMarkers function in Seurat to test for differential expression using the MAST (v1.16.0) method[373].

The macrophages/monocytes from BAL samples were annotated into subsets using two approaches – (i) mapping to macrophages/monocytes from lung reference using Seurat and (ii) using bulk sorted cells as reference with SingleR[331]. The 10X lung scRNA-seq data from three uninfected macaque was obtained from a published study (NCBI GEO: GSE149758)[336]. The following parameters were used to filter cells: (i) nFeature_RNA >=200 & <=4000, (iii) % of mitochondrial genes < 20, (iv) % of RPS/RPL genes < 50 and (v) log10(nFeature_RNA) / log10(nCount_RNA) >= 0.8. The samples were normalized using SCTransform and integrated. The first 40 dimensions were used for the initial clustering. The macrophage/monocyte cells as annotated by SingleR were then selected, split into individual samples and integrated again using 30 dimensions. Louvain clustering resulted in four clusters which were annotated based on the expression of marker genes. This integrated dataset served as the reference to map the macrophages/monocytes from SARS-CoV-2 infected BAL using the FindTransferAnchors and MapQuery with reference.reduction set to pca and umap as the reduction.model.

The BAL samples were also annotated using SingleR library with the IM and AM bulk sorted cells as reference.In order to obtain references for assigning cell types in single-

cell data, bulk RNA-Seq data of interstitial (IM) and alveolar macrophages (AM) from three uninfected cynomolgus macaques[338] was analyzed using DESeq2. The regularized log expression values were obtained using the rlog function with the parameters blind = FALSE and filtType = “parametric.” The significant genes were filtered based on following criteria: padj < 0.05; fold-change > 2 and normalized mean expression > 5000 for either IM or AM samples.

For analysis of human lung data, we obtained the rds object for GEO GSE135893[343] and filtered all cells except those annotated as Macrophages, Monocytes and Proliferating macrophages from Control samples. There were a total of 10 control samples from two different sites. We observed some potential batch effects in UMAP and selected only seven samples from the “Vanderbilt” site. We further dropped one sample as the number of macrophages/monocytes was low resulting in a total of six healthy samples. The object was split based on the Sample_Name and reintegrated using CCA method in Seurat. Based on the expression of markers genes described in Morse et al[344], the four seurat clusters obtained by using 15 dimension and a resolution of 0.1, were annotated as FABP4hi, SPP1hi, FCN1hi and Proliferating macrophages. The rhesus and human macrophage/monocytes from healthy individuals were then integrated using the reference-based approach with human samples as the reference using genes that were classified as one-to-one orthologs according to ENSEMBL between GRCh38 and Mmul10 and shared the same gene name. The UCell (v1.3.1)[374] package was used to obtain enrichment scores for marker gene expression between rhesus and human macrophage/monocyte subsets. The markers for each subset were obtained using the FindMarkers function in Seurat for each species using the MAST method and filtered to

include those with an adjusted p-value < 0.05 and fold-change of > 1.5. These were further filtered to only include genes that were classified as one-to-one orthologs and shared the same gene name between GRCh38 and Mmul10 (**Supplementary Data 6**).

For human BAL, we used the samples available as part of GEO: GSE145926[100]. The cells were filtered based on the following criteria: nFeature_RNA > 100, nFeature_RNA < 3500 and percent.mito < 10 and the samples were integrated using reciprocal PCA. The cells were annotated using BPEncode database in SingleR and only the cells annotated as macrophages/monocytes in the largest cluster comprising of macrophages/monocytes was used for further analysis (**Fig. 2.S8d,e**). These cells were then annotated using the healthy lung macrophage/monocyte as reference using the FindTransferAnchors and MapQuery functions in seurat. The expression of marker genes was used to assess the accuracy of the predictions (**Fig. 2.S8f**).

To calculate the contribution of each cell type towards expression of a gene, the CPM values were obtained using RC normalization method with a scale factor of 1e6. The total CPM value was calculated per gene and the sum of CPM values for a given cell type was divided by the total to obtain a percentage value.

Mesoscale cytokine analysis.

U-PLEX assays (Meso Scale MULTI-ARRAY Technology) were used for plasma and BALF cytokine detection according to manufacturer's instructions, using 25 microliters as input.

Statistics & Reproducibility

No statistical method was used to predetermine sample size. The sample size was largely determined by (i) availability of NHP that, at the time of the study (March 2020), could be infected with SARS-CoV-2 and housed in BSL-3 and (ii) anticipated strong impact of baricitinib in blocking SARS-CoV-2 induced inflammation. The 8 RMs from Cohort 1 were randomized two days after infection into a treated and untreated group each comprising of four RMs. Cohort 2 was comprised of 6 SARS-CoV-2-infected RMs[329]. Nasal sgRNA viral loads at 2dpi were not measured for 4 animals (n=2 Cohort 1 and n=2 baricitinib cohort) and throat sgRNA viral loads at 6dpi and 8dpi were not measured for one Cohort 1 animal due to limited RNA. Whole blood was not stained for flow cytometry at 1dpi for one Cohort 1 and two baricitinib animals and 6dpi for one Cohort 1 animal. BAL fluid supernatant was not collected for one Cohort 1 and one baricitinib animal at 2dpi and subsequently not run for mesoscale analysis. One scRNA-Seq baseline sample from cohort 2 was dropped due to large fraction of epithelial cells. The Investigators were not blinded to allocation during experiments and outcome assessment. Statistical tests were performed using R (version 4.2.2) or GraphPad Prism v7.02 and have been listed accordingly. The specific tests that were used: one-tailed/two-tailed, Mann-Whitney U/Wilcoxon signed-rank test have been indicated for each comaprison. For differential gene expression analysis of bulk and single-cell RNA-Seq data, the adjusted p-values after multiple test correction, determined as part of DESeq2 and MAST analyses were used.

Data availability:

The bulk RNA-Seq data generated in this study for 7dpi and 10dpi/11dpi samples for BAL and -5dpi, 1dpi, 2dpi, 4dpi, 6dpi, 7dpi, 8dpi and 10/11dpi for PBMC has been deposited in NCBI GEO (GSE198882). The scRNA-Seq data for BAL from SARS-CoV-2 infected rhesus macaques and the bulk RNA-Seq data for -5dpi, 2dpi and 4dpi for bulk were obtained from GEO GSE159214[173]. The 10X single-cell uninfected rhesus macaque lung samples were obtained from GEO GSE149758[336]. The bulk RNA-Seq data for sorted interstitial and alveolar macrophages from cynomolgus macaque were obtained GEO [338]. The single-cell uninfected human lung samples and the human BAL samples were obtained from GEO GSE135893[343] and GSE145926[100] respectively. Source data for the figures are provided with the paper.

Code availability:

The scripts used for analysis are available at https://github.com/BosingerLab/NHP_COVID-19_2[375].

Dedication:

We would like to dedicate this manuscript to Dr. Timothy N. Hoang, whose commitment to this project and to scientific discovery were crucial in propelling this study forward. Dr. Hoang will be remembered for his intelligence, drive, and love for science and for all of the lives that he touched during his short but impactful career.

Acknowledgments:

We kindly thank the Emory National Primate Research Center (ENPRC) Director Paul Johnson; Division of Animal Resources, especially Joyce Cohen, Stephanie Ehnert,

Stacey Weissman, Sherrie Jean, Jennifer S. Wood, Fawn Connor-Stroud, Rachelle L. Stammen, Racquel A. Sampson-Harley, Denise Bonenberger, John M. Wambua, Dominic M. D'Urso, Sanjeev Gumber, Kalpana Patel, Maureen Thompson, Ernestine Mahar, Kyndal Goss, Christina Gavegano and Sudhir Kasturi for providing support in animal care, biosafety guidance, technical, computational and cytometry support. We are grateful to Raymond F. Schinazi for providing the baricitinib, and the virus as well as the original idea. We apologize for key publications omitted due to space limitations.

Funding:

NIH Office of Research Infrastructure Programs (ORIP) P51 OD11132 which provides base grant funding to ENPRC and Emory NPRC Genomics Core; and P51 OD11132-61S1 and P51 OD11132-60S4 to M.Pa. Emory University COVID-19 Molecules and Pathogens to Populations and Pandemics (MP3) Initiative Seed Grant to M.Pa., A.P., and R.F.S.

YNPRC Coronavirus Pilot Research Project Program grant (to M.Pa. under award P51 OD11132).

Fast Grants #2144 to M.Pa

The William I.H. and Lula E. Pitts Foundation Grant to M.Pa.

NIH grant 5R01-MH-116695 awarded to R.F.S.

Sequencing data was acquired on an Illumina NovaSeq6000 funded by NIH S10 OD026799 to S.E.B.

Author contributions:

Conceptualization: A.A.U.,T.N.H., E.G.V., M. Pino.,M. Paiardini, R.F.S & S.E.B.;

Methodology: T.N.H., M. Pino., E.G.V.,S.P.R.,M.Y.-H.L.,J.C.,Z.S.,D.A.C.,E.N.B.,T.R.Ho.,S.H.,H.A.,J.L.H.,K.N.,K.L.P.,A.P.,R.D.L., & T.H.V.;

Formal Analysis, A.A.U.,T.N.H.,M. Pino.,A.K.B.,M.Y.-H.L.,C.T.E.,Z.S., E.G.V.,G.K.T., & T.H.V;

Investigation: A.A.U.,T.N.H.,M. Pino.,M. Paiardini., & S.E.B.;

Resources: S.E.B, S.M.B.B.,R.R.A.,R.F.S., R.P.S.,M. Paiardini. & S.E.B.;

Writing: – Original Draft, A.A.U., M.Pino. S.E.B.;

Writing, Review & Editing, T.N.H.,S.P.R.,E.G.V. M. Paiardini, R.F.S.

Visualization, A.A.U.,T.N.H.,M. Pino., A.K.B., G.K.T.

Supervision: M. Paiardini. and S.E.B.;

Funding Acquisition: M. Paiardini & S.E.B., R.F.S.

Competing interests: R.F.S. has served in the past as an unpaid consultant for Eli Lilly whose drugs are being evaluated in the research described in this paper, and owns shares in Eli Lilly. He also receives royalties from the sales of Baricitinib for COVID-19 in the US and Mexico. The terms of this arrangement have been reviewed and approved by Emory University in accordance with its conflict of interest policies. All other authors do not have any conflicts to declare.

Chapter Two Figures

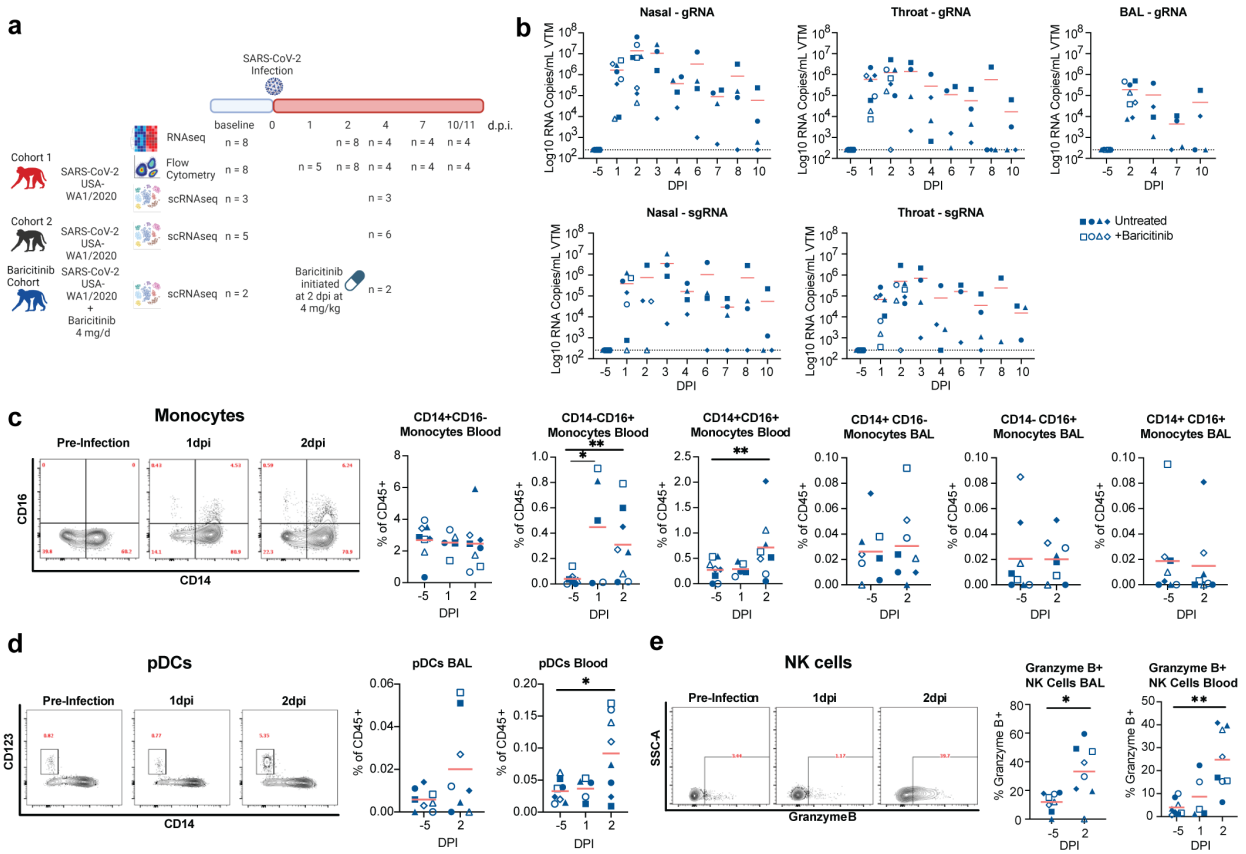

Figure 2.1. Early expansion of inflammatory cells in the blood following infection with SARS-CoV-2. (**a**) Study design; RMs were infected intranasally and intratracheally with SARS-CoV-2 and tracked longitudinally (Cohort 1: n=4, baricitnib cohort: n=4, , Cohort 2: n = 6). Baricitinib was administered daily to 4 RMs (baricitinib cohort) starting at 2dpi and the remaining 4 RMs (Cohort 1) were untreated. (Created with BioRender.com) (**b**) After SARS-CoV-2 inoculation, nasal, throat, and bronchoalveolar lavages (BAL) were collected and viral loads were quantified by qRT-PCR for total gRNA and sgRNA. (**c**) Longitudinal levels of monocytes within BAL and blood depicted as a % of CD45+ cells. p-values: CD14-CD16+ Monocytes Blood: 1 dpi vs -5 dpi = 0.03 and 2 dpi vs -5 dpi = 0.004; CD14+CD16+ Monocytes Blood 2 dpi vs -5 dpi = 0.004 (d) Longitudinal levels of plasmacytoid dendritic cells (pDCs) within BAL and blood depicted as a percentage of CD45+ cells. p-value for pDCs Blood 2 dpi vs -5 dpi = 0.02. (**e**) Longitudinal levels of NK cells expressing Granzyme B in BAL and blood. p-values for Granzyme B+ NK Cells 2 dpi vs -5 dpi BAL = 0.01 and blood = 0.008. n = 8 RM from Cohort 1 & baricitinib cohort) The red bars represent the mean. Statistical analysis was performed using one-tailed Wilcoxon signed-rank test in Graphpad Prism v7.02 comparing each timepoint to -5dpi. * p-value < 0.05, ** p-value < 0.01. Source data (b-e) are provided as a Source Data file.

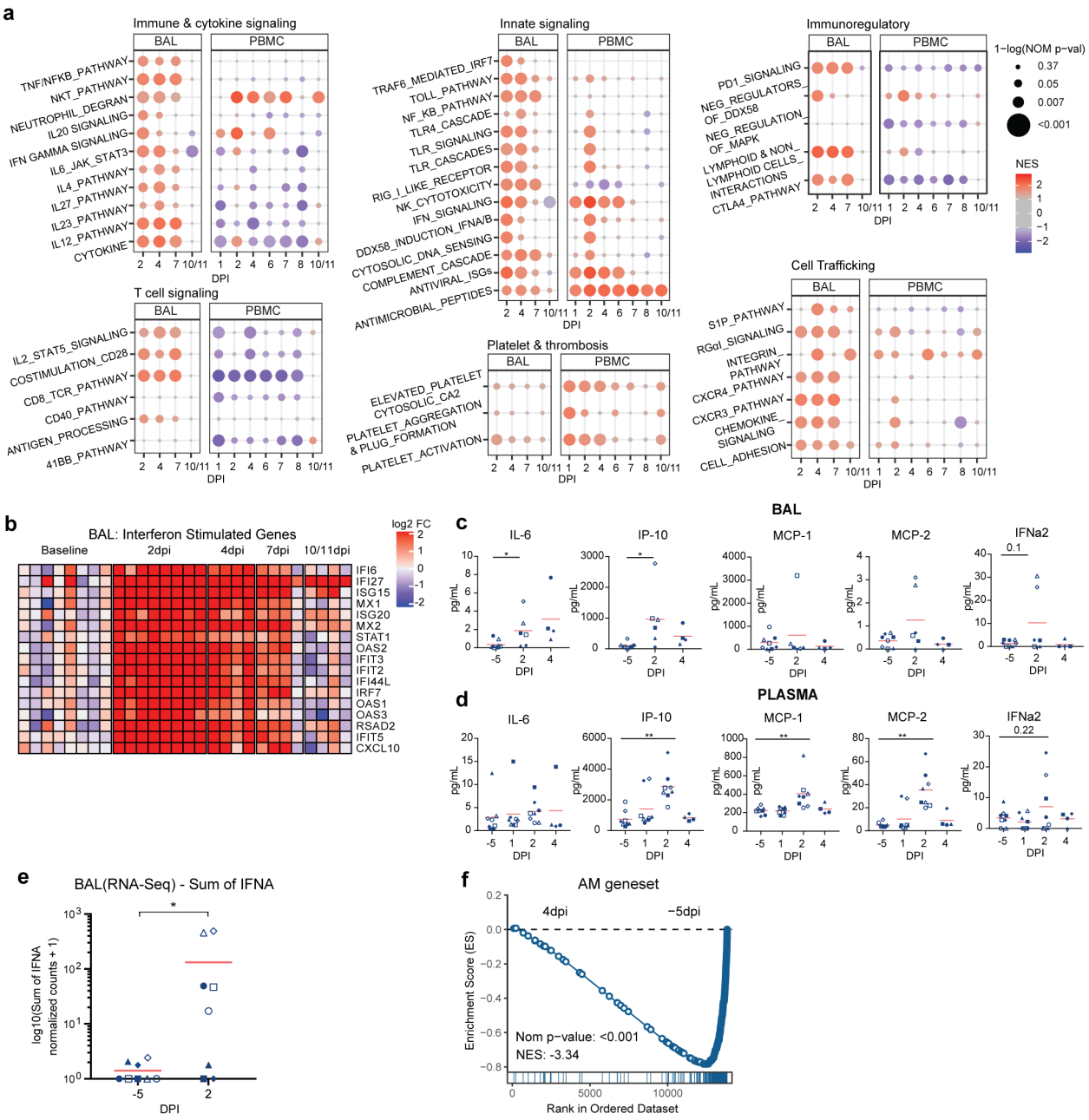

Figure 2.2. Early pro-inflammatory and ISG response observed in airways and peripheral blood by bulk transcriptomics. n = 8 RM from Cohort 1 & baricitinib cohort) for -5 dpi and 2dpi except for (c) where n=6 (3 RM Cohort 1 + 3 RM baricitnib cohort) at 2 dpi. n=4 RM from Cohort 1 starting from 4dpi **(a)** Dot plots showing normalized enrichment scores and nominal p-values for gene sets. Enrichment is indicated by dot color (red: positively enriched vs -5dpi; blue: negatively enriched), dot size indicates significance. Normalized enrichment scores and nominal p-values were determined using GSEA[367]. The exact nominal p-values are included in Supplementary Data 1. **(b)** Heatmap of longitudinal responses for the ISG gene set. The color scale indicates log2 expression relative to the median of the -5dpi samples. **(c)** Cytokines evaluation (Mesoscale) in BALF p-values for 2dpi vs -5 dpi: IL6 = 0.02 and IP-10 = 0.03 and **(d)** Plasma; only significant cytokines are shown (p-values for 2dpi vs -5 dpi: IP-10 = 0.008,

MCP-1 = 0.008, MCP-2 = 0.004). **(e)** Sum of normalized expression of all IFNA genes in BAL. * p-value = 0.04. **(f)** GSEA enrichment plot showing negative enrichment for AM gene signature (derived from SingleR) when comparing bulk BAL RNA-Seq samples from 4dpi to -5dpi (Nominal p-value = 0). The red bar represents the mean. Statistical analysis for (c), (d) and (e) was performed using one-tailed Wilcoxon signed-rank test in R v4.2.2 comparing each timepoint to -5dpi. * p-value < 0.05, ** p-value < 0.01. Source data (c-e) are provided as a Source Data file.

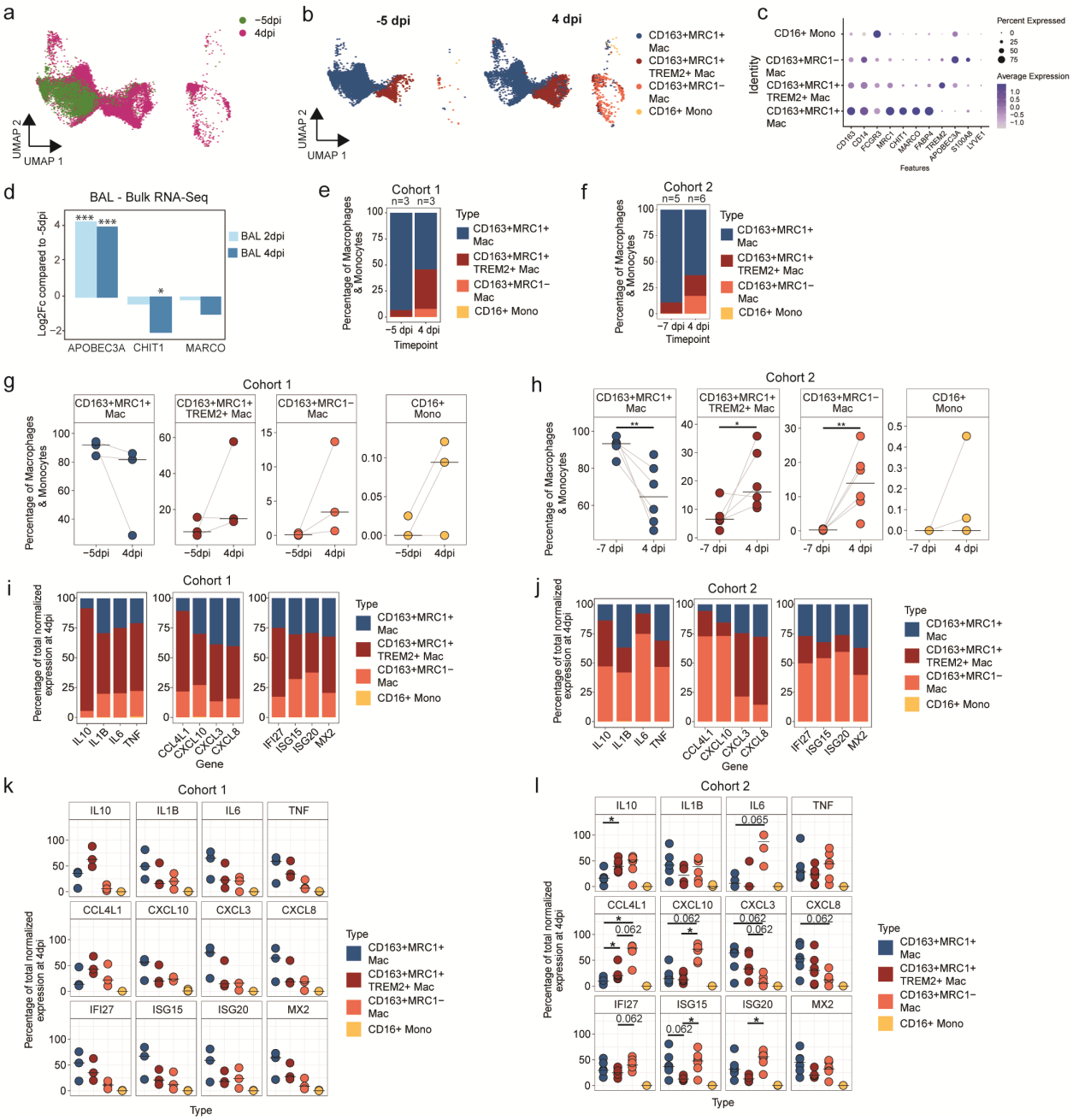

Figure. 2.3. Influx of pro-inflammatory macrophages in BAL (a) Projection of single-cell macrophages/monocytes from -5dpi (green) and 4dpi (magenta) 10X BAL samples

obtained from three SARS-CoV-2 infected rhesus macaques (Cohort 1) onto the reference UMAP of lung macrophage/monocytes from uninfected rhesus macaques (NCBI GEO : GSE149758[336]). **(b)** UMAP projections showing the predicted cell type annotations based on the uninfected lung reference split by time of sample collection (Cohort 1). **(c)** DotPlots showing the expression of marker genes for the different macrophage/monocyte subsets in SARS-CoV-2 infected BAL samples (Cohort 1) **(d)** Log2 fold-changes compared to -5dpi for APOBEC3A, CHIT1 and MARCO in bulk BAL RNA-Seq data (Cohort 1). Signficance was determined using DESeq2. The p-values corrected by the default Benjamini and Hochberg method were used * adj p-value < 0.05, *** adj p-value < 0.001. The exact p-values are included in Supplementary Data 2. **(e and f)** Percentage of a given subset out of all macrophage/monocyte subsets at -5dpi and 4dpi from all three animals pooled (Cohort 1) (e) and at -7dpi and 4 dpi from all six animals pooled (Cohort 2) (f). **(g and h)** Percentage of a given subset out of all macrophage/monocyte subsets for each animal at -5dpi and 4dpi from Cohort 1 (n=3) (g) and at -7dpi (n = 5) and 4 dpi (n=6) for Cohort 2 (h) . The black lines indicate the median. p-values for Cohort 2 (f) for 4 dpi vs – 7 dpi: CD163+MRC1+ = 0.009, CD163+MRC1+TREM2+ = 0.03, and CD163+MRC1- = 0.004 **(i-l)** Contribution of each macrophage/monocyte subset towards the production of the pro-inflammatory genes and ISG – Cohort 1 pooled (i), Cohort 2 pooled (j), Cohort 1 individual (k) and Cohort 2 individual (l). p-values for (l): * = 0.03. The percentage contribution was calculated by dividing the sum of normalized expression of a given gene in a macrophage/monocyte subset by the sum of the normalized expression of the gene in all macrophage/monocyte subsets. (a-c,e,g,i,k) Cohort 1: n=3 for both -5dpi and 4dpi, (d) Cohort 1: n= 8 for 2dpi and n=4 for 4dpi (f,h,j,l) Cohort 2: n=5 for -7dpi and n=6 for 4 dpi. The black lines indicate the median. Statistical analysis was performed using two-tailed Wilcoxon singed rank test for (g, k and l) and two-tailed Mann-Whitney U test for (h) in R v4.2.2. * p-value < 0.05, ** p-value < 0.01. Source data (d-l) are provided as a Source Data file.

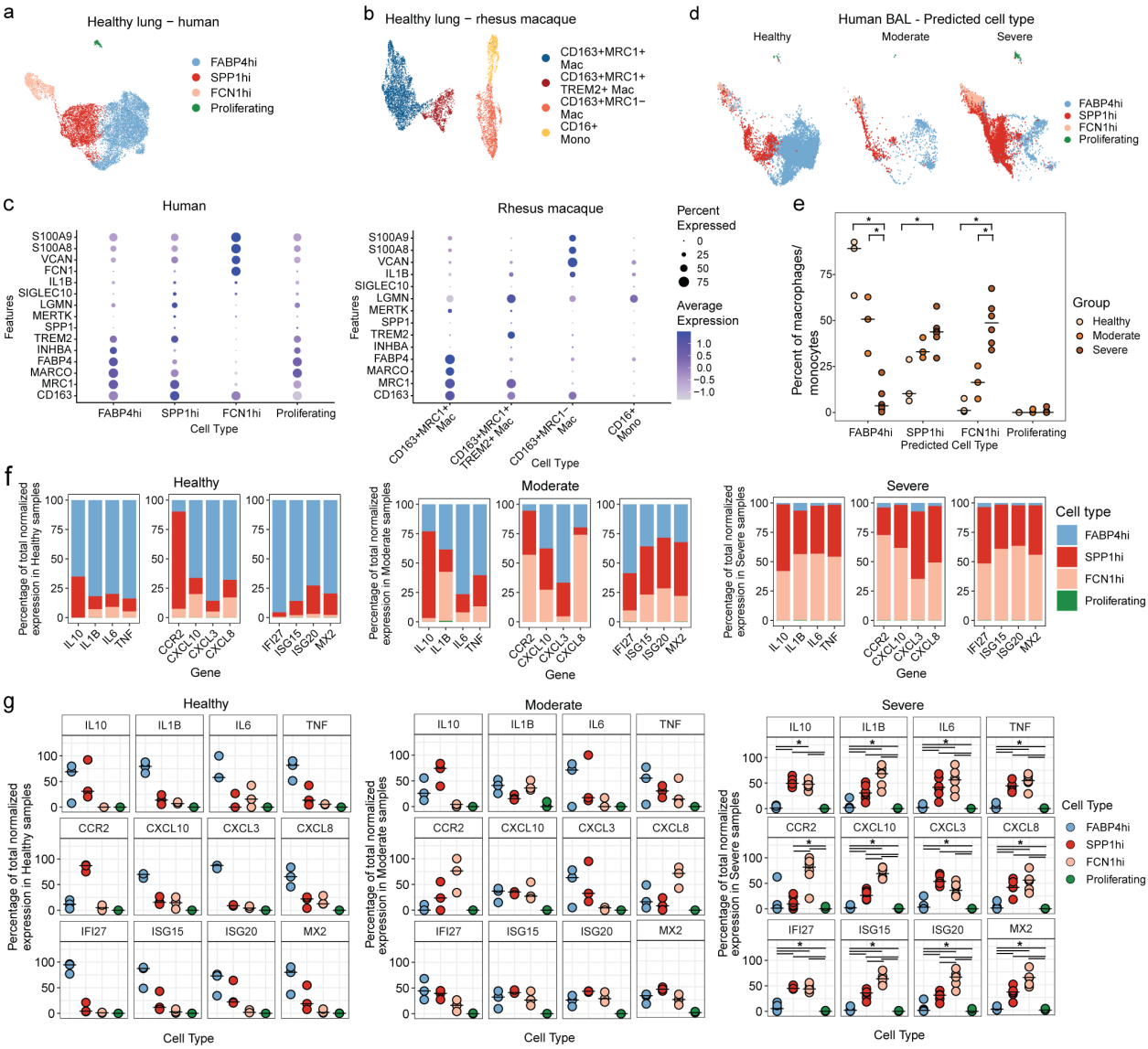

Figure 2.4. Comparison of rhesus and human macrophage subsets. (**a**) Macrophage subsets in lungs from six healthy human donors (GEO: GSE135893). (**b**) Macrophage subsets in lungs from three healthy rhesus macaques (GEO: GSE149758). (**c**) DotPlots showing the expression of marker genes. The color gradient represents the level of expression and the size of the dot represents the percentage of cells expressing a given gene. (**d**) UMAP of BAL samples from human donors that are healthy (n=3), or suffering from moderate (n = 3) or severe (n = 6) COVID-19 (GEO: GSE145926) mapped to the healthy lung reference using the Seurat MapQuery function (**e**) Percent of predicted cell types out of all macrophage/monocytes in each human BAL sample. The black bar indicates the median. Statistical analysis was performed using pairwise two-tailed Mann-Whitney U test in R v4.2.2. p-value * = 0.02 . (**f & g**) Contribution of each predicted macrophage/monocyte subsets in human BAL towards the production of the pro-inflammatory genes and ISG – pooled (f) and individual (g). The percentage contribution was calculated by dividing the sum of normalized expression of a given gene in a macrophage/monocyte subset by the sum of the normalized expression of the gene in all

macrophage/monocyte subsets. The black bars represent the median. Statistical analysis was performed using two-tailed Wilcoxon signed rank test in R v4.2.2. * p-value 0.03 for all except FABP4 vs Proliferating for IL6, IL1B, TNF, CXCL3, CXCL8 and SPP1hi vs Proliferating for CCR2: p-value = 0.04. Source data (e-g) are provided as a Source Data file.

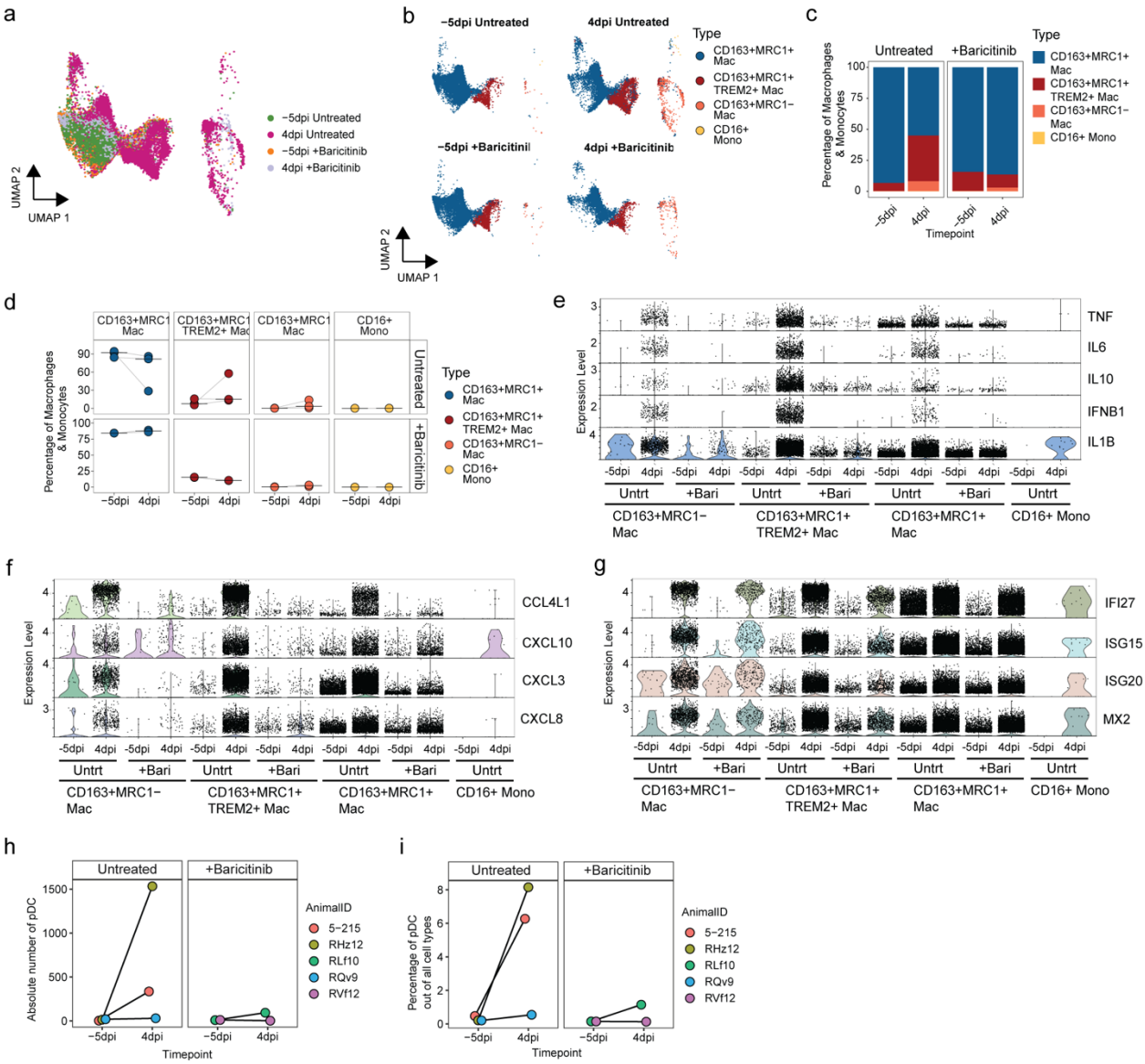

Figure 2.5. Baricitinib reduced the influx of pro-inflammatory macrophages in addition to the pro-inflammatory gene expression profile. **(a)** Projection of macrophages/monocytes from -5dpi and 4dpi 10X BAL samples from three untreated and two baricitinib treated rhesus macaques on the reference UMAP of uninfected lung macrophages/monocytes (NCBI GEO: GSE149758) **(b)** UMAP split by treatment and timepoint showing predicted cells annotations based on mapping to the reference lung macrophages/monocytes **(c & d)** Percentage of a given macrophage/monocyte subset of all the macrophages/monocytes in the BAL samples - pooled (c) and individual (d) **(e, f,**

g) Violin plots showing expression of pro-inflammatory cytokines (e), chemokines (f) and ISG (g) in the different macrophage/monocyte subsets in BAL 10X samples from baricitinib treated and untreated samples. (h) Absolute number of pDC in BAL samples from scRNA-Seq and (i) Percentage of pDC out of all cells in the BAL samples from scRNA-Seq. Source data (c,d,h,i) are provided as a Source Data file.

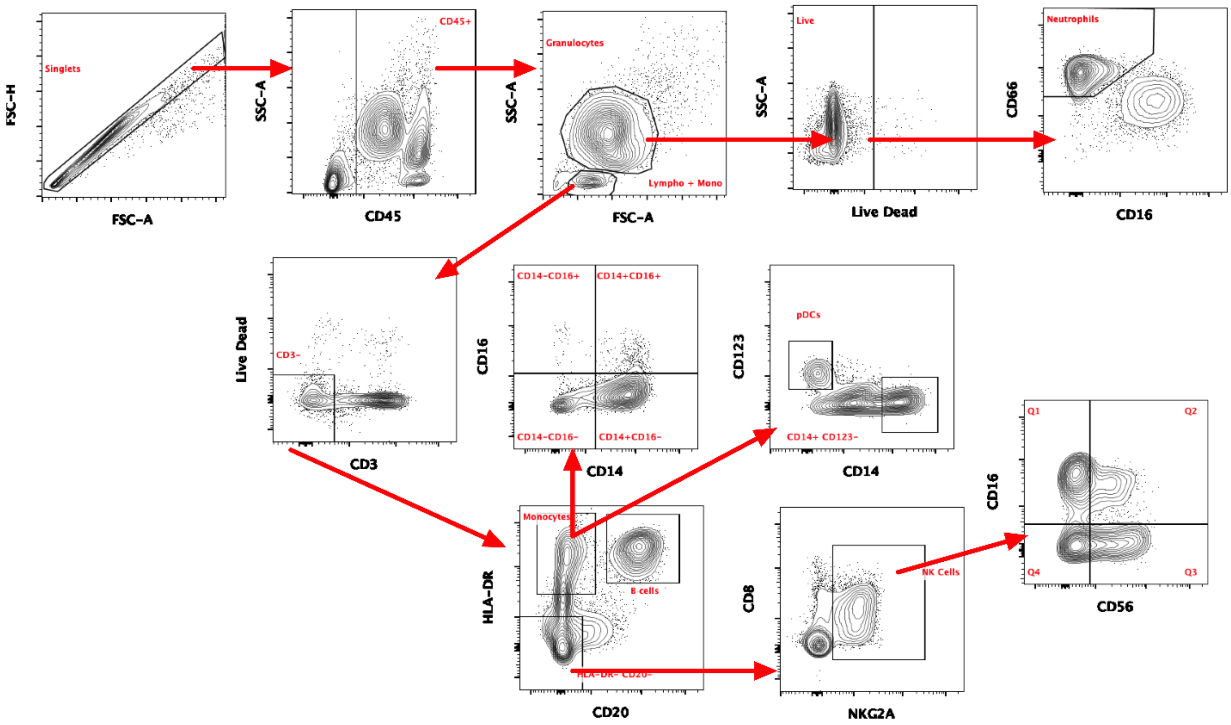

Figure 2.S1. Flow gating strategy for different immune cell populations.

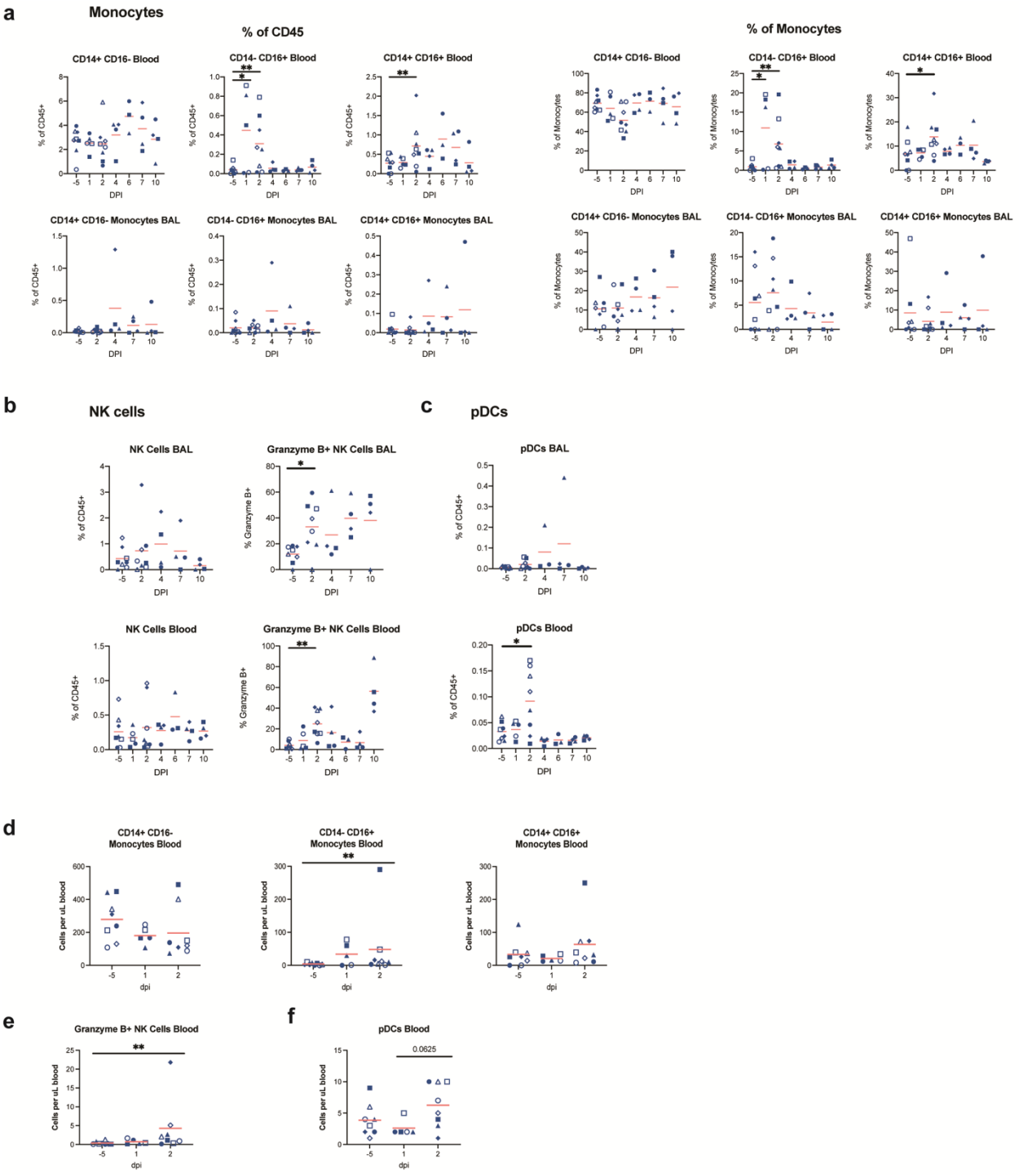

Figure 2.S2. Longitudinal flow cytometric analysis in BAL and blood following SARS-CoV-2 infection. n = 8 RM from Cohort 1 and baricitnib cohort for -5dpi and 2dpi, n= 5 RM from Cohort 1 and baricitinib cohort for 1dpi blood samples and n=4 RM from Cohort 1 at 4dpi, 7dpi, and 10dpi, and n= 3 RM from Cohort 1 at 6dpi. Open symbols represent baricitnib cohort that started receiving treatment at 2dpi and the filled symbols represent RM from Cohort 1 that were untreated. (**a**) Longitudinal levels of monocytes within BAL and blood depicted as the percentage of CD45+ cells and % of monocytes

($CD3^-$ $CD20^-$ HLA-DR^+). p-values for % of CD45+: CD14-CD16+ monocytes blood: 1 dpi vs -5 dpi = 0.03 and 2 dpi vs -5 dpi = 0.004; CD14+CD16+ monocytes blood 2 dpi vs -5 dpi = 0.004. p-values for % of monocytes: CD14-CD16+ monocytes blood: 1 dpi vs -5 dpi = 0.03 and 2 dpi vs -5 dpi = 0.004; CD14+CD16+ monocytes blood 2 dpi vs -5 dpi = 0.02 (**b**) Longitudinal levels of NK cells as a percentage of CD45+ cells and frequency of NK cells expressing Granzyme B in BAL and blood. p-values for Granzyme B+ NK Cells 2 dpi vs -5 dpi BAL = 0.01 and blood = 0.008. (**c**) Longitudinal levels of plasmacytoid dendritic cells (pDCs) within BAL and blood depicted as a % of CD45+ cells. **(d, e, f)** Absolute counts of monocytes (d), Granzyme B expressing NK cells (e) and pDCs (f).p-values for (d) CD14-CD16+ monocytes in blood 2 dpi vs -5 dpi = 0.004, (e) Granzyme B+ NK cells in blood 2 dpi vs -5 dpi = 0.004. The red bars represent the mean. Statistical analysis was performed using one-tailed Wilcoxon signed-rank test (a-c) and two-tailed Wilcoxon test (d-f) in Graphpad Prism v7.02 comparing each time point to -5dpi. * p-value < 0.05, ** p-value < 0.01. Source data (a-f) are provided as a Source Data file.

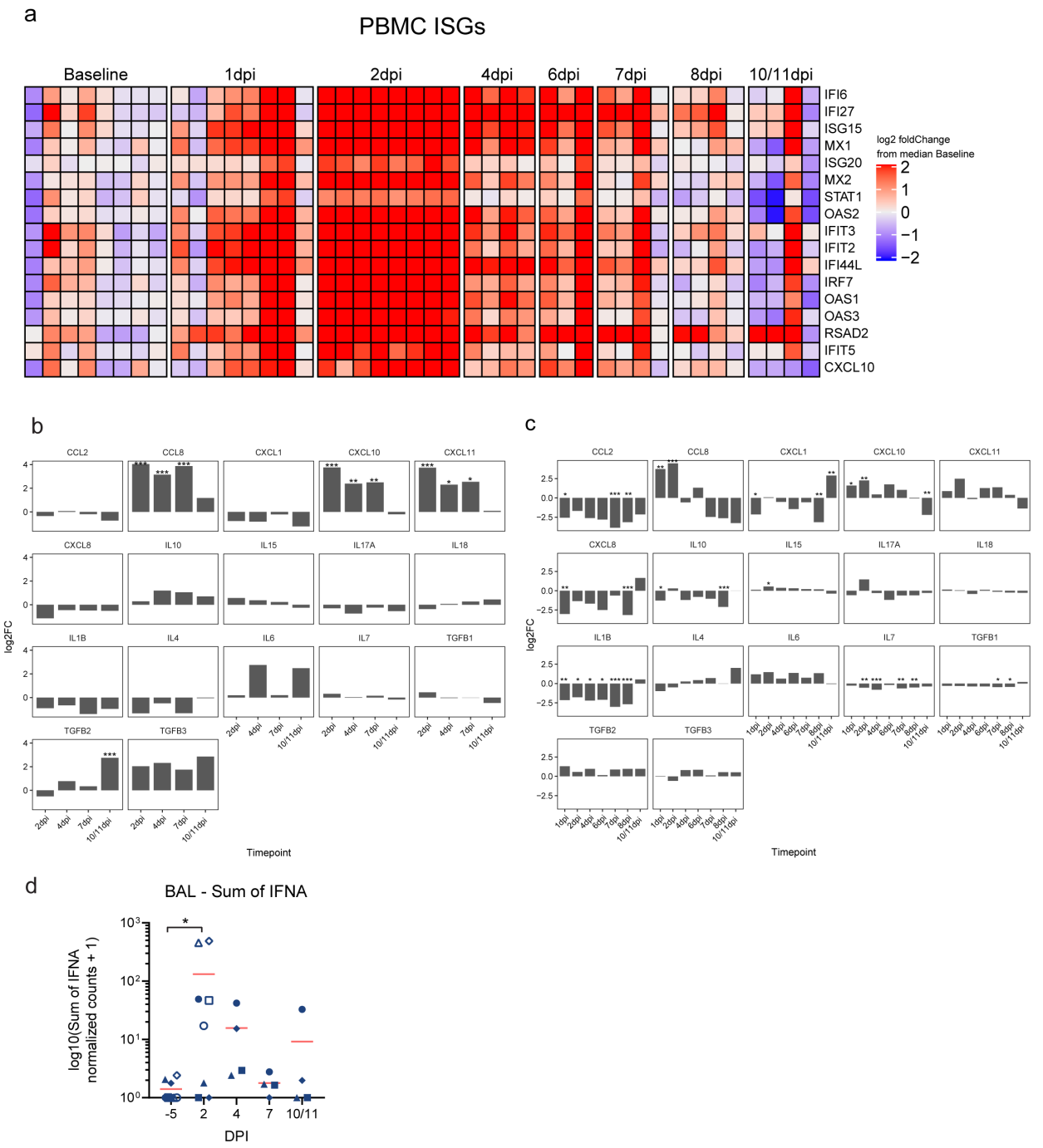

Figure 2.S3. Bulk transcriptomic analysis of airways and peripheral blood. n = 8 RM from Cohort 1 and baricitnib cohort for -5dpi, 1dpi and 2dpi, n= 4 RM from Cohort 1 starting at 4dpi. **(a)** Heatmap showing expression of ISG in PBMC over all sampled time points. The color scale indicates log2 expression relative to the median of -5dpi samples. **(b & c)** Normalized expression of cytokines and chemokines in bulk RNA-Seq in BAL (b) and PBMC(c). Statistical analysis was performed using DESeq2. The p-values corrected by the default Benjamini and Hochberg method were used. * padj < 0.05, ** padj < 0.01, *** padj < 0.001. The exact p-values are included in Supplementary Data 2 and 3. **(d)** Sum of normalized expression of IFNA in longitudinal BAL samples * p-value = 0.04. The

red bars represent the mean. Statistical analysis was performed using one-tailed Wilcoxon signed-rank test in R v4.2.2 comparing each time point to -5dpi. . Source data (d) are provided as a Source Data file.

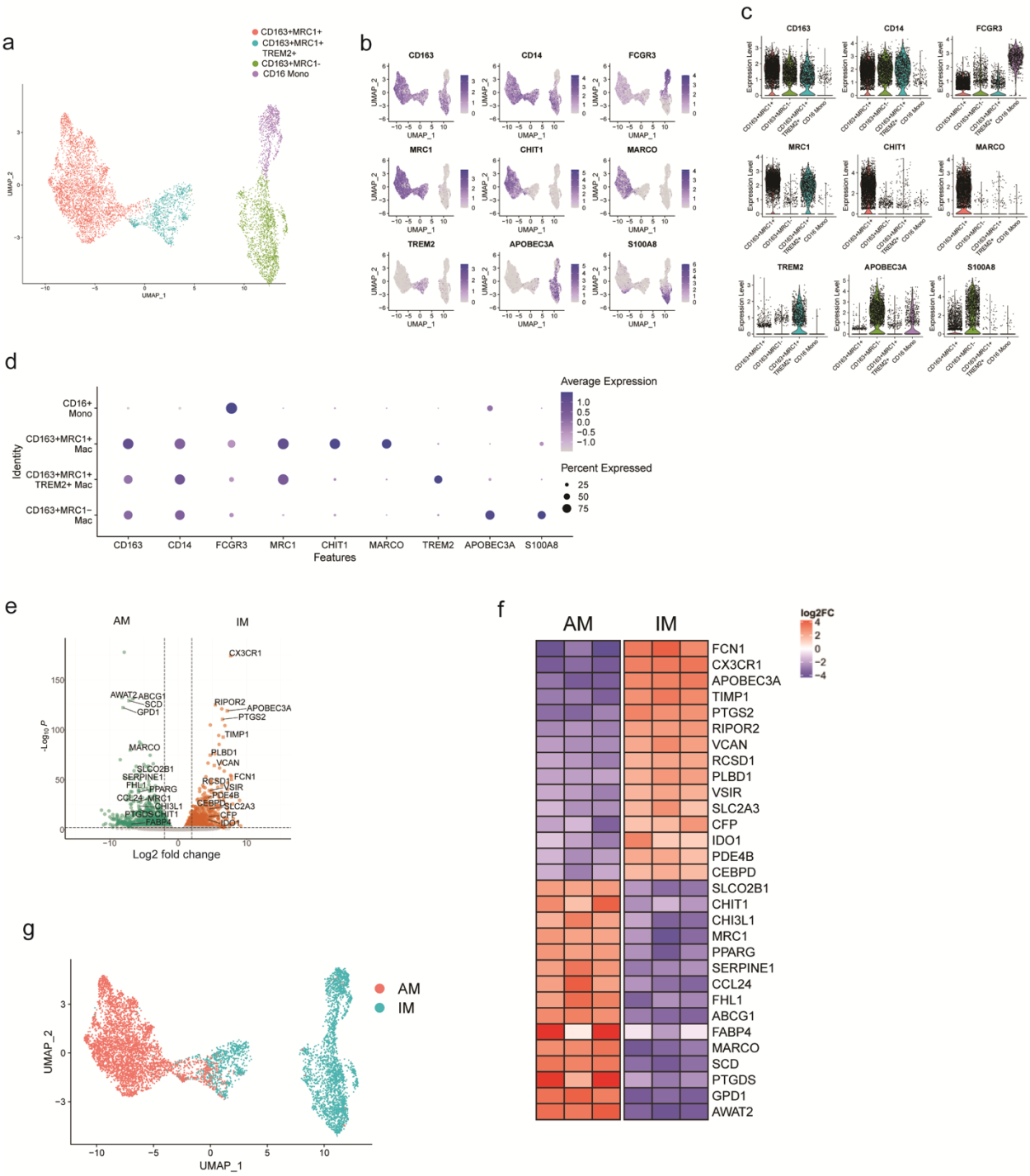

Figure 2.S4. References used for annotating macrophage/monocyte subsets. **(a)** UMAP of macrophages/monocytes from 10X lung samples of three uninfected rhesus macaques (NCBI GEO: GSE149758[336]) showing Louvain clustering. (**b & c**) FeaturePlot

(b) and Violin Plots (c) showing the expression of marker genes in the macrophage/monocyte clusters. **(d)** DotPlot showing expression of marker genes for the different monocyte/macrophage subsets as defined previously[336, 339] **(e)** Volcano plots showing differentially expressed genes for pairwise comparison of alveolar (n=3) and interstitial macrophages (n=3)[338]. The thresholds used are an adjusted p-value < 0.05 and a fold change of 2 for alveolar vs interstitial macrophage. Top 15 genes that have a mean normalized expression of at least 5000 for either type have been indicated. Statistical analysis was performed using DESeq2. The p-values corrected by the default Benjamini and Hochberg method were used. **(f)** Heatmap showing the top 15 genes for each subset. The color scale indicates log2 expression relative to the median of all samples. (**g**) UMAP of single-cell 10X lung samples showing SingleR annotations using the bulk sorted cells as reference.

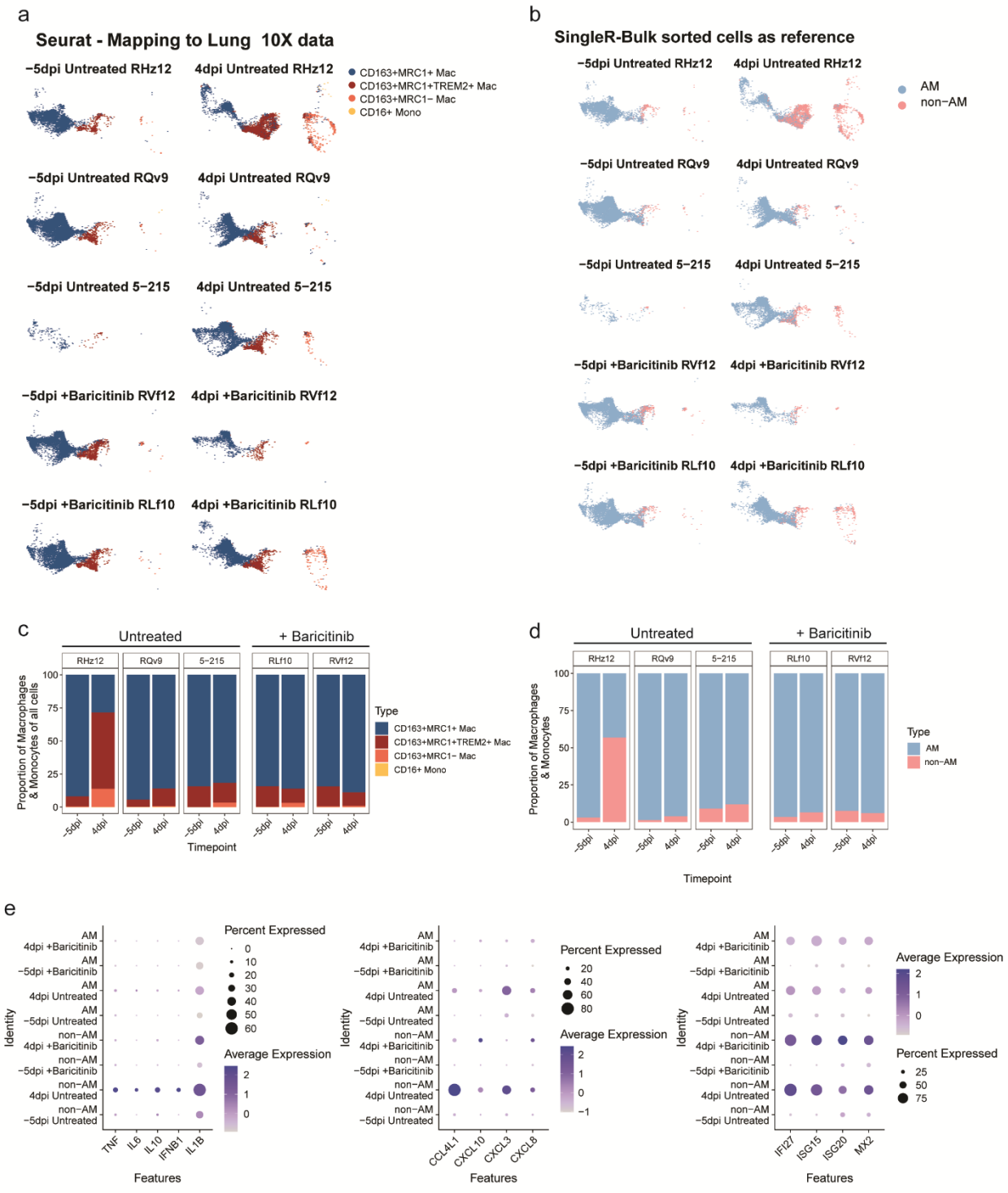

Figure 2.S5. Cell annotation using bulk sorted cells as reference. (a & b) The BAL macrophage/monocytes from SARS-CoV2 infected rhesus macaques (three untreated - Cohort 1 and two baricitinib treated) projected on the 10X lung reference macrophages/monocytes UMAP split by each animal and timepoint. (a) Annotations predicted from mapping to 10X lung samples using Seurat (b) Annotations predicted by SingleR using the bulk sorted AM and IM cells as reference.**(c & d)** Percentage of a

macrophage/monocytes subset out of all the macrophage/monocyte cells in a given sample based on 10X lung reference (c) and the bulk sorted cells as reference (d). **(e)** DotPlots showing expression of pro-inflammatory cytokines, chemokines and ISG in macrophage/monocyte subsets based on the bulk sorted cells reference at -5dpi and 4dpi in BAL samples from untreated (Cohort 1) and baricitinib treated rhesus macaques. Source data (c,d) are provided as a Source Data file.

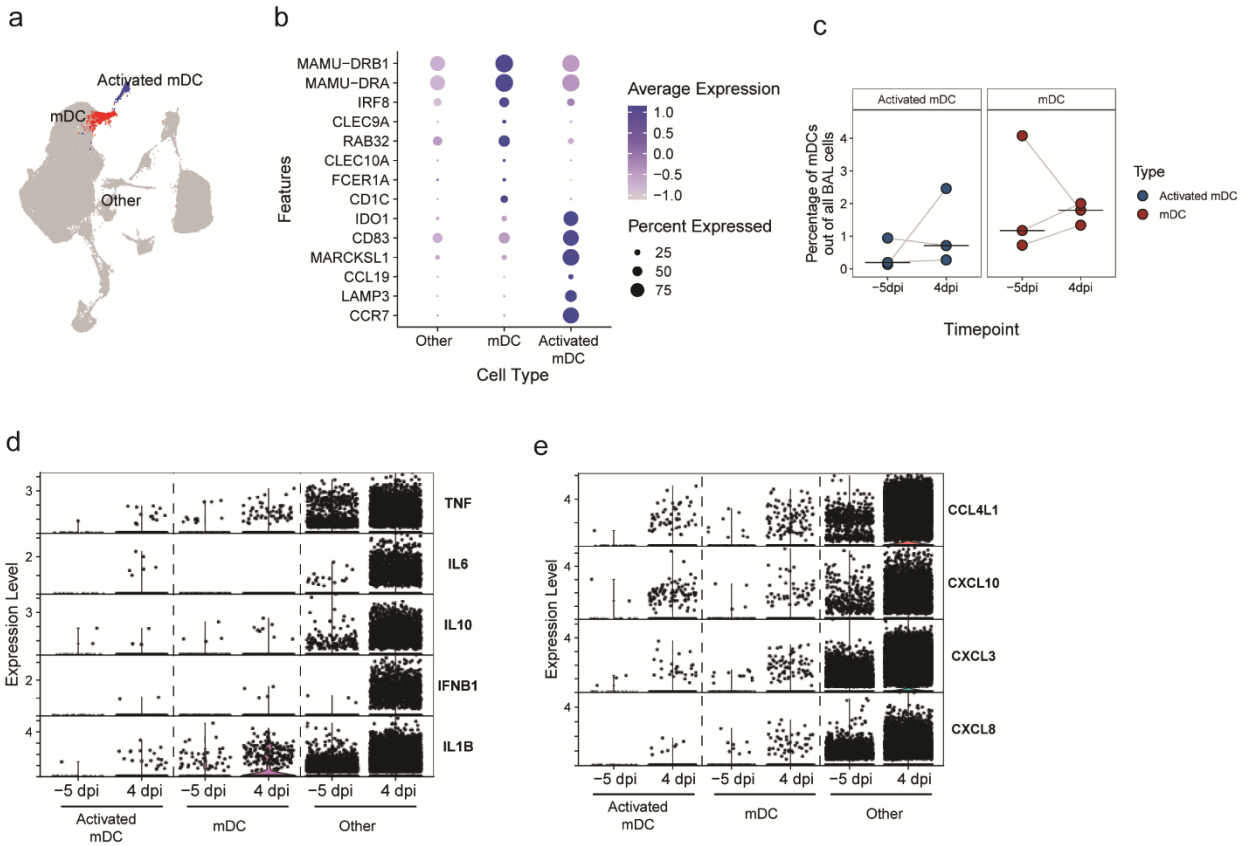

Figure 2.S6. Expression of cytokines and chemokines in mDC from rhesus macaque BAL. n = 3 RM from Cohort 1 for both -5dpi and 4dpi. (a) UMAP showing clusters annotated as mDC and activated mDC in integrated data comprising of untreated (Cohort 1) and baricitnib treated animals. (b) Dot plot showing the expression of marker genes used for annotation of mDC clusters from untreated (Cohort 1) and baricitnib treated animals. **(c)** Percentage of mDCs out of all the BAL cells in untreated animals (Cohort 1). The black lines indicate the median. **(d & e)** Violin plots showing the expression of cytokines (d) and chemokines (e) in mDC subsets compared to all other BAL cells from untreated animals Source data (c) are provided as a Source Data file.

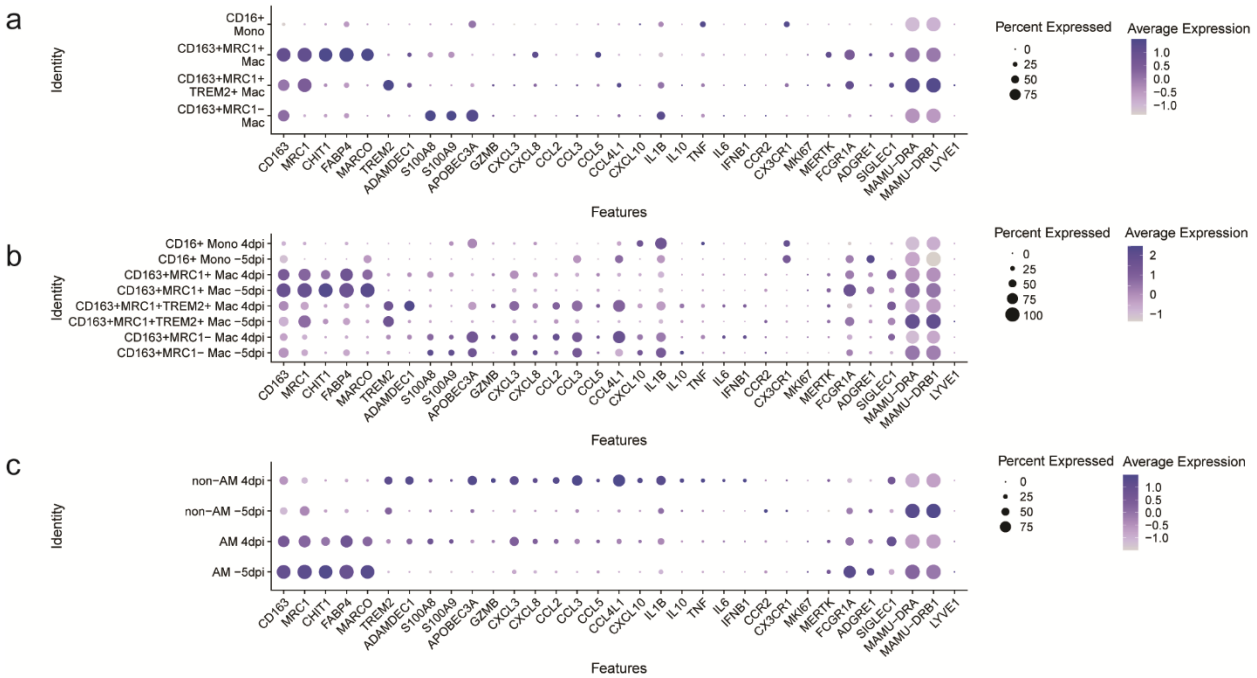

Figure 2.S7. Expression of canonical markers and pro-inflammatory genes in different macrophage/monocyte subsets. (a) 10X lung control samples from three uninfected RM. **(b & c)** BAL samples from three SARS-CoV2 infected RM (Cohort 1) annotated using the 10X lung reference (b) or the bulk sorted cells as reference (c).

Figure 2.S8. Feature plots showing expression of cytokines (a), chemokines (b) and ISG (c) in the different macrophage/monocyte subsets from rhesus macaque BAL (Cohort 1 n = 3).

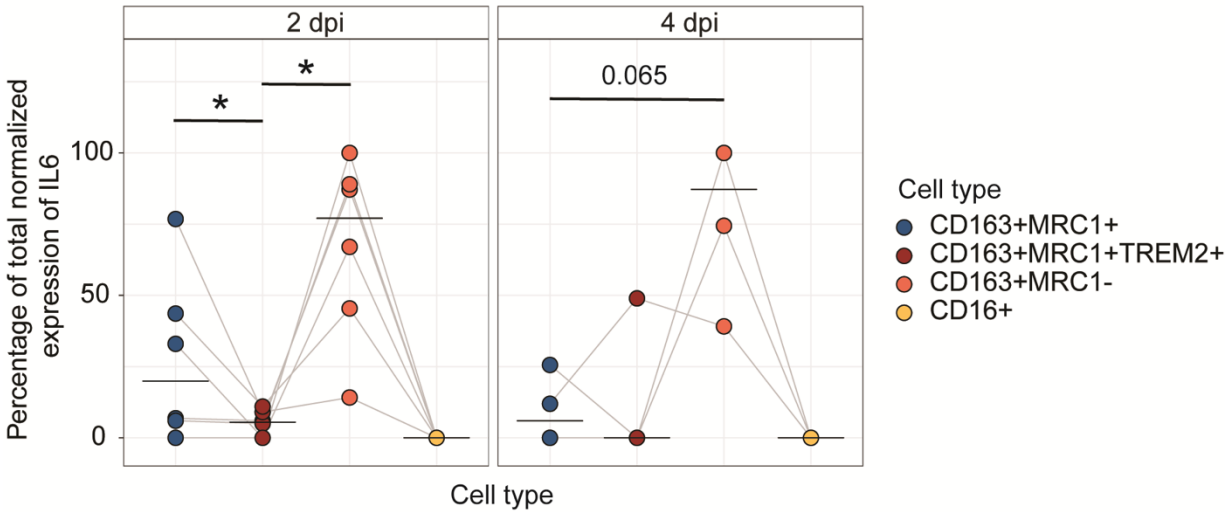

Figure 2.S9. Contribution of each macrophage/monocyte subset towards the production of IL6 at 2 dpi and 4 dpi in Cohort 2 (n = 6). The percentage was obtained by summing

the normalized expression of IL6 for each subset and dividing by the total normalized expression of IL6 from all subsets separately for each time point. The black lines indicate the median. Statistical test was performed using two-tailed Wilcoxon signed rank test in R v4.2.2. p-values: 2dpi CD163+MRC1+ vs CD163+MRC1+TREM2+ = 0.04 and CD163+MRC1+TREM2+ vs CD163+MRC1- = 0.03. . Source data are provided as a Source Data file.

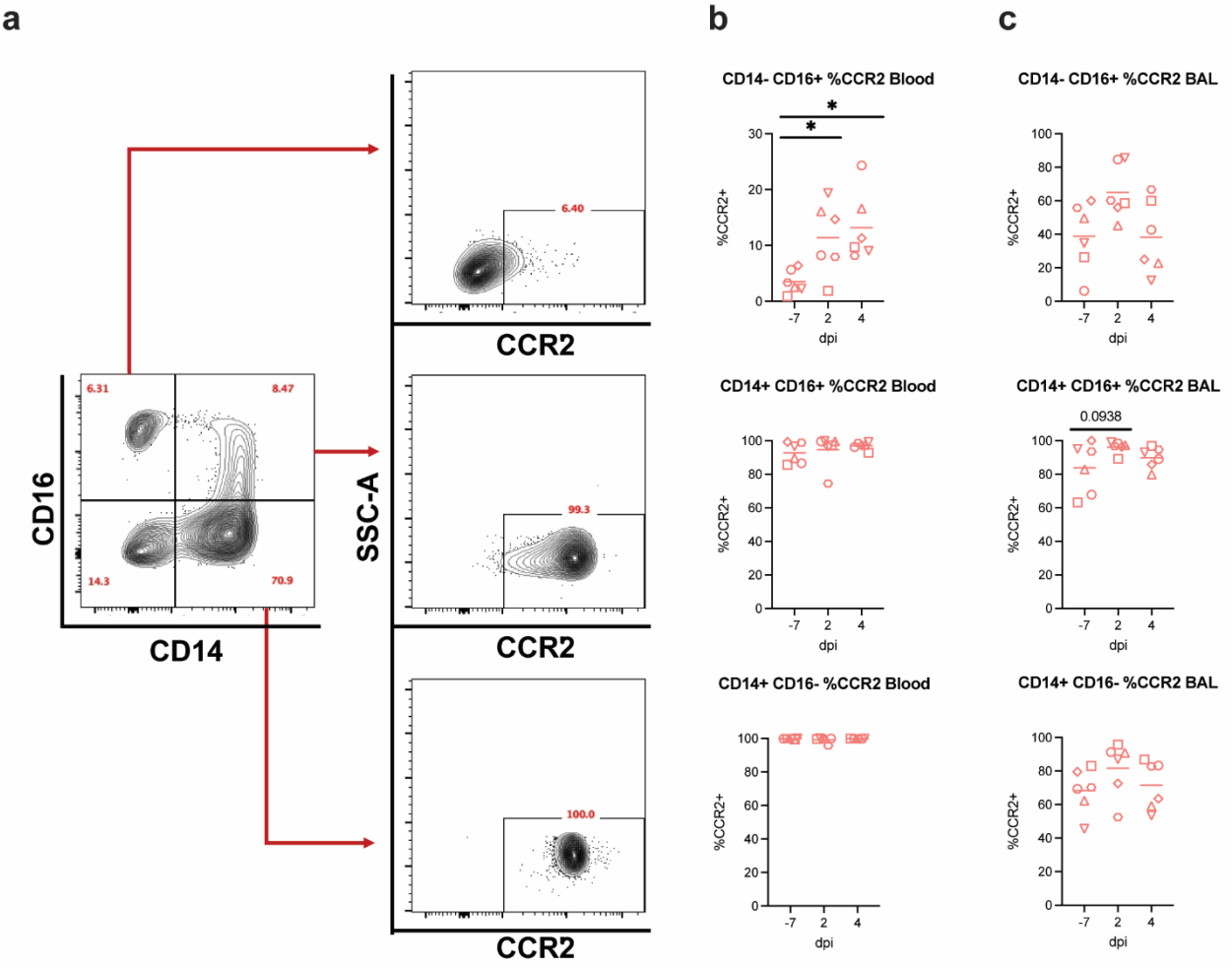

Figure 2.S10. Expression of CCR2 in monocytes in rhesus macaque BAL (Cohort 2 n = 6) (a) Representative Flow plots (b) Percentage of CCR2+ monocytes in blood (c) Percentage of CCR2+ monocytes in BAL. The red bar represents the mean. Statistical analysis was performed using two-tailed Wilcoxon signed-rank test in GraphPad Prism v7.02 comparing each time point. * p-value = 0.0312 . Source data (b,c) are provided as a Source Data file.

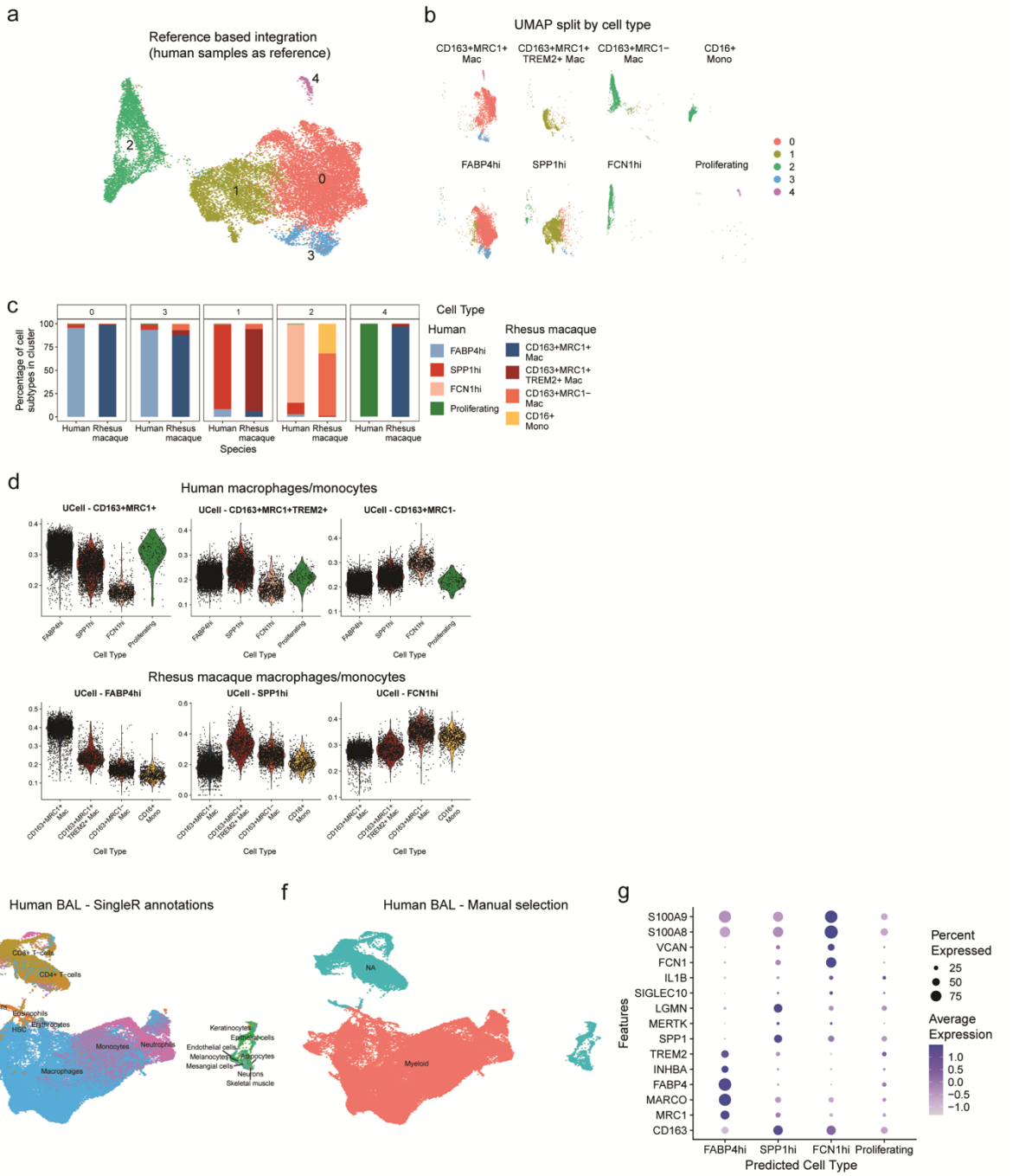

Figure 2.S11. Comparison of human lung macrophage/monocytes subsets with that of rhesus macaque (a) UMAP of macrophages/monocytes from lung samples of six healthy human donors[343] and three healthy rhesus macaques[33619] integrated with the human samples as reference using one-to-one orthologs between GRCh38 and Mmul10 with shared gene names. **(b)** UMAP from (a) split by the cell types. The top row corresponds to the rhesus macrophages/monocytes while the bottom are from human. (**c**) Distribution of different cell types in each seurat cluster. Percentage of a cell type is indicated out of all human or rhesus macrophage/monocyte subsets in a given cluster. **(d)** Violin plots showing the UCell enrichment score for marker gene expression. The top

row shows the enrichment of rhesus macrophage/monocyte marker genes in human macrophages/monocytes and the bottom row shows the enrichment of human macrophage/monocyte marker genes in rhesus macrophages/monocytes (**e & f**) UMAP of integrated human BAL samples[100] (healthy=3, mild COVID-19 = 3 and severe COVID-19 = 6) colored by SingleR-based annotation (d) or manual selection of the myeloid cluster (e). (**g**) DotPlot indicating expression of marker genes in the predicted cell types in human BAL samples based on mapping to the human healthy lung macrophages/monocytes. Source data (c) are provided as a Source Data file.

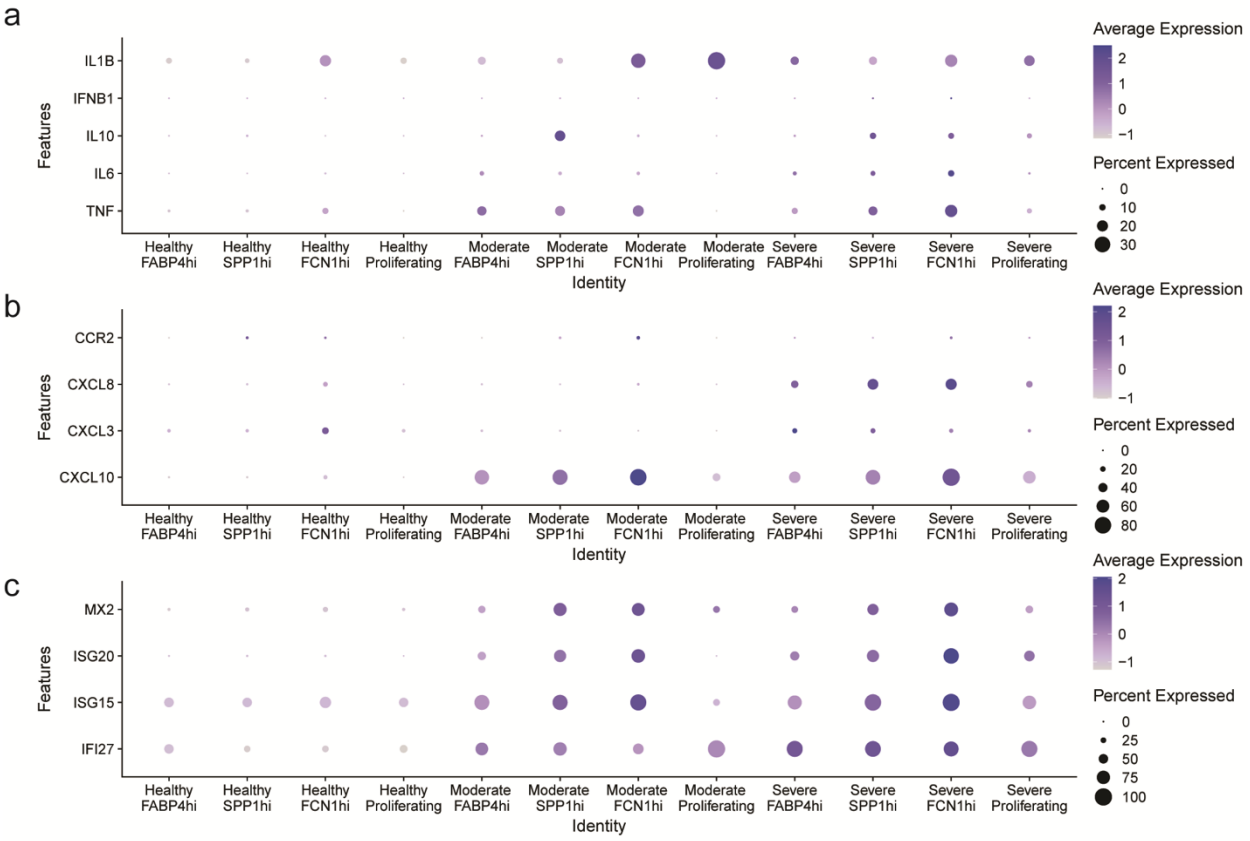

Figure 2.S12. Expression of pro-inflammatory mediators in human BAL samples. Expression of pro-inflammatory cytokines (**a**), chemokines (**b**) and ISG (**c**) in the different macrophage/monocyte subsets predicted in human BAL samples based on mapping to healthy human macrophages/monocytes.

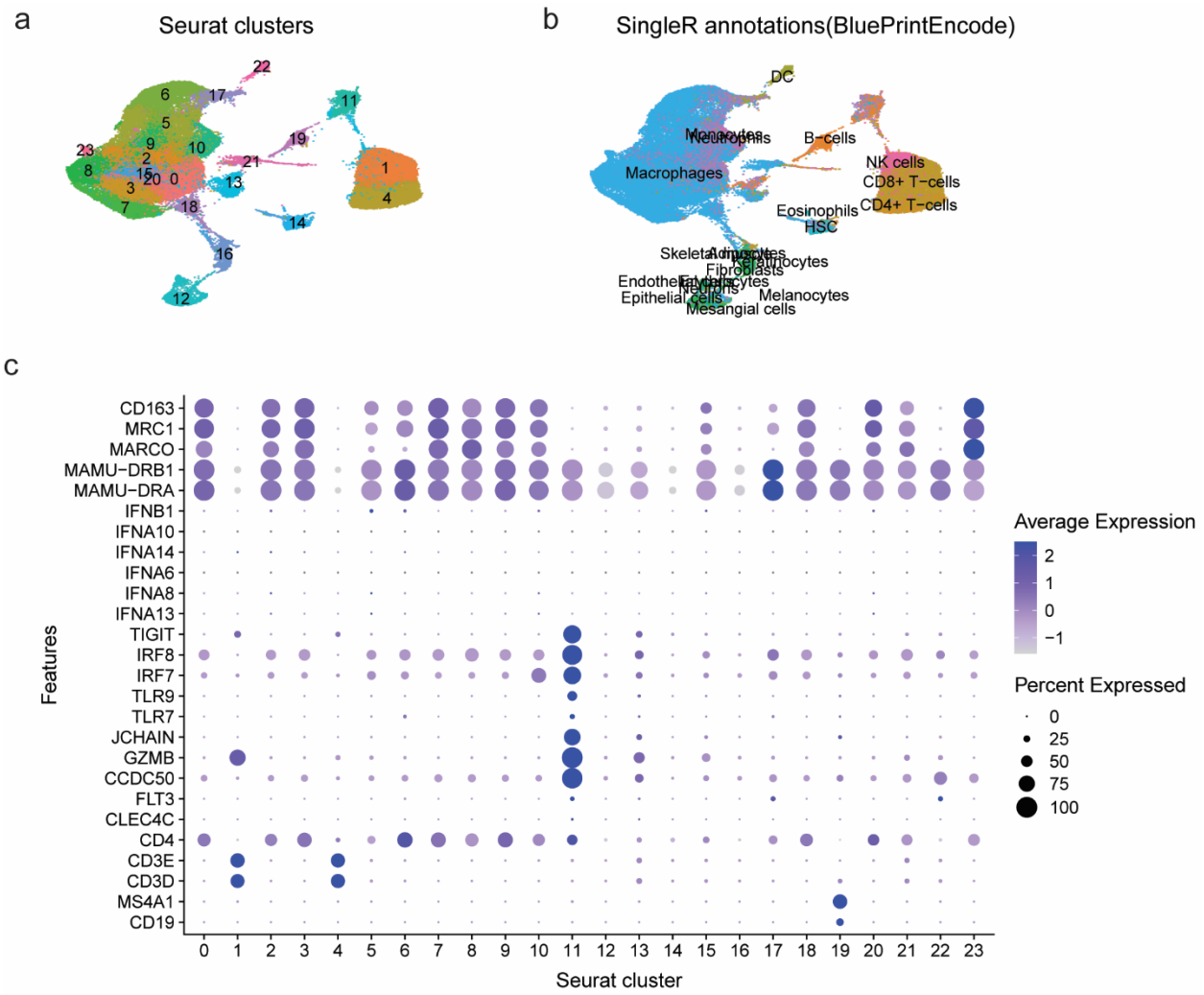

Figure 2.S13. Annotation of pDC in BAL from untreated (n=3 – Cohort 1) and baricitinib treated (n=2) rhesus macaques. (**a** & **b**) UMAP after integration of all five samples colored according to seurat clusters (a) or SingleR-based annotations (b). (**c**) Dot plot showing expression of canonical marker genes for different Seurat clusters for the five rhesus BAL samples. Cluster 11 was annotated as pDC cells.

Chapter Three: Modulation of type I interferon responses potently inhibits SARS-CoV-2 replication and inflammation in rhesus macaques

Elise G. Viox[1,20], Timothy N. Hoang[1,20,†], Amit A. Upadhyay[1,20], Rayhane Nchioua[2], Maximilian Hirschenberger[2], Zachary Strongin[1], Gregory K. Tharp[3], Maria Pino[1], Kevin Nguyen[1], Justin L. Harper[1], Matthew Gagne[4], Shir Marciano[5], Arun K. Boddapati[3], Kathryn L. Pellegrini[3], Arpan Pradhan[1], Jennifer Tisoncik-Go[6], Leanne S. Whitmore[6], Kirti A. Karunakaran[1], Melissa Roy[7], Shannon Kirejczyk[8], Elizabeth H. Curran[7], Chelsea Wallace[9], Jennifer S. Wood[9], Fawn Connor-Stroud[9], Emily A. Voigt[10], Christopher M. Monaco[11], David E. Gordon[11], Sudhir P. Kasturi[1,11], Rebecca D. Levit[12], Michael Gale, Jr.[6], Thomas H. Vanderford[1], Guido Silvestri[1,11], Kathleen Busman-Sahay[13], Jacob D. Estes[13,14,15,16], Monica Vaccari[17,18], Daniel C. Douek[4], Konstantin M.J. Sparrer[2], R. Paul Johnson[1,19], Frank Kirchhoff[2], Gideon Schreiber[5], Steven E. Bosinger[1,3,11*], Mirko Paiardini[1,11*]

[1]Division of Microbiology and Immunology, Emory National Primate Research Center, Emory University, Atlanta, GA 30329, USA

[2]Institute of Molecular Virology, Ulm University Medical Center, 89081 Ulm, Germany

[3]Emory NPRC Genomics Core Emory National Primate Research Center, Emory University, Atlanta, GA 30329, USA

[4]Vaccine Research Center, National Institute of Allergy and Infectious Diseases, National Institutes of Health, Bethesda, MD 20892, USA

[5]Department of Biomolecular Sciences, Weizmann Institute of Science, Rehovot 76100, Israel

[6]Department of Immunology, University of Washington School of Medicine, and the Washington National Primate Research Center, Seattle, WA 98109, USA

[7]Division of Pathology, Emory National Primate Research Center, Emory University, Atlanta, GA 30329, USA

[8]StageBio, 5930 Main St. Mount Jackson, VA 22842, USA

[9]Division of Animal Resources, Emory National Primate Research Center, Emory University, Atlanta, GA 30329, USA

[10]RNA Vaccines Group, Access to Advanced Health Institute, Seattle, WA 98102, USA.

[11]Department of Pathology and Laboratory Medicine, School of Medicine, Emory University, Atlanta, GA 30322, USA

[12]Department of Medicine, School of Medicine, Emory University, Atlanta, GA 30322, USA

[13]Vaccine and Gene Therapy Institute, Oregon Health & Science University, Beaverton, OR 97006, USA

[14]Oregon National Primate Research Center, Oregon Health & Science University, Beaverton, OR 97006, USA

[15]Department of Clinical Medicine, Aarhus University, Aarhus 8000, Denmark

[16]School of Health and Biomedical Sciences, College of Science, Engineering and Health, RMIT University, Melbourne 3000, Australia

[17]Division of Immunology, Tulane National Primate Research Center, Covington, LA 70433, USA

[18]Department of Microbiology and Immunology, Tulane School of Medicine, New Orleans, LA 70112, USA

[19]Infectious Disease Division, Department of Medicine, Emory University School of Medicine, Atlanta, Georgia, USA.

[20]These authors contributed equally

†Deceased

*Correspondence to: mirko.paiardini@emory.edu (M.P; Lead Contact); steven.bosinger@emory.edu (S.E.B.)

Published in *Science Immunology* Volume 8, Issue 85, July 28th, 2023, PMID: 37506197

Abstract: Type-I interferons (IFN-I) are critical mediators of innate control of viral infections, but also drive recruitment of inflammatory cells to sites of infection, a key feature of severe COVID-19. Here, IFN-I signaling was modulated in rhesus macaques (RMs) prior to and during acute SARS-CoV-2 infection using a mutated IFNα2 (IFN-modulator; IFNmod), which has previously been shown to reduce the binding and signaling of endogenous IFN-I. IFNmod treatment in uninfected RMs was observed to induce a modest upregulation of only antiviral IFN-stimulated genes (ISGs); however, in SARS-CoV-2-infected RMs, IFNmod reduced both antiviral and inflammatory ISGs. Notably, IFNmod treatment resulted in a potent reduction in SARS-CoV-2 viral loads both in vitro in Calu-3 cells and in vivo in Bronchoalveolar lavage (BAL), upper airways, lung,

and hilar lymph nodes of RMs. Furthermore, in SARS-CoV-2 infected RMs, IFNmod treatment potently reduced inflammatory cytokines, chemokines, and CD163+MRC1- inflammatory macrophages in BAL and expression of Siglec-1 on circulating monocytes. In the lung, IFNmod also reduced pathogenesis and attenuated pathways of inflammasome activation and stress response during acute SARS-CoV-2 infection. Using an intervention targeting both IFN-α and IFN-β pathways, this study shows that, while early IFN-I restrains SARS-CoV-2 replication, uncontrolled IFN-I-signaling critically contributes to SARS-CoV-2 inflammation and pathogenesis in the moderate disease model of RMs.

One Sentence Summary: Administration of a mutated IFNα2 to rhesus macaques limited viral replication and pathogenesis during SARS-CoV-2 infection.

Main Text:

INTRODUCTION

Coronavirus disease 2019 (COVID-19) is caused by severe acute respiratory syndrome coronavirus 2 (SARS-CoV-2) and is an ongoing pandemic that has resulted in over 6.9 million cumulative deaths [376, 377]. While vaccines are highly effective, vaccine-induced immunity and neutralizing antibody titers wane over time. In addition, the emergence of SARS-CoV-2 variants resulting in breakthrough infections remains worrisome. Thus, it is imperative to fully characterize the viral pathogenesis of SARS-CoV-2 and early COVID-19 immune responses to identify correlates of protection and design therapeutics that can mitigate disease severity and viral replication.

Type-I interferons (IFN-I) are ubiquitously expressed cytokines that play a central role in innate antiviral immunity and cell-intrinsic immunity against viral pathogens [104, 105, 378]. The receptors for IFN-I, IFNAR1 and IFNAR2, are universally expressed and, following formation of the IFN-I ternary complex, trigger the downstream transcription of interferon stimulated genes (ISGs) that mediate a myriad of antiviral effector functions and promote recruitment of inflammatory cells [379]. Work early in the pandemic indicated that the IFN-I system has a protective effect from disease in SARS-CoV-2 infection, as individuals with severe COVID-19 were demonstrated to be more likely to have deficiencies to IFN-I responses, either by the presence of rare inborn errors (*TLR3*, *IRF7*, *TICAM1*, *TBK1*, or *IFNAR1*), neutralizing auto-antibodies against IFN-I, or the lack of production of IFN-I [72, 95, 114, 115, 119, 355, 380-383]. Additionally, Genome Wide Association Studies (GWAS) of critically ill COVID-19 patients have identified multiple critical COVID-19-associated variants in genes that are involved in IFN-I signaling including *IFNA10*, *IFNAR2*, *TYK2,* as well as type III interferon signaling *IL10RB* [384]. These findings contributed to the establishment of a model in which sustained IFN-I responses were deemed to be critical for protecting SARS-CoV-2-infected patients from progressing to severe COVID-19.

However, more recent work has suggested that the role of the IFN-I system in SARS-CoV-2 infection may be more complex than initially thought. In contrast to the aforementioned studies, Povysil et al. found no associations between rare loss-of-function variants in IFN-I and severe COVID-19 [385]. Further, Lee et al. demonstrated that hyper-inflammatory signatures characterized by IFN-I response in conjunction with TNF/IL-1β

were associated with severe COVID-19 in SARS-CoV-2 infected individuals [386] and Blanco-Melo et al. showed that high IFN-I expression in the lung was linked to increased morbidity early in the COVID-19 pandemic [387]. Additionally, prolonged IFN signaling in murine models of respiratory infection has recently been shown to interfere with repair in lung epithelia, increasing disease severity and susceptibility to bacterial infections [121, 388] and blocking IFN-I with anti-IFNAR2 antibodies has been shown to suppress inflammation in SARS-CoV-2-infected MISTRG6-hACE2 mice when combined with remdesivir [389].

In the past year, progress has been made in characterizing the underlying mechanisms of IFN-I mediated pathogenesis in SARS-CoV-2 infection. For example, pro-inflammatory monocytes ($CD14^+$ $CD16^+$) that can be driven to expand by IFN-I have been shown by Junqueira et al. and Sefik et al. to phagocytose antibody-opsonized SARS-CoV-2 via FCγRs, undergo abortive infection, and induce pyroptosis that results in systemic inflammation [80, 389]. Additionally, Laurent et al. demonstrated that pDCs infiltrate into the lungs of COVID-19 patients and IFN-I produced by pDCs in response to SARS-CoV-2 results in transcriptional and epigenetic changes in macrophages that prime them for hyperactivation in vitro; these findings support a model in which pDCs that infiltrate into the lungs directly sense SARS-CoV-2 and produce IFN-I that prime lung macrophages to produce pro-inflammatory cytokines [390].

Further work also has demonstrated the association of multiple ISGs with increased SARS-CoV-2 infection. Specifically, interferon-induced transmembrane proteins (IFITM 1-3) have been shown to be commandeered by SARS-CoV-2 to increase efficiency of

viral infection [391], the IFN-I-inducible receptor sialic acid-binding Ig-like lectin 1 (Siglec-1/CD169) can function as an attachment receptor and enhances ACE2-mediated infection and induction of trans-infection [78], and aberrant cGAS-STING activation has not only been found in the severely damaged lungs of COVID-19 patients post-mortem but has also been detected in macrophages surrounding damaged epithelial cells in COVID-19 skin lesions [90].

Several ongoing and recently completed clinical trials administering IFN-I have shown little to no positive effects of therapy during acute infection, despite treatment with IFN being highly efficient against SARS-CoV-2 *in vitro* [141, 392]. No beneficial effects were observed with either IFNβ-1a or combination IFNβ-1a and remdesivir treatment in hospitalized COVID-19 patients in the WHO Solidarity Trial and Adaptive COVID-19 Treatment Trial (ACTT-3) respectively. In fact, combination IFNβ-1a and remdesivir resulted in worse outcomes and respiratory status in ACTT-3 patients who required high-flow oxygen at baseline when compared to treatment with remdesivir alone [305]. Pegylated IFN-α2b has shown some promise in moderate COVID-19 patients, with a phase 3 randomized open label study showing that patients that received pegylated IFN-α2b experienced a faster time to viral clearance [309]. Recently, there has been renewed interest in pursuing IFN-λ as a COVID-19 therapeutic following completion of the Phase 3 TOGETHER clinical trial which demonstrated that early administration of pegylated IFN-λ resulted in a 51% risk reduction of COVID-19-related hospitalizations or emergency room visits in predominantly vaccinated individuals at high risk of developing severe COVID-19 [315].

Given the discordant effects of IFN treatment observed in the aforementioned trials and the contradictory findings of IFN-I having a protective or detrimental role in COVID-19, it is critical that further research on the mechanisms of IFN-I in regulating SARS-CoV-2 infection is conducted.

Non-human primate (NHP) models, specifically rhesus macaques (RMs), have been used extensively to study pathogenesis and evaluate potential vaccine and antiviral candidates for numerous viral diseases, including HIV and, more recently, SARS-CoV-2 [173, 174, 393, 394]. RMs infected with SARS-CoV-2 develop mild to moderate disease, mimic patterns of viral shedding, and, in similar fashion to humans, rarely progress to severe disease [173, 174, 393, 394]. Multiple previous studies [173, 174, 393, 394] have shown that RMs generate a rapid and robust IFN-I response following SARS-CoV-2 infection, with numerous ISGs upregulated as early as 1 day post-infection (dpi) in both peripheral blood mononuclear cells (PBMCs) and bronchiolar lavage (BAL).

To better understand how downregulating this early IFN-I response in SARS-CoV-2-infection may impact viral replication and pathogenesis in the RM model, we used a mutated IFNα2, here named IFN-I modulator (IFNmod), which binds with high affinity to IFNAR2, but markedly lower affinity to IFNAR1, with a net effect of reducing the binding and signaling of all forms of endogenous IFN-I [395-397], and, as such, previously referred to as IFN-I competitive antagonist (IFN-1ant). IFNmod has been shown to induce low-level stimulation of robust antiviral ISGs without induction of tunable inflammatory genes when

used *in vitro* in cancer cell lines [395, 396]. Importantly, IFNmod has previously been evaluated in vivo in RMs where it was shown to possess a short plasma half-life, allowing us to modulate IFN-I signaling specifically in the early stages of infection, and has been shown to limit the expression of both antiviral and pro-inflammatory ISGs in Simian Immunodeficiency Virus (SIV)-infected RMs [368, 397]. Using an intervention targeting both IFN-α and IFN-β pathways in the moderate disease model of SARS-CoV-2 infected RMs, our data support a model where early IFN-I restrains viral replication, while uncontrolled IFN-I-signaling contributes to SARS-CoV-2 inflammation and pathogenesis.

RESULTS

IFNmod treatment in uninfected RMs modestly upregulated antiviral ISGs without impacting inflammatory genes

We administered IFNmod to four uninfected RMs at a dose of 1 mg/day, intramuscularly, for 4 consecutive days (**Fig. 3.1a, Table 3.S1**) to determine its impact on ISGs in the absence of SARS-CoV-2 infection. Transcript levels of a panel of 16 ISGs previously observed to be induced by SARS-CoV-2 infection [173] in RMs were quantified by RNAseq at pre- and post-treatment timepoints. Similar to what was previously observed in cancer cells treated with IFNmod [395, 396], antiviral ISGs were modestly upregulated following IFNmod administration in both the BAL and PBMCs of uninfected RMs (**Fig. 3.1b-c**) whereas IL-6 signaling and inflammatory genes remained unchanged (**Fig. 3.1d-e)**. Previously, Forerro et al. identified that proinflammatory gene expression triggered by Type I IFNs was largely dependent on the selective induction of the transcription factor IFN regulatory factor 1 (IRF1) [398]. In concordance with the unchanged inflammatory gene

expression, we did not observe any induction of IRF1 in BAL or PBMCs of uninfected, IFNmod-treated RMs **(Fig. 3.1f).** Additionally, IFNmod treatment in uninfected animals did not impact BAL cytokines and chemokines associated with inflammation and recruitment of inflammatory cells including IL-1β, IL-6, IL-8, IL-12p40, TNFβ, IFNγ, MIP1α, and MIP1β **(Fig. 3.1g)**.

Administration of IFNmod in Calu-3 human lung cells modulated IFN-I responses and inhibited SARS-CoV-2 replication to levels comparable to Nirmatrelvir

Consistent with the data in uninfected RMs, IFNmod treatment alone in uninfected Calu-3 human lung cancer cells induced low-level expression of antiviral ISGs OAS1 and Mx1, with very minimal changes in the pro-inflammatory chemokine CXCL10 **(Fig. 3.2a-c).** In the presence of IFNα stimulation, IFNmod inhibited expression of both antiviral ISGs (OAS1, Mx1) and the pro-inflammatory CXCL10 **(Fig. 3.2b-c)**. Taken together, these data indicate that IFNmod stimulates a weak antiviral IFN-I response in the absence of endogenous IFNα, but potently inhibits both antiviral and pro-inflammatory IFN-I pathways induced in response to addition of IFNα.

Given the ability of IFNmod to upregulate antiviral genes in both uninfected RMs and Calu-3 cells, its capacity to limit SARS-CoV-2 replication was explored **(Fig. 3.2d)**. IFNmod was shown to be just as effective as IFN□ and the antiviral Nirmatrelvir (packaged with Ritonavir and sold under the brand name Paxlovid) in inhibiting SARS-CoV-2 infection when treatment was initiated prior to infection **(Fig. 3.2e-f)**. With this reduced viremia, the expression of OAS1 relative to untreated SARS-CoV-2-infected

Calu-3 cells was reduced at all tested concentrations of IFNmod and Nirmatrelvir, but not with the highest tested dose of IFNα **(Fig. 3.2g).** As expected, since viral RNA load was the key driver of inflammation in this *in vitro* model, we observed a potent reduction in CXCL10 mRNA with all three treatments **(Fig. 3.2h)**. We also performed the same experiment with interventions started post-infection **(Fig. 3.S1a)**; although all 3 treatments potently reduced viral loads, in this setting Nirmatrelvir and IFN were slightly more potent than IFNmod at the lowest tested concentrations **(Fig. 3.S1b-c)**. At the highest tested doses, there was a trend towards higher CXCL10 mRNA levels with IFN treatment vs. IFNmod treatment **(Fig. 3.S1d)**, despite similar viral loads, suggesting that uncontrolled IFN-I-signaling contributes to SARS-CoV-2 inflammation.

IFNmod administration decreases SARS-CoV-2 loads in airways of RMs

Since IFNmod treatment resulted in inhibition of SARS-CoV-2 replication *in vitro* and low-level stimulation of antiviral genes without induction of inflammatory genes in uninfected RMs, we then tested the hypothesis that treatment with IFNmod may inhibit viral replication in SARS-CoV-2-infected RMs while limiting systemic inflammation within the host. 18 adult RMs were age and sex matched between two experimental arms to receive 4 doses of IFNmod (intramuscularly, 1 mg/day; IFNmod-treated group) mimicking the 4-day dosing regimen of the uninfected RMs, or to remain untreated (untreated group). To determine how downregulating early IFN-I pathways affects SARS-CoV-2 replication and pathogenesis *in vivo*, animals assigned to the IFNmod-treated group initiated treatment at one day prior to infection (d-1) to allow for IFNmod distribution, binding to the IFNR, and early blocking of endogenous IFN-I and continued daily treatment until 2 days post-

infection (dpi) (**Fig. 3.3a**). On day 0, all 18 RMs were inoculated with a total of $1.1x10^6$ PFU SARS-CoV-2 (2019-nCoV/USA-WA1/2020), administered by intranasal (IN) and intratracheal (IT) routes. 3 IFNmod and 3 untreated RMs were euthanized at 2, 4, and 7 dpi each, respectively. Animals were scored according to the Coronavirus Vaccine and Treatment Evaluation Network (CoVTEN) standard clinical assessment at cageside **(Table 3.S2)** and anesthetic **(Table S3)** accesses. Additionally, vitals including rectal temperature, respiratory rate, heart rate, and SpO_2 were recorded in anesthetized animals. Following infection, untreated RMs experienced increases in rectal temperature (-7 dpi vs.1 dpi, p=0.0117; -7 dpi vs. 2 dpi, p=0.0742), heart rate (-7 dpi vs. 2 dpi, p=0.0391), and respiratory rates (-7 dpi vs. 2 dpi, p=0.0938) **(Fig. 3.S2a)**. IFNmod-treated RMs experienced higher SpO_2 and heart rates than untreated RMs at 2dpi and 4dpi respectively. However, no differences in fold change (FC) of SpO_2 or heart rate from pre-infection baseline (-7dpi) were observed between treatment groups (**Fig. 3.S2b**). Neither treatment group experienced weight changes (**Fig. 3.S2c**) and no differences were observed in cageside, anesthetic, and total clinical scores between untreated and IFNmod-treated RMs **(Fig. 3.S2d)**. Importantly, IFNmod was well tolerated without evidence of treatment induced clinical-pathology, nephrotoxicity, or hepatotoxicity when compared to untreated SARS-CoV-2 infected RMs.

Viral RNA levels were measured using genomic (gRNA) and sub-genomic (sgRNA) qRT-PCR as previously described [173, 399, 400]. During the treatment phase of the study, up to 2 dpi, a drastic reduction in the levels of gRNA N **(Fig. 3.3b-e)** and particularly sgRNA E **(Fig. 3.3f-i)** was observed between untreated and IFNmod-treated RMs in the BAL (**Fig.**

3.3f), nasal swabs (**Fig. 3.3g**), and throat swabs (**Fig. 3.3h)** . Of note, this corresponds to IFNmod treatment resulting in a >3000-fold reduction in median sgRNA E in the BAL at 2 dpi (**Fig. 3.3f**). Additionally, in the nasal swabs at 1 dpi, there was a >1500-fold reduction in median sgRNA E copies in IFNmod-treated RMs (**Fig. 3.3g**). The sgRNA E levels detected at 1 and 2 dpi in the throat showed similar differences, 12-fold and 570-fold less median sgRNA E detected in IFNmod-treated RMs compared to untreated RMs at these respective timepoints (**Fig. 3.3h**). Once treatment was stopped, viral loads remained stable in the treated group up until 7 dpi, both for the genomic and the sub-genomic RNA. As consistently shown in previous studies [173, 174, 393, 394], viral loads decreased in untreated, SARS-CoV-2-infected RMs shortly after the early peak, with swab and BAL viral loads no longer being statistically different between IFNmod-treated and untreated RMs starting from 4 dpi. BAL and nasal swab sgRNA E viral loads were reproduced by an independent laboratory (**Fig. 3.S3a**) and further confirmed by sgRNA targeting the N gene **(Fig. 3.S3b)**.

To assess the impact of IFNmod on viral replication within lung tissue, sections of cranial (upper) and caudal (lower) lung lobes as well as hilar lymph nodes were collected from all animals at necropsy, with 3 RMs from each treatment group euthanized at 2, 4, and 7 dpi. Notably, IFNmod-treated RMs necropsied during the treatment phase at 2 dpi had lower viral gRNA **(Fig. 3.3e)** and sgRNA **(Fig. 3.3i)** levels in their upper and lower lungs as well as hilar LNs than untreated RMs. Although the small sample size at 2 dpi limited statistical power, this difference was substantial, with a 1500-fold and 500-fold reduction in mean gRNA and 250-fold and 300-fold reduction in mean sgRNA E observed in the

upper and lower lung segments respectively of untreated vs. IFNmod-treated RMs. Additionally, when lung viral loads from all three necropsy timepoints were combined, gRNA N levels were found to be lower in the upper lungs of IFNmod treated RMs as compared to untreated RMs **(Fig. 3.S3c-d)**.

In summation, and consistent with the *in vitro* data in Calu-3 cells, *in vivo* treatment with IFNmod resulted in a highly reproducible (1-3 $\log_{10}$) decrease in viremia in the airways of SARS-CoV-2-infected RMs.

IFNmod treatment reduces lung pathology and soluble markers of inflammation in SARS-CoV-2 infected RMs

Consistent with the reduction in SARS-CoV-2 gRNA and sgRNA in the BAL, cranial (upper) lungs, and caudal (lower) lungs of RMs treated with IFNmod at 2 dpi, we observed substantially lower expression of SARS-CoV-2 vRNA in the lungs of treated RMs as compared to untreated RMs at this timepoint by immunohistochemistry **(Fig. 3.S4a)**. Furthermore, SARS-CoV-2 vRNA staining was more diffuse in the untreated RMs, whereas IFNmod-treated RMs had small foci of infected cells. Mx1 was also found to be highly localized to regions of active infection in the lungs of untreated animals at 2 dpi; as expected under normal physiological conditions, Mx1 was more diffuse throughout the lung of IFNmod-treated RMs, regardless of the presence of virus **(Fig. 3.S4a)**.

Pathological analysis of the lungs was performed as previously described [173] by two pathologists, independently and blinded to the treatment arms using the following scoring

criteria: type II pneumocyte hyperplasia, alveolar septal thickening, fibrosis, perivascular cuffing, and peribronchiolar hyperplasia. In both untreated and IFNmod-treated RMs necropsied at 2 dpi, no lung pathology was observed according to our scoring criteria. However, at 4 and 7 dpi, lung pathology was quantifiable, with untreated RMs having higher alveolar septal thickening and perivascular cuffing as compared to IFNmod-treated RMs **(Fig. 3.4a, Fig. 3.S4b**). The total lung pathology score (considering severity and number of effected lobes) and average lung pathology score per lobe (measuring the average severity of abnormalities per lobe, independently of how many lobes had been affected) were lower in the IFNmod-treated group as compared to untreated RMs at 4 and 7 dpi (**Fig. 3.4b-c, Fig. 3.S4b**).

A key feature of severe COVID-19 is the induction of multiple mediators of inflammation and chemotaxis of inflammatory cells to sites of infection [173]. Accordingly, multiple chemokines and cytokines were shown to be highly upregulated in the BAL of untreated RMs at 2 dpi as measured by FC to baseline (-7 dpi); remarkably, at 2 dpi the same cytokines and chemokines remained stable at basal levels in IFNmod-treated RMs (**Fig. 3.4d-k**). More specifically, we observed differences in IL-1β, IL-6, and MCP4 and trending differences in TNFβ, IFN□, and Eotaxin 3 between untreated and IFNmod-treated RMs.

Altogether, IFNmod treatment potently reduced immune mediated pathogenesis in the lung, as well as the levels of multiple cytokines and chemokines in BAL that orchestrate the recruitment of inflammatory cells to sites of infection.

IFNmod-treated RMs display decreased expansion of inflammatory monocytes and rapid downregulation of Siglec-1 expression

Several studies have reported an expansion of circulating inflammatory monocytes in blood of mild/moderate COVID-19 patients [401-403]. High-dimensional flow cytometry was performed on whole blood and BAL of RMs pre- and post-infection to quantify the immunological effects of IFNmod on the frequencies of classical ($CD14^+CD16^-$), non-classical ($CD14^-CD16^+$), and inflammatory ($CD14^+CD16^+$) monocytes as previously described [173] (gating strategy depicted in **Fig. 3.S5a)**. Representative staining of monocyte subsets in untreated and IFNmod-treated animals at pre- and post-infection timepoints is shown in **Fig. 3.5a**. The frequency of $CD14^+CD16^+$ monocytes in blood increased from 11% to 31% of total monocytes from –7 dpi to 2 dpi in untreated RMs, but only from 14% to 18% in IFNmod-treated RMs **(Fig. 3.5b-c).** This difference between treatment groups was maintained at 4 dpi, where CD14+CD16+ monocytes accounted for 19% of total blood monocytes in untreated animals while only accounting for 10% of total blood monocytes in IFNmod-treated RMs **(Fig. 3.5b-c).** Therefore, treatment with IFNmod limited the expansion of inflammatory monocytes, thus reducing the potential for systemic and lower airway inflammation. Of note, at both 2 and 4 dpi, these differences were specific for blood, with no difference observed within the BAL**.**

Siglec-1, an interferon responsive transmembrane protein present on antigen presenting cells, has been shown to function as an attachment receptor for SARS-CoV-2 through enhancement of ACE2-mediated infection and induction of trans-infection [78, 79], and upregulation of Siglec-1 on circulating human monocytes has been identified as an early

marker of SARS-CoV-2 infection and disease severity [404]. There was a strong and rapid upregulation of Siglec-1 on classical and inflammatory monocytes following SARS-CoV-2 infection in all untreated animals, with increases in the frequency of Siglec-1^{+}CD14^{+} blood monocytes (as a percentage of total monocytes) from 0.4% to 70.6% (**Fig. 3.5d-e)**, frequency of CD14^{+} blood monocytes expressing Siglec-1 from 0.5% to 91.7% between –7 dpi and 2 dpi (**Fig. 3.5f),** and mean fluorescence intensity (MFI) of Siglec-1 on CD14^{+} blood monocytes from 1750 to 4050 (**Fig. 3.5g**). All 3 values remained elevated at 4 dpi as compared to -7 dpi. Expression of Siglec-1 was lower in the blood of IFNmod-treated RMs when compared to untreated RMs both at 2 and 4 dpi. The reduced expression of Siglec-1, a well-established downstream molecule of interferon signaling, on blood monocytes in treated RMs is consistent with the observation that IFNmod attenuated antiviral and pro-inflammatory ISGs. Of note, no differences were observed in the expression of Siglec-1 in the smaller myeloid population in the BAL **(Fig. 3.S5b-c).**

To rule out the possibility that IFNmod treatment negatively impacted SARS-CoV-2-specific T cell and neutralizing antibody responses in SARS-CoV-2 infected RMs, we performed ex vivo stimulation of PBMCs with SARS-CoV-2 S peptide pools and NCAP followed by intracellular cytokine staining and serum SARS-CoV-2 pseudovirus neutralization assays at 7 dpi. No differences were observed in SARS-CoV-2-specific T cell or neutralizing antibody responses between treatment groups. Additionally, in line with previous studies [173, 405], we found that SARS-CoV-2-specific CD8 and CD4 T cell responses were weak **(Fig. 3.S6a-e)** and titers of neutralizing antibodies **(Fig. 3.S6f)** were undetectable at 7 dpi.

IFNmod treatment attenuates inflammation and inflammasome activation in the lower airway following SARS-CoV-2 infection

To characterize the pathways that were impacted by IFNmod treatment *in vivo*, bulk RNA-Seq profiling of BAL, PBMCs, and whole blood was performed at multiple timepoints following SARS-CoV-2 infection. SARS-CoV-2 infection induced a robust upregulation of ISG expression in the BAL of untreated animals at 2 dpi. Notably, the transcript levels of ISGs in BAL were substantially attenuated in RMs treated with IFNmod relative to the levels in untreated animals at both 2 and 4 dpi (**Fig. 3.6a, Data File S1),** with 15/16 ISGs being downregulated in IFNmod-treated RMs relative to untreated RMs at 2 dpi (**Fig. 3.6b, Fig. 3.S7a, Data File S1)**. By 7 dpi, ISG expression levels in the BAL of IFNmod-treated animals had returned to basal levels, whereas in untreated RMs, the ISGs in BAL remained elevated (**Fig. 3.6a, Data File S1**).

To assess the impact of IFNmod treatment on inflammation in BAL, the post-infection enrichment of several gene sets in inflammatory pathways, previously associated with severe SARS-CoV-2 infection, was examined at 2 dpi. There was a noticeable loss in enrichment in *IL6 JAK/STAT* **(Fig. 3.6c)** and *TNF* **(Fig. 3.6d)** pathways in IFNmod-treated RMs as compared to untreated RMs. This was even more pronounced for genes associated with neutrophil degranulation **(Fig. 3.6e),** where IFNmod-treated RMs had no enrichment between 2 dpi and baseline, but untreated RMs were enriched. Examination of the leading-edge genes in these pathways (**Fig. 3.6f-h, Data File S1),** and differentially expressed genes (DEGS) identified by *DESeq2* analysis (**Fig. 3.6i-l, Data File S1**),

displayed a stark divergence in the levels of several inflammatory mediators between the IFNmod and untreated groups. Notably, upregulation of IL6 (**Fig. 3.6f**), TNFA-inducing protein 6 (TNFAIP6), PTX3/TNFAIP5, TNF (**Fig. 3.6g, i**), IL10, IFNG, and IL7 (**Fig. 3.6i**) was evident in BAL samples in untreated animals but largely absent in IFNmod-treated animals (**Fig. 3.6f-g, i**). A similar pattern of expression was observed for genes encoding components of azurophilic granules (AZU1/azurocidin 1, RAB44) (**Fig. 3.6h**). In untreated animals, several chemokines involved in migration and recruitment of monocytes and macrophages (CCL2, CCL3, CCL4L1, CCL5, CCL7, CCL8, CCL22), neutrophils (CXCL3), and activated T cells (CXCL9, CXCL10, and CXCL11) were elevated after infection; however, this expression was abrogated in the IFNmod-treated group (**Fig.6j and S7b)**. In agreement with these observed effects on inflammatory mediators, we found that untreated RMs experienced a high induction of IRF1 in BAL at 2 dpi and 4 dpi compared to pre-infection baseline; however, there was no change in IRF1 following SARS-CoV-2-infection in the BAL of IFNmod-treated RMs **(Fig. 3.S7b)**. Thus, in vivo treatment with IFNmod was found to not trigger IRF1 expression in uninfected RMs **(Fig. 3.1f)**, and did not block IFR1 expression in the context of SARS-CoV-2 infection. Of note, while some of these differences in BAL gene expression of inflammatory mediators between treatment groups were maintained at 4 and/or 7 dpi, no differences were observed in protein levels of BAL inflammatory cytokines and chemokines measured via Mesoscale following the cessation of IFNmod treatment **(Fig. 3.4d-k)** This discrepancy between gene expression and protein levels of inflammatory mediators may result from post-transcriptional modification, a higher degree of sensitivity for the transcriptomic measurements as compared to the mesoscale, a higher consumption of those cytokines,

thus masking their increase in BAL fluid while increasing the signaling, or a combination of these factors.

Consistent with reports by Laurent et al. of patients with mild COVID-19 [390], we observed an increase in the abundance of pDCs (defined by CLEC4A/BDCA2 expression) in the BAL of untreated RMs at 2 dpi relative to pre-infection baseline (-7 dpi) by bulk RNA-seq **(Fig. 3.S7c)**. Remarkably, IFNmod-treated RMs experienced a lower level of CLEC4C/BDCA2 and IFNαs in the BAL at 2 dpi as compared to untreated RMs, indicating that IFNmod reduced the recruitment of pDCs to the lower respiratory tract **(Fig. 3.S7d)**. Several genes regulating T cell activation and co-stimulation (CD38, CD69, CD274/PDL1, CD80, CD86, CD40) were upregulated after SARS-CoV-2 infection in untreated animals but minimally changed in IFNmod-treated RMs (**Fig. 3.6k)**. Lastly, consistent with prior reports in human and mice [406-408], the expression of several S100 acute phase proteins (S100A8, S100A9, S100A12) were elevated in BAL samples from untreated animals but were absent in IFNmod-treated RMs. Collectively, these data demonstrate that IFNmod treatment induces a near complete loss of inflammatory activation and a reduction in pathways associated with recruitment and activation of myeloid cells, neutrophils, and pDCs in the lower airway.

Previously, the NLRP3 inflammasome pathway was shown to be the main driver of IFN-I induced pathology in SARS-CoV-2-infected hACE2 mice and inhibition of NLRP3 was observed to attenuate lung tissue pathology [389]. To investigate if NLRP3 signaling was induced by SARS-CoV-2 infection in RMs, we characterized the enrichment of genes

associated with the two phases of NLRP3 signaling: i) priming, in which cytokines and PRRs can upregulate inflammasome components such as NLPR3, CASP1, pro-IL1b and ii) activation, which consists of IL1□ and IL18 release and pyroptosis [409]. Canonical genes in the NLRP3 inflammasome pathway including IL1B, IL1RN/IL1RA, GSDMD, and NLRP3 were upregulated at 2 dpi in BAL samples from untreated animals (**Fig. 3.6l**). Additionally, AIM2 was observed to be upregulated in untreated RM BAL at 2 dpi, consistent with previous findings of AIM2 inflammasome activation in the monocytes of patients with COVID-19 [80]. In IFNmod-treated RMs, however, there was no discernible upregulation from baseline of these inflammasome-associated factors (**Fig. 3.6l**).

Similar to what was described in BAL, IFNmod-treated animals experienced reduced expression of ISGs, inflammatory genes, and innate immune genes in PBMCs and whole blood relative to untreated animals following SARS-CoV-2 infection **(Fig. 3.S8a-f)**. Thus, IFNmod treatment in RMs was not only able to potently attenuate inflammation and inflammasome activation in the lower airway, but also reduce inflammation systemically during SARS-CoV-2 infection.

IFNmod treatment inhibits the accumulation and activation of $CD163^{+}MRC1^{-}$ inflammatory macrophages in the lower airway during SARS-CoV-2 infection

To survey the impact of IFNmod treatment on the landscape of immune cells in the lower airway, droplet-based sc-RNA-Seq was performed on cells obtained from BAL pre- and post- SARS-CoV-2 infection in both IFNmod and untreated animals. After quality filtering, 62,081 cells were clustered using Seurat, followed by more refined annotation with a

curated set of marker genes **(Fig. 3.S9a-c)**. Consistent with prior studies [100, 173], the majority of cells were of myeloid lineage (macrophages and monocytes), with a minority of several other immune phenotypes and epithelial cells observed (**Fig. 3.7a, Fig. 3.S9d**). The expression of the 17 ISG panel utilized above was examined in these subtypes (except for neutrophils) and showed that ISGs peaked at 2 dpi in untreated animals in all subsets, including pDCs **(Fig. 3.S9e-g)** which have previously been shown to possess a strong IFN-I signature in the BAL of mild COVID-19 patients [390]. Remarkably, IFNmod treatment diminished expression of ISGs in all of the cell subsets identified in the BAL of SARS-CoV-2-infected RMs **(Fig. 3.S9e-g)**. Thus, IFNmod was shown to be highly effective at reducing the IFN-I response in all cells identified in the lower airway.

In recent work, we used sc-RNA-Seq to identify two myeloid population of the BAL of RMs, $CD163^{+}MRC1^{+}TREM2^{+}$ and $CD163^{+}MRC1^{-}$, that infiltrated into the lower airway and produced inflammatory cytokines during acute SARS-CoV2 infection [410]. We also showed that blocking the recruitment of these subsets with a JAK/STAT inhibitor abrogated inflammatory signaling [173, 410]. Here, using a reference comprising of the macrophage/monocyte subsets from lungs of three healthy RMs as described previously [410, 411], we divided the clusters of Macrophage/Monocyte cells in the lower airways of RMs into four subsets: $CD163^{+}MRC1^{+}$, $CD163^{+}MRC1^{+}TREM2^{+}$, $CD163^{+}MRC1^{-}$, and $CD16^{+}$ monocytes (**Fig. 3.7b, Fig. 3.S10a-b**). Of note, the CD16+ monocyte subset was omitted from further functional analyses due to its very low frequency. The percentage of $CD163^{+}MRC1^{+}$ macrophages in the BAL of untreated RMs decreased following SARS-CoV-2 infection due to the infiltration of $CD163^{+}MRC1^{-}$ and $CD163^{+}MRC1^{+}TREM2^{+}$ cells

at 2 dpi (**Fig. 3.7c, Fig. 3.S10c**). Conversely, the percentage of $CD163^{+}MRC1^{+}$ macrophages in the BAL of IFNmod-treated RMs remained relatively stable, with $CD163^{+}MRC1^{+}$ macrophages at 2 dpi being higher in IFNmod-treated vs. untreated RMs. Additionally, the $CD163^{+}MRC1^{-}$ population in BAL was shown to have expanded from pre-infection baseline to 2 dpi in untreated animals as compared to IFNmod-treated animals (**Fig. 3.7c, Fig. 3.S10c).** At 2 dpi, viral reads were detected (percentage of viral reads > 0) in macrophages/monocytes in the BAL of untreated RM at a rate of 9.8% (1030/9451 cells, median of individual animals 5.8%) (**Fig. 3.7d, Fig. 3.S10d**) consistent with studies in human COVID-19 patients where an average of 7.8% of lung macrophages were reported to be SARS-CoV-2 positive [412]. IFNmod decreased the frequency of macrophages/monocytes detected in the BAL of treated animals, with a rate of only 0.01% (1/7544) macrophages/monocytes having detectable viral reads (**Fig. 3.7d, Fig. 3.S10d**). Among the macrophage subsets in the untreated group, the CD163+MRC1- subset was primarily associated with viral reads with a median of 11% of cells with detectable viral reads compared to 2.2% of CD163+MRC1+ and 2.4% of CD163+MRC1+TREM2+ (**Fig. 3.7d, Fig. 3.S10e**). The number of cells with detectable viral reads gradually decreased at 4 dpi and was almost absent by 7 dpi **(Fig. 3.S10e)**.

Peak ISG levels in $CD163^{+}MRC1^{+}$, $CD163^{+}MRC1^{+}TREM2^{+}$, and $CD163^{+}MRC1^{-}$ macrophage subsets in BAL were observed at 2 dpi, with the highest and most sustained ISG expression occurring in the $CD163^{+}MRC1^{-}$ population (**Fig. 3.7e, Data File S3**). In all three macrophage subsets in the BAL, IFNmod treatment effectively suppressed ISG expression (**Fig. 3.7e**). The $CD163^{+}MRC1^{-}$ were the predominant subset producing

inflammatory cytokines and chemokines at 2 dpi and other post-infection timepoints in both experimental groups, with IFNmod reducing the transcript levels of both (**Fig. 3.7f-g, Data File S3**).

Since a series of studies in humans and a humanized mouse model linked lower airway inflammation during SARS-CoV-2 infection to inflammasome activation specifically within infiltrating monocytes and resident macrophages [80, 389], we went on to characterize the expression of canonical inflammasome genes within each myeloid subset in the lower airway. We observed that the expression of AIM2, CASP1, GSDMD, IL1B, IL1RN and IL27 increased from -7 dpi to 2 dpi in the CD163+MRC1- subset and was maintained until 7 dpi (**Fig. 3.7h, Data File S3**). Several inflammasome-associated genes were also induced at 2 dpi in $CD163^{+}MRC1^{+}$ and $CD163^{+}MRC1^{+}TREM2^{+}$ macrophages, albeit at lower cellular percentages overall compared to the $CD163^{+}MRC1^{-}$ population **(Fig. 3.7h)**. Across all three myeloid subsets, IFNmod consistently dampened the expression of inflammasome mediators, with the effect being most apparent at 2 dpi **(Fig. 3.7h)**.

Collectively, these data indicate a profound effect of IFNmod treatment in inhibiting the accumulation of $CD163^{+}MRC1^{-}$ macrophages, the most prevalent subset undergoing inflammasome activation and contributing to inflammation, in the lower airway during SARS-CoV-2 infection.

IFNmod treatment dampens inflammasome activation, bystander stress response, and cell death pathways in lung during acute SARS-CoV-2 infection

To further characterize the effect of IFNmod within the lower airway, sc-RNA-Seq was conducted on cell suspensions prepared from caudal (lower) lung lobe sections obtained at necropsy. Based on the expression of canonical markers, these cells were classified into four major groups – Epithelial, Lymphoid, Myeloid and "Other"- stromal and endothelial (**Fig. 3.8a**), which were then each clustered separately. The annotations were further fine-tuned based on the expression of marker genes [413] **(Fig. 3.S11a-d**), yielding 42,699 cells with balanced representation of varying phenotypes across the lung (**Fig. 3.8a and Fig. 3.S11a-d**). Interestingly, the Myeloid cluster in the lung contained an additional subset beyond the four phenotypes described in the BAL that was closely related to the $CD163^{+}MRC1^{+}$ cells and was defined by high expression of SIGLEC1 (**Fig. 3.8a and Fig. 3.S11c**).

Analyses at the pathway level at 2 dpi demonstrated a profound impact of IFNmod treatment in abrogating IFN-I signaling, as observed by an absence of enrichment of several IFN-related gene sets across all cell subsets in the lungs of IFNmod-treated RMs, despite being robustly overrepresented in untreated animals (**Fig. 3.8b, Fig. 3.S12a, Data FIle S4**). At the gene level, analyses of individual cell subsets, including AT1 and AT2 cells (Epithelial cluster), $CD163^{+}MRC1^{-}$ cells (Myeloid cluster), T cells, NK cells, and B cells (in the Lymphoid cluster) showed between 12 to 17 ISGs out of the panel of 17 ISGs being lower in IFNmod-treated RMs as compared to untreated RMs at 2 dpi (**Fig. 3.8c, Fig. 3.S12b, Data FIle S5**).

At 7 dpi, five days after cessation of IFNmod treatment, expression of ISGs had largely normalized and was equivalent between the untreated and IFNmod groups (**Fig. 3.S12c, Data FIle S4**). Taken together, these data demonstrate that IFNmod treatment was able to effectively suppress the IFN-I system across a broad distribution of pulmonary cellular subsets during acute SARS-CoV-2 infection, including epithelium involved in gas exchange, immune cells in the interstitium, and cells in the lung vasculature.

Given the attenuated expression of genes related to inflammasome signaling in the BAL of IFNmod-treated RMs, we investigated if a similar dampening effect occurred in the lungs of treated animals. In untreated animals, we observed an enrichment of genes within the IL1 signaling cascade at 2 dpi relative to pre-infection baseline across several myeloid, lymphocyte, and endothelial subsets. Conversely, in IFNmod-treated RMs, there was no enrichment of the IL1 signaling cascade gene set at 2 dpi (**Fig. 3.8b)**. Additionally, there was an enrichment of gene-sets representing necrotic cell-death pathways observed in untreated RMs, but not IFNmod-treated RMs **(Fig. 3.8b).** Since infection-induced pyroptosis is a process of inflammation-related necrosis that has been shown to largely occur within myeloid cells [414], we next delineated the contribution of individual subsets to the inflammatory state in the lower airway by visualizing DEGs across subsets (**Fig. 3.8d-f, Fig. 3.S12d-h, Data FIle S5**). Notably, expression of components of the inflammasome **(Fig. 3.8d and Fig. 3.S12e)** and classical inflammatory mediators **(Fig. 3.8e and Fig. 3.S12f)** were restricted to the myeloid subsets, suggesting that inflammasome priming and activation in the lung during SARS-CoV-2 infection is largely constrained to monocyte/macrophage populations. Consistent with this model,

expression of GSDMD, a central regulator of NLRP3-regulated pyroptosis, was highest in monocyte/macrophage populations (**Fig. 3.8d**). Importantly, levels of these inflammasome components were all potently reduced by IFNmod treatment (**Fig. 3.8d**).

In untreated RMs, widespread induction of genes from the programmed cell death **(Fig. 3.8f and Fig. 3.S12g)** and response to heat stress (**Fig. 3.S12d, h**) pathways were observed across the landscape of lung cellular subsets, particularly in the Myeloid and Lymphoid classes of phenotypes. In contrast, within the IFNmod-treated group, expression of genes related to programmed cell death and response to heat stress was strikingly attenuated; this effect was particularly apparent in capillary and capillary aerocytes (**Fig. 3.8f, Fig. 3.S12d, g-h**).

These data are consistent with a model in which, during acute SARS-CoV-2 infection, activated monocytes and macrophages cells undergo inflammasome-mediated pyroptosis, which provides secondary stress signals to the non-immune cell classes of the lung. Importantly, IFNmod treatment was also able to abolish induction of these stress and cell death related pathways in these pulmonary subsets.

DISCUSSION

The ways in which IFN-I regulates SARS-CoV-2 replication and disease progression are incompletely understood. Here, we employed an integrated systems approach in a nonhuman primate model of mild to moderate SARS-CoV-2 infection to dissect the roles

of antiviral and pro-inflammatory IFN-I responses in early SARS-CoV-2 infection using a mutated IFNα2 (IFN-I modulator; IFNmod). Notably, this protein was previously demonstrated to have a high affinity to IFNAR2 and markedly lower affinity to IFNAR1, resulting in receptor occupancy, and blocking binding and signaling of all forms of endogenous IFN-I produced in response to viral infection [395-397]. While SARS-CoV-2-infection in untreated RMs was shown to induce a strong IFN-I response with concomitant inflammation and lung damage, IFNmod remarkably and potently reduced viral loads in the upper and lower airways, inflammation, and lung pathology. Therefore, using an *in vivo* intervention targeting IFN-I to understand its role in SARS-CoV-2 infection, our study shows that early IFN-I restrains SARS-CoV-2 replication and an aberrant IFN-I response contributes to SARS-CoV-2 pathogenesis. Furthermore, it also demonstrates a beneficial role of IFNmod in limiting both viral replication and SARS-CoV-2 induced inflammation in NHP when initiated prior to infection.

Initially, we evaluated the effects of administering IFNmod in uninfected RMs and found that IFNmod resulted in a modest and transient stimulation of antiviral ISGs, while genes associated with systemic inflammation remained unchanged. This is consistent with previous in vitro work on cancer cell lines in which low amounts of IFN-I induced the transcription of robust antiviral genes, without the activation of tunable inflammatory genes which often require high concentrations and high affinity IFN-I (*35)*. Next, we showed that IFNmod was capable of substantially reducing SARS-CoV-2 viral loads in vitro in Calu-3 cells to levels equivalent to the antiviral Nirmatrelvir (packaged with ritonavir and sold as Paxlovid), particularly when administered pre-infection. These

results raised the intriguing hypothesis that regulating IFN-I signaling using IFNmod in the early stages of SARS-CoV-2 infection could balance low levels of antiviral genes while blocking the expression of pro-inflammatory genes. Remarkably, the administration of IFNmod prior to and during the first two days of SARS-CoV-2 infection in RMs was found to result in a reduction in viral loads in the BAL (>3 log reduction), nasal, and throat swabs. Additionally, IFNmod reduced viral loads in the upper and lower lungs as well as hilar LNs of RMs during the treatment period and limited lung pathology as well as the production of numerous pro-inflammatory cytokines and chemokines within the lower airways.

We show that IFNmod administration prior to SARS-CoV-2 infection in RMs results in an upregulation of antiviral ISGs, while potently dampening endogenous IFN-I signaling and limiting the immunopathology that has been linked to IFN-I following SARS-CoV-2 infection. Although it is likely that the reduction in inflammatory responses that we observed in IFNmod-treated RMs may be partially attributed to lower viral loads in these animals, our data support a direct action of IFNmod in targeting inflammation independent of reducing viral load. This is evidenced by IFNmod treatment in the presence of IFNα (and absence of SARS-CoV-2 infection) potently inhibiting pro-inflammatory CXCL10 in Calu-3 human lung cancer cells and IFNmod-treated RMs still experiencing lower levels of inflammation at 4 and 7 dpi despite viral loads no longer being different between treatment groups. Consistent with the observation that IFNmod achieved a “goldilocks” effect of upregulating antiviral ISGs while reducing expression of inflammatory mediators, we observed that IFNmod blocked the expression of the transcription factor IFR1, which has previously been shown to be a key regulator of proinflammatory gene expression

triggered by Type I IFNs, during SARS-CoV-2 infection. Altogether, these data support a working model in which early antiviral IFN-I responses restrain SARS-CoV-2 replication, whereas a sustained and systemic IFN-I response, particularly when extended to pro-inflammatory genes, exacerbate SARS-CoV-2 pathology.

Notably, SARS-CoV-2 infection in RMs represents a mild/moderate model of COVID-19; thus, one limitation of our study is that does not address the impact of IFNmod in severe COVID-19. Additionally, while we observed reductions in SARS-CoV-2 infectivity and inflammatory gene expression in Calu-3 cells when IFNmod was administered post-infection, it is also important to note that we initiated IFNmod treatment in RMs prior to infection with SARS-CoV-2 and that changing the timing of administration could also lead to different results in vivo.

IFNmod administration in SIV-infected RMs during the first 4 weeks of infection was previously shown to result in higher plasma viral loads, increased CD4+ T cell depletion, and a more rapid progression to AIDS. These results highlight that modulating IFN-I during infection with inherently different viruses (SARS-CoV-2, which establishes an acute infection that is naturally controlled in a few weeks in RMs and SIV, which establishes a persistent, chronic infection) can have vastly different effects on pathogenesis.

Our data also show a central role of IFN-I in regulating the axis of infiltrating monocytes and subsequent inflammation within the airway and lung interstitium during SARS-CoV-2 infection.

Numerous studies have observed hyperactivation of monocytes and macrophages in COVID-19 (reviewed in [415]). Within the lower airway, an early study identified elevated expression of IL1B, IL6, and TNF within alveolar macrophages in patients with severe COVID-19 [100]. Subsequent work has progressed to dissect the precise phenotypes contributing to SARS-CoV-2 driven inflammation within the monocyte/macrophage axis in mice [416], NHPs [393, 410], and more recently, in humans [417]. In these studies, a consistent model has emerged in which resident tissue alveolar macrophages are displaced by inflammatory, infiltrating monocytes and interstitial macrophages. Notably, we observed IFNmod treatment to profoundly impact monocyte/macrophage populations *in vivo*, decreasing the activation state of the $CD163^{+}MRC1^{-}$ population and its recruitment to the BAL as well as reducing the expansion of $CD14^{+}CD16^{+}$ pro-inflammatory monocytes in the periphery relative to untreated RMs. We also identified the $CD163^{+}MRC1^{-}$ interstitial macrophage-like subset as the predominant population expressing inflammatory cytokines and chemokines and exhibiting inflammasome activation within the alveolar space during SARS-CoV-2 infection. Moreover, and supporting recent studies in humanized mice [389], our work demonstrates that targeted modulation of the IFN-I system during early SARS-CoV-2 can effectively eliminate the level of cell-associated virus on macrophages and broadly dampen induction of the inflammasome.

Autopsies of patients succumbing to severe COVID-19 have linked disease pathology to the accumulation of aberrantly activated macrophages in lungs [418] and hyperactivated Siglec1+ macrophages co-localizing with SARS-CoV-2 in the hilar LNs of autopsy samples [419]. Grant et al proposed a model in which alveolar macrophages act as "Trojan horses" that traffic to adjacent lung regions, ferrying cell-associated virus and propagating inflammation [420]. In this context, the observation that IFNmod was able to potently reduce the expression of the viral attachment receptor Siglec-1 on CD14+ blood monocytes and BAL macrophages, with concomitantly lowered ISG expression and inflammasome activation, provides a possible mechanism by which the IFN system may enhance trans-infection and enable propagation and dissemination of inflamed macrophages in the airspace. Our scRNA-Seq data are consistent with the "Trojan horse" hypothesis and extend it by identifying that the $CD163^{+}MRC1^{-}$ and $CD163^{+}TREM2^{+}$ populations are the predominant populations in the lung in which the inflammasome is induced.

This study, using an intervention targeting both IFN-□ and IFN-□ pathways, demonstrates the central role of IFN-I in regulating the early events of SARS-CoV-2 infection and pathogenesis in RMs, making a strong case that, while rapid and transient stimulation of antiviral ISGs helps restrain SARS-CoV-2 replication, IFN-I driven excessive inflammation has deleterious consequences if left unchecked.

MATERIALS AND METHODS

Study Design

The main objective of our study was to determine how downregulating early IFN-I pathways affects SARS-CoV-2 replication and pathogenesis. We utilized IFN modulator (IFNmod), a mutated IFNα2 with high affinity to IFNAR2, but markedly lower affinity to IFNAR1 that was previously demonstrated to block binding of endogenous IFN-I. We first assessed the impact of IFNmod on interferon stimulated genes (ISGs) in uninfected rhesus macaques (RMs) and uninfected Calu-3 cells. Additionally, we also evaluated the ability of IFNmod to reduce SARS-CoV-2 replication in infected Calu-3 cells. Next, we used the RM model of SARS-CoV-2 to examine the effect of IFNmod on SARS-CoV-2 replication and pathogenesis *in vivo*. 18 RMs (9 untreated and 9 IFNmod-treated from -1 to 2 days post infection (dpi)) were inoculated with WA1/2020 SARS-CoV-2 and necropsied at days 2, 4, and 7dpi. We compared longitudinal BAL, nasopharyngeal swab, and throat swab viral loads as well as lung and hilar LN tissue viral loads at necropsy between untreated and IFNmod-treated animals. Additionally, to evaluate the impact of IFNmod on SARS-CoV-2 pathogenesis, we also performed mesoscale immunoassay, flow cytometry, and bulk RNAseq as well as scRNAseq analysis.

Study Approval

EPC's animal care facilities are accredited by both the U.S. Department of Agriculture (USDA) and by the Association for Assessment and Accreditation of Laboratory Animal Care (AAALAC). All animal procedures were performed in line with institutional regulations and guidelines set forth by the NIH's Guide for the Care and Use of Laboratory Animals, 8th edition, and were conducted under anesthesia with appropriate follow-up pain management to minimize animal suffering. All animal experimentation was reviewed

and approved by Emory University's Institutional Animal Care and Use Committee (IACUC) under permit PROTO202100003.

Animal models

In the uninfected animal study, 4 (2 females and 2 males; average age of 9 years and 2 months) specific-pathogen free (SPF) Indian-origin rhesus macaques (RM; *Macaca mulatta;* **Table 3.S1)** were housed at Emory National Primate Research Center (ENPRC) in the BSL-2 facility. All four uninfected RMs were administered 1 mg/day of IFN-I modulator (IFNmod) for four consecutive days. IFNmod was supplied in solution and diluted with PBS and administered intramuscularly in the thigh. Peripheral blood (PB) and BAL collections were performed at pre- and post-administration timepoints as annotated **(Fig. 3.1a).**

In the SARS-CoV-2-infected animal study, 20 (8 females and 12 males; average age of 11 years and 8 months) SPF Indian-origin rhesus macaques (**Table 3.S1**) were housed at the ENPRC as previously described [364] in the ABSL3 facility. The number of animals was chosen based on (1) viral loads, (2) monocytes inflammation, and (3) RNA transcriptomic data previously published by our group [173] in SARS-CoV-2 infected RMs treated with a JAK1/2 inhibitor. RMs were infected with $1.1x10^6$ plaque forming units (PFU) SARS-CoV-2 via both the intranasal (1 mL) and intratracheal (1 mL) routes concurrently. Two SARS-CoV-2-infected animals were excluded due to error in specimen processing, resulting in missing time points. Nine RMs were administered 1 mg/day of IFN-I modulator (IFNmod) starting one day prior to infection (-1 dpi) until 2 dpi. IFNmod

was supplied in solution and diluted with PBS and administered intramuscularly in the thigh. The other 9 animals served as untreated, SARS-CoV-2 infected group. At each cage-side access, RMs were clinically scored for responsiveness, discharges, respiratory rate, respiratory effort, cough, and fecal consistency **(Table 3.S2)**. Additionally, at each anesthetic access, body weight, body condition score, respiratory rate, pulse oximetry, and rectal temperature was recorded and RMs were clinically scored for discharges, respiratory character, and hydration **(Table S3)**. Longitudinal tissue collections of peripheral blood (PB); bronchoalveolar lavage (BAL); and nasal, and pharyngeal mucosal swabs in addition to thoracic X-rays (ventrodorsal and right lateral views) were performed immediately following IFNmod administration as annotated (**Fig. 3.3a**). In addition to the tissues listed above, at necropsy the following tissues were processed for mononuclear cells: hilar LN, caudal (lower) lung, cranial (upper) lung, and spleen. Additional necropsy tissues harvested for histology included nasopharynx.

IFNmod production

IFNmod (also named IFN-1ant) is an IFNα2 engineered protein, including the R120E mutation and the terminal 5 amino acids of IFNα8. This results in tight binding to IFNAR2, and below detection binding to IFNAR1 [395, 421]. For expression, IFNmod was cloned in a pET28bdSUMO plasmid [422] and grown in BL21 DE3 cells to OD_{600} of 0.6 at 37°C in 2TY broth, after which, cells were transferred to 15°C and 0.2 mM fresh IPTG was added for overnight growth. Cells were harvested and disintegrated in 50 mM Tris, 100 mM NaCl buffer (pH 8) including Benzonase (Sigma-Aldrich, Cat#: E1014-5KU), protease inhibitor cocktail (Sigma-Aldrich, Cat#: P8465-5ML) and lysozyme (Sigma- Aldrich, Cat# 62970-

5G-F), and purified by NiNTA beads (Ni-NTA beads, Merck, cat. 70666-4). IFNmod fused with SUMO was purified by the on-column cleavage using 50 mM Tris pH 8, 100 mM NaCl and BD-Sumo protease (1:200 from 1mg\ml stock, in-house production) for 2 hr at RT, and then moved to over-night cleavage at 4°C [422]. After elution from NiNTA, IFNmod was subjected to size exclusion chromatography using a Superdex 75 26/60 column. For endotoxin removal, IFNmod was subjected to ToxinEraser™ (GenScript, L00338), with endotoxin levels measured using ToxinSensor™ (GenScript, Cat# l00350). Yields were ~15 mg pure protein per liter.

ISGs induction in IFNmod-treated Calu-3 cells

Human epithelial lung adenocarcinoma cells (Calu-3 cells) were acquired through and authenticated by ATCC (HTB-55). Specifications of authentication are available from the manufacturer. qRT-PCR was performed on uninfected Calu-3 cells treated with various concentrations of IFNmod with or without IFNα to assess induction of antiviral ISGs Mx1 and OAS1 and inflammatory gene CXCL10 as described in the Supplementary Materials.

Impact of IFNmod on SARS-CoV-2 replication in Calu-3 cells

The ability of IFNmod treatment to reduce SARS-CoV-2 replication when initiated pre- and post-infection respectively was assessed in Calu-3 cells as described in the Supplementary Materials.

Viral Stocks

The SARS-CoV-2 NL-02-2020 (BetaCoV/Netherlands/01/NL/2020) viral stock used in Calu-3 cell experiments was obtained from the European Virus Archive.

The SARS-CoV-2 viral stock used in RM experiments (USA-WA/2020 strain) was obtained from BEI Resources (Cat no. NR-53899, Lot: 70040383). Prior to infection, stocks were titered on Vero E6 cells by plaque assay (ATCC, CRL-1586) and sequenced to verify the stock's genomic integrity.

Determination of viral load RNA

SARS-CoV-2 gRNA N and sgRNA E were quantified in nasopharyngeal (NP) swabs, throat swabs, and bronchoalveolar lavages (BAL) as described in the Supplementary Materials. Using remaining viral RNA extracted from NP swabs and BAL, sgRNA E mRNA viral loads were repeated by the NIAD Vaccine Research Center (VRC) as described previously [423, 424] and sgRNA N mRNA was also quantified as detailed in the Supplementary Materials.

SARS-CoV-2 quantification from necropsy samples

Upper cranial lung, lower caudal lung, and hilar LN were collected at necropsy, homogenized, and tissue viral RNA was extracted and quantified as detailed in the Supplementary Materials. Additionally, RNAscope in situ hybridization was performed as previously described [158, 172] to characterize the distribution of SARS-CoV-2 vRNA within lung tissue.

Histopathology and immunohistochemistry

Due to study end point, the animals were euthanized, and a complete necropsy was performed. Various tissue samples including lung, nasal turbinates, trachea, and brain were collected for histopathology which was performed as detailed in the Supplementary Materials. Additionally, immunohistochemical (IHC) staining of Mx1 on sections of lung was performed as previously described [158, 172, 174].

Tissue Processing

Peripheral blood (PB), nasopharyngeal swabs, throat swabs, and BAL were collected longitudinally. At necropsy, lower (caudal) lung, upper (cranial) lung, and hilar LNs were also collected. Detailed methods pertaining to the collection and processing of these tissues are included in the Supplementary Materials.

Bulk and single-cell RNA-Seq Library and sequencing from NHP BALs

Single cell suspensions from BAL were prepared in a BSL3 as described above for flow cytometry and libraries for bulk and sc-RNA-Seq were prepared as described previously [173, 410]. For sc-RNA-Seq, 10,000 cells each from two individual animals containing bar-code hashes were pooled and a total of approximately 20,000 cells were loaded onto the 10X Genomics Chromium Controller. In case of BAL samples, 10,000 cells from two individual animals containing barcode hashes were pooled except for two samples. Additional sequencing details can be found in the Supplementary Materials.

Bulk RNA-Seq analysis

Reads were aligned using STAR v2.7.3. [425]. The STAR index was built by combining genome sequences for Macaca mulatta (Mmul10 Ensembl release 100), SARS-CoV2 (strain MT246667.1 - NCBI). Transcript abundance and differential expression testing were performed using htseq-count [426] and DESeq2 [366] as described previously [410]. A detailed listing of methods for expression and pathway analyses is described in the Supplementary Materials.

Bulk RNA-Seq Whole blood analysis

Bulk RNA-Seq sample preparation and bioinformatic analyses of whole blood samples were performed independently of BAL or PBMC samples and are described in detail in the Supplementary Materials.

Single-cell RNA-Seq Bioinformatic Analysis

The cellranger v6.1.0 (10X Genomics) pipeline was used for processing the 10X sequencing data and the downstream analysis was performed using the Seurat v4.0.4 [427] R package as described previously [410]. A composite reference comprising of Mmul10 from Ensembl release 100 and SARS-CoV2 (strain MT246667.1 - NCBI) was used for alignment of sequencing with cellranger. The percentage of SARS-CoV2 reads was determined using the PercentageFeatureSet for SARS-CoV2 genes. For BAL samples, a total of 62,081 cells across all animals passed QC and were used for analyses. For lung samples, a total of 42,699 cells passed upstream QC and were used for analysis. A detailed breakdown of the number of cells per sample/animals is recorded in **Data File**

S2. Detailed methodology for the sc-RNA-Seq bioinformatics are reported in the Supplementary Materials.

Immunophenotyping

23-parameter flow cytometric analysis was performed on whole blood, fresh PBMCs, and mononuclear cells (10^6 cells) derived from LN biopsies, BAL, and lung as detailed in the Supplementary Materials using anti-human monoclonal antibodies (mAbs), which we [364, 365, 428, 429] and others, including databases maintained by the NHP Reagent Resource (MassBiologics), have shown as being cross-reactive in RMs.

T cell stimulation and intracellular cytokine staining assays

The assay was performed as described before [405, 430]. Briefly, ~2 × 10^6 PBMCs from n=3 animals at days -7pi and 7pi were cultured in 200-µl final volume in 5-ml polypropylene tubes (BD Biosciences, San Diego, CA, USA) in the presence of anti-CD28 (1 µg/ml) and anti-CD49d (1 µg/ml) (BD Biosciences) and the following conditions: (i) negative control with dimethyl sulfoxide only, (ii) whole spike (S) peptide pool 1 (*n* = 253 peptides, 15-mers with 10-residue overlap) (Weiskopf and Sette labs, LJI, La Jolla, CA) at a final concentration of 1 µg/ml, (iii) N peptide pool, and (iv) phorbol 12-myristate 13-acetate/ionomycin. Brefeldin A was added to all tubes at 10 µg/ml (Sigma-Aldrich, St Louis, MO) and cells were cultured for 6 hours and transferred to 4°C before staining for flow cytometry as described in the Supplementary Materials.

SARS-CoV-2 Pseudovirus Neutralization Assays

SARS-CoV-2 Pseudovirus neutralization assay was based on protocol in Crawford et al 2020 [431] and conducted with minor changes to how it was previously reported in Voigt et al 2022 [432]. The revised protocol is detailed in the Supplementary Materials.

Mesoscale

Plasma was collected from EDTA blood following centrifugation at 2500 rpm for 15 minutes. BALF supernatant was obtained from BAL that was filtered through a 70µm cell strainer and spun down at 1800rpm for 5 minutes. Both plasma and BALF were frozen at -80C and later thawed immediately prior to use.

Cytokines were measured using Mesoscale Discovery. Pro-and anti-inflammatory cytokines and chemokines were measured as part of V-Plex (#K15058D-1). INF alpha was measured with a U plex (K156VHK-1 Mesoscale Discovery, Rockville, Maryland). Levels for each cytokine/chemokine were determined in double and following the instructions of the kits. The plates were read on a MESO Quick plex 500 SQ120 machine.

Quantities were determined using the discovery Work bench software for PC (version 4.0).

Statistical Analysis

All statistical analyses were performed two-sided with p-values ≤0.05 deemed significant. Ranges of significance were graphically annotated as follows: *, $p<0.05$; **, $p<0.01$; ***, $p<0.001$; ****, $p<0.0001$. Analyses for Figs. 1g, 2b-c, 2e-h, 3b-l, 4a-k, 5b-c, 5e-g, S1b-d, S2a-b, S3a-d, S4b, S5b-c, and S6b-f were performed with Prism version 8 (GraphPad)

while analyses for Figs. 7c, S9d and S10c were performed with R version 4.0.3 (using function wilcox.test with the parameters paired and correct set to FALSE). The Wald test (DESeq2 package) was used to calculate the BH corrected p-values for Figs. 6b and S7.

Acknowledgments:

We would like to dedicate this manuscript to Dr. Timothy N. Hoang, whose commitment to this project and to scientific discovery were crucial in propelling this study forward. Dr. Hoang will be remembered for his intelligence, drive, and love for science and all of the lives that he touched during his short but impactful career. We thank the Emory National Primate Research Center (EPC) Division of Animal Resources, especially Joyce Cohen, Sherrie M. Jean, and Rachelle L. Stammen in Veterinary Medicine and Stephanie Ehnert, Stacey Weissman, Denise Bonenberger, John M. Wambua, and Racquel Sampson-Harley in Research Resources for providing support in animal care. We would also like to thank Sanjeev Gumber in the EPC Division of Pathology, Kalpana Patel in the EPC Safety Office, Shelly Wang in the Emory CFAR Core, Krista Krish in the EPC Virology Core, Nichole Arnett in the EPC Clinical Pathology Lab, and Elizabeth Beagle, Hadj Aoued, Tristan Horton, David Cowan, Sydney Hamilton, and Thomas Hodder in the Emory NPRC Genomics Core. Additionally, we would like to thank Erin Haupt and the Immunologic Core, Department of Immunology, TNPRC for help with MSD analysis, Elise Smith and Jean Chang in the Gale Lab at WaNPRC for blood RNA-Seq library preparation services, Samuel Beaver for pseudovirus neutralization assays services, and Jana-

Romana Fischer and Kerstin Regensburger at Ulm University Medical Center for excellent technical assistance.

Funding: This work was funded by P510D011132-60S4: COVTEN/ACTIV; the Emory MP3 Grant; Fast Grants #2144, and the Pitts Foundation (all to MPa). Support for this work was also provided by award NIH Office of Research Infrastructure Programs (ORIP) P51OD11132 to EPC, P30 AI050409 to the Emory Center for AIDS Research Systems Immunology Core, 1RO1 HL140223 (to RDL), and P51 OD010425 (WaNPRC; to MGal, LSW, JT-G). FK and KMJS were supported by grants from the German Research Foundation (DFG; CRC 1279 and SP1600/4-1) and the German Federal Ministry for Research and Education (BMBF; Restrict SARS-CoV-2 and IMMUNOMOD). MH is part of the International Graduate School of Molecular Medicine, Ulm. Next generation sequencing services and 10X Genomics captures were performed in the Emory NPRC Genomics Core, which is supported in part by NIH P51OD011132. Sequencing data was acquired on an Illumina NovaSeq6000 funded by NIH S10OD026799 to SEB. The content of this publication does not necessarily reflect the views or policies of the U.S. Department of Health and Human Services, nor does it imply endorsement of organizations or commercial products.

Author contributions:

TNH, EGV, MPi, DCD, RPJ, GSc, SEB, and MPa conceptualized the study. SM produced and validated the activity of IFNmod under the supervision of GSc. JLH wrote the IACUC protocol for the animal studies. EGV, ZS, JLH, and KN processed all RM blood samples

in an aBSL-2 facility. TNH, EGV, and MPi processed all SARS-CoV-2 infected samples in an aBSL-3 suite with assistance from KAK. SPK and RDL developed and optimized lung and heart processing protocols, respectively. GKT conducted PBMC and BAL bulk RNA-seq analysis and GKT and SEB graphed bulk RNA-seq data. MV performed Mesoscale analysis on plasma and BAL fluid from uninfected and SARS-CoV-2-infected RMs. MH performed uninfected Calu-3 experiments and qRT-PCR analysis of ISGs in both uninfected and SARS-CoV-2-infected Calu-3 experiments. RN conducted SARS-CoV-2 infection experiments in Calu-3 cells and qRT-PCR analysis of viral RNA. CW, JSW, and FC-S conducted all longitudinal animal collection procedures for SARS-CoV-2-infected RMs in the aBSL-3 and EHC performed necropsy collections. THV measured gRNA-N and sgRNA-E viral loads in nasopharyngeal and throat swabs, BAL, and necropsy tissues. MG performed repeat measurements of sgRNA-E as well as sgRNA-N viral loads in nasopharyngeal swabs and BAL. MR and SK performed lung pathology scoring. KB-S and JDE performed and analyzed IHC and RNAscope in situ hybridization experiments. TNH, EGV, ZS, and KN performed multi-parameter flow cytometry and TNH and EGV analyzed flow data. AP and SPK performed and analyzed T cell stimulation and intracellular cytokine staining assays. EAV assayed serum neutralizing antibody titers. JT-G and LSW performed and analyzed whole blood RNA-seq under the supervision of MGal. KLP performed 10X Genomics scRNA-seq and AKB performed pre-processing for single-cell BAL data. AAU conducted and graphed all scRNA-seq analyses. CMM performed targeted mass spectrometry to measure IFNmod in uninfected animals under the supervision of DEG. Funding was acquired by RDL, FK, RPJ, and MPa. EGV, TNH,

AAU, SEB, and MPa wrote the manuscript with critical inputs from ZS, MPi, JLH, MGal, GSi, KMJS, RPJ, FK, and GSc.

Competing interests:

The authors declare that they have no competing interests.

Data and materials availability:

Data tables for expression counts for bulk and single-cell RNA-Seq for BAL are deposited in NCBI's Gene Expression Omnibus and are accessible through the Gene Expression Omnibus (GEO) accession GSE205429. Transcriptomics data sets from whole blood RNA sequencing are deposited at the GEO accession number GSE207665. The processed single-cell lung macrophages reference dataset [410] was originally obtained from GEO GSE14975833 [433]. Custom scripts and supporting documentation on the RNA-Seq analyses will be made available at https://github.com/BosingerLab/NHP_COVID_IFNmod.(DOI 10.5281/zenodo.8082029) The R markdown code applied to the analyses of whole blood can be accessed at https://github.com/galelab/Paiardini_Modulation_type_I_Interferon. The R markdown code applied to the analyses of whole blood can be accessed at https://github.com/galelab/Paiardini_Modulation_type_I_Interferon.

All data needed to evaluate the conclusions in the paper are present in the paper or the Supplementary Materials.

Supplementary Materials

Materials and Methods

ISGs induction in IFNmod-treated Calu-3 cells

Calu-3 cells were seeded in 48 well plates. 24 hours post-seeding, cells were treated with 0, 0.004, 0.04, or 0.4 *μ*g/ml IFNmod with or without 0.04 μg/ml IFNα. 24 hours later, cells were harvested for qRT-PCR analysis. Total RNA extraction was performed using the Quick-RNA Microprep Kit (Zymo research) according to the manufacturer's instructions. On a StepOnePlus Real-Time PCR System (Applied Biosystems), reverse transcription and qRT–PCR were performed in one step using a SuperScript III Platinum Kit (Thermo Fisher Scientific) following the manufacturer's instructions. Each TaqMan probe (OAS1, Hs05048921_s1; Mx1, Hs00895608_m1; CXCL10, Hs00171042_m1; β-Actin, Hs99999903_m1) was acquired as premixed TaqMan Gene Expression Assays (Thermo Fisher Scientific) and added to the reaction. Expression levels of each target gene were calculated by normalizing to Actin levels using the ΔΔCT method.

Impact of IFNmod on SARS-CoV-2 replication in Calu-3 cells

For pre-infection treatment initiation experiments, 30,000 Calu-3 cells were seeded in 96 well plates and allowed to rest for 24 hours. Cells were then either treated with IFNmod (0.004, 0.04, or 0.4 μg/ml) or IFNα (20, 100 and 500 IU/ml) 24 hours prior to infection, treated with Nirmatrelvir (0.1, 1, and 10μM) 1 hour prior to infection, or left untreated. Cells were then infected with SARS CoV-2 NL-02-2020 (MOI 0.1) and, 5h post infection, were washed once with PBS, supplemented with fresh media, and treated again with IFNmod,

IFNα, or Nirmatrelvir respectively. 48h later, supernatants and cells were harvested for qRT-PCR analysis.

For post-infection treatment initiation experiments, 30,000 Calu-3 cells were seeded in 96 well plates and allowed to rest for 48 hours. Cells were then infected with SARS CoV-2 NL-02-2020 (MOI 0.1) and, 5h post infection, were washed once with PBS, supplemented with fresh media, and treated with IFNmod (0.004, 0.04, or 0.4 µg/ml), IFNα (20, 100 and 500 IU/ml), or Nirmatrelvir ((0.1, 1, and 10µM) respectively. 48h later, supernatants and cells were harvested for qRT-PCR analysis.

N (nucleoprotein) transcript levels were determined in supernatants collected from SARS-CoV-2 infected Calu-3 cells. Total RNA was isolated using the Viral RNA Mini Kit (Qiagen, Cat#52906) according to the manufacturer's instructions. RT-qPCR was performed as previously described using TaqMan Fast Virus 1-Step Master Mix (Thermo Fisher, Cat#4444436) and a OneStepPlus Real-Time PCR System (96-well format, fast mode). Primers were purchased from Biomers (Ulm, Germany) and dissolved in RNAse free water. Synthetic SARS-CoV-2-RNA (Twist Bioscience, Cat#102024) or RNA isolated from BetaCoV/France/IDF0372/2020 viral stocks quantified via this synthetic RNA (for low CT samples) were used as a quantitative standard to obtain viral copy numbers. All reactions were run in duplicates. Forward primer (HKU-NF): 5'-TAA TCA GAC AAG GAA CTG ATT A-3'; Reverse primer (HKU-NR): 5'-CGA AGG TGT GAC TTC CAT G-3'; Probe (HKU-NP): 5'-FAM-GCA AAT TGT GCA ATT TGC GG-TAMRA-3'.

Determination of viral load RNA

Nasopharyngeal and throat swabs were placed in 2mL of PBS (CORNING). Virus was inactivated by mixing 1:1 with Buffer ATL (Qiagen) prior to viral RNA extraction from NP swabs, throat swabs, and BAL on fresh, inactivated specimens. Viral RNA was extracted on the QIASymphony SP platform using the DSP virus/pathogen kit according to the manufacturer's protocols. Quantitative PCR (qPCR) was performed on viral RNA samples using the N2 primer and probe set designed by the CDC for their diagnostic algorithm: CoV2-N2-F: 5'-TTACAAACATTGGCCGCAAA-3', CoV2-N2-R: 5'-GCGCGACATTCCGAAGAA-3', and CoV2-N2-Pr: 5'-FAM-ACAATTTGCCCCCAGCGCTTCAG-BHQ-3'. The primer and probe sequences for the sub-genomic mRNA or sgRNA transcript of the E gene are SGMRNA-E-F: 5'-CGATCTCTTGTAGATCTGTTCTC-3', SGMRNA-E-R: 5'-ATATTGCAGCAGTACGCACACA-3', and SGMRNA-E-Pr: 5'-FAM-ACACTAGCCATCCTTACTGCGCTTCG-3'. qPCR reactions were performed in duplicate with the TaqMan Fast Virus 1-step Master Mix using the manufacturer's cycling conditions, 200nM of each primer, and 125nM of the probe. The limit of detection in this assay was 70 copies per mL of PBS or BAL. To verify sample quality the CDC RNase P p30 subunit qPCR was modified to account for rhesus macaque specific polymorphisms. The primer and probe sequences are RM-RPP30-F 5'-AGACTTGGACGTGCGAGCG-3', RM-RPP30-R 5'-GAGCCGCTGTCTCCACAAGT-3', and RPP30-Pr 5'-FAM-TTCTGACCTGAAGGCTCTGCGCG-BHQ1-3'. A single well from each extraction was run as above to verify RNA integrity and sample quality via detectable and consistent cycle threshold values. All quantities were determined using *in vitro* transcribed RNA

standards that were verified with quantified viral RNA stocks acquired from ATCC and BEI Resources. For repeat sgRNA E mRNA viral loads, the following primer and probe sets were used: sgLeadSARSCoV2_F (5′-CGATCTCTTGTAGATCTGTTCTC-3′), E_Sarbeco_P (5′-FAM-ACACTAGCCATCCTTACTGCGCTTCG-BHQ1-3′), and E_Sarbeco_R (5′-ATATTGCAGCAGTACGCACACA-3′). Viral sgRNA N mRNA was also quantified by the VRC using the following primer and probe sets: Forward: 5′-CGATCTCTTGTAGATCTGTTCTC-3′, Probe: 5′-FAM-TAACCAGAATGGAGAACGCAGTGGG-BHQ1–3′, Reverse: 5′-GGTGAACCAAGACGCAGTAT-3′). The lower limit of detection for the assay conducted at the VRC was 50 copies per mL of PBS or BAL.

SARS-CoV-2 quantification from necropsy samples

An approximately 0.5 cm^3 sample of each tissue (lower caudal lung, upper cranial lung, and hilar LN) was collected at necropsy, placed in 1mL RNAlater Solution (invitrogen), stored at 4°C for 24 hours, and then frozen at -80°C. ~50mg of each thawed sample was transferred to a microcentrifuge tube containing a 5mm stainless steel bead (Qiagen, Part No. 69989) and 1200 µL Buffer RLT Plus, and homogenized twice for 1-5 minutes each at 25Hz using a TissueLyser LT sample disruptor (Qiagen, Part No. 85600) with a 12 tube Tissue Lyser LT adapter (Qiagen, Part No. 69980). Following centrifugation of the samples at maximum speed for 3 minutes, the supernatant of the samples was collected. Tissue RNA was extracted from homogenized supernatants on the Qiasymphony SP platform using the QIAsymphony RNA Kit (Qiagen, Part No. 931636). Viral RNA was quantified as above and normalized to the copy number of RPP30.

Histopathology and immunohistochemistry

For histopathologic examination, tissue samples including lung, nasal turbinates, trachea, and brain were fixed in 4% neutral-buffered paraformaldehyde for 24h at room temperature, routinely processed, paraffin-embedded, sectioned at 4μm, and stained with hematoxylin and eosin (H& E). The H&E slides from all tissues were examined by two board certified veterinary pathologists. For each animal, all the lung lobes were used for analysis and affected microscopic fields were scored. Scoring was performed based on these criteria: number of lung lobes affected, type 2 pneumocyte hyperplasia, alveolar septal thickening, fibrosis, perivascular cuffing, peribronchiolar hyperplasia, inflammatory infiltrates, hyaline membrane formation. An average lung lobe score was calculated by combining scores from each criterion. Digital images of H&E stained slides were captured at 40× and 200× magnification with an Olympus BX43 microscope equipped with a digital camera (DP27, Olympus) using Cellsens® Standard 2.3 digital imaging software (Olympus).

Tissue Processing

PB was collected from the femoral vein in sodium citrate, serum separation, and EDTA tubes from which plasma or serum was separated by centrifugation within 1 hour of phlebotomy. Serum from blood collected in serum separator tubes and plasma from blood collected in sodium citrate tubes were used for comprehensive blood chemistry panels. EDTA PB was used for complete blood counts, whole blood staining, and PBMC isolation and staining. Following the centrifugation of EDTA PB and the removal of plasma, 500uL

of the remaining fraction of blood was lysed with ACK lysis buffer, pelleted via centrifugation, and washed twice with PBS in preparation for whole blood flow cytometry staining. Peripheral blood mononuclear cells (PBMCs) were also isolated from the fraction of EDTA blood remaining following the removal of plasma using a Ficoll-Paque Premium density gradient (GE Healthcare), and washed with R-10 medium. R-10 medium was composed of RPMI 1640 (Corning) supplemented with 10% heat-inactivated fetal bovine serum (FBS), 100 IU/mL penicillin, 100 µg/mL streptomycin, and 200 mM L-glutamine (GeminiBio).

Nasopharyngeal swabs were collected under anesthesia by using a clean flocked nylon-tipped swab (Azer Scientific Inc, Nasopharyngeal swab Individually wrapped, sterile, 76422-824, VWR International) placed approximately 2-3cm into the nares. Oropharyngeal swabs were collected under anesthesia using polyester tipped swabs (Puritan Standard Polyester Tipped applicator, polystyrene handle, 25-806 2PD, VWR International) to streak the tonsils and back of throat bilaterally (throat/pharyngeal). The swabs were dipped in 2 mL PBS (Corning) and vortexed for 30 sec, and the eluate was collected.

To collect BAL, a fiberoptic bronchoscope (Olympus BF-XP190 EVIS EXERA III ULTRA SLM BRNCH and BF-P190 EVIS EXERA 4.1mm) was manipulated into the trachea, directed into the primary bronchus, and secured into a distal subsegmental bronchus upon which 35-70 mL of normal saline (0.9% NaCl) was administered into the bronchus and re-aspirated to obtain a minimum of 20ml of lavage fluid. At necropsy, a large sterile

syringe with the plunger removed was inserted into the tracheal opening and approximately 150 ml of sterile 1 x PBS was poured into both sides of the lungs. The syringe was then removed and re-inserted into the tracheal opening with the plunger replaced. Lavage fluid was then pulled back into the syringe and dispensed into conical tubes. BAL was filtered through a 70µm cell strainer and multiple aliquots were collected for viral loads. Next, the remaining BAL was centrifuged at 2200rpm for 5 minutes and the BAL fluid supernatant was collected for mesoscale analysis. Pelleted BAL cells were resuspended in R10 and used for downstream analyses including 10x, Bulk RNAseq, and flow cytometry.

The lower portions of the cranial (upper) lung lobes and the bilateral upper portions of the caudal (lower) lung lobes were collected at necropsy. Lung tissue was injected with digestion media containing 0.4mg/mL DNase I (StemCell Technologies), 2.5 mg/mL of Collagenase D (Roche), and 0.2mg/mL Liberase TL Research Grade (Sigma-Aldrich) in HBSS using a blunt end needle. Next, lung tissue was cut into small pieces using blunt end scissors and incubated in digestion media at 37C for 1 hour. Lung tissue was then transferred into gentleMACS C tubes (Miltenyi Biotec) and homogenized using a gentleMACS Dissociator, program “Lung 02_01” (Miltenyi Biotec). The resulting homogenized tissue was filtered through a 100µm BD Falcon cell strainer and washed with R-10 medium.

Hilar LN biopsies were collected at necropsy, sectioned using blunt, micro-dissection scissors and mechanically disrupted through a 70µm cell strainer and washed with R-10 media.

Mononuclear cells were counted for viability using a Countess II Automated Cell Counter (Thermo Fisher) with trypan blue stain and were cryo-preserved in aliquots of up to $2x10^7$ cells in 10% DMSO in heat-inactivated FBS. Whole tissue segments (0.5 cm^3) were snap frozen dry or stored in RNAlater (Qiagen) for analyses of RNA-seq and tissue viral quantification, respectively.

Bulk and single-cell RNA-Seq Library and sequencing of BAL samples
For bulk RNA-Seq, 50,000 cells were lysed directly into 700 ul of QIAzol reagent and RNA was isolated using the miRNeasy Micro kit (Qiagen) with on-column DNase digestion. RNA quality was assessed using an Agilent Fragment Analyzer and ten nanograms of total RNA was used as input for cDNA synthesis using the Clontech SMART-Seq v4 Ultra Low Input RNA kit (Takara Bio) according to the manufacturer's instructions. Amplified cDNA was fragmented and appended with dual-indexed bar codes using the NexteraXT DNA Library Preparation kit (Illumina). Libraries were validated by capillary electrophoresis on an Agilent Fragment Analyzer, pooled at equimolar concentrations, and sequenced on an Illumina NovaSeq6000. For single-cell RNA-Seq, approximately 20,000 cells were loaded onto the 10X Genomics Chromium Controller in the BSL3 facility using the Chromium NextGEM Single Cell 5' Library & Gel Bead kit according to manufacturer instructions [434]. The resulting gene expression libraries were sequenced as

paired-end 26x91 reads on an Illumina NovaSeq6000 targeting a depth of 50,000 reads per cell. Cell Ranger software was used to perform demultiplexing of cellular transcript data, and mapping and annotation of UMIs and transcripts for downstream data analysis.

Bulk RNA-Seq analysis

Reads were aligned using STAR v2.7.3. (*73*). The STAR index was built by combining genome sequences for Macaca mulatta (Mmul10 Ensembl release 100), SARS-CoV2 (strain MT246667.1 - NCBI). The gffread utility (https://github.com/gpertea/gffread) was used to convert gff3 file for SARS-CoV2 and the resulting gtf file for SARS-CoV2 was edited to include exon entries which had the same coordinates as CDS to get counts with STAR. The combined genomic and gtf files were used for generating the STAR index. Transcript abundance estimates were calculated internal to the STAR aligner using the algorithm of htseq-count [426]. The ReadsPerGene files were read in R constructing a count matrix that was imported in DESeq2 using the DESeqDataSetFromMatrix function. DESeq2 was used for normalization [366], producing both a normalized read count table and a regularized log expression table. Only the protein coding genes defined in the gtf file were used for analysis. The design used was: ~ Subject + Treatment * Timepoint. The regularized log expression values were obtained using the rlog function with the parameters blind =FALSE and filtType = “parametric”. GSEA 4.1.0 (https://www.gsea-msigdb.org/) was used for gene set enrichment analysis with the following gene sets: Hallmark and Reactome and Biocarta Canonical pathways (MsigDB), NHP ISGs (*40*). GSEA was run with default parameters with the permutation type set to gene_set. The input for GSEA was the regularized log expression values obtained from DESeq2 which

was filtered to remove genes with mean expression <=0. The regularized log expression values were also used to generate heatmaps using the Complex Heatmap R library.

Bulk RNA-Seq Whole blood analysis

Whole blood was collected from RM into PAXgene RNA tubes (PreAnalytiX) according to the manufacturer's instructions. RNA was isolated using RNAdvance Blood Kit (Beckman) following the manufacturer's instructions. mRNAseq libraries were constructed using KAPA RNA HyperPrep Kit with RiboErase (HMR) Globin in conjunction with the KAPA mRNA Capture Kit (Roche Sequencing). Libraries were sequenced on an Illumina NextSeq500 sequencer using Illumina NextSeq 500/550 High Output v23 (150 cycles) following the manufacturer's protocol for sample handling and loading. Reads were initially filtered for hemoglobin and rRNA reads using bowtie 2.4.2, and then aligned to the *Macaca mulatta* (Mmul10 Ensembl release 100) genome using STAR v2.7.5a. Final counts were then generated with HTSeq-count v0.13 [425, 426, 435]. Genes with a mean count across samples lower than 5 were filtered from the analysis. Counts were normalized using TMM normalization/voom [436-438]. Differential gene analysis was done using limma with design (~0 +time:treatment + animal) with an adjusted pval cutoff of 0.05 and absolute LFC value greater than 0.58 comparing 1,2,4,5 and 7 dpi to baseline at each time-point for animals treated with IFNmod and untreated animals (infected with SARS-CoV-2) [438]. Over representation analysis was performed on significant DE genes using SetRank [439]. To identify pathways significantly enriched (adjusted P val < 0.05). Activity of pathways of interest were illustrated by calculating the mean logCPM value of genes in each pathway across time.

Single-cell RNA-Seq Bioinformatic Analysis

The cellranger v6.1.0 (10X Genomics) pipeline was used for processing the 10X sequencing data and the downstream analysis was performed using the Seurat v4.0.4 [427] R package. A composite reference comprising of Mmul10 from Ensembl release 100 and SARS-CoV2 (strain MT246667.1 - NCBI) was used for alignment with cellranger. The percentage of SARS-CoV2 reads was determined using the PercentageFeatureSet for SARS-CoV2 genes.

For BAL samples, the samples were demultiplexed using HTODemux function in Seurat. The gene expression matrix was filtered to include protein coding genes and exclude genes encoded on Y chromosome, B and T cell receptor genes, mitochondrial genes, RPS and RPL genes and SARS-CoV2 genes. The cells were further filtered on the following criteria: nFeature_RNA >=500 and <= 3500, ncount_RNA >=250 and log10GenesPerUMI > 0.8. After filtering, the samples were normalized using SCTransform method [440] and integrated using the first 30 dimensions with the default CCA method [441]. Three samples were dropped - two due to low cell numbers (RNi17 4 dpi and RZs14 7 dpi) and one for large proportion of epithelial cells (CD68 baseline). The downstream analyses was carried out with the remaining samples comprising of 62,081 cells. The number of cells per sample is shown in **Data File 2**. The integrated object was split into individual samples and after filtering the three samples, the remaining samples were normalized using the SCTransform method [440] and then integrated using the reciprocal PCA method [441]. The first 30 dimensions were used with the

FindIntegrationAnchors, FindUMAP and FindNeighbors method. Clustering was carried out using the default Louvain method and the resolution was set to 1. Cell annotations were carried out based on the expression of canonical markers in seurat clusters and SingleR v1.4.0 library (Blueprint Encode database) [331] annotations were used as a guide. As a distinct cluster could not be determined for neutrophils based on the expression of canonical marker genes, the SingleR annotations were used for neutrophils. Differential gene expression analysis was carried out using the FindMarkers function with "MAST" [373] method.

To further classify the macrophages/monocytes in BAL, only cells in the largest cluster comprising the macrophages/monocytes were further processed. The subset function was used to get these cells followed by splitting the object in individual samples. The MapQuery function was used to map individual samples to a reference lung macrophage/monocyte dataset from three healthy rhesus macaques obtained from a previously published study [433] using the same approach that we have previously described [410].

For lung samples, we processed sections of lower (caudal) lung obtained from animals necropsied at 2 dpi (n=3 Untreated, n=3 IFNmod) and 7 dpi (n=1 Untreated, n=1 IFNmod). Two of the 2 dpi samples were dropped (one from each group), due to low cell recovery. The cellranger pipeline was used as described above. The filtered counts were read into Seurat using the Read10X_h5 function. The gene expression matrix was filtered to include protein coding genes and exclude genes encoded on Y chromosome, B and T cell receptor genes, mitochondrial genes, RPS and RPL genes and SARS-CoV2 genes.

The cells were filtered based on the following criteria: (i) nFeature_RNA between 500 and 5000 and (ii) percent mitochondrial genes <= 25%. Normalization was performed using SCTransform and the samples were integrated using reciprocal PCA. The first 30 dimensions were used and clustering was carried out with the resolution set to 0.1 using the default Louvain algorithm in seurat. The clusters were annotated based on the expression of canonical markers and roughly divided into four major subsets: epithelial, myeloid, lymphoid and others. Each subset was then clustered separately to fine tune the cell type annotations. The human Lung v1 reference [413] in Azimuth (https://azimuth.hubmapconsortium.org/) was used to guide the cell annotations. Based on the expression of canonical markers, some clusters were classified as doublets and some remained unassigned. After removing the doublets and unassigned clusters, UMAPs showed some additional cells that coincided with the removed doublets/unassigned clusters and these were removed as well. Finally, a total of 42,699 cells were used subsequently for downstream analysis. The number of cells per sample is recorded in **Data File 2.** Differential gene expression analysis was carried out using the FindMarkers function with "MAST" method. Over –representation analysis was carried out using clusterProfiler v4.5.0.992 [442] with Hallmark, Reactome, KEGG and BioCarta genesets from the msigdb database [367, 443, 444]. The msigdbr v7.5.1 library (https://igordot.github.io/msigdbr/) was used for retrieving the msigdb databases.

Immunophenotyping

A panel of the following mAbs was used for longitudinal T-cell phenotyping in PBMCs: anti-CCR7-BB700 (clone 3D12; 2.5 µL; cat. # 566437), anti-CXCR3-BV421 (clone IC6; 2.5 µL; cat. # 562558), anti-Ki-67-BV480 (clone B56; 5 µL; cat. # 566109), anti-CCR4-BV750 (clone 1G1 1E5; 2.5 µL; cat. # 746980), anti-CD3-BUV395 (clone SP34-2; 2.5 µL; cat. # 564117), anti-CD8-BUV496 (clone RPA-T8; 2.5 µL; cat. # 612942), anti-CD45-BUV563 (clone D058-1283; 2.5 µL; cat. # 741414), anti-CD49a-BUV661 (clone SR84; 2.5 µL; cat. # 750628), anti-CD28-BUV737 (clone CD28.2; 5 µL; cat. # 612815), anti-CD69-BUV805 (clone FN50; 2.5 µL; cat. # 748763), and Fixable Viability Stain 700 (2 µL; cat. # 564997) all from BD Biosciences; anti-CD95-BV605 (clone DX2; 5 µL; cat. # 305628), anti-HLA-DR-BV650 (clone L243; 5 µL; cat. # 307650), anti-CD25-BV711 (clone BC96; 5 µL; cat. # 302636), anti-PD-1-BV785 (clone EH12.2H7; 5 µL; cat. # 329930), anti-CD101-PE-Cy7 (clone BB27; 2.5 µL; cat. # 331014), anti-FoxP3-AF647 (clone 150D; 5 µL; cat. # 320014), and anti-CD4-APC-Cy7 (clone OKT4; 2.5 µL; cat. # 317418) all from Biolegend; anti-CD38-FITC (clone AT1; 5 µL; cat. # 60131FI) from STEMCELL Technologies; and anti-CXCR5-PE (clone MU5UBEE; 5 µL; cat. # 12-9185-42), anti-GranzymeB-PE-TexasRed (clone GB11; 2.5 µL; cat. # GRB17), and anti-CD127-PE-Cy5 (clone eBioRDR5; 5 µL; cat. # 15-1278-42) all from Thermo Fisher. mAbs for chemokine receptors (i.e. CCR7) were incubate at 37°C for 15 min, and cells were fixed and permeabilized for 30 min at room temperature using a FoxP3 / Transcription Factor Staining Buffer Kit (Tonbo Biosciences; cat. # TNB-0607-KIT). A panel of the following mAbs was used for the longitudinal phenotyping of innate immune cells in whole blood (500 µL), as described in [445], and mononuclear cells ($2x10^6$ cells) derived from LN biopsies, BAL, and lung: anti-CD20-BB700 (clone 2H7; 2.5 µL; cat. # 745889), anti-

CD11b-BV421 (clone ICRFF44; 2.5 µL; cat. # 562632), anti-Ki-67-BV480 (clone B56; 5 µL; cat. # 566109), anti-CD14-BV605 (clone M5E2; 2.5 µL; cat. # 564054), anti-CD56-BV711 (clone B159; 2.5 µL; cat. # 740781), anti-CD163-BV750 (clone GHI/61; 2.5 µL; cat. # 747185), anti-CD3-BUV395 (clone SP34-2; 2.5 µL; cat. # 564117), anti-CD8-BUV496 (clone RPA-T8; 2.5 µL; cat. # 612942), anti-CD45-BUV563 (clone D058-1283; 2.5 µL; cat. # 741414), anti-CCR2-BUV661 (clone LS132.1D9; 2.5 µL; cat. # 750472), anti-CD16-BUV737 (clone 3G8; 2.5 µL; cat. # 564434), anti-CD101-BUV805 (clone V7.1; 2.5 µL; cat. # 749163), anti-CD169-PE (clone 7-239; 2.5 µL; cat. # 565248), and anti-CD206-PE-Cy5 (clone 19.2; 20 µL; cat. # 551136) and Fixable Viability Stain 700 (2 µL; cat. # 564997) all from BD Biosciences; anti-ACE2-AF488 (clone Polyclonal; 5 µL; cat. # FAB9332G-100UG) from R & D; anti-HLA-DR-BV650 (clone L243; 5 µL; cat. # 307650), anti-CD11c-BV785 (clone 3.9; 5 µL; cat. # 301644), and anti-CD123-APC-Fire750 (clone 315; 2.5 µL; cat. # 306042) all from Biolegend; anti-GranzymeB-PE-TexasRed (clone GB11; 2.5 µL; cat. # GRB17) from Thermo Fisher; anti-CD66abce-PE-Vio770 (clone TET2; 1 µL; cat. # 130-119-849) from Miltenyi Biotec; anti-NKG2A-APC (clone Z199; 5 µL; cat. # A60797) from Beckman Coulter. mAbs for chemokine receptors (i.e. CCR2) were incubated at 37°C for 15 min, and cells were fixed and permeabilized at room temperature for 15 min with Fixation/Permeabilization Solution Kit (BD Biosciences; cat. #554714). All samples were fixed with 4% paraformaldehyde and acquired within 24 hours of fixation. For each sample a minimum of $1.2x10^5$ stopping gate events (live $CD3^+$ T-cells) were recorded. Acquisition of data was performed on a FACSymphony A5 (BD Biosciences) driven by FACS DiVa software and analyzed with FlowJo (version 10.7; Becton, Dickinson, and Company).

T cell stimulation and intracellular cytokine staining assays

E-fluor 780 Viability dye (E-bioscience/Thermofisher) was used to stain for dead cells and the following antibodies known to cross-react with RM cells were used in staining cells as described before [405, 430] (BV421, anti-human CD4 (Clone; OKT4) and PerCP Cy5.5, anti-human CD8a (Clone; RPA-T8) antibodies from Biolegend were used in surface staining. BV655 anti-human CD3 (Clone; SP34-2, BD Biosciences), Alexa-488 anti human IL-2 (Clone; MQ1-17H12) and Alexa-647 anti human IFN-γ (Clone; 4S.B3) from Biolegend, PE-Cy7 anti human TNF (Clone; Mab11) from Thermofisher and PE anti human IL-4 (Clone; 7A3-3) was procured from Miltenyi Biotec. Stained cells were acquired using a Fortessa Flow Cytometer (BD Biosciences, CA). Flow cytometry data was analyzed using Flow Jo (TreeStar, Or).

SARS-CoV-2 Pseudovirus Neutralization Assays

Human Angiotensin-Converting Enzyme 2-expressing HEK-293 cells (BEI Resources, #NR-52511) were plated at $5*10^4$ cells/well in 96 well flat bottom tissue culture treated plates and incubated overnight at 37° C + 5% CO_2. The following day, the experimental NHP sera along with a SARS-Cov-2 convalescent NHP control (BEI resources NR52401) and Naïve mouse sera were initially diluted 1:10 in media (Gibco DMEM with GlutaMAX and 10% FBS) and then serially diluted 1:2 across a 96 well round bottom plate for a total of 11 dilutions. Pseudovirus expressing the wild-type SARS-Cov-2 spike protein was thawed at room temperature and then diluted to a normalized value of $1*10^8$ total integrated intensity units/mL. The diluted pseudovirus was added 1:1 to samples on the

plate after which the plates were incubated at 37°C + 5% CO_2 for 1 hour. After the 1-hour incubation, the pseudovirus/serum mixtures were added to the HEK 293T Human-Ace-2 cells, which each sample repeated in quadruplicate. Polybrene (Sigma-Aldrich TRG1003) was added at a final concentration of 5ug/mL to each well of the plate. The plates were incubated for 72 hours at 37° C + 5% CO_2. Plates were imaged on a fluorescent plate imager for Zs green expression (ImageXpress Pico Automated Cell Imaging System, Molecular Devices, San Jose, CA). The total integrated intensity per well output was used to calculate the percent pseudovirus inhibition in each well. The percent pseudovirus inhibition was fit with a four-parameter sigmoidal curve to calculate IC_{50} values for each sample.

Chapter Three Figures

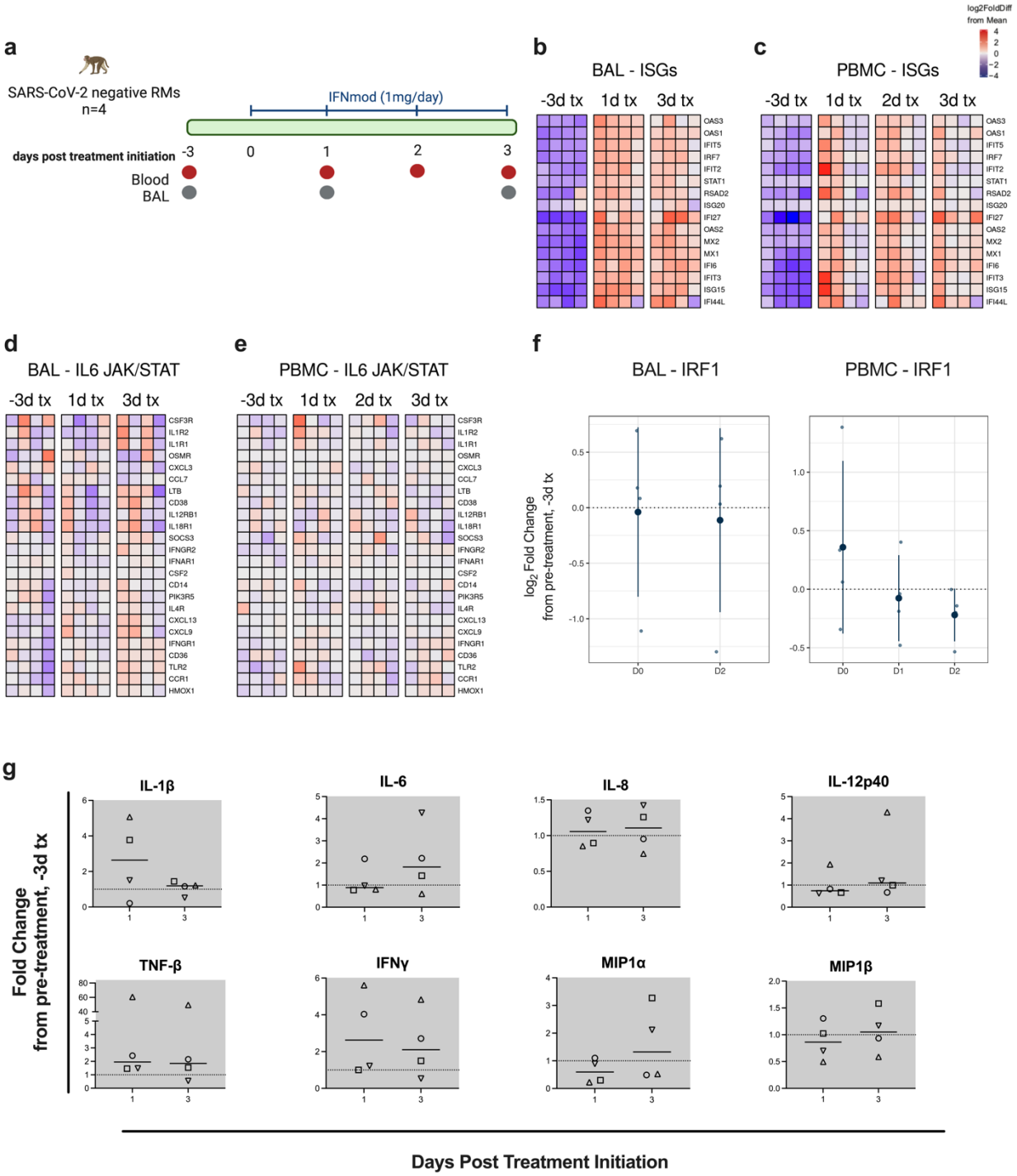

Figure 3.1. Administration of IFNmod in uninfected RMs resulted in modest upregulation of ISGs without changes to inflammatory genes or inflammatory cytokines and chemokines. (a) Study design of IFNmod treatment in uninfected RMs; 1mg IFNmod was administered intramuscularly to n=4 uninfected RMs (7-10 years old, median = 9.5 years) for four consecutive days. Blood and BAL were collected at pre-treatment baseline (3 days before treatment initiation) and once a day from days 1-3 post

treatment initiation, with the exception of day 2 post treatment initiation, where only blood was collected. Heatmaps of ISG expression in **(b)** BAL and **(c)** PBMC of uninfected RMs before and after IFNmod treatment. Heatmaps of genes associated with IL-6 signaling and inflammation in **(d)** BAL and **(e)** PBMC of uninfected RMs before and after IFNmod treatment. **(f)** Distribution of log2 fold-changes of IRF1 relative to pre-treatment baseline (-3d tx). Filled dots represent the mean, and lighter dots are individual data points. **(g)** Fold change of cytokines and chemokines in BAL fluid relative to pre-treatment baseline (-3d tx) measured by mesoscale. Statistical analyses for mesoscale analysis were performed using one-tailed Wilcoxon signed-rank tests. Each black, open symbol represents an uninfected RM. Black lines represent median fold change. Gray-shaded boxes indicate that timepoint occurred during IFNmod treatment. The color scale depicted in the top right of panel c indicates log2 expression relative to the mean of all samples and is applicable to panels b-e.

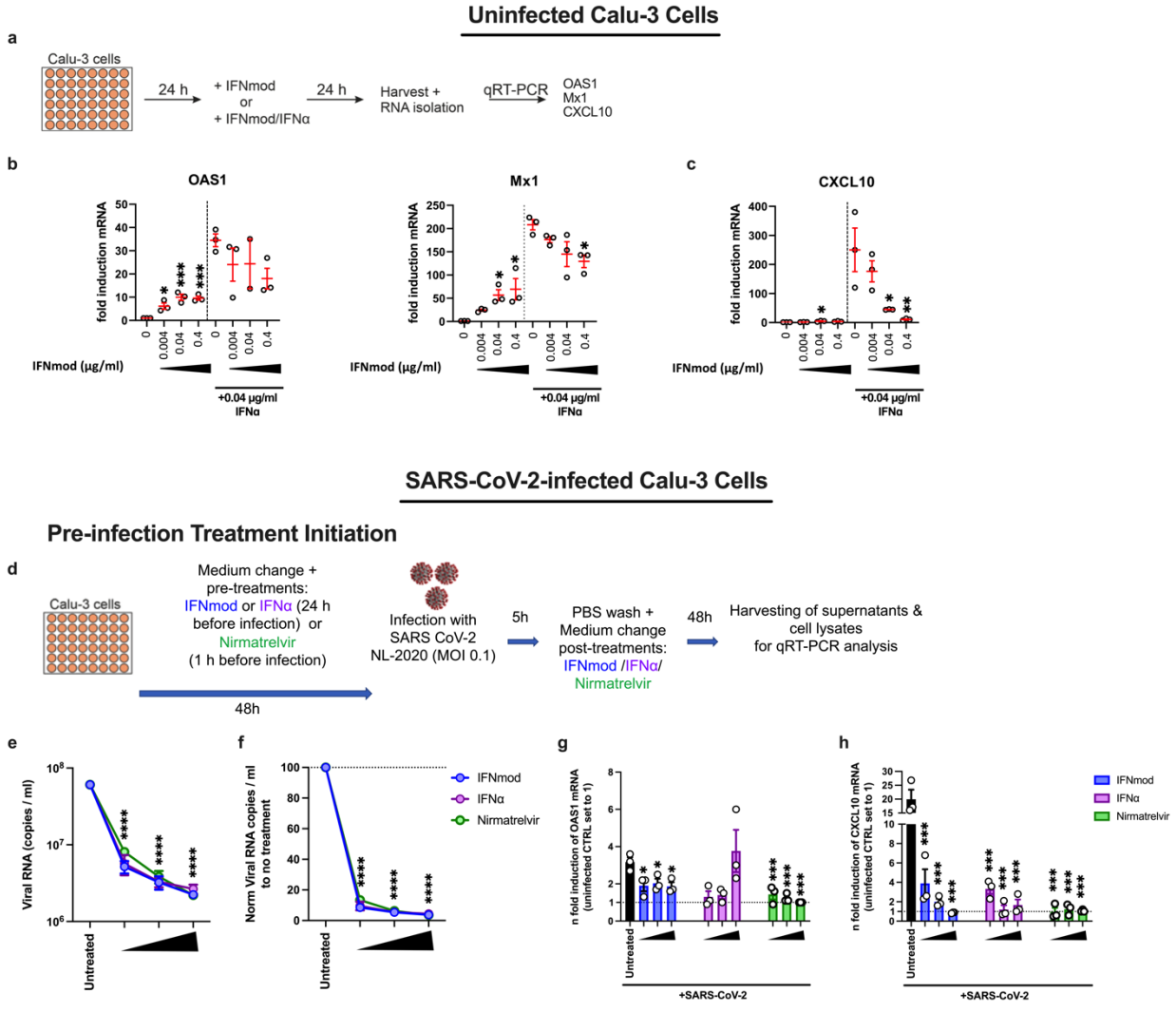

Figure 3.2. Administration of IFNmod in Calu-3 human lung cells modulated type I IFN responses and inhibited SARS-CoV-2 replication to levels comparable to

Nirmatrelvir. (a) Overview of uninfected Calu-3 cell culture setup with IFNmod (0.004, 0.04, and 0.4 µg/ml) +/- IFNα (0.04 µg/ml) treatment. mRNA fold induction of **(b)** antiviral genes OAS1 and Mx1 and **(c)** inflammatory gene CXCL10 in Calu-3 cells following IFNmod (0.004, 0.04, or 0.4 µg/ml) +/- IFNα (0.04 µg/ml) treatment from three independent Calu-3 experiments. Statistical analyses were performed using ordinary ANOVA with Dunnett's multiple comparisons tests comparing IFNmod +/- IFNα treated samples to the respective no IFNmod controls. **(d)** Overview of Calu-3 SARS-CoV-2 cell culture setups with IFNmod (0.004, 0.04, and 0.4 µg/ml), IFNα (20, 100 and 500 IU/ml), or Nirmatrelvir (0.1, 1, and 10µM) treatment initiated pre-infection. **(e)** Viral N RNA copies/mL quantified by qRT-PCR and **(f)** normalized relative to the no treatment condition (N= 3 +/- SEM). Statistical analyses were performed using ordinary ANOVA with Dunnett's multiple comparisons tests comparing untreated to IFNmod-treated samples. mRNA fold induction of **(g)** antiviral gene OAS1 and **(h)** inflammatory gene CXCL10 in SARS-CoV-2-infected Calu-3 cells following IFNmod (0.004, 0.04, or 0.4 µg/ml), IFNα (20, 100 and 500 IU/ml), or Nirmatrelvir (0.1, 1, and 10µM) treatment that was initiated pre-infection relative to untreated, uninfected controls. Statistical analyses for were performed using ordinary ANOVA with Dunnett's multiple comparisons test comparing untreated, infected samples to treated, infected samples. * p-value < 0.05, ** p-value < 0.01, *** p-value < 0.001, **** p-value <0.0001.

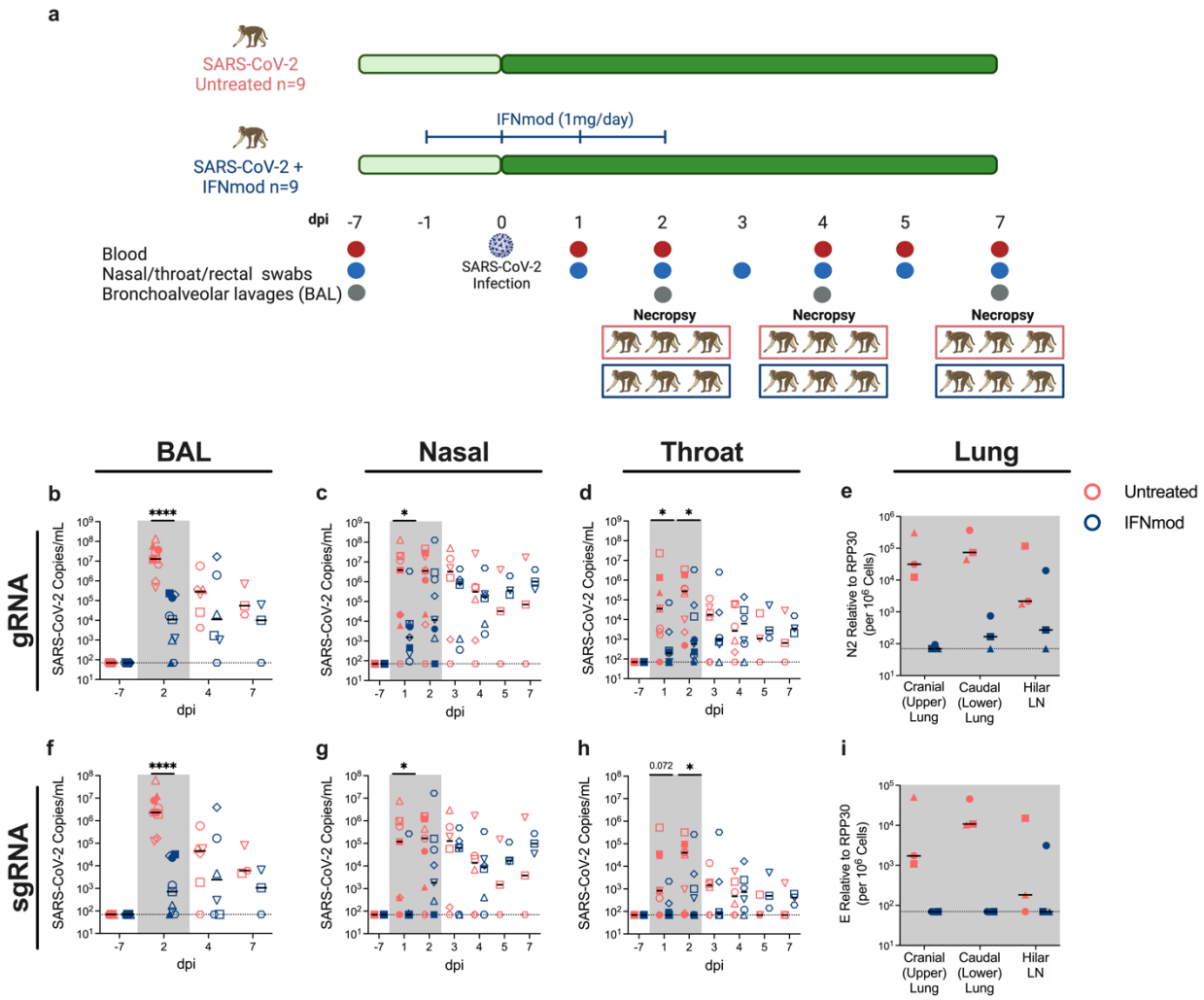

Figure 3.3. IFNmod administration reduced viral loads of SARS-CoV-2 infected RMs. (a) Study Design; n=18 RMs (6-20 years old, mean = 10 years; 10 males and 8 females) were infected intranasally and intratracheally with SARS-CoV-2. 1 day prior to infection (-1 dpi), n=9 RMs started a 4-dose regimen of IFNmod (1mg/day) that continued up until 2 dpi while the other n=9 RMs remained untreated. RMs were sacrificed at 2 dpi (n=3 RMs per treatment arm), 4 dpi (n=3 RMs per treatment arm), or 7 dpi (n=3 RMs per treatment arm). Levels of SARS-CoV-2 **(b-e)** gRNA N and **(f-i)** sgRNA E in BAL, nasopharyngeal swabs, throat swabs, and cranial (upper) lung, caudal (lower) lung, and hilar lymph nodes (LNs) of RMs. For BAL viral loads, n=9 RMs per treatment arm for -7 and 2 dpi, n=6 RMs per treatment arm for 4 dpi, and n=3 RMs per treatment arm for 7 dpi. For nasopharyngeal and throat swab viral loads, n=9 RMs per treatment arm for -7, 1, and 2 dpi, n=6 RMs per treatment arm for 3 and 4 dpi, and n=3 RMs per treatment arm for 5 and 7 dpi. Lung and hilar LN viral loads are from RMs necropsied at 2 dpi (n=3 RMs per treatment arm). Untreated animals are depicted in red and IFNmod-treated animals are depicted in blue. Black lines in h-m represent median viral loads for each treatment group at each timepoint. Gray-shaded boxes indicate that timepoint occurred during IFNmod treatment. Statistical analyses were performed using non-parametric Mann-

Whitney tests. * p-value < 0.05, ** p-value < 0.01, *** p-value < 0.001, **** p-value <0.0001.

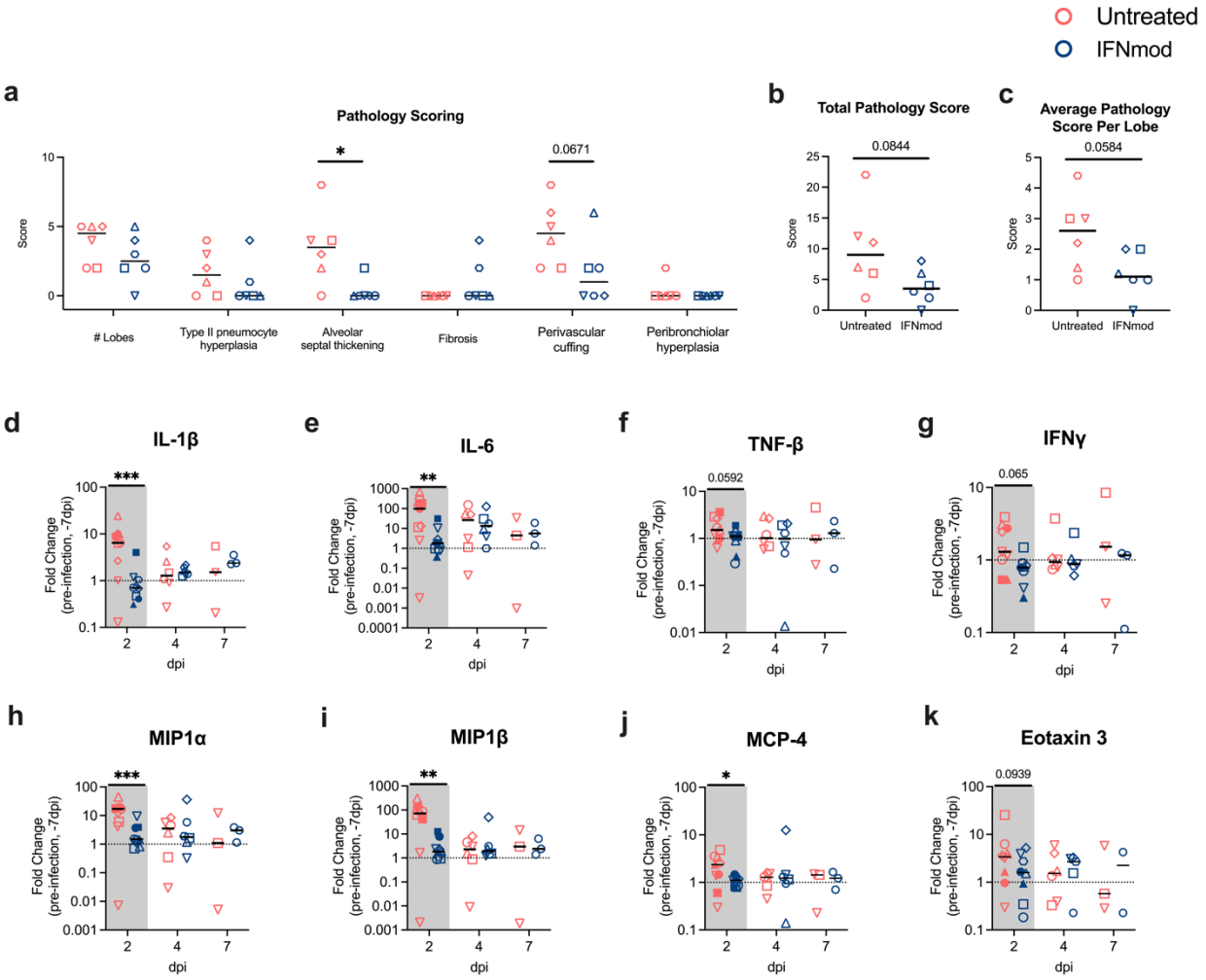

Figure 3.4. IFNmod administration resulted in lower levels of lung pathology and inflammatory cytokines and chemokines in SARS-CoV-2-infected RMs. (a) Individual lung pathology scoring parameters, **(b)** total lung pathology scores, and **(c)** average lung pathology scores per lobe of RMs necropsied at 4 and 7 dpi (n=6 RMs per treatment arm). (**d-k**) Fold change of cytokines and chemokines in BAL fluid relative to –7 dpi measured by mesoscale. One untreated animal was excluded from all mesoscale analysis due to abnormally high baseline levels. n=8 Untreated and 9 IFNmod for 2 dpi, n=5 Untreated and 6 IFNmod for 4 dpi, and n=2 Untreated and 3 IFNmod for 7 dpi. Untreated animals are depicted in red and IFNmod treated animals are depicted in blue. Black lines represent the median viral load, pathology score, or fold change in animals from each respective treatment group. Gray-shaded boxes indicate that timepoint occurred during IFNmod treatment. Statistical analyses were performed using two-sided non-parametric Mann-Whitney tests. * p-value < 0.05, ** p-value < 0.01, *** p-value < 0.001, **** p-value <0.0001.

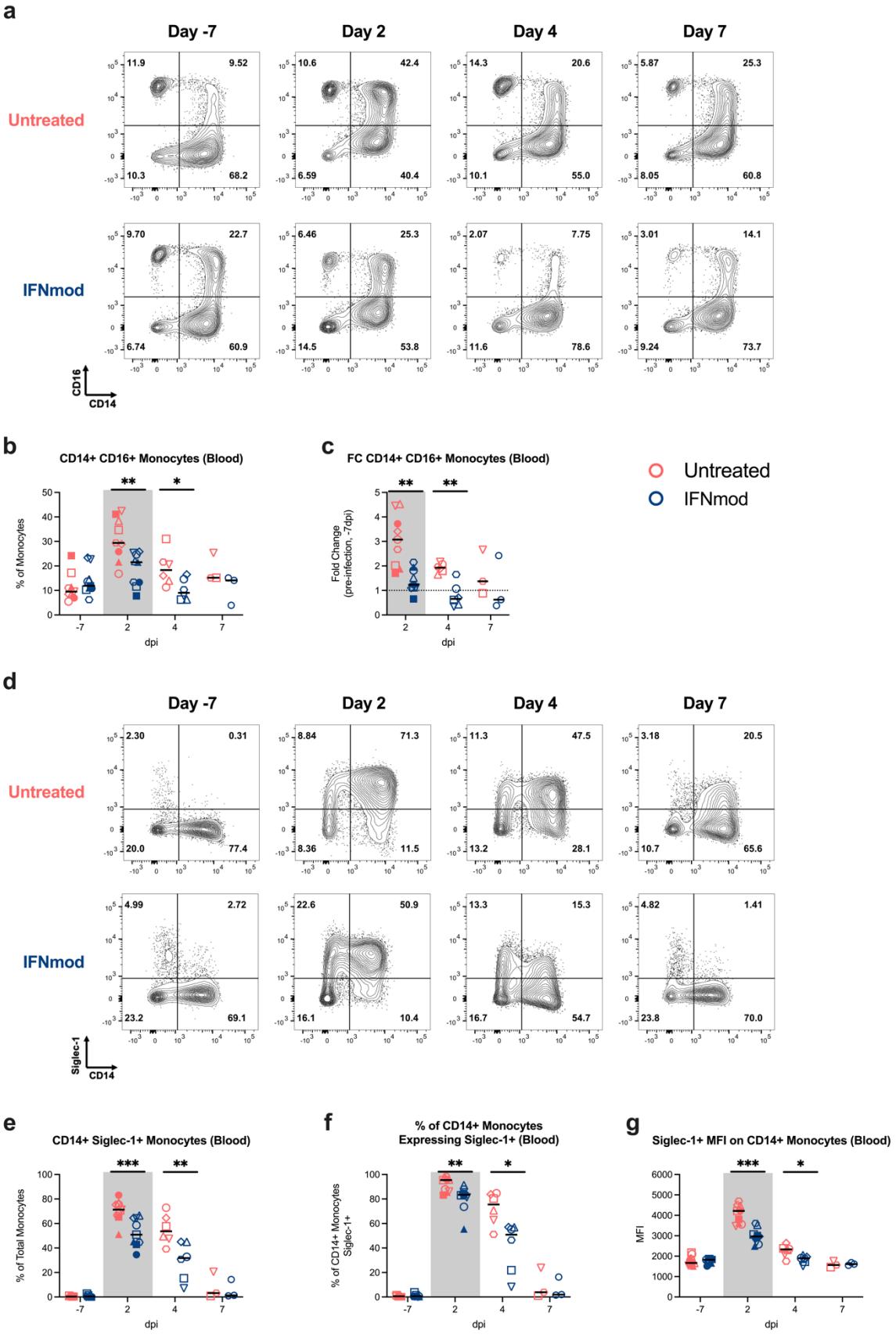
a
Day -7
Day 2
Day 4
Day 7
Untreated
IFNmod
11.9
9.52
10.3
68.2
10.6
42.4
6.59
40.4
14.3
20.6
10.1
55.0
5.87
25.3
8.05
60.8
9.70
22.7
6.74
60.9
6.46
25.3
14.5
53.8
2.07
7.75
11.6
78.6
3.01
14.1
9.24
73.7
CD16
CD14
b
CD14+ CD16+ Monocytes (Blood)
% of Monocytes
dpi
c
FC CD14+ CD16+ Monocytes (Blood)
Fold Change (pre-infection, -7dpi)
dpi
Untreated
IFNmod
d
Day -7
Day 2
Day 4
Day 7
Untreated
IFNmod
2.30
0.31
20.0
77.4
8.84
71.3
8.36
11.5
11.3
47.5
13.2
28.1
3.18
20.5
10.7
65.6
4.99
2.72
23.2
69.1
22.6
50.9
16.1
10.4
13.3
15.3
16.7
54.7
4.82
1.41
23.8
70.0
Siglec-1
CD14
e
CD14+ Siglec-1+ Monocytes (Blood)
% of Total Monocytes
dpi
f
% of CD14+ Monocytes Expressing Siglec-1+ (Blood)
% of CD14+ Monocytes Siglec-1+
dpi
g
Siglec-1+ MFI on CD14+ Monocytes (Blood)
MFI
dpi

Figure 3.5. IFNmod-treated RMs had lower frequencies of CD14+CD16+ monocytes and expression of Siglec-1 compared to untreated RMs. (a) Representative staining of classical (CD14+CD16-), non-classical (CD14-CD16+), and inflammatory (CD14+CD16+) monocytes in peripheral blood throughout the course of infection with frequency as a percentage of total monocytes. **(b-c)** Frequency as a percentage of total monocytes and fold change relative to pre-infection baseline (-7 dpi) of inflammatory (CD14+CD16+) monocytes in peripheral blood. **(d)** Representative staining and **(e)** frequency as a percentage of total monocytes of Siglec-1+ CD14+ monocytes in peripheral blood. **(f)** Frequency as a percentage of CD14+ monocytes that were Siglec-1+ in peripheral blood. **(g)** MFI of Siglec-1 on CD14+ monocytes in peripheral blood. Untreated animals are depicted in red and IFNmod treated animals are depicted in blue. In representative staining plots, frequencies of each quadrant are bolded. Black lines represent the median frequency or fold change in animals from each respective treatment group. Gray-shaded boxes indicate that timepoint occurred during IFNmod treatment. Statistical analyses were performed using two-sided non-parametric Mann-Whitney tests. * p-value < 0.05, ** p-value < 0.01, *** p-value < 0.001, **** p-value <0.0001.

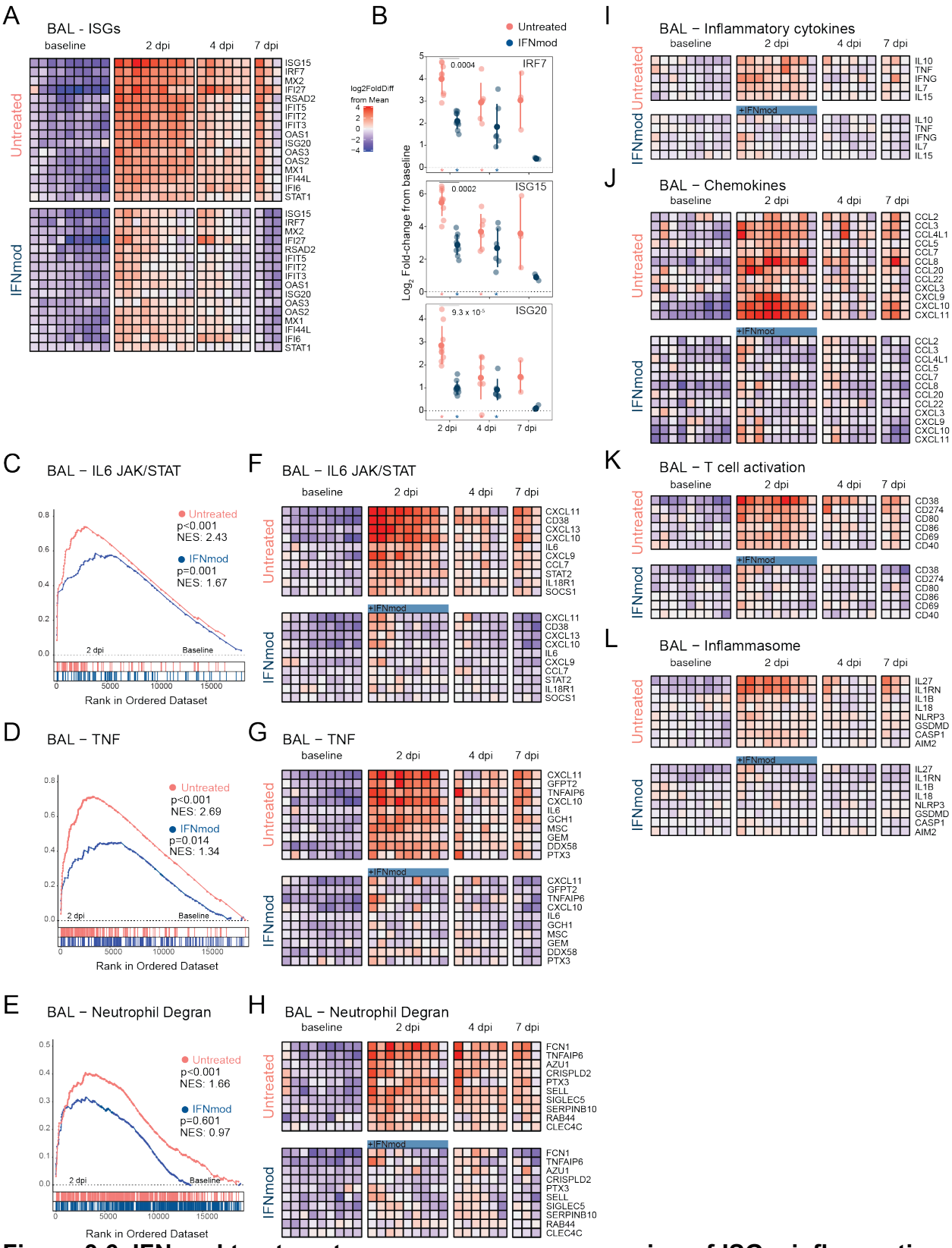

Figure 3.6. IFNmod treatment suppresses gene expression of ISGs, inflammation, and neutrophil degranulation in the BAL of SARS-CoV-2 infected NHPs. Bulk RNA-

Seq profiles of BAL cell suspensions obtained at -7 dpi (n=9 per treatment arm), 2 dpi (n=9 per treatment arm), 4 dpi (n=6 per treatment arm), and 7 dpi (n=3 per treatment arm). **(a)** Heatmap of longitudinal gene expression in BAL prior to and following SARS-CoV-2 infection for the ISG gene panel. The color scale indicates log2 expression relative to the mean of all samples. Samples obtained while the animals were receiving IFNmod administration are depicted by a blue bar. **(b)** Distribution of log2 fold-changes of select ISGs relative to baseline. Filled dots represent the mean, and lighter dots are individual data points. Asterisks indicate statistical significance ($p_{adj} < 0.05$) of gene expression relative to baseline within treatment groups; black horizontal bars indicate BH corrected p-values of direct contrasts of the gene expression between groups at time-points (i.e. IFNmod vs Untreated) using the Wald test and the DESeq2 package. **(c-e)** GSEA enrichment plots depicting pairwise comparison of gene expression of 2 dpi samples vs -7 dpi samples within treatment groups. The untreated group is depicted by red symbols, and data for the IFNmod treated group is shown in blue. The top-scoring (i.e. leading edge) genes are indicated by solid dots. The hash plot under GSEA curves indicate individual genes and their rank in the dataset. Left-leaning curves (i.e. positive enrichment scores) indicate enrichment, or higher expression, of pathways at 2 dpi, right-leaning curves (negative enrichment scores) indicate higher expression at -7 dpi. Sigmoidal curves indicate a lack of enrichment, i.e. equivalent expression between the groups being compared. The normalized enrichment scores and nominal p-values testing the significance of each comparison are indicated. Gene sets were obtained from the MSIGDB (Hallmark and Canonical Pathways) database. **(f-h)** Heatmaps of longitudinal gene expression after SARS-CoV-2. Genes plotted are the top 10 genes in the leading edge of gene set enrichment analysis calculated in panels c-e for each pathway in the Untreated 2 dpi vs -7 dpi comparison. (**i-l**) Longitudinal gene expression for selected DEGs in immune signaling pathways. The expression scale is depicted in the top right of panel a and is applicable to panels a, f, g, h, i, j, k, and l.

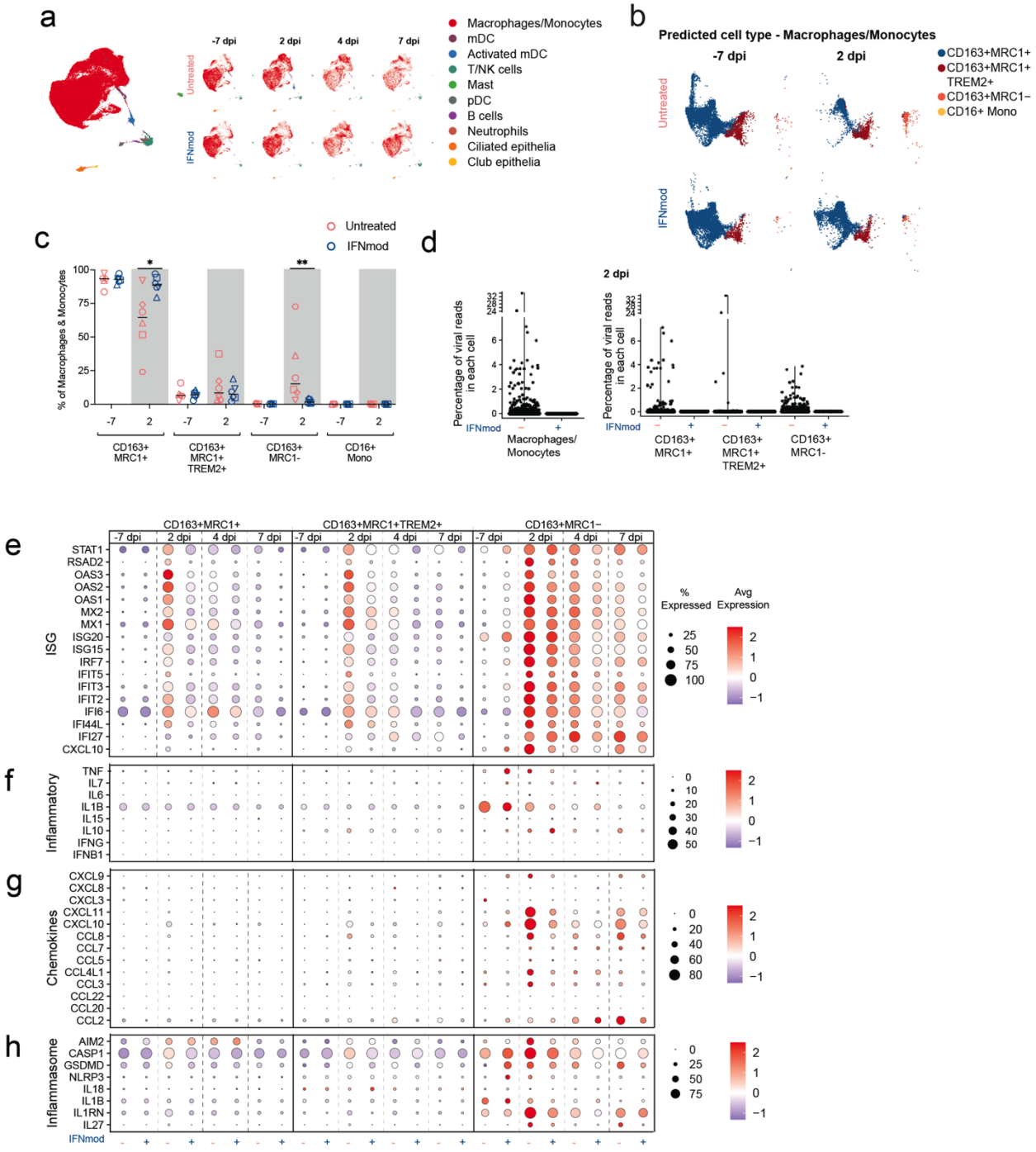

Figure 3.7. Effect of IFNmod treatment on gene expression of BAL single-cells using 10X. (n=6 Untreated, n=6 IFNmod except n=5 for Untreated -7dpi, IFNmod 4dpi, and IFNmod 7 dpi) **(a)** UMAP of BAL samples (62,081 cells) integrated using reciprocal PCA showing cell type annotations. UMAP split by treatment and time points are also shown. **(b)** Mapping of macrophage/monocyte cells in the BAL of SARS-CoV-2-infected untreated and IFNmod treated RMs to different lung macrophage/monocyte subsets from healthy rhesus macaque [433]. **(c)** Percentage of different macrophage/monocyte subsets out of all the macrophage/monocytes in BAL at -7 dpi and 2 dpi from untreated and

IFNmod treated RMs. The black bars represent the median. Statistical analyses between treatment groups were performed using non-parametric Mann-Whitney tests. * p-value < 0.05, ** p-value < 0.01, *** p-value < 0.001, **** p-value <0.0001. **(d)** Violin Plots showing the percentage of viral reads in each cell for total macrophages/monocytes and individual macrophages/monocytes subsets at 2 dpi determined using the PercentageFeatureSet in Seurat. **(e-h)** Dot Plots showing expression of selected **(e)** ISGs**, (f)** inflammatory genes, **(g)** chemokines, and **(h)** inflammasome genes**.** The size of the dot indicates the percentage of cells that express a given a gene and the color indicates the level of expression. The numbers of CD16+ monocytes were very low and have been thus omitted.

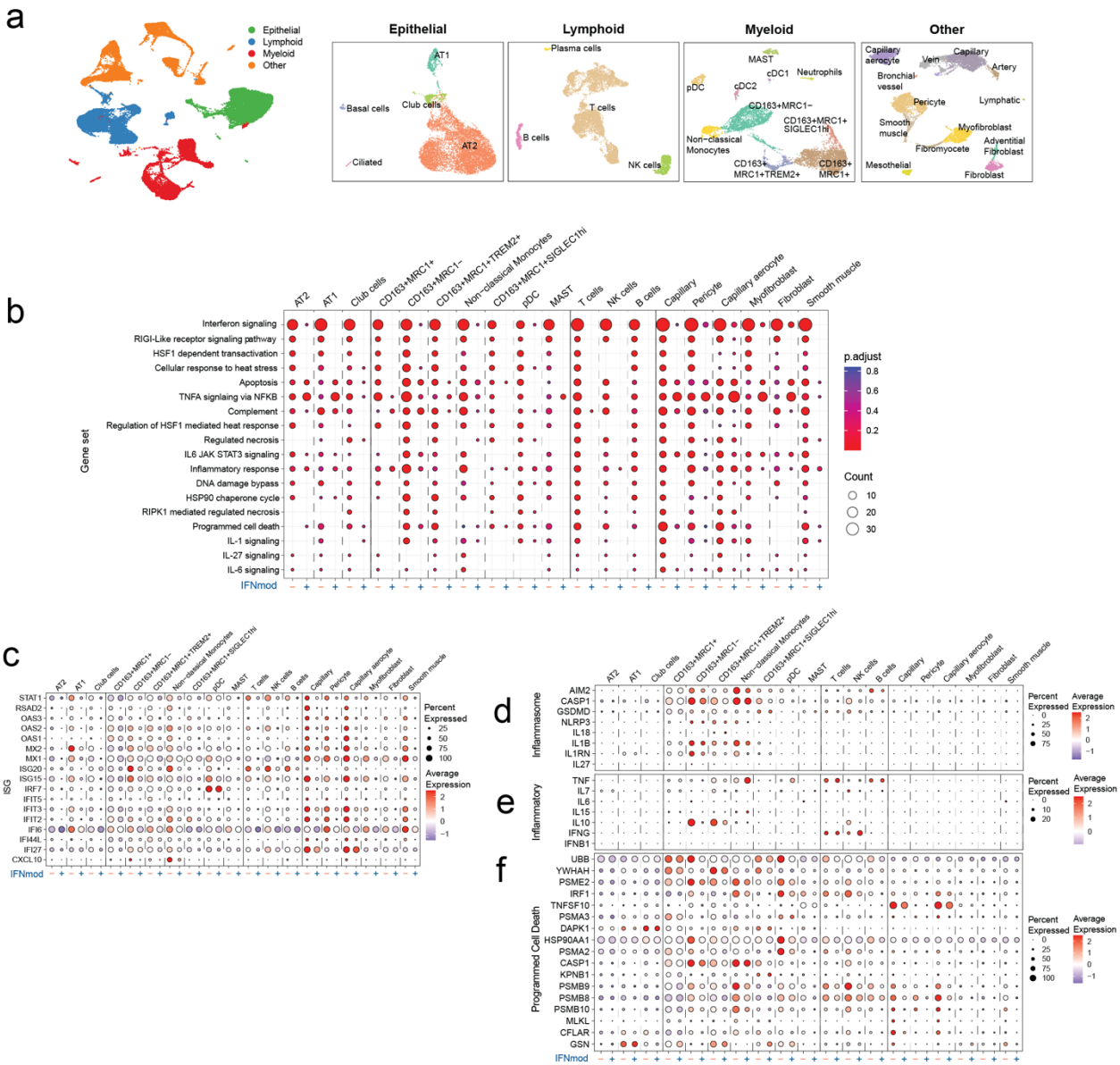

Figure 3.8. Effect of IFNmod treatment on lung cells. (a) UMAP based on reciprocal PCA of lung single cells collected at 2 dpi (n = 2 Untreated, 2 IFNmod) and 7 dpi (n = 1

Untreated, 1 IFNmod). The cells were classified into four broad categories – epithelial, lymphoid, myeloid and others (stromal and endothelial). The cells from each category were subset and clustered separately. UMAPs for each category with cell type annotations are also shown. **(b)** Selected gene sets that were found to be enriched (p-adjusted value < 0.05) in lung cells from untreated RMs at 2 dpi based on over-representation analysis using Hallmark, Reactome, KEGG, and BioCarta gene sets from msigdb. The size of the dots represents the number of genes that were enriched in the gene set and the color indicates the p-adjusted value. The gene set id in order are: M983, M15913, M27255, M27253, M5902, M5890, M5921, M27250, M41804, M5897, M5932, M27698, M27251, M29666, M27436, M27895, M27897, M1014. **(c-f)** Dot plots showing gene expression in lung cells present at higher frequencies from untreated and IFNmod treated macaques at 2 dpi **(c)** ISG, **(d)** genes related to inflammasome, **(e)** inflammation, and **(f)** programmed cell death. The size of the dot represents the percent of cells expressing a given gene and the color indicates the average expression.

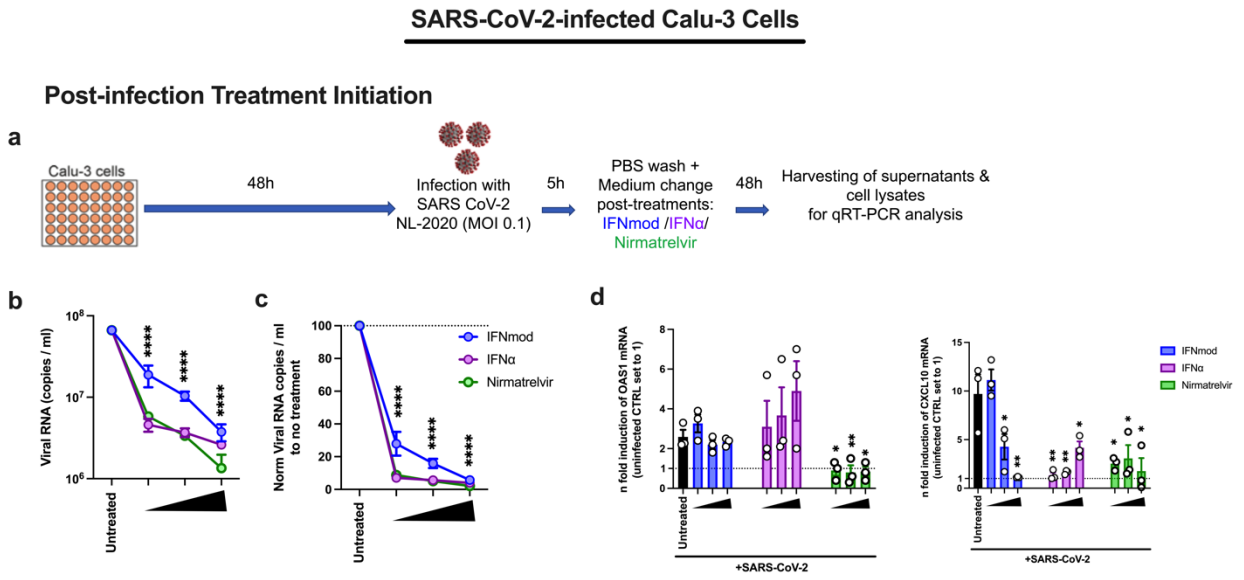

Fig. 3.S1. IFNmod treatment initiated post-SARS-CoV-2 infection leads to reduction in viral RNA loads and inflammatory gene expression. (a) Overview of Calu-3 SARS-CoV-2 cell culture setups with IFNmod (0.004, 0.04, and 0.4 µg/ml), IFNα (20, 100 and 500 IU/ml), or Nirmatrelvir (0.1, 1, and 10µM) treatment initiated post-infection. **(b)** Viral N RNA copies/mL quantified by qRT-PCR and **(c)** normalized relative to the no treatment condition. Bars show the mean of 3 independent experiments (+/- SEM), each measured in technical duplicates. Statistical analyses were performed using ordinary ANOVA with Dunnett's multiple comparisons test comparing IFNmod-treated samples to untreated samples. **(d)** mRNA fold induction of antiviral gene OAS1 and inflammatory gene CXCL10 in SARS-CoV-2-infected Calu-3 cells following IFNmod (0.004, 0.04, or 0.4 µg/ml), IFNα (20, 100 and 500 IU/ml), or Nirmatrelvir (0.1, 1, and 10µM) treatment initiated post-infection relative to untreated, uninfected control samples. Statistical analyses were performed using ordinary ANOVA with Dunnett's multiple comparisons test comparing

untreated, infected samples to treated, infected samples. * p-value < 0.05, ** p-value < 0.01, *** p-value < 0.001, **** p-value <0.0001.

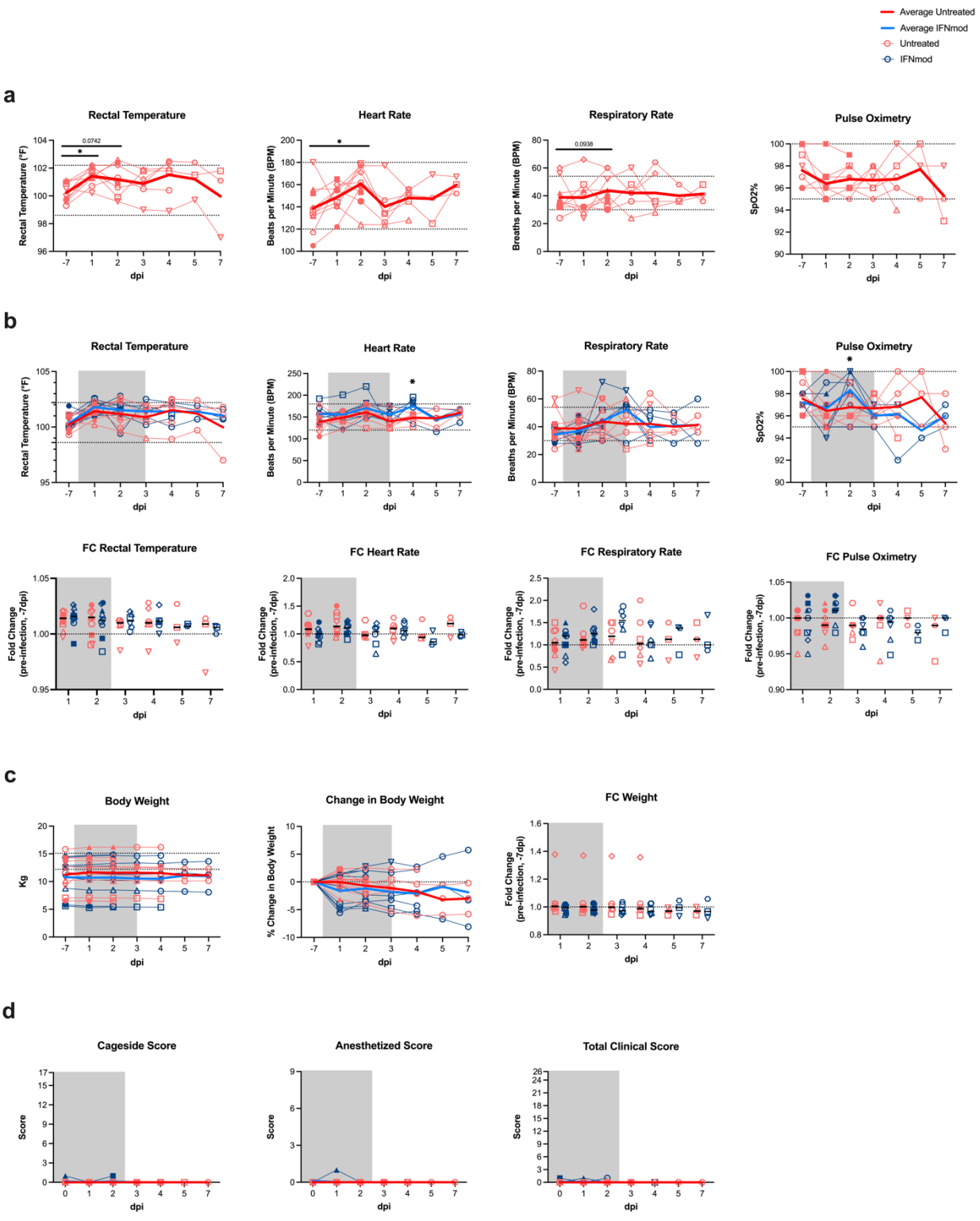

Fig. 3.S2. Administration of IFNmod was safe and well-tolerated in SARS-CoV-2-infected RMs. **(a)** Longitudinal measurements of rectal temperature, heart rate, respiratory rate, and pulse oximetry in untreated SARS-CoV-2-infected RMs. n=9 RMs at -7, 1, and 2 dpi, n=6 RMs at 3 and 4 dpi, and n=3 RMs at 5 and 7 dpi. Statistical analysis

between timepoints was performed using two-sided Wilcoxon matched-pairs signed rank tests. * p-value < 0.05, ** p-value < 0.01. (**b**) Longitudinal measurements and fold changes relative to pre-infection baseline of rectal temperature, heart rate, respiratory rate, and pulse oximetry in untreated and IFNmod-treated SARS-CoV-2-infected RMs. **(c)** Longitudinal measurements of body weight and changes in body weight from pre-infection baseline calculated as percentages and fold changes in untreated and IFNmod-treated SARS-CoV-2-infected RMs. (**d**) Cage-side scores, anesthetized scores, and total clinical scores of untreated and IFNmod-treated SARS-CoV-2-infected RMs. For panels b-d, n=9 RMs per treatment arm at -7, 1, and 2 dpi, n=6 RMs per treatment arm at 3 and 4 dpi, and n=3 RMs per treatment arm at 5 and 7 dpi. Statistical analyses for panels b-d were performed using non-parametric Mann-Whitney tests. * p-value < 0.05, ** p-value < 0.01, *** p-value < 0.001, **** p-value <0.0001. Black dotted horizontal lines indicate normal ranges for measured parameters for adult indoor RMs. Bolded red and blue lines indicate averages for Untreated and IFNmod-treated RMs respectively. Black bolded lines represent the median fold changes of measured parameters for animals from each respective treatment group. Red symbols indicate individual untreated animals and blue symbols indicate individual IFNmod animals. Gray-shaded boxes indicate that timepoint occurred during IFNmod treatment.

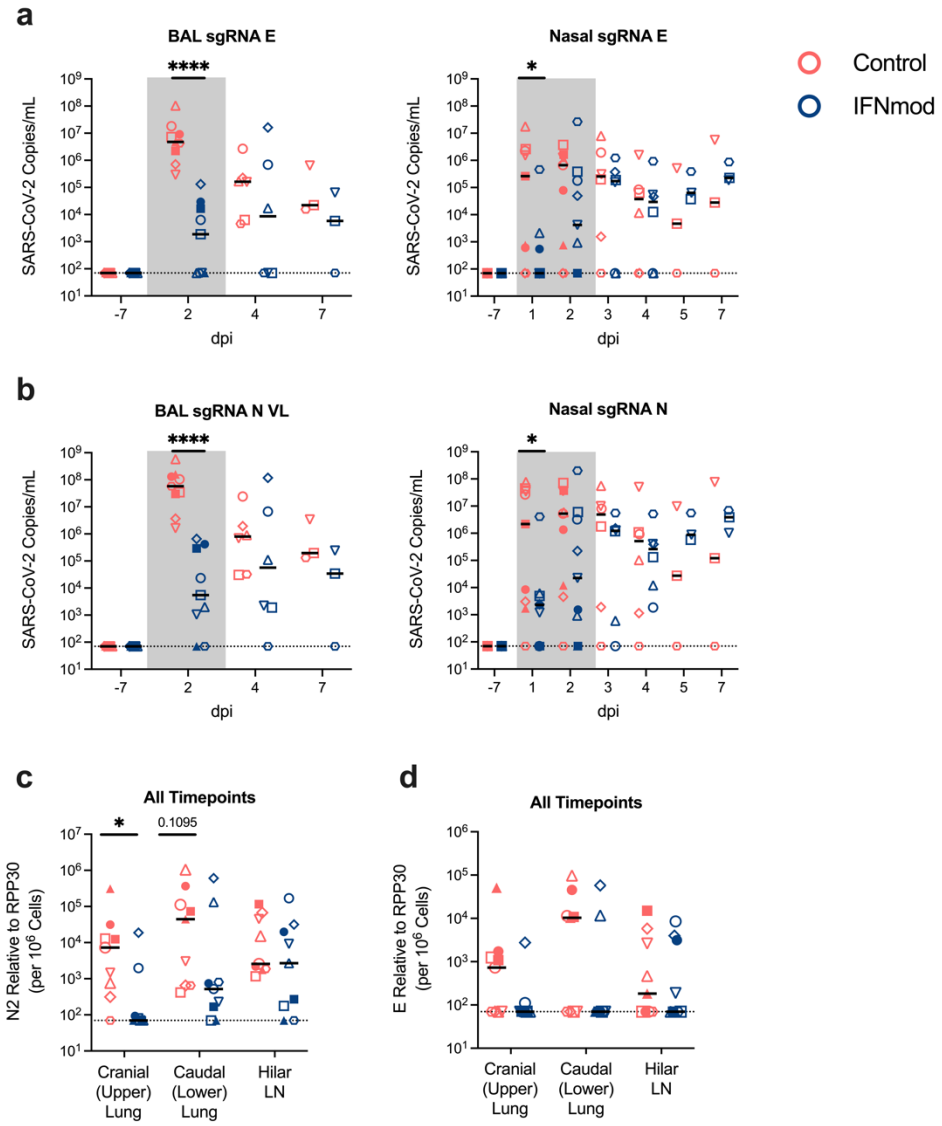

Fig. 3.S3. IFNmod reduced nasopharyngeal, BAL, and lung viral loads in SARS-CoV-2-infected RMs. (a) sgRNA-E viral loads were repeated along with **(b)** sgRNA-N viral loads for BAL and nasopharyngeal swabs by a second lab. For BAL sgRNA-E and sgRNA-N, n=9 per treatment group at -7 and 2 dpi, n=6 per treatment group at 4 dpi, and n=3 per treatment group at 7 dpi. For nasopharyngeal swab sgRNA-E and sgRNA-N, n=9 per treatment group at -7, 1, and 2 dpi, n=6 per treatment group at 3 and 4 dpi, and n=3 per treatment group at 5 and 7 dpi. Levels of SARS-CoV-2 **(c)** gRNA and **(d)** sgRNA in cranial (upper) lung, caudal (lower) lung, and hilar lymph nodes (LNs) of RMs necropsied at all timepoints (n=9 per treatment group). Individual untreated animals are depicted by red symbols and individual IFNmod treated animals are depicted by blue symbols. Black lines represent the median viral load or score of animals from each respective treatment group. Statistical analyses were performed using non-parametric Mann-Whitney tests. * p-value < 0.05, ** p-value < 0.01, *** p-value < 0.001, **** p-value <0.0001.

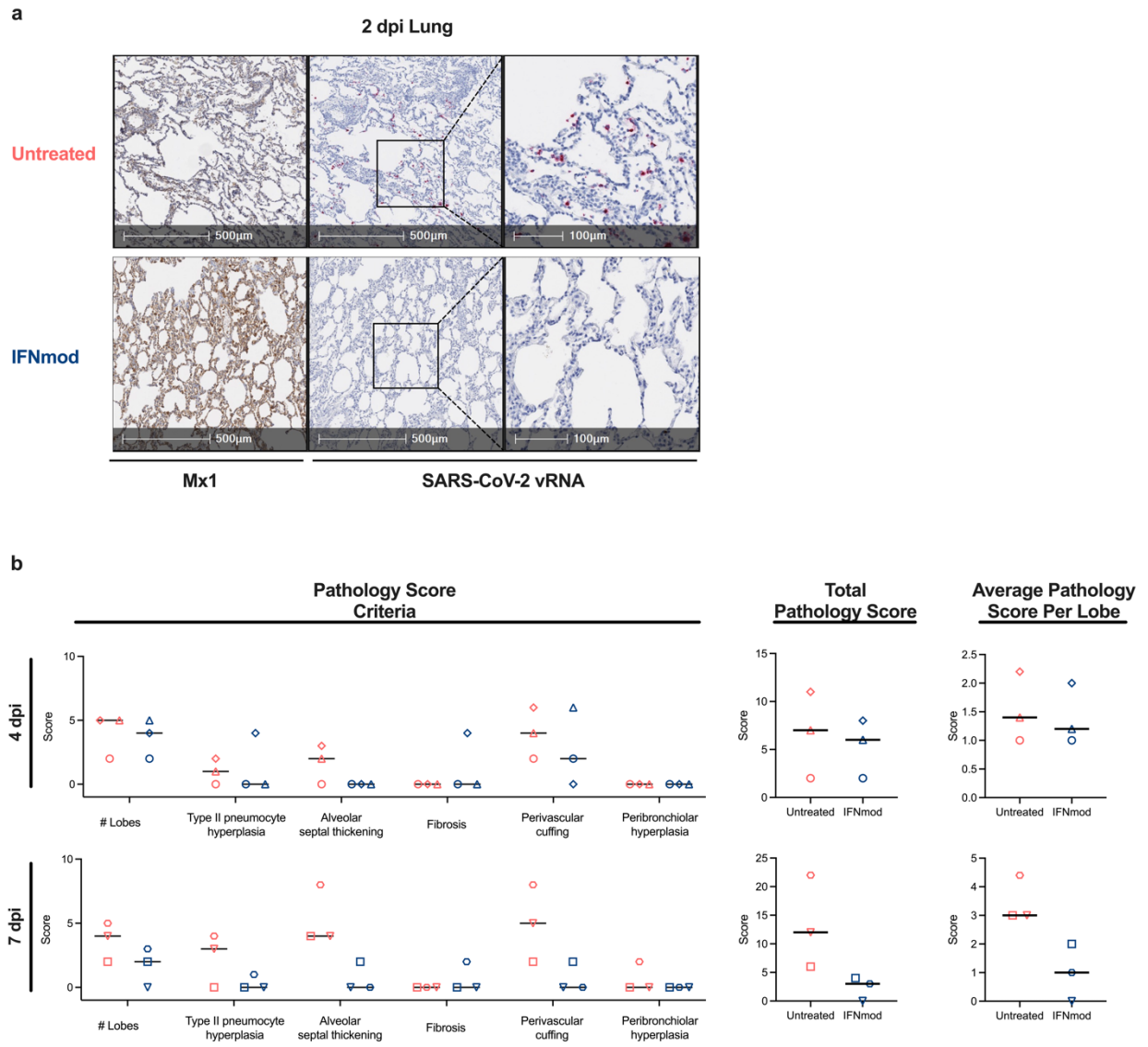

Fig. 3.S4. Mx1 is more highly localized to viral foci in untreated SARS-CoV-2-infected RMs and IFNmod treatment decreases lung pathology. Representative staining for **(a)** Mx1 and SARS-CoV-2 vRNA in lungs of untreated and IFNmod-treated RMs necropsied at 2 dpi. Right column contains zoomed-in images of black box regions in center column. **(b)** Scores for individual parameters of lung pathology, total lung pathology scores, and average pathology scores per lung lobe of RMs necropsied at 4 dpi (n=3 RMs per treatment group) and 7 dpi (n=3 RMs per treatment group) respectively. Untreated animals are depicted in red and IFNmod treated animals are depicted in blue. Black lines represent the median viral load or score of animals from each respective treatment group. Statistical analyses were performed using non-parametric Mann-Whitney tests. * p-value < 0.05, ** p-value < 0.01, *** p-value < 0.001, **** p-value <0.0001.

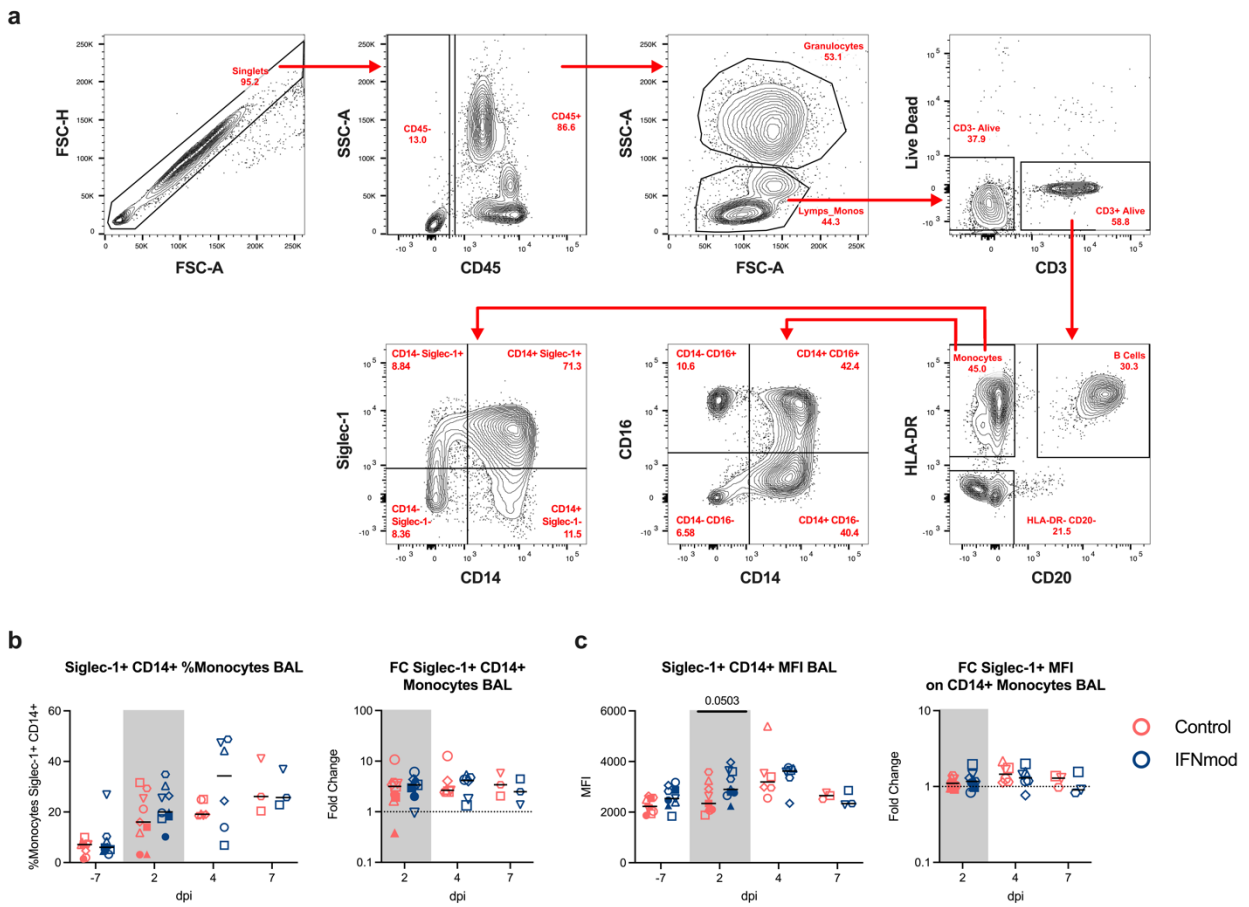

Fig. 3.S5. Flow gating strategy and expression of Siglec1+ in BAL. (a) Gating strategy for innate immune cell phenotyping panel used in whole blood and BAL. **(b)** Frequency of CD14+ monocytes that were Siglec-1+ in BAL mononuclear cells and fold change relative to -7 dpi. **(c)** MFI of Siglec-1 on CD14+ monocytes in BAL mononuclear cells and fold change relative to -7 dpi. n=9 RMs per treatment group at -7 and 2dpi, n=6 RMs per treatment group at 4dpi, and n=3 RMs per treatment group at 7 dpi. Untreated animals are depicted in red and IFNmod treated animals are depicted in blue. Black lines represent the median frequency or fold change in animals from each respective treatment group. Gray-shaded boxes indicate that timepoint occurred during IFNmod treatment. Statistical analyses were performed using two-sided non-parametric Mann-Whitney tests. * p-value < 0.05, ** p-value < 0.01, *** p-value < 0.001, **** p-value <0.0001.

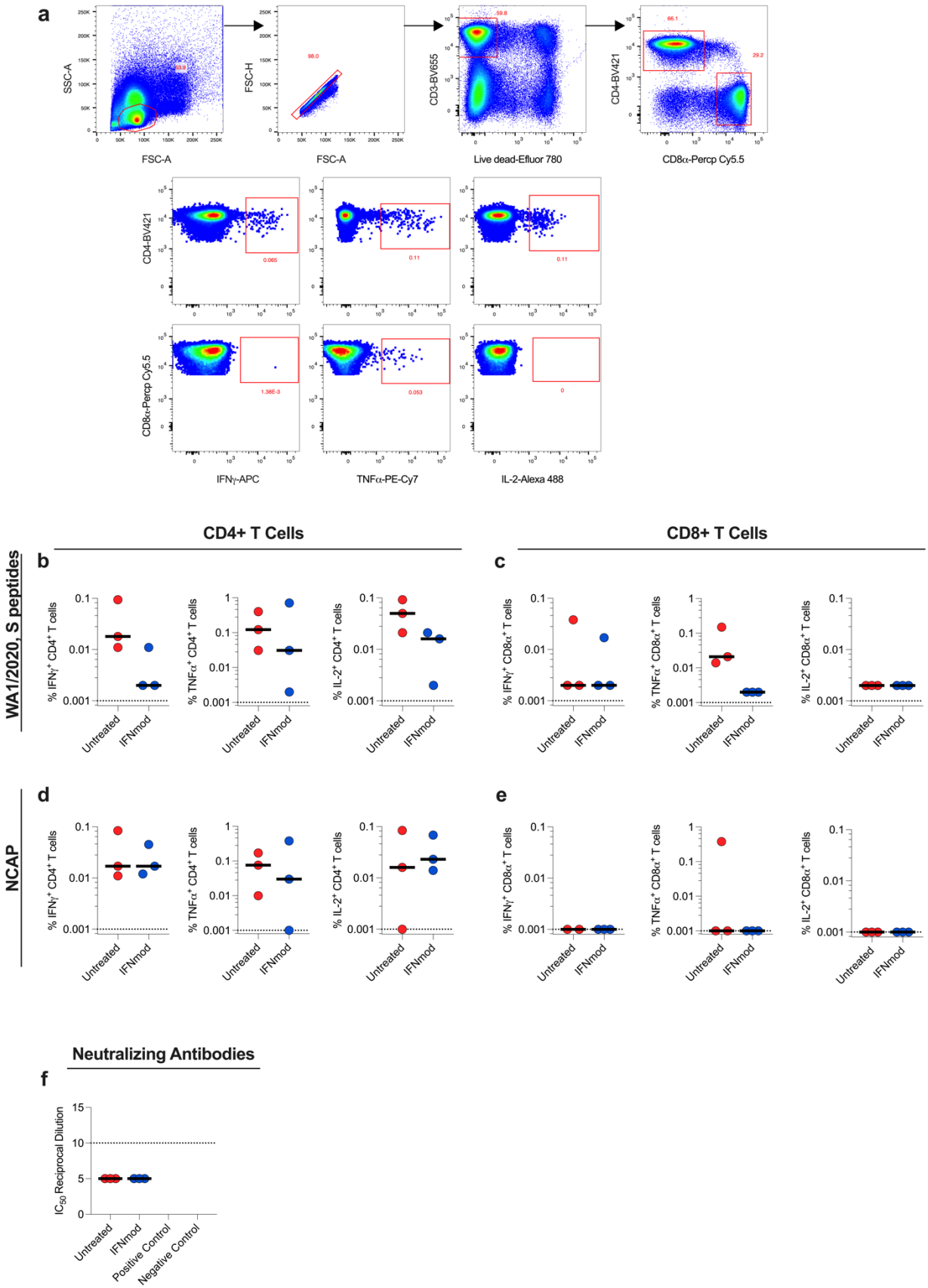
a
SSC-A
FSC-A
FSC-H
FSC-A
CD3-BV655
Live dead-Efluor 780
CD4-BV421
CD8α-Percp Cy5.5
CD4-BV421
CD8α-Percp Cy5.5
IFNγ-APC
TNFα-PE-Cy7
IL-2-Alexa 488
CD4+ T Cells
CD8+ T Cells
WA1/2020, S peptides
NCAP
b
c
d
e
% IFNγ+ CD4+ T cells
% TNFα+ CD4+ T cells
% IL-2+ CD4+ T cells
% IFNγ+ CD8α+ T cells
% TNFα+ CD8α+ T cells
% IL-2+ CD8α+ T cells
Untreated
IFNmod
Neutralizing Antibodies
f
IC50 Reciprocal Dilution
Untreated
IFNmod
Positive Control
Negative Control

Fig. 3.S6. IFNmod treatment does not impact SARS-CoV-2-specific T cell or neutralizing antibody responses. (a) Gating strategy for identifying IFNγ, TNFα, or IL-2 positive CD8+ and CD4+ T cells. IFNγ, TNFα, or IL-2 frequency levels in CD4+ and CD8 + T cells from 7 dpi PBMCs following ex-vivo stimulation with SARS-CoV-2 **(b,c)** S peptide pool and **(d,e)** NCAP**. (f)** SARS-CoV-2 pseudovirus neutralizing antibody titers in 7 dpi serum. Statistical analyses were performed using two-sided non-parametric Mann-Whitney tests. * p-value < 0.05, ** p-value < 0.01, *** p-value < 0.001, **** p-value <0.0001.

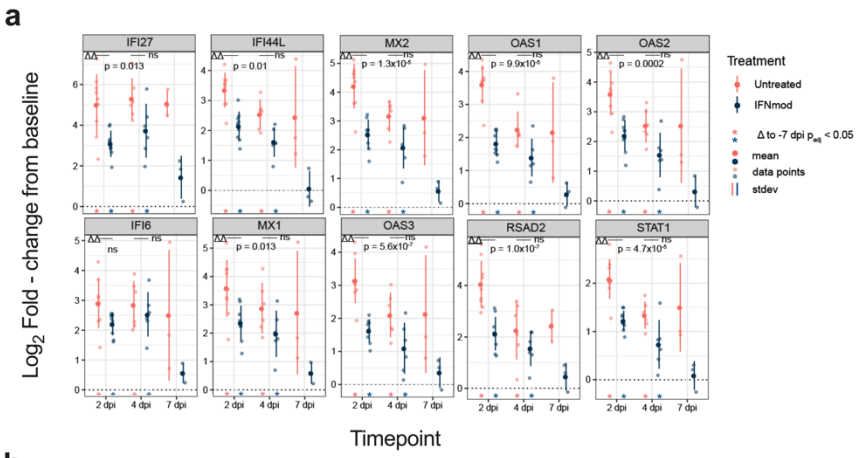
a
IFI27
IFI44L
MX2
OAS1
OAS2
IFI6
MX1
OAS3
RSAD2
STAT1
Treatment
Untreated
IFNmod
mean
data points
stdev
Log2 Fold - change from baseline
Timepoint
2 dpi
4 dpi
7 dpi

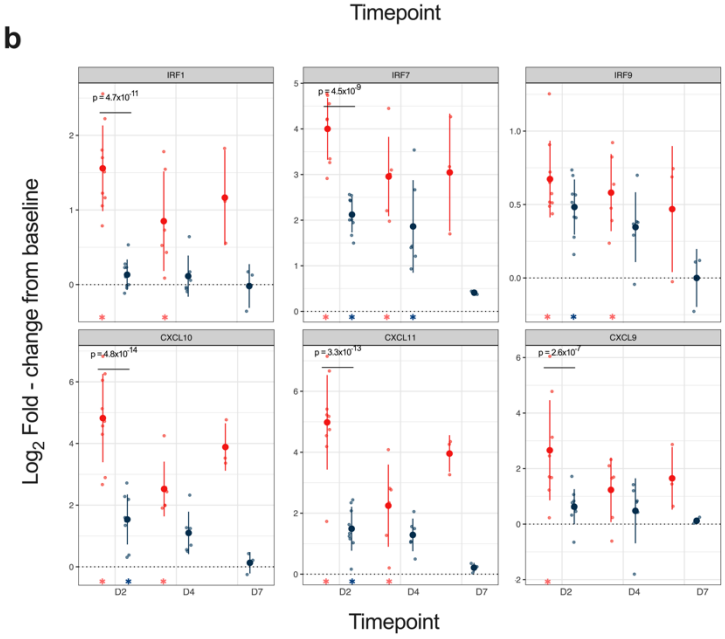
b
IRF1
IRF7
IRF9
CXCL10
CXCL11
CXCL9
Log2 Fold - change from baseline
Timepoint
D2
D4
D7

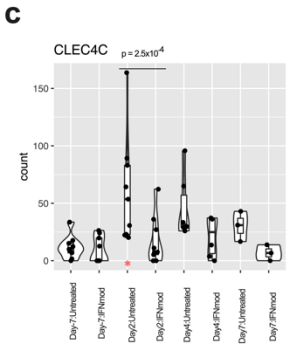
c
CLEC4C
count

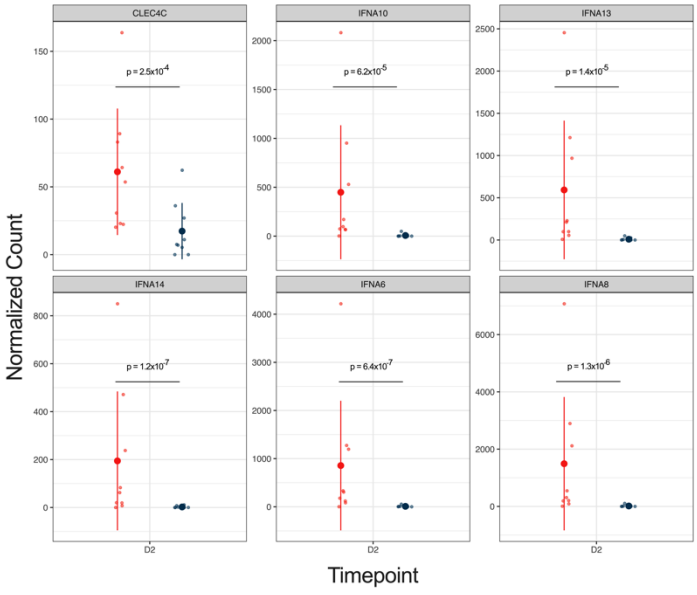
d
CLEC4C
IFNA10
IFNA13
IFNA14
IFNA6
IFNA8
Normalized Count
Timepoint
D2

Fig. 3.S7. Gene expression in BAL in rhesus macaques infected with SARS-CoV-2 after treatment with IFNmod. Log2 fold-changes in **(a)** ISGs, **(b)** IRFs (IRF1, IRF7, IRF9), and CXCR3 ligands (CXCL10, CXCL11, and CXCL9) in the BAL of untreated and IFNmod-treated SARS-CoV-2-infected RMs relative to pre-infection baseline (-7 dpi). **(c)** Violin plot showing the longitudinal normalized RNA-seq read counts of CLEC4C in BAL of untreated and IFNmod-treated SARS-CoV-2-infected RMs. **(d)** Normalized RNA-seq read counts of pDC-specific marker CLEC4C and IFNA genes in the BAL of untreated and IFNmod-treated SARS-CoV-2-infected RMs at 2 dpi. Filled dots represent the mean, and lighter dots are individual data points (n=9 per treatment arm at -7 and 2 dpi, n=6 RMs per treatment arm at 4 dpi, and n=3 RMs per treatment arm at 7 dpi). Asterisks indicate statistical significance ($p_{adj} < 0.05$) of gene expression relative to baseline within treatment groups; black horizontal bars indicate BH corrected p-values of direct contrasts of the gene expression between groups at time-points (i.e. IFNmod vs Untreated) using the Wald test and the DESeq2 package. Vertical colored bars depict the standard deviation of each distribution.

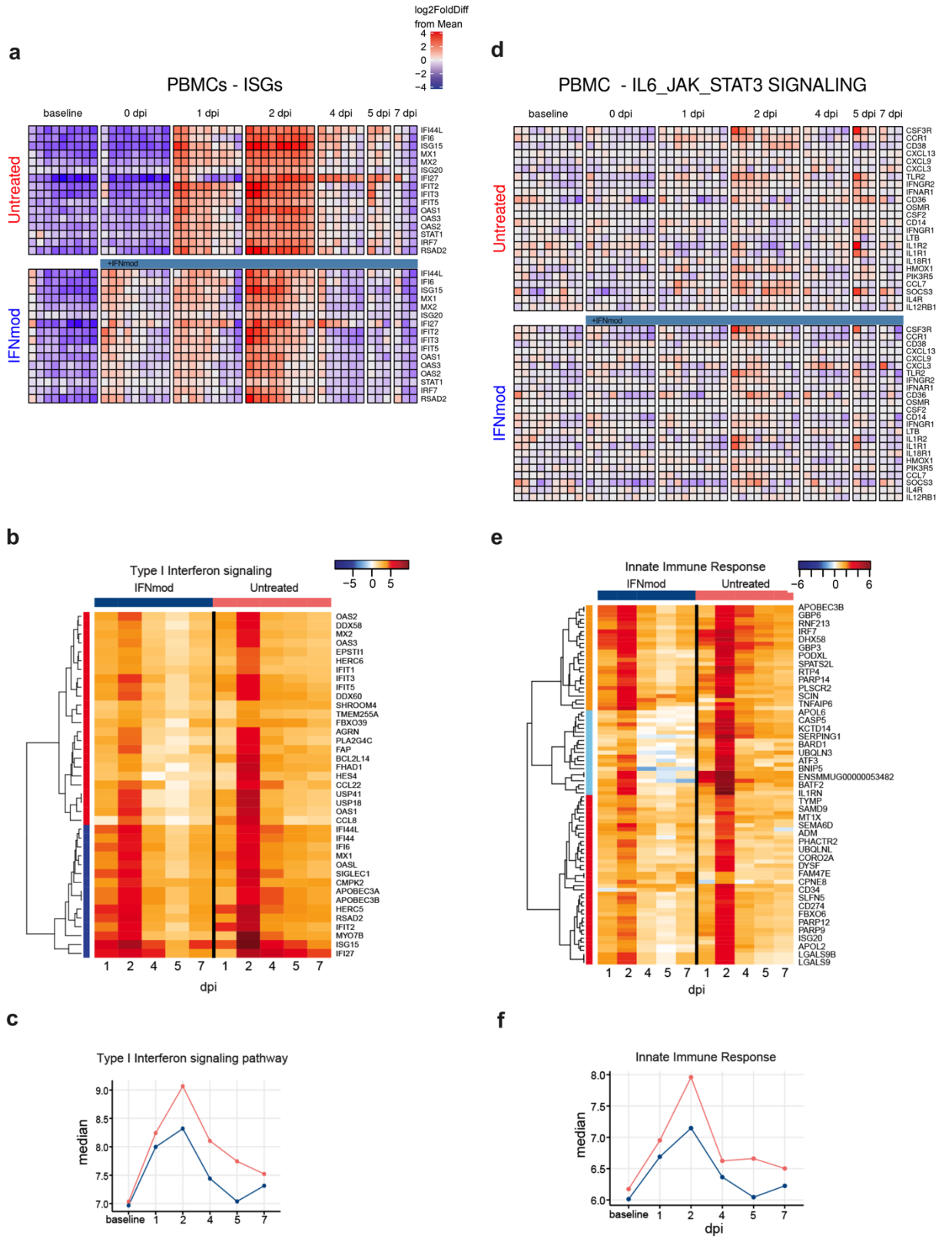

Fig. 3.S8. Gene expression in PBMCs and whole blood in rhesus macaques infected with SARS-CoV-2 after treatment with IFNmod. (a) Heatmap of longitudinal

gene expression in PBMCs after SARS-CoV-2 infection for the ISG panel (n=9 RMs per treatment arm at -7, 0, 1, and 2 dpi, n=6 RMs per treatment arm at 4 dpi and n=3 RMs per treatment arm at 5 and 7 dpi). The color scale indicates log2 expression relative to the mean of all samples. Samples obtained while the animals were receiving IFNmod administration are depicted by a blue bar. **(b)** Heatmap depicting log-fold changes for DEGs in significantly enriched type I interferon signaling pathways for both IFNmod and untreated animals in whole blood. **(c)** Median logCPM values for genes in the type I interferon signaling pathways in whole blood. **(d)** Heatmap of longitudinal gene expression in PBMCs after SARS-CoV-2 infection for genes in the IL-6 JAK/STAT pathway (sample numbers as for panel a). The color scale depicted in panel a is applicable to panel d. Samples obtained while the animals were receiving IFNmod administration are depicted by a blue bar. **(e)** Heatmap depicting log-fold changes for DEGs in significantly enriched innate immune response pathways for both IFNmod and untreated animals in whole blood. **(f)** Median logCPM values for genes in the innate immune response pathway in whole blood.

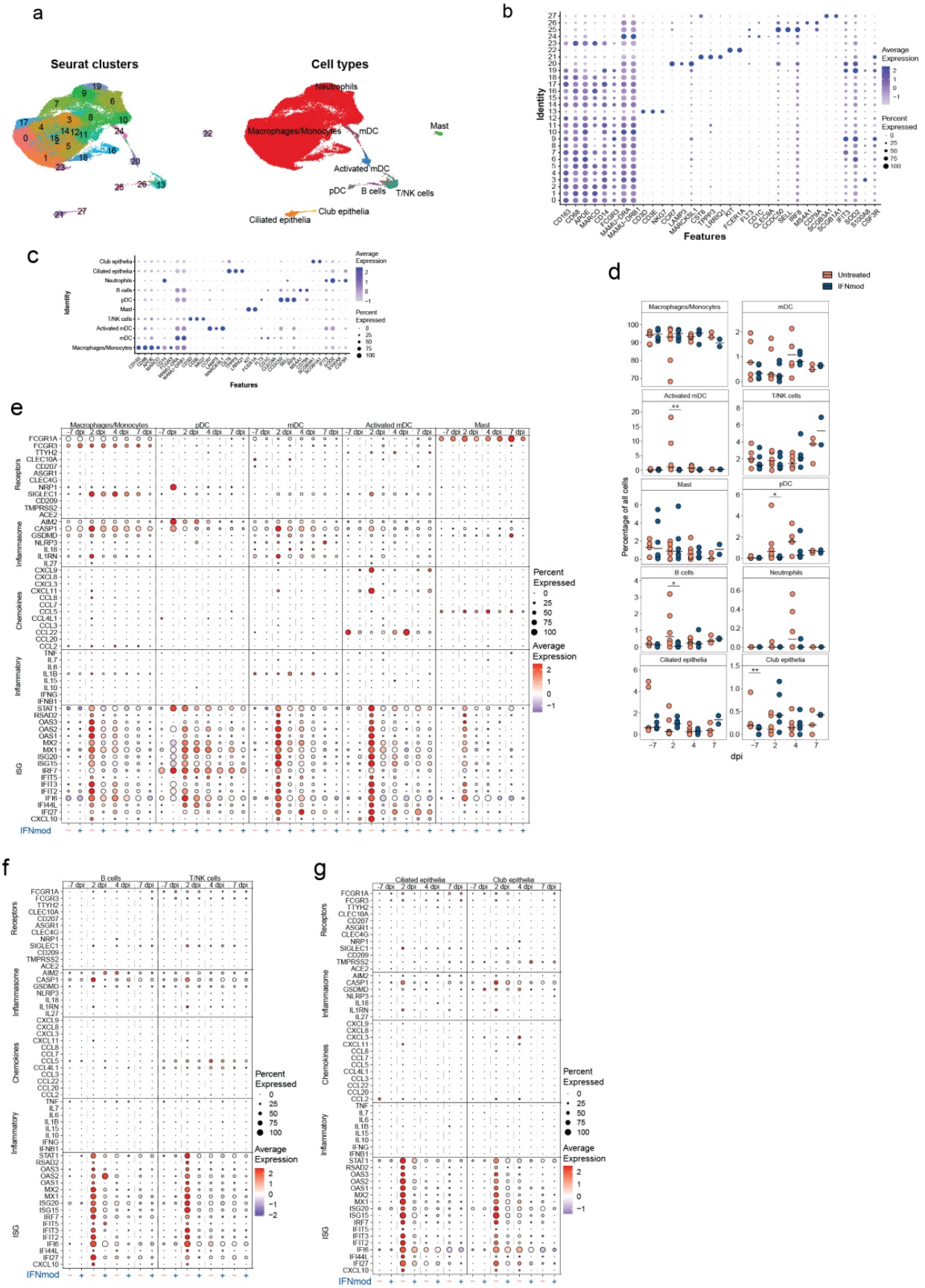
a
Seurat clusters
Cell types
Neutrophils
Macrophages/Monocytes
mDC
Mast
Activated mDC
pDC
B cells
T/NK cells
Club epithelia
Ciliated epithelia
b
Identity
Features
Average Expression
Percent Expressed
c
Club epithelia
Ciliated epithelia
Neutrophils
B cells
pDC
Mast
T/NK cells
Activated mDC
mDC
Macrophages/Monocytes
d
Untreated
IFNmod
Percentage of all cells
dpi
e
Receptors
Inflammasome
Chemokines
Inflammatory
ISG
IFNmod
f
g

Fig. 3.S9. Expression of marker genes in BAL single-cells. (n=6 Untreated, n=6 IFNmod except n=5 for Untreated -7dpi, IFNmod 4dpi, and IFNmod 7 dpi) **(a)** UMAP of BAL samples colored by clusters determined using Seurat and annotated cell types. **(b)** Dot Plot showing expression of canonical marker genes in seurat clusters. **(c)** Dot Plot showing expression of canonical marker genes in annotated cell types. **(d)** Percentage of each cell type out of all BAL cells in a given sample. The black bar represents the median. Two-tailed Mann-Whitney test was used to calculate p-values. * p-value < 0.05, ** p-value < 0.01, *** p-value < 0.001, **** p-value <0.0001. **(e-g)** Dot Plot showing expression of select ISGs, inflammatory cytokines, chemokines, inflammasome-related and receptor genes in **(e)** myeloid cells (neutrophils excluded due to low frequency)**, (f)** lymphocytes**,** and **(g)** epithelial cells**.**

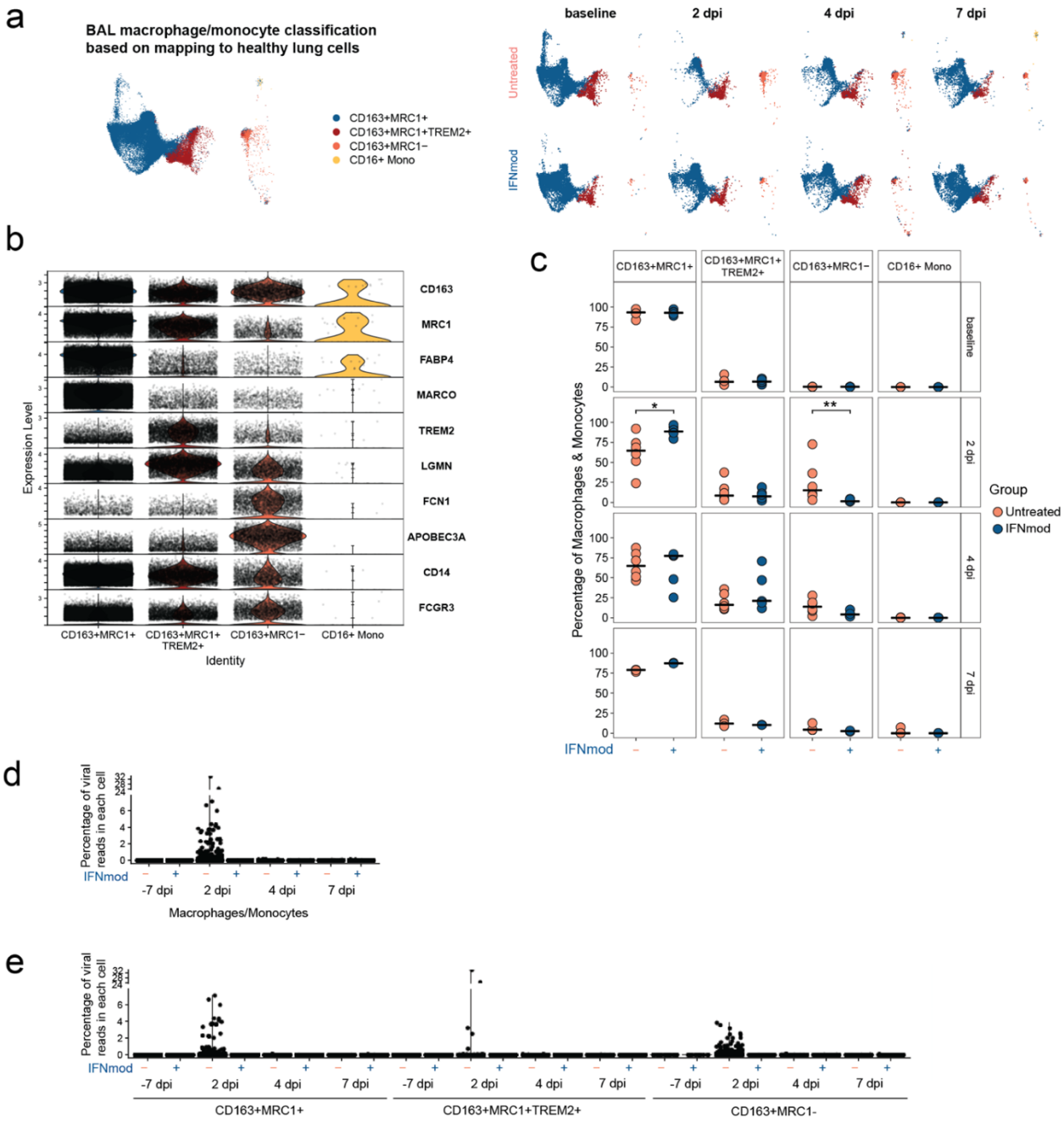

Fig. 3.S10. Effect of IFNmod treatment on different BAL cell types. (n = 6 Untreated, n = 6 IFNmod except n=5 for Untreated -7dpi, IFNmod 4dpi, and IFNmod 7 dpi) **(a)** UMAP showing BAL macrophages/monocytes mapped to the reference macrophage/monocytes from lungs of healthy rhesus macaques. The UMAP split by time point and treatment are also shown. **(b)** Expression of marker genes for macrophage/monocyte subsets in BAL. **(c)** Percentage of different macrophage/monocyte subsets out of all the macrophages/monocytes in BAL at different time points between the untreated and IFNmod treated rhesus macaques. The black bars represent the median. Two-tailed Mann-Whitney test was used to calculate p-values. * p-value < 0.05, ** p-value < 0.01, *** p-value < 0.001, **** p-value <0.0001. Violin plots showing the percentage of viral

reads in BAL **(d)** total macrophages/monocytes and **(e)** individual macrophage/monocyte subsets between the untreated and IFNmod treated macaques at different time points. The percentages were determined using the PercentageFeatureSet in Seurat for SARS-CoV2 genes. CD16+ monocytes were very excluded due to low frequency.

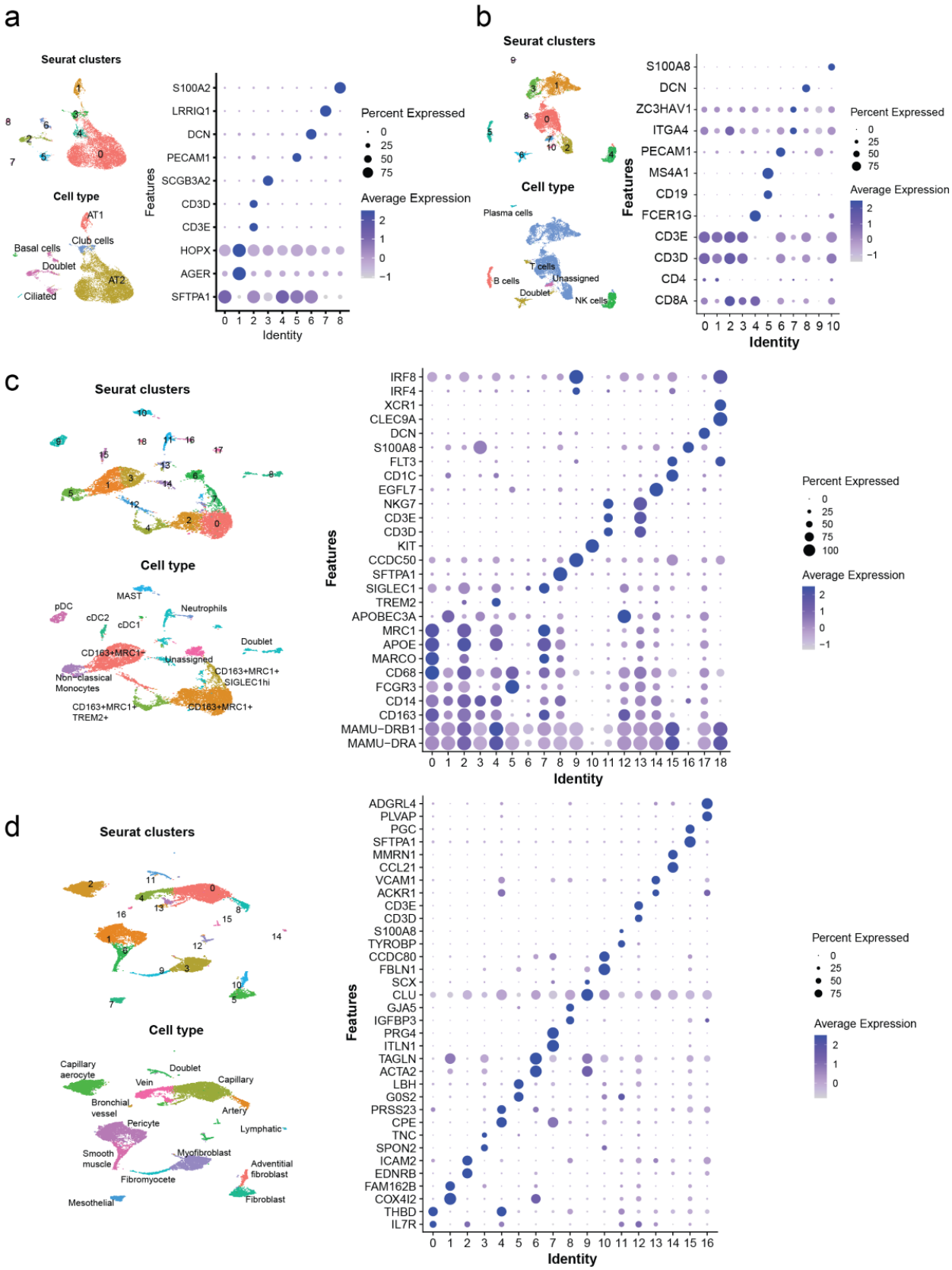

Fig. 3.S11. Cell annotation of lung samples (n = 2 Untreated, 2 IFNmod at 2dpi and n

= 1 Untreated, 1 IFNmod at 7dpi). The cells were divided into four major categories - **(a)** epithelial**, (b)** lymphoid**, (c)** myeloid**,** and **(d)** other (stromal and endothelial) and clustered separately. The clusters so obtained were annotated based on the expression of canonical markers. For each category, a UMAP and a DotPlot with canonical marker genes are shown based on seurat clustering. The second UMAP shows the cell type annotations based on the expression of marker genes.

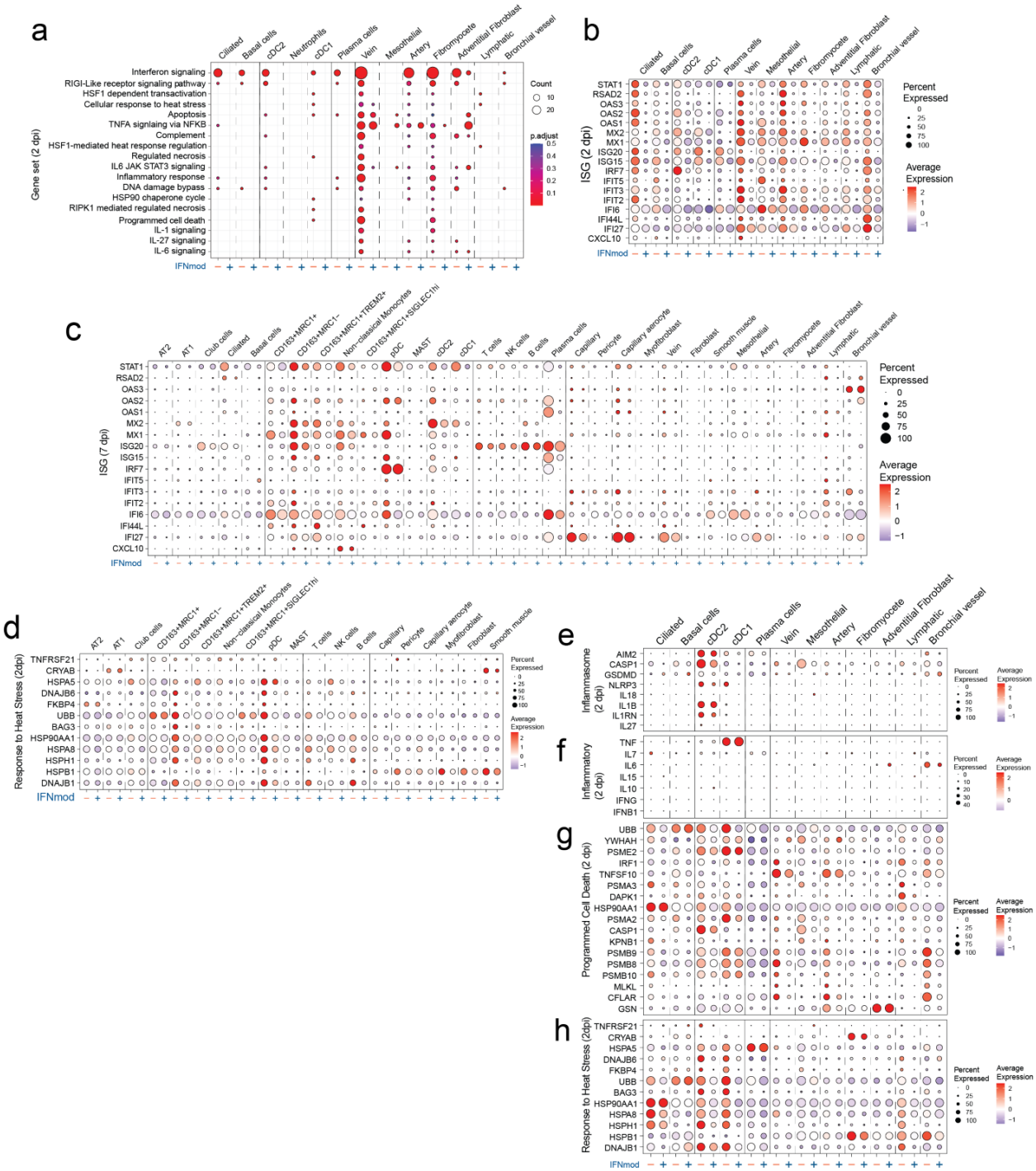

Fig. 3.S12. Effect of IFNmod treatment on gene expression of lung cells (n = 2 Untreated, 2 IFNmod at 2dpi and n = 1 Untreated, 1 IFNmod at 7dpi)**. (a)** Enrichment of gene sets in lung cell types that were present at low frequency at 2 dpi based on over-representation analysis using Hallmark, Reactome, KEGG, and BioCarta gene sets from msigdb. Selected gene sets that were enriched in untreated RM samples at 2 dpi (p-adjusted value < 0.05) are shown. The size of the dots represents the number of genes that were enriched in the gene set and the color indicates the p-adjusted value. The gene set id in order are: M983, M15913, M27255, M27253, M5902, M5890, M5921, M27250,

M41804, M5897, M5932, M27698, M27251, M29666, M27436, M27895, M27897, M1014. **(b-h)** Dot plots showing gene expression in lung cells (neutrophils not shown due to low frequency) from untreated and IFNmod treated animals. **(b)** Expression of ISG in cells present at low frequencies at 2 dpi. **(c)** Expression of ISGs in all lung cells at 7 dpi. **(d)** Expression of genes related to response to heat stress in lung cells that were present at higher frequencies at 2 dpi. Expression of genes related to **(e)** inflammasome**, (f)** inflammation**, (g)** programmed cell death**,** and **(h)** response to heat stress at 2 dpi in lung cell types that were present at low frequencies.

Chapter Three Tables

Animal Name	Sex	Age (months)	Weight (kgs)	Infection Status	Treatment	Day of Necropsy (dpi)	Annotated Symbol
RCh15	M	114	12.08	Uninfected	IFNmod	N/A	○
RIo15	M	112	14.14	Uninfected	IFNmod	N/A	□
RUy14	F	123	12.92	Uninfected	IFNmod	N/A	△
14D002	F	91	6.72	Uninfected	IFNmod	N/A	▽
RMs8	F	236	16.26	SARS-CoV-2	Untreated	4	○
CD68	F	80	11.51	SARS-CoV-2	Untreated	7	□
RRc17	F	71	7.08	SARS-CoV-2	Untreated	4	△
RGo9	F	216	10.31	SARS-CoV-2	Untreated	7	▽
LG92	M	72	12.825	SARS-CoV-2	Untreated	4	◇
LC10	M	84	12.465	SARS-CoV-2	Untreated	7	⬡
KV30	M	98	13.9	SARS-CoV-2	Untreated	2	●
RAa17	F	77	6.58	SARS-CoV-2	Untreated	2	■
RCd8	M	246	14.4	SARS-CoV-2	Untreated	2	▲
RMj8	M	239	14.655	SARS-CoV-2	IFNmod	4	○
KV31	M	91	11.35	SARS-CoV-2	IFNmod	7	□
RCk17	F	70	5.5	SARS-CoV-2	IFNmod	4	△
RRj11	F	181	8.51	SARS-CoV-2	IFNmod	7	▽
RNi17	M	70	10.445	SARS-CoV-2	IFNmod	4	◇
RZs14	M	118	13.39	SARS-CoV-2	IFNmod	7	⬡
LD22	M	88	14.75	SARS-CoV-2	IFNmod	2	●
X17	F	89	5.64	SARS-CoV-2	IFNmod	2	■
RAz8	M	234	12.7	SARS-CoV-2	IFNmod	2	▲

Table 3.S1. Uninfected and SARS-CoV-2-infected macaque characteristics. Animal ID. Sex. Age in months and weight at beginning of study in kg. Infection status. Treatment group assignment. Day post infection that necropsy was performed. Annotated symbol in figures. For infected animals, open symbols indicate that the animal was necropsied at 4 dpi or 7 dpi while filled symbols indicate that the animal was necropsied at 2 dpi.

Coronavirus Vaccine and Treatment Evaluation Network
Standard Clinical Assessment

Parameter	Rating/Description	Assessment Score
Responsiveness	**0** - Normal - bright, alert, responsive	
	1 - Mildly affected - slightly depressed, acts disinterested with personnel in room, lies down in cage but gets up when approached	
	2 - Moderately affected/obtunded - non-responsive, very disinterested in personnel, hunched or lying down, will get up when stimulated	
	3 - Severely affected/comatose - lying down completely unresponsive to stimuli	
Discharges	**0** - Normal	
	1 - Mild nasal/ocular	
	3 - Severe nasal/ocular	
Respiratory Rate	**0** - Normal	
	1 - Mild tachypnea	
	3 - Severe tachypnea	
Respiratory Effort	**0** - Normal - no apparent changes in breathing	
	1 - Mild - slightly increased effort breathing	
	3 - Severe-open mouth breathing, abdominal breathing	
Cough	**0** - Normal (normal skin turgor, moist mucous membranes)	
	1 - Mild dehydration (5-10%)	
	3 - Severe dehydration (>10%)	
Fecal consistency	**0** - Normal	
	1 - Soft	
	2 - Fluid	
	Total	
Notes		

Table 3.S2. Coronavirus Vaccine and Treatment Evaluation Network (CoVTEN) standard clinical assessment for cage-side scores, related to Fig. 3.S2b. Cage-side scores were performed at 0, 1, 2, 3, 4, 5, and 7 dpi and added to anesthetized scores to obtain the total clinical score for each dpi. Cageside scores were based on responsiveness, discharges, respiratory rate, respiratory effect, cough, and fecal consistency and were completed prior to anesthesia.

Coronavirus Vaccine and Treatment Evaluation Network
Standard Clinical Assessment

Parameter	Description	Assessment Score
Discharges	**0** - Normal	
	1 - Mild (ocular/nasal)	
	3 - Severe (ocular/nasal)	
Respiratory character	**0** - Normal	
	1 - Mild dyspnea	
	3 - Severe dyspnea	
Hydration	**0** - Normal (normal skin turgor, moist mucous membranes)	
	1 - Mild dehydration (5-10%)	
	3 - Severe dehydration (>10%)	
	Total	

Physical Examination Under Anesthesia - Objective measures

	Body Weight (kg)	Body Condition Score	Respiratory rate (bpm)	SpO2	Rectal Temperature (°F)	
Value						
Notes						

Table 3.S3. Coronavirus Vaccine and Treatment Evaluation Network (CoVTEN) standard clinical assessment for anesthetized scores, related to Fig. 3.S2b. Anesthetized scores were performed at 0, 1, 2, 3, 4, 5, and 7 dpi and added to cageside scores to obtain the total clinical score for each dpi. Anesthetized scores were based on discharges, respiratory character, and hydration. Body weights (kg), body condition scores, respiratory rates (bpm), SpO2 (%), and rectal temperatures (°F) were also recorded during anesthetic accesses.

Chapter Four: Discussion

The COVID-19 pandemic has resulted in significant morbidity and mortality, with over 770 million confirmed cases of SARS-CoV-2 infection and 6.9 million COVID-19-related deaths [13]. Although COVID-19 vaccines have been shown to be effective in protecting against severe disease, the emergence of variants of concern that are capable of evading vaccine-induced immunity and immunity from natural infection is a significant threat to global health. At present, SARS-CoV-2 variant EG.5 is the fastest growing variant in multiple areas of the world and COVID-19 test positivity, wastewater levels, hospitalizations, and deaths are on the rise, with COVID-19 related deaths increasing by 17.6% within the U.S. in the last week alone [29]. Although it is unclear if EG.5 is driving the current COVID-19 wave, this new variant has been shown to possess mutations that are linked to increased transmissibility and decreased susceptibility to antibodies induced by current vaccines [446]. In addition to the threat of EG.5, the emergence of SARS-CoV-2 variant BA.2.86 which possesses 30 mutations in its spike protein compared to XBB.1.5 is of great concern [228].

While vaccines are actively being updated to keep up with the emergence of these new variants, there is a significant need for effective COVID-19 therapeutics to treat individuals with breakthrough infections and those that are unvaccinated. Current therapies approved or authorized for emergency use in COVID-19 patients are limited and some of these medications have multiple drug interactions or are contraindicated in populations that are most at-risk for severe disease such as patients with chronic kidney disease [447]. The identification of SARS-CoV-2 clinical isolates that are resistant to approved direct-acting antivirals such as Paxlovid underscores the importance for

expanding available treatment options, pursuing more broad-spectrum antivirals such as host-directed antivirals, and potentially administering a combination of antivirals to prevent the emergence of treatment-resistant strains [448]. Additionally, while currently available therapies have been shown to reduce mortality rates in severe and critical COVID-19 patients, mortality in treated patients still remains high, necessitating the development of more effective treatment options [449].

Although some cases of COVID-19 progress to severe and even critical disease, the majority of individuals experience mild to moderate disease [26]. Currently, there are several therapeutics approved for use in patients with mild to moderate COVID-19 that are at high risk of progressing to severe disease including Nirmatrelvir/Ritonavir, Remdesivir, and Molnupiravir [239]. However, to date, no therapeutic has been approved for the treatment of individuals with mild to moderate infection who have not been defined as being at high risk for progressing to severe disease. The development of a therapeutic capable of reducing the duration of viral shedding and time to symptom resolution in individuals with mild to moderate COVID-19 not only has the capacity to reduce the spread of SARS-CoV-2 but also lessen the economic burden of COVID-19. Additionally, given that individuals who have had mild to moderate COVID-19 are still susceptible to developing long COVID/ post-COVID syndrome, the identification of therapeutics that are effective at mitigating this risk is of great importance [450].

In order to develop more targeted and effective therapies, it is essential that further research is conducted to more fully characterize SARS-CoV-2 pathogenesis and immune-mediated pathology. Animal models of SARS-CoV-2 infection continue to play important roles in advancing COVID-19 research, allowing for the control of key

parameters and the collection of tissues otherwise not available in human studies. Given the wide spectrum of disease that is observed in individuals with COVID-19, it is essential that animal models that mimic the pathogenesis of mild, moderate, and severe COVID-19 are utilized. Rhesus macaques are physiologically and genetically similar to humans and, like humans, the majority of SARS-CoV-2-infected rhesus macaques develop mild to moderate COVID-19. Therefore, we believe that the NHP model of SARS-CoV-2 remains uniquely appropriate to investigate SARS-CoV-2 pathogenesis and to develop novel therapies for mild and moderate COVID in humans.

Use of the rhesus macaque model of SARS-CoV-2 infection in both of the included studies enabled us to control for parameters that may impact clinical outcome in humans (i.e., virus strain, dose, and route of challenge) and allowed us to perform both longitudinal collections of BAL fluid and in-depth histological examination of lung tissues at necropsy. Furthermore, use of an RM model enabled the characterization of some of the earliest immune events following infection, something that would only be possible in humans through SARS-CoV-2 human challenge studies, the ethics of which are hotly debated due to potential risk for developing severe disease or post-COVID syndrome. As such, these studies produced an unprecedented in-depth mechanistic characterization of the early immunological events following SARS-CoV-2 infection and the effect of baricitinib and IFNmod on COVID-19 pathogenesis, including single-cell RNA sequencing analyses of BAL and lung-derived cells (i.e., macrophages, epithelial cells, endothelial cells, etc.) at the peak of infection.

Previously, our group showed that myeloid cells were primarily responsible for the production of pro-inflammatory cytokines in the lower airways of SARS-CoV-2-infected

RMs at 4 days post infection [173]. Here, we identified the specific myeloid subsets contributing to these pro-inflammatory cytokines as CD163+MRC1+TREM2+ and CD163+MRC1− macrophages and show that these two populations infiltrate into the lower airways of RMs during hyperacute SARS-CoV-2 infection. We also show that baricitinib, a JAK1/JAK2 inhibitor that was the first immunomodulatory agent FDA approved for the treatment of COVID-19, was able to reduce the infiltration of both of these macrophage populations and decrease the expression of pro-inflammatory cytokines. Importantly, comparative analysis of our NHP sc-RNA-Seq data with published human studies showed that the CD163+MRC1+TREM2+ and CD163+MRC1− macrophages that we had defined transcriptionally in NHPs had analogous populations in the human lung, further supporting the relevance of NHPs as a model for human SARS-CoV-2 infection.

In the first included study, we also observed an increase in pDCs in the lower airway following SARS-CoV-2 infection, consistent with what was observed by Laurent et al. in patients with mild COVID-19 [390]. This increase in pDCs coincided with the peak of IFN-I signaling in SARS-CoV-2-infected RMs. Since the role of IFN-I in regulating SARS-CoV-2 replication and pathogenesis is incompletely understood and carries important clinical and therapeutic implications for COVID-19 patients, we pursued a second study to dissect the role of this early IFN response in SARS-CoV-2 infection using the rhesus macaque model. Here, we present the first *in vivo* study showing the direct impact of blocking IFN-I using IFNmod in SARS-CoV-2 infected RMs. The key result of this study is that IFNmod treatment was highly effective in attenuating antiviral and inflammatory ISGs in PBMCs, whole blood, BAL, and lung of SARS-CoV-2 infected RMs when initiated

pre-infection. Based on the results of previous studies, one may expect that a lower IFN-I response would be associated with higher viremia[114, 119, 354, 355]. However, we found that IFNmod-treated SARS-CoV-2-infected RMs consistently showed: (i) >3 $\log_{10}$ reduction of viremia in upper and lower airways, (ii) decreased COVID-19 pathogenesis; (iii) attenuation of canonical pro-inflammatory genes and pathways; and (iv) markedly reduced levels of soluble and cellular markers of inflammation and disease severity, as compared to treatment-naïve, SARS-CoV-2-infected controls. In addition, our single-cell transcriptomic analyses of BAL and lung-derived cells showed a central role of IFN-I in regulating the axis of infiltrating macrophages and subsequent inflammation within the airway and lung interstitium, and demonstrated that targeted modulation of the IFN-I system during early SARS-CoV-2 infection reduces the level of cell-associated virus on macrophages and suppresses the induction of the inflammasome.

There are several limitations of the two included studies. For both studies, we were unable to validate the scRNAseq findings pertaining to BAL macrophages through conventional flow cytometry. This was due to the autofluorescence of the large population of macrophages in the BAL in multiple channels, which prohibited us from confidently identifying CD163+/CD206+ BAL macrophages. Importantly, however, we did not observe autofluorescence in the smaller monocyte population in the BAL, thereby supporting that our flow cytometry data on the smaller monocyte population in both studies is robust.

Furthermore, in the second study, we were not able to directly determine if IFNmod treatment reduced inflammatory responses in SARS-CoV-2-infected animals i) solely due to it inhibiting endogenous IFN-I responses or ii) if the lower viral loads in IFNmod-treated

animals were also contributing to lower inflammatory responses. Importantly, we showed in Calu-3 cells that IFNmod treatment in the presence of IFNα (and absence of SARS-CoV-2 infection) potently inhibits both antiviral and pro-inflammatory IFN-I pathways. Thus, IFNmod was shown in vitro to reduce inflammation independent of viral loads. Furthermore, *in vivo* we show that despite viral loads being similar between treated and untreated animals at 4 and 7dpi, IFNmod-treated RMs still experienced significantly lower levels of inflammation, including (i) lower frequency of blood CD14+CD16+ monocytes and pDCs; (ii) decreased expression of IL-6 JAK/STAT, TNF, inflammatory cytokine and chemokine genes; and (iv) reduced total lung pathology score and average score per lung lobe. However, when we compared the effect of direct inhibition of SARS-CoV-2 viral replication with Nirmatrelvir vs. IFNmod treatment on the expression of antiviral and inflammatory ISGs in vitro, we found that both treatments resulted in a potent reduction in CXCL10 mRNA, supporting the idea that reduction of viral loads is associated with reduced inflammation. Taken together, these data indicate that the reduced inflammation observed in SARS-CoV-2-infected, IFNmod-treated RMs may be influenced by both inhibition of endogenous IFN-I responses as well as the lower viral loads.

While IFNmod significantly decreased viral loads and pathology when initiated pre-infection in the rhesus macaques in our study, it is important to note that the using IFNmod clinically as a COVID-19 prophylactic has low feasibility. Previous studies administering IFNmod in uninfected rhesus macaques (referred to as IFN1ant) reported that IFNmod had a relatively short half-life, resulting in a need for daily dosing [397]. While this short life-span was part of the rationale for our mechanistically-oriented study where we wanted to modulate the IFN-I pathways only at the very early phase of infection, this short half-life

would make prophylactic treatment in the setting of a multi-year-long pandemic with a respiratory virus difficult and long-term treatment may not be well-tolerated. A prophylactic similar to Evusheld, a combination of anti-SARS-CoV-2 monoclonal antibodies previously authorized for use as a COVID-19 prophylactic that required dosing once every six months, would be a much more practical option [451]. Furthermore, although we show that IFNmod results in a decrease in viral RNA when administered post-SARS-CoV-2-infection in Calu-3 cells, we did not conduct post-infection IFNmod treatment initiation in RMs. Therefore, very limited conclusions can be drawn from our study about IFNmod as a candidate COVID-19 therapeutic.

Importantly, IFNmod was previously observed to have vastly different effects in rhesus macaques when it was administered during different phases of SIV infection. While IFNmod administration during acute SIV infection was shown to lead to an increase in the SIV reservoir size and a faster rate of CD4 T cell decline and progression of AIDS, IFNmod had beneficial effects in chronically SIV-infected animals that were ART-suppressed or ART-untreated, resulting in the suppression of IFN-I-mediated inflammatory pathways [368, 397]. The stark differences in the effects of IFNmod initiated at different post-SIV infection timepoints highlights the importance of timing in IFN responses to viral infections as well as the importance for determining the optimal treatment window for IFNmod in SARS-CoV-2 infection.

While further studies are needed to evaluate IFNmod as a candidate therapeutic, our in vivo mechanistic study supports a critical role of IFN-I in regulating COVID-19 pathogenesis. Together, our two studies contribute to a deeper understanding of the early immune events in hyperacute SARS-CoV-2 infection and support a model where an early

and controlled IFN-I response is beneficial following SARS-CoV-2 infection, whereas uncontrolled IFN-I-signaling leads to an influx of inflammatory macrophages in the lower airways and critically contributes to SARS-CoV-2 inflammation.

REFERENCES

1. Wu JT, Leung K, Leung GM. Nowcasting and forecasting the potential domestic and international spread of the 2019-nCoV outbreak originating in Wuhan, China: a modelling study. Lancet. 2020;395(10225):689-97. Epub 20200131. doi: 10.1016/S0140-6736(20)30260-9. PubMed PMID: 32014114; PMCID: PMC7159271.

2. Gralinski LE, Menachery VD. Return of the Coronavirus: 2019-nCoV. Viruses. 2020;12(2). Epub 20200124. doi: 10.3390/v12020135. PubMed PMID: 31991541; PMCID: PMC7077245.

3. Zhou H, Ji J, Chen X, Bi Y, Li J, Wang Q, Hu T, Song H, Zhao R, Chen Y, Cui M, Zhang Y, Hughes AC, Holmes EC, Shi W. Identification of novel bat coronaviruses sheds light on the evolutionary origins of SARS-CoV-2 and related viruses. Cell. 2021;184(17):4380-91 e14. Epub 20210609. doi: 10.1016/j.cell.2021.06.008. PubMed PMID: 34147139; PMCID: PMC8188299.

4. Zhu N, Zhang D, Wang W, Li X, Yang B, Song J, Zhao X, Huang B, Shi W, Lu R, Niu P, Zhan F, Ma X, Wang D, Xu W, Wu G, Gao GF, Tan W, China Novel Coronavirus I, Research T. A Novel Coronavirus from Patients with Pneumonia in China, 2019. N Engl J Med. 2020;382(8):727-33. Epub 2020/01/25. doi: 10.1056/NEJMoa2001017. PubMed PMID: 31978945; PMCID: PMC7092803.

5. Wu F, Zhao S, Yu B, Chen YM, Wang W, Song ZG, Hu Y, Tao ZW, Tian JH, Pei YY, Yuan ML, Zhang YL, Dai FH, Liu Y, Wang QM, Zheng JJ, Xu L, Holmes EC, Zhang YZ. A new coronavirus associated with human respiratory disease in China. Nature. 2020;579(7798):265-9. Epub 20200203. doi: 10.1038/s41586-020-2008-3. PubMed PMID: 32015508; PMCID: PMC7094943.

6. Coronaviridae Study Group of the International Committee on Taxonomy of V. The species Severe acute respiratory syndrome-related coronavirus: classifying 2019-nCoV and naming it SARS-CoV-2. Nat Microbiol. 2020;5(4):536-44. Epub 20200302. doi: 10.1038/s41564-020-0695-z. PubMed PMID: 32123347; PMCID: PMC7095448.

7. Chan JF, Yuan S, Kok KH, To KK, Chu H, Yang J, Xing F, Liu J, Yip CC, Poon RW, Tsoi HW, Lo SK, Chan KH, Poon VK, Chan WM, Ip JD, Cai JP, Cheng VC, Chen H, Hui CK, Yuen KY. A familial cluster of pneumonia associated with the 2019 novel coronavirus indicating person-to-person transmission: a study of a family cluster. Lancet. 2020;395(10223):514-23. Epub 20200124. doi: 10.1016/S0140-6736(20)30154-9. PubMed PMID: 31986261; PMCID: PMC7159286.

8. Rothe C, Schunk M, Sothmann P, Bretzel G, Froeschl G, Wallrauch C, Zimmer T, Thiel V, Janke C, Guggemos W, Seilmaier M, Drosten C, Vollmar P, Zwirglmaier K, Zange S, Wolfel R, Hoelscher M. Transmission of 2019-nCoV Infection from an Asymptomatic Contact in Germany. N Engl J Med. 2020;382(10):970-1. Epub 20200130. doi: 10.1056/NEJMc2001468. PubMed PMID: 32003551; PMCID: PMC7120970.

9. Riou J, Althaus CL. Pattern of early human-to-human transmission of Wuhan 2019 novel coronavirus (2019-nCoV), December 2019 to January 2020. Euro Surveill. 2020;25(4). doi: 10.2807/1560-7917.ES.2020.25.4.2000058. PubMed PMID: 32019669; PMCID: PMC7001239.

10. Cucinotta D, Vanelli M. WHO Declares COVID-19 a Pandemic. Acta Biomed. 2020;91(1):157-60. Epub 20200319. doi: 10.23750/abm.v91i1.9397. PubMed PMID: 32191675; PMCID: PMC7569573.

11. HHS. Determination That A Public Health Emergency Exists 2020. Available from: https://aspr.hhs.gov/legal/PHE/Pages/2019-nCoV.aspx.

12. CDC. CDC Museum COVID-19 Timeline: CDC; 2023 [updated 2023-03-15T02:17:05Z]. Available from: https://www.cdc.gov/museum/timeline/covid19.html.

13. WHO Coronavirus (COVID-19) Dashboard: World Health Organization; 2020 [updated August 30, 2023; cited 2023 September]. Available from: https://covid19.who.int/.

14. Cui J, Li F, Shi ZL. Origin and evolution of pathogenic coronaviruses. Nat Rev Microbiol. 2019;17(3):181-92. doi: 10.1038/s41579-018-0118-9. PubMed PMID: 30531947; PMCID: PMC7097006.

15. Donaldson EF, Haskew AN, Gates JE, Huynh J, Moore CJ, Frieman MB. Metagenomic analysis of the viromes of three North American bat species: viral diversity among different bat species that share a common habitat. J Virol. 2010;84(24):13004-18. Epub 20101006. doi: 10.1128/JVI.01255-10. PubMed PMID: 20926577; PMCID: PMC3004358.

16. Pfefferle S, Oppong S, Drexler JF, Gloza-Rausch F, Ipsen A, Seebens A, Muller MA, Annan A, Vallo P, Adu-Sarkodie Y, Kruppa TF, Drosten C. Distant relatives of severe acute respiratory syndrome coronavirus and close relatives of human coronavirus 229E in bats, Ghana. Emerg Infect Dis. 2009;15(9):1377-84. doi: 10.3201/eid1509.090224. PubMed PMID: 19788804; PMCID: PMC2819850.

17. Huynh J, Li S, Yount B, Smith A, Sturges L, Olsen JC, Nagel J, Johnson JB, Agnihothram S, Gates JE, Frieman MB, Baric RS, Donaldson EF. Evidence supporting a zoonotic origin of human coronavirus strain NL63. J Virol. 2012;86(23):12816-25. Epub 20120919. doi: 10.1128/JVI.00906-12. PubMed PMID: 22993147; PMCID: PMC3497669.

18. Andersen KG, Rambaut A, Lipkin WI, Holmes EC, Garry RF. The proximal origin of SARS-CoV-2. Nat Med. 2020;26(4):450-2. doi: 10.1038/s41591-020-0820-9. PubMed PMID: 32284615; PMCID: PMC7095063.

19. Zhou P, Yang XL, Wang XG, Hu B, Zhang L, Zhang W, Si HR, Zhu Y, Li B, Huang CL, Chen HD, Chen J, Luo Y, Guo H, Jiang RD, Liu MQ, Chen Y, Shen XR, Wang X, Zheng XS, Zhao K, Chen QJ, Deng F, Liu LL, Yan B, Zhan FX, Wang YY, Xiao GF, Shi

ZL. A pneumonia outbreak associated with a new coronavirus of probable bat origin. Nature. 2020;579(7798):270-3. Epub 20200203. doi: 10.1038/s41586-020-2012-7. PubMed PMID: 32015507; PMCID: PMC7095418.

20. Huang C, Wang Y, Li X, Ren L, Zhao J, Hu Y, Zhang L, Fan G, Xu J, Gu X, Cheng Z, Yu T, Xia J, Wei Y, Wu W, Xie X, Yin W, Li H, Liu M, Xiao Y, Gao H, Guo L, Xie J, Wang G, Jiang R, Gao Z, Jin Q, Wang J, Cao B. Clinical features of patients infected with 2019 novel coronavirus in Wuhan, China. Lancet. 2020;395(10223):497-506. Epub 20200124. doi: 10.1016/S0140-6736(20)30183-5. PubMed PMID: 31986264; PMCID: PMC7159299.

21. Wan Y, Shang J, Graham R, Baric RS, Li F. Receptor Recognition by the Novel Coronavirus from Wuhan: an Analysis Based on Decade-Long Structural Studies of SARS Coronavirus. J Virol. 2020;94(7). Epub 20200317. doi: 10.1128/JVI.00127-20. PubMed PMID: 31996437; PMCID: PMC7081895.

22. Shi H, Han X, Jiang N, Cao Y, Alwalid O, Gu J, Fan Y, Zheng C. Radiological findings from 81 patients with COVID-19 pneumonia in Wuhan, China: a descriptive study. Lancet Infect Dis. 2020;20(4):425-34. Epub 20200224. doi: 10.1016/S1473-3099(20)30086-4. PubMed PMID: 32105637; PMCID: PMC7159053.

23. NIH. Clinical Spectrum of SARS-CoV-2 Infection 2023 [updated 3/6/2023; cited 2023 9/4]. Available from: https://www.covid19treatmentguidelines.nih.gov/overview/clinical-spectrum/.

24. Chen C, Zhu C, Yan D, Liu H, Li D, Zhou Y, Fu X, Wu J, Ding C, Tian G, Lan L, Liu X, Huang C, Hecht R, Li L, Yang S. The epidemiological and radiographical characteristics of asymptomatic infections with the novel coronavirus (COVID-19): A systematic review and meta-analysis. Int J Infect Dis. 2021;104:458-64. Epub 20210112. doi: 10.1016/j.ijid.2021.01.017. PubMed PMID: 33444755; PMCID: PMC7833455.

25. Shang W, Kang L, Cao G, Wang Y, Gao P, Liu J, Liu M. Percentage of Asymptomatic Infections among SARS-CoV-2 Omicron Variant-Positive Individuals: A Systematic Review and Meta-Analysis. Vaccines (Basel). 2022;10(7). Epub 20220630. doi: 10.3390/vaccines10071049. PubMed PMID: 35891214; PMCID: PMC9321237.

26. Wu Z, McGoogan JM. Characteristics of and Important Lessons From the Coronavirus Disease 2019 (COVID-19) Outbreak in China: Summary of a Report of 72 314 Cases From the Chinese Center for Disease Control and Prevention. JAMA. 2020;323(13):1239-42. doi: 10.1001/jama.2020.2648. PubMed PMID: 32091533.

27. de Wit E, van Doremalen N, Falzarano D, Munster VJ. SARS and MERS: recent insights into emerging coronaviruses. Nat Rev Microbiol. 2016;14(8):523-34. Epub 20160627. doi: 10.1038/nrmicro.2016.81. PubMed PMID: 27344959; PMCID: PMC7097822.

28. Ahmad FB, Cisewski JA, Minino A, Anderson RN. Provisional Mortality Data - United States, 2020. MMWR Morb Mortal Wkly Rep. 2021;70(14):519-22. Epub

20210409. doi: 10.15585/mmwr.mm7014e1. PubMed PMID: 33830988; PMCID: PMC8030985.

29. Cdc. COVID Data Tracker2020.

30. Fadini GP, Morieri ML, Boscari F, Fioretto P, Maran A, Busetto L, Bonora BM, Selmin E, Arcidiacono G, Pinelli S, Farnia F, Falaguasta D, Russo L, Voltan G, Mazzocut S, Costantini G, Ghirardini F, Tresso S, Cattelan AM, Vianello A, Avogaro A, Vettor R. Newly-diagnosed diabetes and admission hyperglycemia predict COVID-19 severity by aggravating respiratory deterioration. Diabetes Res Clin Pract. 2020;168:108374. Epub 20200815. doi: 10.1016/j.diabres.2020.108374. PubMed PMID: 32805345; PMCID: PMC7428425.

31. Fadini GP, Morieri ML, Longato E, Avogaro A. Prevalence and impact of diabetes among people infected with SARS-CoV-2. J Endocrinol Invest. 2020;43(6):867-9. Epub 20200328. doi: 10.1007/s40618-020-01236-2. PubMed PMID: 32222956; PMCID: PMC7103097.

32. Saini KS, Tagliamento M, Lambertini M, McNally R, Romano M, Leone M, Curigliano G, de Azambuja E. Mortality in patients with cancer and coronavirus disease 2019: A systematic review and pooled analysis of 52 studies. Eur J Cancer. 2020;139:43-50. Epub 20200902. doi: 10.1016/j.ejca.2020.08.011. PubMed PMID: 32971510; PMCID: PMC7467090.

33. Zhou Y, Yang Q, Chi J, Dong B, Lv W, Shen L, Wang Y. Comorbidities and the risk of severe or fatal outcomes associated with coronavirus disease 2019: A systematic review and meta-analysis. Int J Infect Dis. 2020;99:47-56. Epub 20200725. doi: 10.1016/j.ijid.2020.07.029. PubMed PMID: 32721533; PMCID: PMC7381888.

34. Kompaniyets L, Pennington AF, Goodman AB, Rosenblum HG, Belay B, Ko JY, Chevinsky JR, Schieber LZ, Summers AD, Lavery AM, Preston LE, Danielson ML, Cui Z, Namulanda G, Yusuf H, Mac Kenzie WR, Wong KK, Baggs J, Boehmer TK, Gundlapalli AV. Underlying Medical Conditions and Severe Illness Among 540,667 Adults Hospitalized With COVID-19, March 2020-March 2021. Prev Chronic Dis. 2021;18:E66. Epub 20210701. doi: 10.5888/pcd18.210123. PubMed PMID: 34197283; PMCID: PMC8269743.

35. Kissler SM, Fauver JR, Mack C, Tai CG, Breban MI, Watkins AE, Samant RM, Anderson DJ, Metti J, Khullar G, Baits R, MacKay M, Salgado D, Baker T, Dudley JT, Mason CE, Ho DD, Grubaugh ND, Grad YH. Viral Dynamics of SARS-CoV-2 Variants in Vaccinated and Unvaccinated Persons. N Engl J Med. 2021;385(26):2489-91. Epub 20211201. doi: 10.1056/NEJMc2102507. PubMed PMID: 34941024; PMCID: PMC8693673.

36. Sun K, Tempia S, Kleynhans J, von Gottberg A, McMorrow ML, Wolter N, Bhiman JN, Moyes J, du Plessis M, Carrim M, Buys A, Martinson NA, Kahn K, Tollman S, Lebina L, Wafawanaka F, du Toit JD, Gomez-Olive FX, Mkhencele T, Viboud C, Cohen C. SARS-CoV-2 transmission, persistence of immunity, and estimates of Omicron's impact in South

African population cohorts. Sci Transl Med. 2022;14(659):eabo7081. Epub 20220824. doi: 10.1126/scitranslmed.abo7081. PubMed PMID: 35638937; PMCID: PMC9161370.

37. Cevik M, Tate M, Lloyd O, Maraolo AE, Schafers J, Ho A. SARS-CoV-2, SARS-CoV, and MERS-CoV viral load dynamics, duration of viral shedding, and infectiousness: a systematic review and meta-analysis. Lancet Microbe. 2021;2(1):e13-e22. Epub 20201119. doi: 10.1016/S2666-5247(20)30172-5. PubMed PMID: 33521734; PMCID: PMC7837230.

38. Hakki S, Zhou J, Jonnerby J, Singanayagam A, Barnett JL, Madon KJ, Koycheva A, Kelly C, Houston H, Nevin S, Fenn J, Kundu R, Crone MA, Pillay TD, Ahmad S, Derqui-Fernandez N, Conibear E, Freemont PS, Taylor GP, Ferguson N, Zambon M, Barclay WS, Dunning J, Lalvani A, investigators As. Onset and window of SARS-CoV-2 infectiousness and temporal correlation with symptom onset: a prospective, longitudinal, community cohort study. Lancet Respir Med. 2022;10(11):1061-73. Epub 20220818. doi: 10.1016/S2213-2600(22)00226-0. PubMed PMID: 35988572; PMCID: PMC9388060.

39. Who. Coronavirus disease 2019 (COVID-19) Situation Report – 73 2020 [updated 4/2/2020]. Available from: https://apps.who.int/iris/bitstream/handle/10665/331686/nCoVsitrep02Apr2020-eng.pdf?sequence=1&isAllowed=y.

40. WHO. Post COVID-19 condition (Long COVID) 2022 [updated 12/7/2022; cited 2023 9/4]. Available from: https://www.who.int/europe/news-room/fact-sheets/item/post-covid-19-condition.

41. Davis HE, Assaf GS, McCorkell L, Wei H, Low RJ, Re'em Y, Redfield S, Austin JP, Akrami A. Characterizing long COVID in an international cohort: 7 months of symptoms and their impact. EClinicalMedicine. 2021;38:101019. Epub 20210715. doi: 10.1016/j.eclinm.2021.101019. PubMed PMID: 34308300; PMCID: PMC8280690.

42. Davis HE, McCorkell L, Vogel JM, Topol EJ. Author Correction: Long COVID: major findings, mechanisms and recommendations. Nat Rev Microbiol. 2023;21(6):408. doi: 10.1038/s41579-023-00896-0. PubMed PMID: 37069455; PMCID: PMC10408714.

43. Larsen NW, Stiles LE, Shaik R, Schneider L, Muppidi S, Tsui CT, Geng LN, Bonilla H, Miglis MG. Characterization of autonomic symptom burden in long COVID: A global survey of 2,314 adults. Front Neurol. 2022;13:1012668. Epub 20221019. doi: 10.3389/fneur.2022.1012668. PubMed PMID: 36353127; PMCID: PMC9639503.

44. Xie Y, Xu E, Bowe B, Al-Aly Z. Long-term cardiovascular outcomes of COVID-19. Nat Med. 2022;28(3):583-90. Epub 20220207. doi: 10.1038/s41591-022-01689-3. PubMed PMID: 35132265; PMCID: PMC8938267.

45. Xie Y, Al-Aly Z. Risks and burdens of incident diabetes in long COVID: a cohort study. Lancet Diabetes Endocrinol. 2022;10(5):311-21. Epub 20220321. doi: 10.1016/S2213-8587(22)00044-4. PubMed PMID: 35325624; PMCID: PMC8937253.

46. Mancini DM, Brunjes DL, Lala A, Trivieri MG, Contreras JP, Natelson BH. Use of Cardiopulmonary Stress Testing for Patients With Unexplained Dyspnea Post-Coronavirus Disease. JACC Heart Fail. 2021;9(12):927-37. doi: 10.1016/j.jchf.2021.10.002. PubMed PMID: 34857177; PMCID: PMC8629098.

47. Kedor C, Freitag H, Meyer-Arndt L, Wittke K, Hanitsch LG, Zoller T, Steinbeis F, Haffke M, Rudolf G, Heidecker B, Bobbert T, Spranger J, Volk HD, Skurk C, Konietschke F, Paul F, Behrends U, Bellmann-Strobl J, Scheibenbogen C. A prospective observational study of post-COVID-19 chronic fatigue syndrome following the first pandemic wave in Germany and biomarkers associated with symptom severity. Nat Commun. 2022;13(1):5104. Epub 20220830. doi: 10.1038/s41467-022-32507-6. PubMed PMID: 36042189; PMCID: PMC9426365.

48. Ceban F, Ling S, Lui LMW, Lee Y, Gill H, Teopiz KM, Rodrigues NB, Subramaniapillai M, Di Vincenzo JD, Cao B, Lin K, Mansur RB, Ho RC, Rosenblat JD, Miskowiak KW, Vinberg M, Maletic V, McIntyre RS. Fatigue and cognitive impairment in Post-COVID-19 Syndrome: A systematic review and meta-analysis. Brain Behav Immun. 2022;101:93-135. Epub 20211229. doi: 10.1016/j.bbi.2021.12.020. PubMed PMID: 34973396; PMCID: PMC8715665.

49. Su Y, Yuan D, Chen DG, Ng RH, Wang K, Choi J, Li S, Hong S, Zhang R, Xie J, Kornilov SA, Scherler K, Pavlovitch-Bedzyk AJ, Dong S, Lausted C, Lee I, Fallen S, Dai CL, Baloni P, Smith B, Duvvuri VR, Anderson KG, Li J, Yang F, Duncombe CJ, McCulloch DJ, Rostomily C, Troisch P, Zhou J, Mackay S, DeGottardi Q, May DH, Taniguchi R, Gittelman RM, Klinger M, Snyder TM, Roper R, Wojciechowska G, Murray K, Edmark R, Evans S, Jones L, Zhou Y, Rowen L, Liu R, Chour W, Algren HA, Berrington WR, Wallick JA, Cochran RA, Micikas ME, Unit IS-SC-B, Wrin T, Petropoulos CJ, Cole HR, Fischer TD, Wei W, Hoon DSB, Price ND, Subramanian N, Hill JA, Hadlock J, Magis AT, Ribas A, Lanier LL, Boyd SD, Bluestone JA, Chu H, Hood L, Gottardo R, Greenberg PD, Davis MM, Goldman JD, Heath JR. Multiple early factors anticipate post-acute COVID-19 sequelae. Cell. 2022;185(5):881-95 e20. Epub 20220125. doi: 10.1016/j.cell.2022.01.014. PubMed PMID: 35216672; PMCID: PMC8786632.

50. Bowe B, Xie Y, Al-Aly Z. Acute and postacute sequelae associated with SARS-CoV-2 reinfection. Nat Med. 2022;28(11):2398-405. Epub 20221110. doi: 10.1038/s41591-022-02051-3. PubMed PMID: 36357676; PMCID: PMC9671810.

51. Ayoubkhani D, Bosworth ML, King S, Pouwels KB, Glickman M, Nafilyan V, Zaccardi F, Khunti K, Alwan NA, Walker AS. Risk of Long COVID in People Infected With Severe Acute Respiratory Syndrome Coronavirus 2 After 2 Doses of a Coronavirus Disease 2019 Vaccine: Community-Based, Matched Cohort Study. Open Forum Infect Dis. 2022;9(9):ofac464. Epub 20220912. doi: 10.1093/ofid/ofac464. PubMed PMID: 36168555; PMCID: PMC9494414.

52. Lu R, Zhao X, Li J, Niu P, Yang B, Wu H, Wang W, Song H, Huang B, Zhu N, Bi Y, Ma X, Zhan F, Wang L, Hu T, Zhou H, Hu Z, Zhou W, Zhao L, Chen J, Meng Y, Wang J, Lin Y, Yuan J, Xie Z, Ma J, Liu WJ, Wang D, Xu W, Holmes EC, Gao GF, Wu G, Chen

W, Shi W, Tan W. Genomic characterisation and epidemiology of 2019 novel coronavirus: implications for virus origins and receptor binding. Lancet. 2020;395(10224):565-74. Epub 20200130. doi: 10.1016/S0140-6736(20)30251-8. PubMed PMID: 32007145; PMCID: PMC7159086.

53. Llanes A, Restrepo CM, Caballero Z, Rajeev S, Kennedy MA, Lleonart R. Betacoronavirus Genomes: How Genomic Information has been Used to Deal with Past Outbreaks and the COVID-19 Pandemic. Int J Mol Sci. 2020;21(12). Epub 20200626. doi: 10.3390/ijms21124546. PubMed PMID: 32604724; PMCID: PMC7352669.

54. Ellis P, Somogyvari F, Virok DP, Noseda M, McLean GR. Decoding Covid-19 with the SARS-CoV-2 Genome. Curr Genet Med Rep. 2021;9(1):1-12. Epub 20210109. doi: 10.1007/s40142-020-00197-5. PubMed PMID: 33457109; PMCID: PMC7794078.

55. Gordon DE, Jang GM, Bouhaddou M, Xu J, Obernier K, White KM, O'Meara MJ, Rezelj VV, Guo JZ, Swaney DL, Tummino TA, Huttenhain R, Kaake RM, Richards AL, Tutuncuoglu B, Foussard H, Batra J, Haas K, Modak M, Kim M, Haas P, Polacco BJ, Braberg H, Fabius JM, Eckhardt M, Soucheray M, Bennett MJ, Cakir M, McGregor MJ, Li Q, Meyer B, Roesch F, Vallet T, Mac Kain A, Miorin L, Moreno E, Naing ZZC, Zhou Y, Peng S, Shi Y, Zhang Z, Shen W, Kirby IT, Melnyk JE, Chorba JS, Lou K, Dai SA, Barrio-Hernandez I, Memon D, Hernandez-Armenta C, Lyu J, Mathy CJP, Perica T, Pilla KB, Ganesan SJ, Saltzberg DJ, Rakesh R, Liu X, Rosenthal SB, Calviello L, Venkataramanan S, Liboy-Lugo J, Lin Y, Huang XP, Liu Y, Wankowicz SA, Bohn M, Safari M, Ugur FS, Koh C, Savar NS, Tran QD, Shengjuler D, Fletcher SJ, O'Neal MC, Cai Y, Chang JCJ, Broadhurst DJ, Klippsten S, Sharp PP, Wenzell NA, Kuzuoglu-Ozturk D, Wang HY, Trenker R, Young JM, Cavero DA, Hiatt J, Roth TL, Rathore U, Subramanian A, Noack J, Hubert M, Stroud RM, Frankel AD, Rosenberg OS, Verba KA, Agard DA, Ott M, Emerman M, Jura N, von Zastrow M, Verdin E, Ashworth A, Schwartz O, d'Enfert C, Mukherjee S, Jacobson M, Malik HS, Fujimori DG, Ideker T, Craik CS, Floor SN, Fraser JS, Gross JD, Sali A, Roth BL, Ruggero D, Taunton J, Kortemme T, Beltrao P, Vignuzzi M, Garcia-Sastre A, Shokat KM, Shoichet BK, Krogan NJ. A SARS-CoV-2 protein interaction map reveals targets for drug repurposing. Nature. 2020;583(7816):459-68. Epub 20200430. doi: 10.1038/s41586-020-2286-9. PubMed PMID: 32353859; PMCID: PMC7431030.

56. Gao T, Gao Y, Liu X, Nie Z, Sun H, Lin K, Peng H, Wang S. Identification and functional analysis of the SARS-COV-2 nucleocapsid protein. BMC Microbiol. 2021;21(1):58. Epub 20210222. doi: 10.1186/s12866-021-02107-3. PubMed PMID: 33618668; PMCID: PMC7898026.

57. Cubuk J, Alston JJ, Incicco JJ, Singh S, Stuchell-Brereton MD, Ward MD, Zimmerman MI, Vithani N, Griffith D, Wagoner JA, Bowman GR, Hall KB, Soranno A, Holehouse AS. The SARS-CoV-2 nucleocapsid protein is dynamic, disordered, and phase separates with RNA. Nat Commun. 2021;12(1):1936. Epub 20210329. doi: 10.1038/s41467-021-21953-3. PubMed PMID: 33782395; PMCID: PMC8007728.

58. Mu J, Xu J, Zhang L, Shu T, Wu D, Huang M, Ren Y, Li X, Geng Q, Xu Y, Qiu Y, Zhou X. SARS-CoV-2-encoded nucleocapsid protein acts as a viral suppressor of RNA interference in cells. Sci China Life Sci. 2020;63(9):1413-6. Epub 20200410. doi: 10.1007/s11427-020-1692-1. PubMed PMID: 32291557; PMCID: PMC7154568.

59. Li JY, Liao CH, Wang Q, Tan YJ, Luo R, Qiu Y, Ge XY. The ORF6, ORF8 and nucleocapsid proteins of SARS-CoV-2 inhibit type I interferon signaling pathway. Virus Res. 2020;286:198074. Epub 20200623. doi: 10.1016/j.virusres.2020.198074. PubMed PMID: 32589897; PMCID: PMC7309931.

60. Neuman BW, Kiss G, Kunding AH, Bhella D, Baksh MF, Connelly S, Droese B, Klaus JP, Makino S, Sawicki SG, Siddell SG, Stamou DG, Wilson IA, Kuhn P, Buchmeier MJ. A structural analysis of M protein in coronavirus assembly and morphology. J Struct Biol. 2011;174(1):11-22. Epub 20101203. doi: 10.1016/j.jsb.2010.11.021. PubMed PMID: 21130884; PMCID: PMC4486061.

61. Thomas S. The Structure of the Membrane Protein of SARS-CoV-2 Resembles the Sugar Transporter SemiSWEET. Pathog Immun. 2020;5(1):342-63. Epub 20201019. doi: 10.20411/pai.v5i1.377. PubMed PMID: 33154981; PMCID: PMC7608487.

62. Mandala VS, McKay MJ, Shcherbakov AA, Dregni AJ, Kolocouris A, Hong M. Structure and drug binding of the SARS-CoV-2 envelope protein transmembrane domain in lipid bilayers. Nat Struct Mol Biol. 2020;27(12):1202-8. Epub 20201111. doi: 10.1038/s41594-020-00536-8. PubMed PMID: 33177698; PMCID: PMC7718435.

63. Huang Y, Yang C, Xu XF, Xu W, Liu SW. Structural and functional properties of SARS-CoV-2 spike protein: potential antivirus drug development for COVID-19. Acta Pharmacol Sin. 2020;41(9):1141-9. Epub 20200803. doi: 10.1038/s41401-020-0485-4. PubMed PMID: 32747721; PMCID: PMC7396720.

64. Jaimes JA, Andre NM, Chappie JS, Millet JK, Whittaker GR. Phylogenetic Analysis and Structural Modeling of SARS-CoV-2 Spike Protein Reveals an Evolutionary Distinct and Proteolytically Sensitive Activation Loop. J Mol Biol. 2020;432(10):3309-25. Epub 20200419. doi: 10.1016/j.jmb.2020.04.009. PubMed PMID: 32320687; PMCID: PMC7166309.

65. Hoffmann M, Kleine-Weber H, Schroeder S, Kruger N, Herrler T, Erichsen S, Schiergens TS, Herrler G, Wu NH, Nitsche A, Muller MA, Drosten C, Pohlmann S. SARS-CoV-2 Cell Entry Depends on ACE2 and TMPRSS2 and Is Blocked by a Clinically Proven Protease Inhibitor. Cell. 2020;181(2):271-80 e8. Epub 20200305. doi: 10.1016/j.cell.2020.02.052. PubMed PMID: 32142651; PMCID: PMC7102627.

66. Li MY, Li L, Zhang Y, Wang XS. Expression of the SARS-CoV-2 cell receptor gene ACE2 in a wide variety of human tissues. Infect Dis Poverty. 2020;9(1):45. Epub 20200428. doi: 10.1186/s40249-020-00662-x. PubMed PMID: 32345362; PMCID: PMC7186534.

67. Zhao Y, Zhao Z, Wang Y, Zhou Y, Ma Y, Zuo W. Single-Cell RNA Expression Profiling of ACE2, the Receptor of SARS-CoV-2. Am J Respir Crit Care Med. 2020;202(5):756-9. doi: 10.1164/rccm.202001-0179LE. PubMed PMID: 32663409; PMCID: PMC7462411.

68. Jackson CB, Farzan M, Chen B, Choe H. Mechanisms of SARS-CoV-2 entry into cells. Nat Rev Mol Cell Biol. 2022;23(1):3-20. Epub 20211005. doi: 10.1038/s41580-021-00418-x. PubMed PMID: 34611326; PMCID: PMC8491763.

69. Matsuyama S, Nagata N, Shirato K, Kawase M, Takeda M, Taguchi F. Efficient activation of the severe acute respiratory syndrome coronavirus spike protein by the transmembrane protease TMPRSS2. J Virol. 2010;84(24):12658-64. Epub 20101006. doi: 10.1128/JVI.01542-10. PubMed PMID: 20926566; PMCID: PMC3004351.

70. Shirato K, Kawase M, Matsuyama S. Middle East respiratory syndrome coronavirus infection mediated by the transmembrane serine protease TMPRSS2. J Virol. 2013;87(23):12552-61. Epub 20130911. doi: 10.1128/JVI.01890-13. PubMed PMID: 24027332; PMCID: PMC3838146.

71. Bertram S, Dijkman R, Habjan M, Heurich A, Gierer S, Glowacka I, Welsch K, Winkler M, Schneider H, Hofmann-Winkler H, Thiel V, Pohlmann S. TMPRSS2 activates the human coronavirus 229E for cathepsin-independent host cell entry and is expressed in viral target cells in the respiratory epithelium. J Virol. 2013;87(11):6150-60. Epub 20130327. doi: 10.1128/JVI.03372-12. PubMed PMID: 23536651; PMCID: PMC3648130.

72. Ziegler CGK, Allon SJ, Nyquist SK, Mbano IM, Miao VN, Tzouanas CN, Cao Y, Yousif AS, Bals J, Hauser BM, Feldman J, Muus C, Wadsworth MH, 2nd, Kazer SW, Hughes TK, Doran B, Gatter GJ, Vukovic M, Taliaferro F, Mead BE, Guo Z, Wang JP, Gras D, Plaisant M, Ansari M, Angelidis I, Adler H, Sucre JMS, Taylor CJ, Lin B, Waghray A, Mitsialis V, Dwyer DF, Buchheit KM, Boyce JA, Barrett NA, Laidlaw TM, Carroll SL, Colonna L, Tkachev V, Peterson CW, Yu A, Zheng HB, Gideon HP, Winchell CG, Lin PL, Bingle CD, Snapper SB, Kropski JA, Theis FJ, Schiller HB, Zaragosi LE, Barbry P, Leslie A, Kiem HP, Flynn JL, Fortune SM, Berger B, Finberg RW, Kean LS, Garber M, Schmidt AG, Lingwood D, Shalek AK, Ordovas-Montanes J. SARS-CoV-2 Receptor ACE2 Is an Interferon-Stimulated Gene in Human Airway Epithelial Cells and Is Detected in Specific Cell Subsets across Tissues. Cell. 2020;181(5):1016-35.e19. Epub 20200427. doi: 10.1016/j.cell.2020.04.035. PubMed PMID: 32413319; PMCID: PMC7252096.

73. Bayati A, Kumar R, Francis V, McPherson PS. SARS-CoV-2 infects cells after viral entry via clathrin-mediated endocytosis. J Biol Chem. 2021;296:100306. Epub 20210119. doi: 10.1016/j.jbc.2021.100306. PubMed PMID: 33476648; PMCID: PMC7816624.

74. Koch J, Uckeley ZM, Doldan P, Stanifer M, Boulant S, Lozach PY. TMPRSS2 expression dictates the entry route used by SARS-CoV-2 to infect host cells. EMBO J. 2021;40(16):e107821. Epub 20210713. doi: 10.15252/embj.2021107821. PubMed PMID: 34159616; PMCID: PMC8365257.

75. V'Kovski P, Kratzel A, Steiner S, Stalder H, Thiel V. Coronavirus biology and replication: implications for SARS-CoV-2. Nat Rev Microbiol. 2021;19(3):155-70. Epub 20201028. doi: 10.1038/s41579-020-00468-6. PubMed PMID: 33116300; PMCID: PMC7592455.

76. Hoffmann M, Kleine-Weber H, Pohlmann S. A Multibasic Cleavage Site in the Spike Protein of SARS-CoV-2 Is Essential for Infection of Human Lung Cells. Mol Cell. 2020;78(4):779-84 e5. Epub 20200501. doi: 10.1016/j.molcel.2020.04.022. PubMed PMID: 32362314; PMCID: PMC7194065.

77. Shang J, Wan Y, Luo C, Ye G, Geng Q, Auerbach A, Li F. Cell entry mechanisms of SARS-CoV-2. Proc Natl Acad Sci U S A. 2020;117(21):11727-34. Epub 20200506. doi: 10.1073/pnas.2003138117. PubMed PMID: 32376634; PMCID: PMC7260975.

78. Lempp FA, Soriaga LB, Montiel-Ruiz M, Benigni F, Noack J, Park YJ, Bianchi S, Walls AC, Bowen JE, Zhou J, Kaiser H, Joshi A, Agostini M, Meury M, Dellota E, Jr., Jaconi S, Cameroni E, Martinez-Picado J, Vergara-Alert J, Izquierdo-Useros N, Virgin HW, Lanzavecchia A, Veesler D, Purcell LA, Telenti A, Corti D. Lectins enhance SARS-CoV-2 infection and influence neutralizing antibodies. Nature. 2021;598(7880):342-7. Epub 20210831. doi: 10.1038/s41586-021-03925-1. PubMed PMID: 34464958.

79. Perez-Zsolt D, Muñoz-Basagoiti J, Rodon J, Elosua-Bayes M, Raïch-Regué D, Risco C, Sachse M, Pino M, Gumber S, Paiardini M, Chojnacki J, Erkizia I, Muñiz-Trabudua X, Ballana E, Riveira-Muñoz E, Noguera-Julian M, Paredes R, Trinité B, Tarrés-Freixas F, Blanco I, Guallar V, Carrillo J, Blanco J, Telenti A, Heyn H, Segalés J, Clotet B, Martinez-Picado J, Vergara-Alert J, Izquierdo-Useros N. SARS-CoV-2 interaction with Siglec-1 mediates trans-infection by dendritic cells. Cell Mol Immunol. 2021;18(12):2676-8. Epub 20211115. doi: 10.1038/s41423-021-00794-6. PubMed PMID: 34782760; PMCID: PMC8591443.

80. Junqueira C, Crespo Â, Ranjbar S, de Lacerda LB, Lewandrowski M, Ingber J, Parry B, Ravid S, Clark S, Schrimpf MR, Ho F, Beakes C, Margolin J, Russell N, Kays K, Boucau J, Das Adhikari U, Vora SM, Leger V, Gehrke L, Henderson LA, Janssen E, Kwon D, Sander C, Abraham J, Goldberg MB, Wu H, Mehta G, Bell S, Goldfeld AE, Filbin MR, Lieberman J. FcγR-mediated SARS-CoV-2 infection of monocytes activates inflammation. Nature. 2022;606(7914):576-84. Epub 20220406. doi: 10.1038/s41586-022-04702-4. PubMed PMID: 35385861.

81. Zheng M, Karki R, Williams EP, Yang D, Fitzpatrick E, Vogel P, Jonsson CB, Kanneganti TD. TLR2 senses the SARS-CoV-2 envelope protein to produce inflammatory cytokines. Nat Immunol. 2021;22(7):829-38. Epub 20210507. doi: 10.1038/s41590-021-00937-x. PubMed PMID: 33963333; PMCID: PMC8882317.

82. Potapov I, Kanneganti TD, Del Sol A. Fostering experimental and computational synergy to modulate hyperinflammation. Trends Immunol. 2022;43(1):4-7. Epub 20211126. doi: 10.1016/j.it.2021.11.004. PubMed PMID: 34844849; PMCID: PMC9375712.

83. Jung S, Potapov I, Chillara S, Del Sol A. Leveraging systems biology for predicting modulators of inflammation in patients with COVID-19. Sci Adv. 2021;7(6). Epub 20210203. doi: 10.1126/sciadv.abe5735. PubMed PMID: 33536217.

84. Choudhury A, Mukherjee S. In silico studies on the comparative characterization of the interactions of SARS-CoV-2 spike glycoprotein with ACE-2 receptor homologs and human TLRs. J Med Virol. 2020;92(10):2105-13. Epub 20200517. doi: 10.1002/jmv.25987. PubMed PMID: 32383269; PMCID: PMC7267663.

85. Zhao Y, Kuang M, Li J, Zhu L, Jia Z, Guo X, Hu Y, Kong J, Yin H, Wang X, You F. SARS-CoV-2 spike protein interacts with and activates TLR41. Cell Res. 2021;31(7):818-20. Epub 20210319. doi: 10.1038/s41422-021-00495-9. PubMed PMID: 33742149; PMCID: PMC7975240.

86. Bortolotti D, Gentili V, Rizzo S, Schiuma G, Beltrami S, Strazzabosco G, Fernandez M, Caccuri F, Caruso A, Rizzo R. TLR3 and TLR7 RNA Sensor Activation during SARS-CoV-2 Infection. Microorganisms. 2021;9(9). Epub 20210826. doi: 10.3390/microorganisms9091820. PubMed PMID: 34576716; PMCID: PMC8465566.

87. Thorne LG, Reuschl AK, Zuliani-Alvarez L, Whelan MVX, Turner J, Noursadeghi M, Jolly C, Towers GJ. SARS-CoV-2 sensing by RIG-I and MDA5 links epithelial infection to macrophage inflammation. EMBO J. 2021;40(15):e107826. Epub 20210702. doi: 10.15252/embj.2021107826. PubMed PMID: 34101213; PMCID: PMC8209947.

88. Sipila M, Karma P, Pukander J, Timonen M, Kataja M. The Bayesian approach to the evaluation of risk factors in acute and recurrent acute otitis media. Acta Otolaryngol. 1988;106(1-2):94-101. doi: 10.3109/00016488809107375. PubMed PMID: 3421103.

89. Ma R, Ortiz Serrano TP, Davis J, Prigge AD, Ridge KM. The cGAS-STING pathway: The role of self-DNA sensing in inflammatory lung disease. FASEB J. 2020;34(10):13156-70. Epub 20200828. doi: 10.1096/fj.202001607R. PubMed PMID: 32860267; PMCID: PMC8121456.

90. Domizio JD, Gulen MF, Saidoune F, Thacker VV, Yatim A, Sharma K, Nass T, Guenova E, Schaller M, Conrad C, Goepfert C, de Leval L, Garnier CV, Berezowska S, Dubois A, Gilliet M, Ablasser A. The cGAS-STING pathway drives type I IFN immunopathology in COVID-19. Nature. 2022;603(7899):145-51. Epub 20220119. doi: 10.1038/s41586-022-04421-w. PubMed PMID: 35045565; PMCID: PMC8891013.

91. Lee S, Channappanavar R, Kanneganti TD. Coronaviruses: Innate Immunity, Inflammasome Activation, Inflammatory Cell Death, and Cytokines. Trends Immunol. 2020;41(12):1083-99. Epub 20201015. doi: 10.1016/j.it.2020.10.005. PubMed PMID: 33153908; PMCID: PMC7561287.

92. Zheng M, Williams EP, Malireddi RKS, Karki R, Banoth B, Burton A, Webby R, Channappanavar R, Jonsson CB, Kanneganti TD. Impaired NLRP3 inflammasome activation/pyroptosis leads to robust inflammatory cell death via caspase-8/RIPK3 during

coronavirus infection. J Biol Chem. 2020;295(41):14040-52. Epub 20200806. doi: 10.1074/jbc.RA120.015036. PubMed PMID: 32763970; PMCID: PMC7549031.

93. Campbell GR, To RK, Hanna J, Spector SA. SARS-CoV-2, SARS-CoV-1, and HIV-1 derived ssRNA sequences activate the NLRP3 inflammasome in human macrophages through a non-classical pathway. iScience. 2021;24(4):102295. Epub 20210309. doi: 10.1016/j.isci.2021.102295. PubMed PMID: 33718825; PMCID: PMC7939994.

94. Schultze JL, Aschenbrenner AC. COVID-19 and the human innate immune system. Cell. 2021;184(7):1671-92. Epub 20210216. doi: 10.1016/j.cell.2021.02.029. PubMed PMID: 33743212; PMCID: PMC7885626.

95. Lucas C, Wong P, Klein J, Castro TBR, Silva J, Sundaram M, Ellingson MK, Mao T, Oh JE, Israelow B, Takahashi T, Tokuyama M, Lu P, Venkataraman A, Park A, Mohanty S, Wang H, Wyllie AL, Vogels CBF, Earnest R, Lapidus S, Ott IM, Moore AJ, Muenker MC, Fournier JB, Campbell M, Odio CD, Casanovas-Massana A, Herbst R, Shaw AC, Medzhitov R, Schulz WL, Grubaugh ND, Dela Cruz C, Farhadian S, Ko AI, Omer SB, Iwasaki A. Longitudinal analyses reveal immunological misfiring in severe COVID-19. Nature. 2020;584(7821):463-9. Epub 20200727. doi: 10.1038/s41586-020-2588-y. PubMed PMID: 32717743; PMCID: PMC7477538.

96. Manson JJ, Crooks C, Naja M, Ledlie A, Goulden B, Liddle T, Khan E, Mehta P, Martin-Gutierrez L, Waddington KE, Robinson GA, Ribeiro Santos L, McLoughlin E, Snell A, Adeney C, Schim van der Loeff I, Baker KF, Duncan CJA, Hanrath AT, Lendrem BC, De Soyza A, Peng J, J'Bari H, Greenwood M, Hawkins E, Peckham H, Marks M, Rampling T, Luintel A, Williams B, Brown M, Singer M, West J, Jury EC, Collin M, Tattersall RS. COVID-19-associated hyperinflammation and escalation of patient care: a retrospective longitudinal cohort study. Lancet Rheumatol. 2020;2(10):e594-e602. Epub 20200821. doi: 10.1016/S2665-9913(20)30275-7. PubMed PMID: 32864628; PMCID: PMC7442426.

97. Short SAP, Gupta S, Brenner SK, Hayek SS, Srivastava A, Shaefi S, Singh H, Wu B, Bagchi A, Al-Samkari H, Dy R, Wilkinson K, Zakai NA, Leaf DE, Investigators S-C. d-dimer and Death in Critically Ill Patients With Coronavirus Disease 2019. Crit Care Med. 2021;49(5):e500-e11. doi: 10.1097/CCM.0000000000004917. PubMed PMID: 33591017; PMCID: PMC8275993.

98. Qin C, Zhou L, Hu Z, Zhang S, Yang S, Tao Y, Xie C, Ma K, Shang K, Wang W, Tian DS. Dysregulation of Immune Response in Patients With Coronavirus 2019 (COVID-19) in Wuhan, China. Clin Infect Dis. 2020;71(15):762-8. doi: 10.1093/cid/ciaa248. PubMed PMID: 32161940; PMCID: PMC7108125.

99. Ruan Q, Yang K, Wang W, Jiang L, Song J. Clinical predictors of mortality due to COVID-19 based on an analysis of data of 150 patients from Wuhan, China. Intensive Care Med. 2020;46(5):846-8. Epub 20200303. doi: 10.1007/s00134-020-05991-x. PubMed PMID: 32125452; PMCID: PMC7080116.

100. Liao M, Liu Y, Yuan J, Wen Y, Xu G, Zhao J, Cheng L, Li J, Wang X, Wang F, Liu L, Amit I, Zhang S, Zhang Z. Single-cell landscape of bronchoalveolar immune cells in patients with COVID-19. Nat Med. 2020;26(6):842-4. Epub 20200512. doi: 10.1038/s41591-020-0901-9. PubMed PMID: 32398875.

101. Burke DC, Isaacs A. Further studies on interferon. Br J Exp Pathol. 1958;39(1):78-84. PubMed PMID: 13510551; PMCID: PMC2082203.

102. Isaacs A, Burke DC. Mode of action of interferon. Nature. 1958;182(4642):1073-4. doi: 10.1038/1821073a0. PubMed PMID: 13590226.

103. Lindenmann J, Burke DC, Isaacs A. Studies on the production, mode of action and properties of interferon. Br J Exp Pathol. 1957;38(5):551-62. PubMed PMID: 13479681; PMCID: PMC2082625.

104. Isaacs A, Lindenmann J. Virus interference. I. The interferon. Proc R Soc Lond B Biol Sci. 1957;147(927):258-67. doi: 10.1098/rspb.1957.0048. PubMed PMID: 13465720.

105. Isaacs A, Lindenmann J, Valentine RC. Virus interference. II. Some properties of interferon. Proc R Soc Lond B Biol Sci. 1957;147(927):268-73. doi: 10.1098/rspb.1957.0049. PubMed PMID: 13465721.

106. Pestka S, Krause CD, Walter MR. Interferons, interferon-like cytokines, and their receptors. Immunol Rev. 2004;202:8-32. doi: 10.1111/j.0105-2896.2004.00204.x. PubMed PMID: 15546383.

107. McNab F, Mayer-Barber K, Sher A, Wack A, O'Garra A. Type I interferons in infectious disease. Nat Rev Immunol. 2015;15(2):87-103. doi: 10.1038/nri3787. PubMed PMID: 25614319; PMCID: PMC7162685.

108. Siegal FP, Kadowaki N, Shodell M, Fitzgerald-Bocarsly PA, Shah K, Ho S, Antonenko S, Liu YJ. The nature of the principal type 1 interferon-producing cells in human blood. Science. 1999;284(5421):1835-7. doi: 10.1126/science.284.5421.1835. PubMed PMID: 10364556.

109. Ivashkiv LB, Donlin LT. Regulation of type I interferon responses. Nat Rev Immunol. 2014;14(1):36-49. doi: 10.1038/nri3581. PubMed PMID: 24362405; PMCID: PMC4084561.

110. Yang E, Li MMH. All About the RNA: Interferon-Stimulated Genes That Interfere With Viral RNA Processes. Front Immunol. 2020;11:605024. Epub 20201209. doi: 10.3389/fimmu.2020.605024. PubMed PMID: 33362792; PMCID: PMC7756014.

111. Schreiber G. The molecular basis for differential type I interferon signaling. J Biol Chem. 2017;292(18):7285-94. Epub 20170313. doi: 10.1074/jbc.R116.774562. PubMed PMID: 28289098; PMCID: PMC5418031.

112. Chen J, Subbarao K. The Immunobiology of SARS*. Annu Rev Immunol. 2007;25:443-72. doi: 10.1146/annurev.immunol.25.022106.141706. PubMed PMID: 17243893.

113. Park A, Iwasaki A. Type I and Type III Interferons - Induction, Signaling, Evasion, and Application to Combat COVID-19. Cell Host Microbe. 2020;27(6):870-8. Epub 20200527. doi: 10.1016/j.chom.2020.05.008. PubMed PMID: 32464097; PMCID: PMC7255347.

114. Zhang Q, Bastard P, Liu Z, Le Pen J, Moncada-Velez M, Chen J, Ogishi M, Sabli IKD, Hodeib S, Korol C, Rosain J, Bilguvar K, Ye J, Bolze A, Bigio B, Yang R, Arias AA, Zhou Q, Zhang Y, Onodi F, Korniotis S, Karpf L, Philippot Q, Chbihi M, Bonnet-Madin L, Dorgham K, Smith N, Schneider WM, Razooky BS, Hoffmann HH, Michailidis E, Moens L, Han JE, Lorenzo L, Bizien L, Meade P, Neehus AL, Ugurbil AC, Corneau A, Kerner G, Zhang P, Rapaport F, Seeleuthner Y, Manry J, Masson C, Schmitt Y, Schlüter A, Le Voyer T, Khan T, Li J, Fellay J, Roussel L, Shahrooei M, Alosaimi MF, Mansouri D, Al-Saud H, Al-Mulla F, Almourfi F, Al-Muhsen SZ, Alsohime F, Al Turki S, Hasanato R, van de Beek D, Biondi A, Bettini LR, D'Angio M, Bonfanti P, Imberti L, Sottini A, Paghera S, Quiros-Roldan E, Rossi C, Oler AJ, Tompkins MF, Alba C, Vandernoot I, Goffard JC, Smits G, Migeotte I, Haerynck F, Soler-Palacin P, Martin-Nalda A, Colobran R, Morange PE, Keles S, Çölkesen F, Ozcelik T, Yasar KK, Senoglu S, Karabela Ş N, Rodríguez-Gallego C, Novelli G, Hraiech S, Tandjaoui-Lambiotte Y, Duval X, Laouénan C, Snow AL, Dalgard CL, Milner JD, Vinh DC, Mogensen TH, Marr N, Spaan AN, Boisson B, Boisson-Dupuis S, Bustamante J, Puel A, Ciancanelli MJ, Meyts I, Maniatis T, Soumelis V, Amara A, Nussenzweig M, García-Sastre A, Krammer F, Pujol A, Duffy D, Lifton RP, Zhang SY, Gorochov G, Béziat V, Jouanguy E, Sancho-Shimizu V, Rice CM, Abel L, Notarangelo LD, Cobat A, Su HC, Casanova JL. Inborn errors of type I IFN immunity in patients with life-threatening COVID-19. Science. 2020;370(6515). Epub 20200924. doi: 10.1126/science.abd4570. PubMed PMID: 32972995; PMCID: PMC7857407.

115. Bastard P, Rosen LB, Zhang Q, Michailidis E, Hoffmann HH, Zhang Y, Dorgham K, Philippot Q, Rosain J, Béziat V, Manry J, Shaw E, Haljasmägi L, Peterson P, Lorenzo L, Bizien L, Trouillet-Assant S, Dobbs K, de Jesus AA, Belot A, Kallaste A, Catherinot E, Tandjaoui-Lambiotte Y, Le Pen J, Kerner G, Bigio B, Seeleuthner Y, Yang R, Bolze A, Spaan AN, Delmonte OM, Abers MS, Aiuti A, Casari G, Lampasona V, Piemonti L, Ciceri F, Bilguvar K, Lifton RP, Vasse M, Smadja DM, Migaud M, Hadjadj J, Terrier B, Duffy D, Quintana-Murci L, van de Beek D, Roussel L, Vinh DC, Tangye SG, Haerynck F, Dalmau D, Martinez-Picado J, Brodin P, Nussenzweig MC, Boisson-Dupuis S, Rodríguez-Gallego C, Vogt G, Mogensen TH, Oler AJ, Gu J, Burbelo PD, Cohen JI, Biondi A, Bettini LR, D'Angio M, Bonfanti P, Rossignol P, Mayaux J, Rieux-Laucat F, Husebye ES, Fusco F, Ursini MV, Imberti L, Sottini A, Paghera S, Quiros-Roldan E, Rossi C, Castagnoli R, Montagna D, Licari A, Marseglia GL, Duval X, Ghosn J, Tsang JS, Goldbach-Mansky R, Kisand K, Lionakis MS, Puel A, Zhang SY, Holland SM, Gorochov G, Jouanguy E, Rice CM, Cobat A, Notarangelo LD, Abel L, Su HC, Casanova JL. Autoantibodies against type I IFNs in patients with life-threatening COVID-19. Science. 2020;370(6515). Epub 20200924. doi: 10.1126/science.abd4585. PubMed PMID: 32972996; PMCID: PMC7857397.

116. Troya J, Bastard P, Planas-Serra L, Ryan P, Ruiz M, de Carranza M, Torres J, Martinez A, Abel L, Casanova JL, Pujol A. Neutralizing Autoantibodies to Type I IFNs in >10% of Patients with Severe COVID-19 Pneumonia Hospitalized in Madrid, Spain. J Clin Immunol. 2021;41(5):914-22. Epub 20210413. doi: 10.1007/s10875-021-01036-0. PubMed PMID: 33851338; PMCID: PMC8043439.

117. Koning R, Bastard P, Casanova JL, Brouwer MC, van de Beek D, with the Amsterdam UMCC-BI. Autoantibodies against type I interferons are associated with multi-organ failure in COVID-19 patients. Intensive Care Med. 2021;47(6):704-6. Epub 20210409. doi: 10.1007/s00134-021-06392-4. PubMed PMID: 33835207; PMCID: PMC8034036.

118. van der Made CI, Simons A, Schuurs-Hoeijmakers J, van den Heuvel G, Mantere T, Kersten S, van Deuren RC, Steehouwer M, van Reijmersdal SV, Jaeger M, Hofste T, Astuti G, Corominas Galbany J, van der Schoot V, van der Hoeven H, Hagmolen Of Ten Have W, Klijn E, van den Meer C, Fiddelaers J, de Mast Q, Bleeker-Rovers CP, Joosten LAB, Yntema HG, Gilissen C, Nelen M, van der Meer JWM, Brunner HG, Netea MG, van de Veerdonk FL, Hoischen A. Presence of Genetic Variants Among Young Men With Severe COVID-19. JAMA. 2020;324(7):663-73. doi: 10.1001/jama.2020.13719. PubMed PMID: 32706371; PMCID: PMC7382021.

119. Hadjadj J, Yatim N, Barnabei L, Corneau A, Boussier J, Smith N, Péré H, Charbit B, Bondet V, Chenevier-Gobeaux C, Breillat P, Carlier N, Gauzit R, Morbieu C, Pène F, Marin N, Roche N, Szwebel TA, Merkling SH, Treluyer JM, Veyer D, Mouthon L, Blanc C, Tharaux PL, Rozenberg F, Fischer A, Duffy D, Rieux-Laucat F, Kernéis S, Terrier B. Impaired type I interferon activity and inflammatory responses in severe COVID-19 patients. Science. 2020;369(6504):718-24. Epub 20200713. doi: 10.1126/science.abc6027. PubMed PMID: 32661059; PMCID: PMC7402632.

120. Kwon JS, Kim JY, Kim MC, Park SY, Kim BN, Bae S, Cha HH, Jung J, Kim MJ, Lee MJ, Choi SH, Chung JW, Shin EC, Kim SH. Factors of Severity in Patients with COVID-19: Cytokine/Chemokine Concentrations, Viral Load, and Antibody Responses. Am J Trop Med Hyg. 2020;103(6):2412-8. Epub 20201027. doi: 10.4269/ajtmh.20-1110. PubMed PMID: 33124544; PMCID: PMC7695090.

121. Broggi A, Ghosh S, Sposito B, Spreafico R, Balzarini F, Lo Cascio A, Clementi N, De Santis M, Mancini N, Granucci F, Zanoni I. Type III interferons disrupt the lung epithelial barrier upon viral recognition. Science. 2020;369(6504):706-12. Epub 20200611. doi: 10.1126/science.abc3545. PubMed PMID: 32527925; PMCID: PMC7292499.

122. Totura AL, Baric RS. SARS coronavirus pathogenesis: host innate immune responses and viral antagonism of interferon. Curr Opin Virol. 2012;2(3):264-75. Epub 20120507. doi: 10.1016/j.coviro.2012.04.004. PubMed PMID: 22572391; PMCID: PMC7102726.

123. Wathelet MG, Orr M, Frieman MB, Baric RS. Severe acute respiratory syndrome coronavirus evades antiviral signaling: role of nsp1 and rational design of an attenuated strain. J Virol. 2007;81(21):11620-33. Epub 20070822. doi: 10.1128/JVI.00702-07. PubMed PMID: 17715225; PMCID: PMC2168762.

124. Kamitani W, Huang C, Narayanan K, Lokugamage KG, Makino S. A two-pronged strategy to suppress host protein synthesis by SARS coronavirus Nsp1 protein. Nat Struct Mol Biol. 2009;16(11):1134-40. Epub 20091018. doi: 10.1038/nsmb.1680. PubMed PMID: 19838190; PMCID: PMC2784181.

125. Huang C, Lokugamage KG, Rozovics JM, Narayanan K, Semler BL, Makino S. SARS coronavirus nsp1 protein induces template-dependent endonucleolytic cleavage of mRNAs: viral mRNAs are resistant to nsp1-induced RNA cleavage. PLoS Pathog. 2011;7(12):e1002433. Epub 20111208. doi: 10.1371/journal.ppat.1002433. PubMed PMID: 22174690; PMCID: PMC3234236.

126. Devaraj SG, Wang N, Chen Z, Chen Z, Tseng M, Barretto N, Lin R, Peters CJ, Tseng CT, Baker SC, Li K. Regulation of IRF-3-dependent innate immunity by the papain-like protease domain of the severe acute respiratory syndrome coronavirus. J Biol Chem. 2007;282(44):32208-21. Epub 20070830. doi: 10.1074/jbc.M704870200. PubMed PMID: 17761676; PMCID: PMC2756044.

127. Frieman M, Ratia K, Johnston RE, Mesecar AD, Baric RS. Severe acute respiratory syndrome coronavirus papain-like protease ubiquitin-like domain and catalytic domain regulate antagonism of IRF3 and NF-kappaB signaling. J Virol. 2009;83(13):6689-705. Epub 20090415. doi: 10.1128/JVI.02220-08. PubMed PMID: 19369340; PMCID: PMC2698564.

128. Sun L, Xing Y, Chen X, Zheng Y, Yang Y, Nichols DB, Clementz MA, Banach BS, Li K, Baker SC, Chen Z. Coronavirus papain-like proteases negatively regulate antiviral innate immune response through disruption of STING-mediated signaling. PLoS One. 2012;7(2):e30802. Epub 20120201. doi: 10.1371/journal.pone.0030802. PubMed PMID: 22312431; PMCID: PMC3270028.

129. Kopecky-Bromberg SA, Martinez-Sobrido L, Frieman M, Baric RA, Palese P. Severe acute respiratory syndrome coronavirus open reading frame (ORF) 3b, ORF 6, and nucleocapsid proteins function as interferon antagonists. J Virol. 2007;81(2):548-57. Epub 20061115. doi: 10.1128/JVI.01782-06. PubMed PMID: 17108024; PMCID: PMC1797484.

130. Freundt EC, Yu L, Park E, Lenardo MJ, Xu XN. Molecular determinants for subcellular localization of the severe acute respiratory syndrome coronavirus open reading frame 3b protein. J Virol. 2009;83(13):6631-40. Epub 20090429. doi: 10.1128/JVI.00367-09. PubMed PMID: 19403678; PMCID: PMC2698541.

131. Siu KL, Kok KH, Ng MJ, Poon VKM, Yuen KY, Zheng BJ, Jin DY. Severe acute respiratory syndrome coronavirus M protein inhibits type I interferon production by impeding the formation of TRAF3.TANK.TBK1/IKKepsilon complex. J Biol Chem.

2009;284(24):16202-9. Epub 20090420. doi: 10.1074/jbc.M109.008227. PubMed PMID: 19380580; PMCID: PMC2713514.

132. Frieman M, Yount B, Heise M, Kopecky-Bromberg SA, Palese P, Baric RS. Severe acute respiratory syndrome coronavirus ORF6 antagonizes STAT1 function by sequestering nuclear import factors on the rough endoplasmic reticulum/Golgi membrane. J Virol. 2007;81(18):9812-24. Epub 20070627. doi: 10.1128/JVI.01012-07. PubMed PMID: 17596301; PMCID: PMC2045396.

133. Hussain S, Perlman S, Gallagher TM. Severe acute respiratory syndrome coronavirus protein 6 accelerates murine hepatitis virus infections by more than one mechanism. J Virol. 2008;82(14):7212-22. Epub 20080430. doi: 10.1128/JVI.02406-07. PubMed PMID: 18448520; PMCID: PMC2446958.

134. Hussain S, Gallagher T. SARS-coronavirus protein 6 conformations required to impede protein import into the nucleus. Virus Res. 2010;153(2):299-304. Epub 20100826. doi: 10.1016/j.virusres.2010.08.017. PubMed PMID: 20800627; PMCID: PMC2954772.

135. Lu X, Pan J, Tao J, Guo D. SARS-CoV nucleocapsid protein antagonizes IFN-beta response by targeting initial step of IFN-beta induction pathway, and its C-terminal region is critical for the antagonism. Virus Genes. 2011;42(1):37-45. Epub 20101026. doi: 10.1007/s11262-010-0544-x. PubMed PMID: 20976535; PMCID: PMC7088804.

136. Mohammed MEA. The percentages of SARS-CoV-2 protein similarity and identity with SARS-CoV and BatCoV RaTG13 proteins can be used as indicators of virus origin. J Proteins Proteom. 2021;12(2):81-91. Epub 20210409. doi: 10.1007/s42485-021-00060-3. PubMed PMID: 33850392; PMCID: PMC8033097.

137. Wolff G, Melia CE, Snijder EJ, Barcena M. Double-Membrane Vesicles as Platforms for Viral Replication. Trends Microbiol. 2020;28(12):1022-33. Epub 20200611. doi: 10.1016/j.tim.2020.05.009. PubMed PMID: 32536523; PMCID: PMC7289118.

138. Menachery VD, Debbink K, Baric RS. Coronavirus non-structural protein 16: evasion, attenuation, and possible treatments. Virus Res. 2014;194:191-9. Epub 20140930. doi: 10.1016/j.virusres.2014.09.009. PubMed PMID: 25278144; PMCID: PMC4260984.

139. Liu Y, Qin C, Rao Y, Ngo C, Feng JJ, Zhao J, Zhang S, Wang TY, Carriere J, Savas AC, Zarinfar M, Rice S, Yang H, Yuan W, Camarero JA, Yu J, Chen XS, Zhang C, Feng P. SARS-CoV-2 Nsp5 Demonstrates Two Distinct Mechanisms Targeting RIG-I and MAVS To Evade the Innate Immune Response. mBio. 2021;12(5):e0233521. Epub 20210921. doi: 10.1128/mBio.02335-21. PubMed PMID: 34544279; PMCID: PMC8546575.

140. Xia H, Cao Z, Xie X, Zhang X, Chen JY, Wang H, Menachery VD, Rajsbaum R, Shi PY. Evasion of Type I Interferon by SARS-CoV-2. Cell Rep. 2020;33(1):108234. Epub 20200919. doi: 10.1016/j.celrep.2020.108234. PubMed PMID: 32979938; PMCID: PMC7501843.

141. Hayn M, Hirschenberger M, Koepke L, Nchioua R, Straub JH, Klute S, Hunszinger V, Zech F, Prelli Bozzo C, Aftab W, Christensen MH, Conzelmann C, Muller JA, Srinivasachar Badarinarayan S, Sturzel CM, Forne I, Stenger S, Conzelmann KK, Munch J, Schmidt FI, Sauter D, Imhof A, Kirchhoff F, Sparrer KMJ. Systematic functional analysis of SARS-CoV-2 proteins uncovers viral innate immune antagonists and remaining vulnerabilities. Cell Rep. 2021;35(7):109126. Epub 20210427. doi: 10.1016/j.celrep.2021.109126. PubMed PMID: 33974846; PMCID: PMC8078906.

142. Wang R, Yang X, Chang M, Xue Z, Wang W, Bai L, Zhao S, Liu E. ORF3a Protein of Severe Acute Respiratory Syndrome Coronavirus 2 Inhibits Interferon-Activated Janus Kinase/Signal Transducer and Activator of Transcription Signaling via Elevating Suppressor of Cytokine Signaling 1. Front Microbiol. 2021;12:752597. Epub 20210928. doi: 10.3389/fmicb.2021.752597. PubMed PMID: 34650546; PMCID: PMC8506155.

143. Melin AD, Janiak MC, Marrone F, 3rd, Arora PS, Higham JP. Comparative ACE2 variation and primate COVID-19 risk. Commun Biol. 2020;3(1):641. Epub 20201027. doi: 10.1038/s42003-020-01370-w. PubMed PMID: 33110195; PMCID: PMC7591510.

144. Shi J, Wen Z, Zhong G, Yang H, Wang C, Huang B, Liu R, He X, Shuai L, Sun Z, Zhao Y, Liu P, Liang L, Cui P, Wang J, Zhang X, Guan Y, Tan W, Wu G, Chen H, Bu Z. Susceptibility of ferrets, cats, dogs, and other domesticated animals to SARS-coronavirus 2. Science. 2020;368(6494):1016-20. Epub 20200408. doi: 10.1126/science.abb7015. PubMed PMID: 32269068; PMCID: PMC7164390.

145. Chan JF, Zhang AJ, Yuan S, Poon VK, Chan CC, Lee AC, Chan WM, Fan Z, Tsoi HW, Wen L, Liang R, Cao J, Chen Y, Tang K, Luo C, Cai JP, Kok KH, Chu H, Chan KH, Sridhar S, Chen Z, Chen H, To KK, Yuen KY. Simulation of the Clinical and Pathological Manifestations of Coronavirus Disease 2019 (COVID-19) in a Golden Syrian Hamster Model: Implications for Disease Pathogenesis and Transmissibility. Clin Infect Dis. 2020;71(9):2428-46. doi: 10.1093/cid/ciaa325. PubMed PMID: 32215622; PMCID: PMC7184405.

146. Bao L, Deng W, Huang B, Gao H, Liu J, Ren L, Wei Q, Yu P, Xu Y, Qi F, Qu Y, Li F, Lv Q, Wang W, Xue J, Gong S, Liu M, Wang G, Wang S, Song Z, Zhao L, Liu P, Zhao L, Ye F, Wang H, Zhou W, Zhu N, Zhen W, Yu H, Zhang X, Guo L, Chen L, Wang C, Wang Y, Wang X, Xiao Y, Sun Q, Liu H, Zhu F, Ma C, Yan L, Yang M, Han J, Xu W, Tan W, Peng X, Jin Q, Wu G, Qin C. The pathogenicity of SARS-CoV-2 in hACE2 transgenic mice. Nature. 2020;583(7818):830-3. Epub 20200507. doi: 10.1038/s41586-020-2312-y. PubMed PMID: 32380511.

147. Rockx B, Kuiken T, Herfst S, Bestebroer T, Lamers MM, Oude Munnink BB, de Meulder D, van Amerongen G, van den Brand J, Okba NMA, Schipper D, van Run P, Leijten L, Sikkema R, Verschoor E, Verstrepen B, Bogers W, Langermans J, Drosten C, Fentener van Vlissingen M, Fouchier R, de Swart R, Koopmans M, Haagmans BL. Comparative pathogenesis of COVID-19, MERS, and SARS in a nonhuman primate model. Science. 2020;368(6494):1012-5. Epub 20200417. doi: 10.1126/science.abb7314. PubMed PMID: 32303590; PMCID: PMC7164679.

148. Munster VJ, Feldmann F, Williamson BN, van Doremalen N, Perez-Perez L, Schulz J, Meade-White K, Okumura A, Callison J, Brumbaugh B, Avanzato VA, Rosenke R, Hanley PW, Saturday G, Scott D, Fischer ER, de Wit E. Respiratory disease in rhesus macaques inoculated with SARS-CoV-2. Nature. 2020;585(7824):268-72. Epub 20200512. doi: 10.1038/s41586-020-2324-7. PubMed PMID: 32396922; PMCID: PMC7486227.

149. Schlottau K, Rissmann M, Graaf A, Schon J, Sehl J, Wylezich C, Hoper D, Mettenleiter TC, Balkema-Buschmann A, Harder T, Grund C, Hoffmann D, Breithaupt A, Beer M. SARS-CoV-2 in fruit bats, ferrets, pigs, and chickens: an experimental transmission study. Lancet Microbe. 2020;1(5):e218-e25. Epub 20200707. doi: 10.1016/S2666-5247(20)30089-6. PubMed PMID: 32838346; PMCID: PMC7340389.

150. Wang J, Shuai L, Wang C, Liu R, He X, Zhang X, Sun Z, Shan D, Ge J, Wang X, Hua R, Zhong G, Wen Z, Bu Z. Mouse-adapted SARS-CoV-2 replicates efficiently in the upper and lower respiratory tract of BALB/c and C57BL/6J mice. Protein Cell. 2020;11(10):776-82. doi: 10.1007/s13238-020-00767-x. PubMed PMID: 32749592; PMCID: PMC7401472.

151. Leist SR, Dinnon KH, 3rd, Schafer A, Tse LV, Okuda K, Hou YJ, West A, Edwards CE, Sanders W, Fritch EJ, Gully KL, Scobey T, Brown AJ, Sheahan TP, Moorman NJ, Boucher RC, Gralinski LE, Montgomery SA, Baric RS. A Mouse-Adapted SARS-CoV-2 Induces Acute Lung Injury and Mortality in Standard Laboratory Mice. Cell. 2020;183(4):1070-85 e12. Epub 20200923. doi: 10.1016/j.cell.2020.09.050. PubMed PMID: 33031744; PMCID: PMC7510428.

152. Huang K, Zhang Y, Hui X, Zhao Y, Gong W, Wang T, Zhang S, Yang Y, Deng F, Zhang Q, Chen X, Yang Y, Sun X, Chen H, Tao YJ, Zou Z, Jin M. Q493K and Q498H substitutions in Spike promote adaptation of SARS-CoV-2 in mice. EBioMedicine. 2021;67:103381. Epub 20210514. doi: 10.1016/j.ebiom.2021.103381. PubMed PMID: 33993052; PMCID: PMC8118724.

153. Sun SH, Chen Q, Gu HJ, Yang G, Wang YX, Huang XY, Liu SS, Zhang NN, Li XF, Xiong R, Guo Y, Deng YQ, Huang WJ, Liu Q, Liu QM, Shen YL, Zhou Y, Yang X, Zhao TY, Fan CF, Zhou YS, Qin CF, Wang YC. A Mouse Model of SARS-CoV-2 Infection and Pathogenesis. Cell Host Microbe. 2020;28(1):124-33 e4. Epub 20200527. doi: 10.1016/j.chom.2020.05.020. PubMed PMID: 32485164; PMCID: PMC7250783.

154. Hassan AO, Case JB, Winkler ES, Thackray LB, Kafai NM, Bailey AL, McCune BT, Fox JM, Chen RE, Alsoussi WB, Turner JS, Schmitz AJ, Lei T, Shrihari S, Keeler SP, Fremont DH, Greco S, McCray PB, Jr., Perlman S, Holtzman MJ, Ellebedy AH, Diamond MS. A SARS-CoV-2 Infection Model in Mice Demonstrates Protection by Neutralizing Antibodies. Cell. 2020;182(3):744-53 e4. Epub 20200610. doi: 10.1016/j.cell.2020.06.011. PubMed PMID: 32553273; PMCID: PMC7284254.

155. Sun J, Zhuang Z, Zheng J, Li K, Wong RL, Liu D, Huang J, He J, Zhu A, Zhao J, Li X, Xi Y, Chen R, Alshukairi AN, Chen Z, Zhang Z, Chen C, Huang X, Li F, Lai X, Chen

D, Wen L, Zhuo J, Zhang Y, Wang Y, Huang S, Dai J, Shi Y, Zheng K, Leidinger MR, Chen J, Li Y, Zhong N, Meyerholz DK, McCray PB, Jr., Perlman S, Zhao J. Generation of a Broadly Useful Model for COVID-19 Pathogenesis, Vaccination, and Treatment. Cell. 2020;182(3):734-43 e5. Epub 20200610. doi: 10.1016/j.cell.2020.06.010. PubMed PMID: 32643603; PMCID: PMC7284240.

156. Jiang RD, Liu MQ, Chen Y, Shan C, Zhou YW, Shen XR, Li Q, Zhang L, Zhu Y, Si HR, Wang Q, Min J, Wang X, Zhang W, Li B, Zhang HJ, Baric RS, Zhou P, Yang XL, Shi ZL. Pathogenesis of SARS-CoV-2 in Transgenic Mice Expressing Human Angiotensin-Converting Enzyme 2. Cell. 2020;182(1):50-8 e8. Epub 20200521. doi: 10.1016/j.cell.2020.05.027. PubMed PMID: 32516571; PMCID: PMC7241398.

157. Winkler ES, Bailey AL, Kafai NM, Nair S, McCune BT, Yu J, Fox JM, Chen RE, Earnest JT, Keeler SP, Ritter JH, Kang LI, Dort S, Robichaud A, Head R, Holtzman MJ, Diamond MS. SARS-CoV-2 infection of human ACE2-transgenic mice causes severe lung inflammation and impaired function. Nat Immunol. 2020;21(11):1327-35. Epub 20200824. doi: 10.1038/s41590-020-0778-2. PubMed PMID: 32839612; PMCID: PMC7578095.

158. Tostanoski LH, Wegmann F, Martinot AJ, Loos C, McMahan K, Mercado NB, Yu J, Chan CN, Bondoc S, Starke CE, Nekorchuk M, Busman-Sahay K, Piedra-Mora C, Wrijil LM, Ducat S, Custers J, Atyeo C, Fischinger S, Burke JS, Feldman J, Hauser BM, Caradonna TM, Bondzie EA, Dagotto G, Gebre MS, Jacob-Dolan C, Lin Z, Mahrokhian SH, Nampanya F, Nityanandam R, Pessaint L, Porto M, Ali V, Benetiene D, Tevi K, Andersen H, Lewis MG, Schmidt AG, Lauffenburger DA, Alter G, Estes JD, Schuitemaker H, Zahn R, Barouch DH. Ad26 vaccine protects against SARS-CoV-2 severe clinical disease in hamsters. Nat Med. 2020;26(11):1694-700. Epub 20200903. doi: 10.1038/s41591-020-1070-6. PubMed PMID: 32884153; PMCID: PMC7671939.

159. Corbett KS, Flynn B, Foulds KE, Francica JR, Boyoglu-Barnum S, Werner AP, Flach B, O'Connell S, Bock KW, Minai M, Nagata BM, Andersen H, Martinez DR, Noe AT, Douek N, Donaldson MM, Nji NN, Alvarado GS, Edwards DK, Flebbe DR, Lamb E, Doria-Rose NA, Lin BC, Louder MK, O'Dell S, Schmidt SD, Phung E, Chang LA, Yap C, Todd JM, Pessaint L, Van Ry A, Browne S, Greenhouse J, Putman-Taylor T, Strasbaugh A, Campbell TA, Cook A, Dodson A, Steingrebe K, Shi W, Zhang Y, Abiona OM, Wang L, Pegu A, Yang ES, Leung K, Zhou T, Teng IT, Widge A, Gordon I, Novik L, Gillespie RA, Loomis RJ, Moliva JI, Stewart-Jones G, Himansu S, Kong WP, Nason MC, Morabito KM, Ruckwardt TJ, Ledgerwood JE, Gaudinski MR, Kwong PD, Mascola JR, Carfi A, Lewis MG, Baric RS, McDermott A, Moore IN, Sullivan NJ, Roederer M, Seder RA, Graham BS. Evaluation of the mRNA-1273 Vaccine against SARS-CoV-2 in Nonhuman Primates. N Engl J Med. 2020;383(16):1544-55. Epub 20200728. doi: 10.1056/NEJMoa2024671. PubMed PMID: 32722908; PMCID: PMC7449230.

160. Mercado NB, Zahn R, Wegmann F, Loos C, Chandrashekar A, Yu J, Liu J, Peter L, McMahan K, Tostanoski LH, He X, Martinez DR, Rutten L, Bos R, van Manen D, Vellinga J, Custers J, Langedijk JP, Kwaks T, Bakkers MJG, Zuijdgeest D, Rosendahl Huber SK, Atyeo C, Fischinger S, Burke JS, Feldman J, Hauser BM, Caradonna TM,

Bondzie EA, Dagotto G, Gebre MS, Hoffman E, Jacob-Dolan C, Kirilova M, Li Z, Lin Z, Mahrokhian SH, Maxfield LF, Nampanya F, Nityanandam R, Nkolola JP, Patel S, Ventura JD, Verrington K, Wan H, Pessaint L, Van Ry A, Blade K, Strasbaugh A, Cabus M, Brown R, Cook A, Zouantchangadou S, Teow E, Andersen H, Lewis MG, Cai Y, Chen B, Schmidt AG, Reeves RK, Baric RS, Lauffenburger DA, Alter G, Stoffels P, Mammen M, Van Hoof J, Schuitemaker H, Barouch DH. Single-shot Ad26 vaccine protects against SARS-CoV-2 in rhesus macaques. Nature. 2020;586(7830):583-8. Epub 20200730. doi: 10.1038/s41586-020-2607-z. PubMed PMID: 32731257; PMCID: PMC7581548.

161. Routhu NK, Cheedarla N, Gangadhara S, Bollimpelli VS, Boddapati AK, Shiferaw A, Rahman SA, Sahoo A, Edara VV, Lai L, Floyd K, Wang S, Fischinger S, Atyeo C, Shin SA, Gumber S, Kirejczyk S, Cohen J, Jean SM, Wood JS, Connor-Stroud F, Stammen RL, Upadhyay AA, Pellegrini K, Montefiori D, Shi PY, Menachery VD, Alter G, Vanderford TH, Bosinger SE, Suthar MS, Amara RR. A modified vaccinia Ankara vector-based vaccine protects macaques from SARS-CoV-2 infection, immune pathology, and dysfunction in the lungs. Immunity. 2021;54(3):542-56 e9. Epub 20210204. doi: 10.1016/j.immuni.2021.02.001. PubMed PMID: 33631118; PMCID: PMC7859620.

162. Trichel AM. Overview of Nonhuman Primate Models of SARS-CoV-2 Infection. Comp Med. 2021;71(5):411-32. Epub 20210921. doi: 10.30802/AALAS-CM-20-000119. PubMed PMID: 34548126; PMCID: PMC8594265.

163. Cross RW, Agans KN, Prasad AN, Borisevich V, Woolsey C, Deer DJ, Dobias NS, Geisbert JB, Fenton KA, Geisbert TW. Intranasal exposure of African green monkeys to SARS-CoV-2 results in acute phase pneumonia with shedding and lung injury still present in the early convalescence phase. Virol J. 2020;17(1):125. Epub 20200818. doi: 10.1186/s12985-020-01396-w. PubMed PMID: 32811514; PMCID: PMC7431901.

164. Hartman AL, Nambulli S, McMillen CM, White AG, Tilston-Lunel NL, Albe JR, Cottle E, Dunn MD, Frye LJ, Gilliland TH, Olsen EL, O'Malley KJ, Schwarz MM, Tomko JA, Walker RC, Xia M, Hartman MS, Klein E, Scanga CA, Flynn JL, Klimstra WB, McElroy AK, Reed DS, Duprex WP. SARS-CoV-2 infection of African green monkeys results in mild respiratory disease discernible by PET/CT imaging and shedding of infectious virus from both respiratory and gastrointestinal tracts. PLoS Pathog. 2020;16(9):e1008903. Epub 20200918. doi: 10.1371/journal.ppat.1008903. PubMed PMID: 32946524; PMCID: PMC7535860.

165. Johnston SC, Ricks KM, Jay A, Raymond JL, Rossi F, Zeng X, Scruggs J, Dyer D, Frick O, Koehler JW, Kuehnert PA, Clements TL, Shoemaker CJ, Coyne SR, Delp KL, Moore J, Berrier K, Esham H, Shamblin J, Sifford W, Fiallos J, Klosterman L, Stevens S, White L, Bowling P, Garcia T, Jensen C, Ghering J, Nyakiti D, Bellanca S, Kearney B, Giles W, Alli N, Paz F, Akers K, Danner D, Barth J, Johnson JA, Durant M, Kim R, Hooper JW, Smith JM, Kugelman JR, Beitzel BF, Gibson KM, Pitt MLM, Minogue TD, Nalca A. Development of a coronavirus disease 2019 nonhuman primate model using airborne exposure. PLoS One. 2021;16(2):e0246366. Epub 20210202. doi: 10.1371/journal.pone.0246366. PubMed PMID: 33529233; PMCID: PMC7853502.

166. Speranza E, Williamson BN, Feldmann F, Sturdevant GL, Pérez LP, Meade-White K, Smith BJ, Lovaglio J, Martens C, Munster VJ, Okumura A, Shaia C, Feldmann H, Best SM, Wit Ed. Single-cell RNA sequencing reveals SARS-CoV-2 infection dynamics in lungs of African green monkeys. Sci Transl Med. 2021;13(578):eabe8146. doi: 10.1126/scitranslmed.abe8146 PMID - 33431511.

167. Woolsey C, Borisevich V, Prasad AN, Agans KN, Deer DJ, Dobias NS, Heymann JC, Foster SL, Levine CB, Medina L, Melody K, Geisbert JB, Fenton KA, Geisbert TW, Cross RW. Establishment of an African green monkey model for COVID-19 and protection against re-infection. Nat Immunol. 2021;22(1):86-98. Epub 20201124. doi: 10.1038/s41590-020-00835-8. PubMed PMID: 33235385; PMCID: PMC7790436.

168. Blair RV, Vaccari M, Doyle-Meyers LA, Roy CJ, Russell-Lodrigue K, Fahlberg M, Monjure CJ, Beddingfield B, Plante KS, Plante JA, Weaver SC, Qin X, Midkiff CC, Lehmicke G, Golden N, Threeton B, Penney T, Allers C, Barnes MB, Pattison M, Datta PK, Maness NJ, Birnbaum A, Fischer T, Bohm RP, Rappaport J. Acute Respiratory Distress in Aged, SARS-CoV-2-Infected African Green Monkeys but Not Rhesus Macaques. Am J Pathol. 2021;191(2):274-82. Epub 20201107. doi: 10.1016/j.ajpath.2020.10.016. PubMed PMID: 33171111; PMCID: PMC7648506.

169. Ishigaki H, Nakayama M, Kitagawa Y, Nguyen CT, Hayashi K, Shiohara M, Gotoh B, Itoh Y. Neutralizing antibody-dependent and -independent immune responses against SARS-CoV-2 in cynomolgus macaques. Virology. 2021;554:97-105. Epub 20201229. doi: 10.1016/j.virol.2020.12.013. PubMed PMID: 33412411; PMCID: PMC7771262.

170. Koo BS, Oh H, Kim G, Hwang EH, Jung H, Lee Y, Kang P, Park JH, Ryu CM, Hong JJ. Transient Lymphopenia and Interstitial Pneumonia With Endotheliitis in SARS-CoV-2-Infected Macaques. J Infect Dis. 2020;222(10):1596-600. doi: 10.1093/infdis/jiaa486. PubMed PMID: 32745172; PMCID: PMC7454693.

171. Lu S, Zhao Y, Yu W, Yang Y, Gao J, Wang J, Kuang D, Yang M, Yang J, Ma C, Xu J, Qian X, Li H, Zhao S, Li J, Wang H, Long H, Zhou J, Luo F, Ding K, Wu D, Zhang Y, Dong Y, Liu Y, Zheng Y, Lin X, Jiao L, Zheng H, Dai Q, Sun Q, Hu Y, Ke C, Liu H, Peng X. Comparison of nonhuman primates identified the suitable model for COVID-19. Signal Transduct Target Ther. 2020;5(1):157. Epub 20201019. doi: 10.1038/s41392-020-00269-6. PubMed PMID: 32814760; PMCID: PMC7434851.

172. Chandrashekar A, Liu J, Martinot AJ, McMahan K, Mercado NB, Peter L, Tostanoski LH, Yu J, Maliga Z, Nekorchuk M, Busman-Sahay K, Terry M, Wrijil LM, Ducat S, Martinez DR, Atyeo C, Fischinger S, Burke JS, Slein MD, Pessaint L, Van Ry A, Greenhouse J, Taylor T, Blade K, Cook A, Finneyfrock B, Brown R, Teow E, Velasco J, Zahn R, Wegmann F, Abbink P, Bondzie EA, Dagotto G, Gebre MS, He X, Jacob-Dolan C, Kordana N, Li Z, Lifton MA, Mahrokhian SH, Maxfield LF, Nityanandam R, Nkolola JP, Schmidt AG, Miller AD, Baric RS, Alter G, Sorger PK, Estes JD, Andersen H, Lewis MG, Barouch DH. SARS-CoV-2 infection protects against rechallenge in rhesus macaques. Science. 2020;369(6505):812-7. Epub 2020/05/22. doi: 10.1126/science.abc4776. PubMed PMID: 32434946; PMCID: PMC7243369.

173. Hoang TN, Pino M, Boddapati AK, Viox EG, Starke CE, Upadhyay AA, Gumber S, Nekorchuk M, Busman-Sahay K, Strongin Z, Harper JL, Tharp GK, Pellegrini KL, Kirejczyk S, Zandi K, Tao S, Horton TR, Beagle EN, Mahar EA, Lee MYH, Cohen J, Jean SM, Wood JS, Connor-Stroud F, Stammen RL, Delmas OM, Wang S, Cooney KA, Sayegh MN, Wang L, Filev PD, Weiskopf D, Silvestri G, Waggoner J, Piantadosi A, Kasturi SP, Al-Shakhshir H, Ribeiro SP, Sekaly RP, Levit RD, Estes JD, Vanderford TH, Schinazi RF, Bosinger SE, Paiardini M. Baricitinib treatment resolves lower-airway macrophage inflammation and neutrophil recruitment in SARS-CoV-2-infected rhesus macaques. Cell. 2021;184(2):460-75.e21. Epub 20201110. doi: 10.1016/j.cell.2020.11.007. PubMed PMID: 33278358; PMCID: PMC7654323.

174. Aid M, Busman-Sahay K, Vidal SJ, Maliga Z, Bondoc S, Starke C, Terry M, Jacobson CA, Wrijil L, Ducat S, Brook OR, Miller AD, Porto M, Pellegrini KL, Pino M, Hoang TN, Chandrashekar A, Patel S, Stephenson K, Bosinger SE, Andersen H, Lewis MG, Hecht JL, Sorger PK, Martinot AJ, Estes JD, Barouch DH. Vascular Disease and Thrombosis in SARS-CoV-2-Infected Rhesus Macaques. Cell. 2020;183(5):1354-66.e13. Epub 20201009. doi: 10.1016/j.cell.2020.10.005. PubMed PMID: 33065030; PMCID: PMC7546181.

175. McLellan JS, Chen M, Joyce MG, Sastry M, Stewart-Jones GB, Yang Y, Zhang B, Chen L, Srivatsan S, Zheng A, Zhou T, Graepel KW, Kumar A, Moin S, Boyington JC, Chuang GY, Soto C, Baxa U, Bakker AQ, Spits H, Beaumont T, Zheng Z, Xia N, Ko SY, Todd JP, Rao S, Graham BS, Kwong PD. Structure-based design of a fusion glycoprotein vaccine for respiratory syncytial virus. Science. 2013;342(6158):592-8. doi: 10.1126/science.1243283. PubMed PMID: 24179220; PMCID: PMC4461862.

176. Kirchdoerfer RN, Cottrell CA, Wang N, Pallesen J, Yassine HM, Turner HL, Corbett KS, Graham BS, McLellan JS, Ward AB. Pre-fusion structure of a human coronavirus spike protein. Nature. 2016;531(7592):118-21. doi: 10.1038/nature17200. PubMed PMID: 26935699; PMCID: PMC4860016.

177. Pallesen J, Wang N, Corbett KS, Wrapp D, Kirchdoerfer RN, Turner HL, Cottrell CA, Becker MM, Wang L, Shi W, Kong WP, Andres EL, Kettenbach AN, Denison MR, Chappell JD, Graham BS, Ward AB, McLellan JS. Immunogenicity and structures of a rationally designed prefusion MERS-CoV spike antigen. Proc Natl Acad Sci U S A. 2017;114(35):E7348-E57. Epub 20170814. doi: 10.1073/pnas.1707304114. PubMed PMID: 28807998; PMCID: PMC5584442.

178. Loomis RJ, DiPiazza AT, Falcone S, Ruckwardt TJ, Morabito KM, Abiona OM, Chang LA, Caringal RT, Presnyak V, Narayanan E, Tsybovsky Y, Nair D, Hutchinson GB, Stewart-Jones GBE, Kueltzo LA, Himansu S, Mascola JR, Carfi A, Graham BS. Chimeric Fusion (F) and Attachment (G) Glycoprotein Antigen Delivery by mRNA as a Candidate Nipah Vaccine. Front Immunol. 2021;12:772864. Epub 20211208. doi: 10.3389/fimmu.2021.772864. PubMed PMID: 34956199; PMCID: PMC8692728.

179. Loomis RJ, Stewart-Jones GBE, Tsybovsky Y, Caringal RT, Morabito KM, McLellan JS, Chamberlain AL, Nugent ST, Hutchinson GB, Kueltzo LA, Mascola JR,

Graham BS. Structure-Based Design of Nipah Virus Vaccines: A Generalizable Approach to Paramyxovirus Immunogen Development. Front Immunol. 2020;11:842. Epub 20200611. doi: 10.3389/fimmu.2020.00842. PubMed PMID: 32595632; PMCID: PMC7300195.

180. FDA U. COVID-19 Vaccines | FDA2023.

181. Jackson LA, Anderson EJ, Rouphael NG, Roberts PC, Makhene M, Coler RN, McCullough MP, Chappell JD, Denison MR, Stevens LJ, Pruijssers AJ, McDermott A, Flach B, Doria-Rose NA, Corbett KS, Morabito KM, O'Dell S, Schmidt SD, Swanson PA, 2nd, Padilla M, Mascola JR, Neuzil KM, Bennett H, Sun W, Peters E, Makowski M, Albert J, Cross K, Buchanan W, Pikaart-Tautges R, Ledgerwood JE, Graham BS, Beigel JH, m RNASG. An mRNA Vaccine against SARS-CoV-2 - Preliminary Report. N Engl J Med. 2020;383(20):1920-31. Epub 20200714. doi: 10.1056/NEJMoa2022483. PubMed PMID: 32663912; PMCID: PMC7377258.

182. Walsh EE, Frenck RW, Jr., Falsey AR, Kitchin N, Absalon J, Gurtman A, Lockhart S, Neuzil K, Mulligan MJ, Bailey R, Swanson KA, Li P, Koury K, Kalina W, Cooper D, Fontes-Garfias C, Shi PY, Tureci O, Tompkins KR, Lyke KE, Raabe V, Dormitzer PR, Jansen KU, Sahin U, Gruber WC. Safety and Immunogenicity of Two RNA-Based Covid-19 Vaccine Candidates. N Engl J Med. 2020;383(25):2439-50. Epub 20201014. doi: 10.1056/NEJMoa2027906. PubMed PMID: 33053279; PMCID: PMC7583697.

183. Sahin U, Muik A, Vogler I, Derhovanessian E, Kranz LM, Vormehr M, Quandt J, Bidmon N, Ulges A, Baum A, Pascal KE, Maurus D, Brachtendorf S, Lorks V, Sikorski J, Koch P, Hilker R, Becker D, Eller AK, Grutzner J, Tonigold M, Boesler C, Rosenbaum C, Heesen L, Kuhnle MC, Poran A, Dong JZ, Luxemburger U, Kemmer-Bruck A, Langer D, Bexon M, Bolte S, Palanche T, Schultz A, Baumann S, Mahiny AJ, Boros G, Reinholz J, Szabo GT, Kariko K, Shi PY, Fontes-Garfias C, Perez JL, Cutler M, Cooper D, Kyratsous CA, Dormitzer PR, Jansen KU, Tureci O. BNT162b2 vaccine induces neutralizing antibodies and poly-specific T cells in humans. Nature. 2021;595(7868):572-7. Epub 20210527. doi: 10.1038/s41586-021-03653-6. PubMed PMID: 34044428.

184. Polack FP, Thomas SJ, Kitchin N, Absalon J, Gurtman A, Lockhart S, Perez JL, Perez Marc G, Moreira ED, Zerbini C, Bailey R, Swanson KA, Roychoudhury S, Koury K, Li P, Kalina WV, Cooper D, Frenck RW, Jr., Hammitt LL, Tureci O, Nell H, Schaefer A, Unal S, Tresnan DB, Mather S, Dormitzer PR, Sahin U, Jansen KU, Gruber WC, Group CCT. Safety and Efficacy of the BNT162b2 mRNA Covid-19 Vaccine. N Engl J Med. 2020;383(27):2603-15. Epub 20201210. doi: 10.1056/NEJMoa2034577. PubMed PMID: 33301246; PMCID: PMC7745181.

185. Baden LR, El Sahly HM, Essink B, Kotloff K, Frey S, Novak R, Diemert D, Spector SA, Rouphael N, Creech CB, McGettigan J, Khetan S, Segall N, Solis J, Brosz A, Fierro C, Schwartz H, Neuzil K, Corey L, Gilbert P, Janes H, Follmann D, Marovich M, Mascola J, Polakowski L, Ledgerwood J, Graham BS, Bennett H, Pajon R, Knightly C, Leav B, Deng W, Zhou H, Han S, Ivarsson M, Miller J, Zaks T, Group CS. Efficacy and Safety of the mRNA-1273 SARS-CoV-2 Vaccine. N Engl J Med. 2021;384(5):403-16. Epub

20201230. doi: 10.1056/NEJMoa2035389. PubMed PMID: 33378609; PMCID: PMC7787219.

186. FDA U. FDA Takes Key Action in Fight Against COVID-19 By Issuing Emergency Use Authorization for First COVID-19 Vaccine | FDA2020.

187. FDA U. FDA Takes Additional Action in Fight Against COVID-19 By Issuing Emergency Use Authorization for Second COVID-19 Vaccine | FDA: US FDA; 2020 [updated Fri, 12/18/2020 - 19:25]. Available from: https://www.fda.gov/news-events/press-announcements/fda-takes-additional-action-fight-against-covid-19-issuing-emergency-use-authorization-second-covid.

188. Fda US. FDA Approves First COVID-19 Vaccine | FDA: US FDA; 2021 [updated Mon, 08/23/2021 - 00:00]. Available from: https://www.fda.gov/news-events/press-announcements/fda-approves-first-covid-19-vaccine.

189. FDA U. Coronavirus (COVID-19) Update: FDA Takes Key Action by Approving Second COVID-19 Vaccine | FDA: US FDA; 2022 [updated Mon, 01/31/2022 - 11:15]. Available from: https://www.fda.gov/news-events/press-announcements/coronavirus-covid-19-update-fda-takes-key-action-approving-second-covid-19-vaccine.

190. FDA U. Coronavirus (COVID-19) Update: FDA Authorizes Moderna, Pfizer-BioNTech Bivalent COVID-19 Vaccines for Use as a Booster Dose | FDA: US FDA; 2022 [updated Wed, 08/31/2022 - 09:00]. Available from: https://www.fda.gov/news-events/press-announcements/coronavirus-covid-19-update-fda-authorizes-moderna-pfizer-biontech-bivalent-covid-19-vaccines-use.

191. Sadoff J, Gray G, Vandebosch A, Cardenas V, Shukarev G, Grinsztejn B, Goepfert PA, Truyers C, Fennema H, Spiessens B, Offergeld K, Scheper G, Taylor KL, Robb ML, Treanor J, Barouch DH, Stoddard J, Ryser MF, Marovich MA, Neuzil KM, Corey L, Cauwenberghs N, Tanner T, Hardt K, Ruiz-Guinazu J, Le Gars M, Schuitemaker H, Van Hoof J, Struyf F, Douoguih M, Group ES. Safety and Efficacy of Single-Dose Ad26.COV2.S Vaccine against Covid-19. N Engl J Med. 2021;384(23):2187-201. Epub 20210421. doi: 10.1056/NEJMoa2101544. PubMed PMID: 33882225; PMCID: PMC8220996.

192. Muir KL, Kallam A, Koepsell SA, Gundabolu K. Thrombotic Thrombocytopenia after Ad26.COV2.S Vaccination. N Engl J Med. 2021;384(20):1964-5. Epub 20210414. doi: 10.1056/NEJMc2105869. PubMed PMID: 33852795; PMCID: PMC8063883.

193. Greinacher A, Thiele T, Warkentin TE, Weisser K, Kyrle PA, Eichinger S. Thrombotic Thrombocytopenia after ChAdOx1 nCov-19 Vaccination. N Engl J Med. 2021;384(22):2092-101. Epub 20210409. doi: 10.1056/NEJMoa2104840. PubMed PMID: 33835769; PMCID: PMC8095372.

194. FDA U. Coronavirus (COVID-19) Update: FDA Limits Use of Janssen COVID-19 Vaccine to Certain Individuals | FDA2022.

195. Marks P. Revocation of EUA 27205-Janssen COVID-19 Vaccine 2023. Available from: https://www.fda.gov/media/169003/download.

196. Tian JH, Patel N, Haupt R, Zhou H, Weston S, Hammond H, Logue J, Portnoff AD, Norton J, Guebre-Xabier M, Zhou B, Jacobson K, Maciejewski S, Khatoon R, Wisniewska M, Moffitt W, Kluepfel-Stahl S, Ekechukwu B, Papin J, Boddapati S, Jason Wong C, Piedra PA, Frieman MB, Massare MJ, Fries L, Bengtsson KL, Stertman L, Ellingsworth L, Glenn G, Smith G. SARS-CoV-2 spike glycoprotein vaccine candidate NVX-CoV2373 immunogenicity in baboons and protection in mice. Nat Commun. 2021;12(1):372. Epub 20210114. doi: 10.1038/s41467-020-20653-8. PubMed PMID: 33446655; PMCID: PMC7809486.

197. Dunkle LM, Kotloff KL, Gay CL, Anez G, Adelglass JM, Barrat Hernandez AQ, Harper WL, Duncanson DM, McArthur MA, Florescu DF, McClelland RS, Garcia-Fragoso V, Riesenberg RA, Musante DB, Fried DL, Safirstein BE, McKenzie M, Jeanfreau RJ, Kingsley JK, Henderson JA, Lane DC, Ruiz-Palacios GM, Corey L, Neuzil KM, Coombs RW, Greninger AL, Hutter J, Ake JA, Smith K, Woo W, Cho I, Glenn GM, Dubovsky F, nCo VSG. Efficacy and Safety of NVX-CoV2373 in Adults in the United States and Mexico. N Engl J Med. 2022;386(6):531-43. Epub 20211215. doi: 10.1056/NEJMoa2116185. PubMed PMID: 34910859; PMCID: PMC8693692.

198. Who. COVID-19 Vaccines with WHO Emergency Use Listing2021.

199. Andrews N, Tessier E, Stowe J, Gower C, Kirsebom F, Simmons R, Gallagher E, Thelwall S, Groves N, Dabrera G, Myers R, Campbell CNJ, Amirthalingam G, Edmunds M, Zambon M, Brown K, Hopkins S, Chand M, Ladhani SN, Ramsay M, Lopez Bernal J. Duration of Protection against Mild and Severe Disease by Covid-19 Vaccines. N Engl J Med. 2022;386(4):340-50. Epub 20220112. doi: 10.1056/NEJMoa2115481. PubMed PMID: 35021002; PMCID: PMC8781262.

200. Bedston S, Akbari A, Jarvis CI, Lowthian E, Torabi F, North L, Lyons J, Perry M, Griffiths LJ, Owen RK, Beggs J, Chuter A, Bradley DT, de Lusignan S, Fry R, Richard Hobbs FD, Hollinghurst J, Katikireddi SV, Murphy S, O'Reily D, Robertson C, Shi T, Tsang RSM, Sheikh A, Lyons RA. COVID-19 vaccine uptake, effectiveness, and waning in 82,959 health care workers: A national prospective cohort study in Wales. Vaccine. 2022;40(8):1180-9. Epub 20220115. doi: 10.1016/j.vaccine.2021.11.061. PubMed PMID: 35042645; PMCID: PMC8760602.

201. Chemaitelly H, Tang P, Hasan MR, AlMukdad S, Yassine HM, Benslimane FM, Al Khatib HA, Coyle P, Ayoub HH, Al Kanaani Z, Al Kuwari E, Jeremijenko A, Kaleeckal AH, Latif AN, Shaik RM, Abdul Rahim HF, Nasrallah GK, Al Kuwari MG, Al Romaihi HE, Butt AA, Al-Thani MH, Al Khal A, Bertollini R, Abu-Raddad LJ. Waning of BNT162b2 Vaccine Protection against SARS-CoV-2 Infection in Qatar. N Engl J Med. 2021;385(24):e83. Epub 20211006. doi: 10.1056/NEJMoa2114114. PubMed PMID: 34614327; PMCID: PMC8522799.

202. Corrao G, Franchi M, Cereda D, Bortolan F, Zoli A, Leoni O, Borriello CR, Valle GPD, Tirani M, Pavesi G, Barone A, Ercolanoni M, Jara J, Galli M, Bertolaso G, Mancia G. Persistence of protection against SARS-CoV-2 clinical outcomes up to 9 months since vaccine completion: a retrospective observational analysis in Lombardy, Italy. Lancet Infect Dis. 2022;22(5):649-56. Epub 20220128. doi: 10.1016/S1473-3099(21)00813-6. PubMed PMID: 35093194; PMCID: PMC8797009.

203. Goldberg Y, Mandel M, Bar-On YM, Bodenheimer O, Freedman L, Haas EJ, Milo R, Alroy-Preis S, Ash N, Huppert A. Waning Immunity after the BNT162b2 Vaccine in Israel. N Engl J Med. 2021;385(24):e85. Epub 20211027. doi: 10.1056/NEJMoa2114228. PubMed PMID: 34706170; PMCID: PMC8609604.

204. Mizrahi B, Lotan R, Kalkstein N, Peretz A, Perez G, Ben-Tov A, Chodick G, Gazit S, Patalon T. Correlation of SARS-CoV-2-breakthrough infections to time-from-vaccine. Nat Commun. 2021;12(1):6379. Epub 20211104. doi: 10.1038/s41467-021-26672-3. PubMed PMID: 34737312; PMCID: PMC8569006.

205. Accorsi EK, Britton A, Fleming-Dutra KE, Smith ZR, Shang N, Derado G, Miller J, Schrag SJ, Verani JR. Association Between 3 Doses of mRNA COVID-19 Vaccine and Symptomatic Infection Caused by the SARS-CoV-2 Omicron and Delta Variants. JAMA. 2022;327(7):639-51. doi: 10.1001/jama.2022.0470. PubMed PMID: 35060999; PMCID: PMC8848203.

206. Peacock TP, Penrice-Randal R, Hiscox JA, Barclay WS. SARS-CoV-2 one year on: evidence for ongoing viral adaptation. J Gen Virol. 2021;102(4). doi: 10.1099/jgv.0.001584. PubMed PMID: 33855951; PMCID: PMC8290271.

207. Cdc. SARS-CoV-2 Variant Classifications and Definitions2023.

208. MacLean OA, Lytras S, Weaver S, Singer JB, Boni MF, Lemey P, Kosakovsky Pond SL, Robertson DL. Natural selection in the evolution of SARS-CoV-2 in bats created a generalist virus and highly capable human pathogen. PLoS Biol. 2021;19(3):e3001115. Epub 20210312. doi: 10.1371/journal.pbio.3001115. PubMed PMID: 33711012; PMCID: PMC7990310.

209. England PH. Investigation of novel SARS-CoV-2 variant: Variant of Concern 202012/01 - Variant_of_Concern_VOC_202012_01_Technical_Briefing_3.pdf 2023 [9/4/23]. Available from: https://assets.publishing.service.gov.uk/government/uploads/system/uploads/attachment_data/file/959360/Variant_of_Concern_VOC_202012_01_Technical_Briefing_3.pdf.

210. Davies NG, Abbott S, Barnard RC, Jarvis CI, Kucharski AJ, Munday JD, Pearson CAB, Russell TW, Tully DC, Washburne AD, Wenseleers T, Gimma A, Waites W, Wong KLM, van Zandvoort K, Silverman JD, Group CC-W, Consortium C-GU, Diaz-Ordaz K, Keogh R, Eggo RM, Funk S, Jit M, Atkins KE, Edmunds WJ. Estimated transmissibility and impact of SARS-CoV-2 lineage B.1.1.7 in England. Science. 2021;372(6538). Epub 20210303. doi: 10.1126/science.abg3055. PubMed PMID: 33658326; PMCID: PMC8128288.

211. Tegally H, Wilkinson E, Giovanetti M, Iranzadeh A, Fonseca V, Giandhari J, Doolabh D, Pillay S, San EJ, Msomi N, Mlisana K, von Gottberg A, Walaza S, Allam M, Ismail A, Mohale T, Glass AJ, Engelbrecht S, Van Zyl G, Preiser W, Petruccione F, Sigal A, Hardie D, Marais G, Hsiao NY, Korsman S, Davies MA, Tyers L, Mudau I, York D, Maslo C, Goedhals D, Abrahams S, Laguda-Akingba O, Alisoltani-Dehkordi A, Godzik A, Wibmer CK, Sewell BT, Lourenco J, Alcantara LCJ, Kosakovsky Pond SL, Weaver S, Martin D, Lessells RJ, Bhiman JN, Williamson C, de Oliveira T. Detection of a SARS-CoV-2 variant of concern in South Africa. Nature. 2021;592(7854):438-43. Epub 20210309. doi: 10.1038/s41586-021-03402-9. PubMed PMID: 33690265.

212. Wibmer CK, Ayres F, Hermanus T, Madzivhandila M, Kgagudi P, Oosthuysen B, Lambson BE, de Oliveira T, Vermeulen M, van der Berg K, Rossouw T, Boswell M, Ueckermann V, Meiring S, von Gottberg A, Cohen C, Morris L, Bhiman JN, Moore PL. SARS-CoV-2 501Y.V2 escapes neutralization by South African COVID-19 donor plasma. Nat Med. 2021;27(4):622-5. Epub 20210302. doi: 10.1038/s41591-021-01285-x. PubMed PMID: 33654292.

213. Mwenda M, Saasa N, Sinyange N, Busby G, Chipimo PJ, Hendry J, Kapona O, Yingst S, Hines JZ, Minchella P, Simulundu E, Changula K, Nalubamba KS, Sawa H, Kajihara M, Yamagishi J, Kapin'a M, Kapata N, Fwoloshi S, Zulu P, Mulenga LB, Agolory S, Mukonka V, Bridges DJ. Detection of B.1.351 SARS-CoV-2 Variant Strain - Zambia, December 2020. MMWR Morb Mortal Wkly Rep. 2021;70(8):280-2. Epub 20210226. doi: 10.15585/mmwr.mm7008e2. PubMed PMID: 33630820; PMCID: PMC8344984.

214. Wang P, Casner RG, Nair MS, Wang M, Yu J, Cerutti G, Liu L, Kwong PD, Huang Y, Shapiro L, Ho DD. Increased resistance of SARS-CoV-2 variant P.1 to antibody neutralization. Cell Host Microbe. 2021;29(5):747-51 e4. Epub 20210418. doi: 10.1016/j.chom.2021.04.007. PubMed PMID: 33887205; PMCID: PMC8053237.

215. Faria NR, Mellan TA, Whittaker C, Claro IM, Candido DDS, Mishra S, Crispim MAE, Sales FCS, Hawryluk I, McCrone JT, Hulswit RJG, Franco LAM, Ramundo MS, de Jesus JG, Andrade PS, Coletti TM, Ferreira GM, Silva CAM, Manuli ER, Pereira RHM, Peixoto PS, Kraemer MUG, Gaburo N, Jr., Camilo CDC, Hoeltgebaum H, Souza WM, Rocha EC, de Souza LM, de Pinho MC, Araujo LJT, Malta FSV, de Lima AB, Silva JDP, Zauli DAG, Ferreira ACS, Schnekenberg RP, Laydon DJ, Walker PGT, Schluter HM, Dos Santos ALP, Vidal MS, Del Caro VS, Filho RMF, Dos Santos HM, Aguiar RS, Proenca-Modena JL, Nelson B, Hay JA, Monod M, Miscouridou X, Coupland H, Sonabend R, Vollmer M, Gandy A, Prete CA, Jr., Nascimento VH, Suchard MA, Bowden TA, Pond SLK, Wu CH, Ratmann O, Ferguson NM, Dye C, Loman NJ, Lemey P, Rambaut A, Fraiji NA, Carvalho M, Pybus OG, Flaxman S, Bhatt S, Sabino EC. Genomics and epidemiology of the P.1 SARS-CoV-2 lineage in Manaus, Brazil. Science. 2021;372(6544):815-21. Epub 20210414. doi: 10.1126/science.abh2644. PubMed PMID: 33853970; PMCID: PMC8139423.

216. Choi JY, Smith DM. SARS-CoV-2 Variants of Concern. Yonsei Med J. 2021;62(11):961-8. doi: 10.3349/ymj.2021.62.11.961. PubMed PMID: 34672129; PMCID: PMC8542474.

217. Mlcochova P, Kemp SA, Dhar MS, Papa G, Meng B, Ferreira I, Datir R, Collier DA, Albecka A, Singh S, Pandey R, Brown J, Zhou J, Goonawardane N, Mishra S, Whittaker C, Mellan T, Marwal R, Datta M, Sengupta S, Ponnusamy K, Radhakrishnan VS, Abdullahi A, Charles O, Chattopadhyay P, Devi P, Caputo D, Peacock T, Wattal C, Goel N, Satwik A, Vaishya R, Agarwal M, Indian S-C-GC, Genotype to Phenotype Japan C, Collaboration C-NBC-, Mavousian A, Lee JH, Bassi J, Silacci-Fegni C, Saliba C, Pinto D, Irie T, Yoshida I, Hamilton WL, Sato K, Bhatt S, Flaxman S, James LC, Corti D, Piccoli L, Barclay WS, Rakshit P, Agrawal A, Gupta RK. SARS-CoV-2 B.1.617.2 Delta variant replication and immune evasion. Nature. 2021;599(7883):114-9. Epub 20210906. doi: 10.1038/s41586-021-03944-y. PubMed PMID: 34488225; PMCID: PMC8566220.

218. Hoffmann M, Hofmann-Winkler H, Kruger N, Kempf A, Nehlmeier I, Graichen L, Arora P, Sidarovich A, Moldenhauer AS, Winkler MS, Schulz S, Jack HM, Stankov MV, Behrens GMN, Pohlmann S. SARS-CoV-2 variant B.1.617 is resistant to bamlanivimab and evades antibodies induced by infection and vaccination. Cell Rep. 2021;36(3):109415. Epub 20210629. doi: 10.1016/j.celrep.2021.109415. PubMed PMID: 34270919; PMCID: PMC8238662.

219. Twohig KA, Nyberg T, Zaidi A, Thelwall S, Sinnathamby MA, Aliabadi S, Seaman SR, Harris RJ, Hope R, Lopez-Bernal J, Gallagher E, Charlett A, De Angelis D, Presanis AM, Dabrera G, consortium C-GU. Hospital admission and emergency care attendance risk for SARS-CoV-2 delta (B.1.617.2) compared with alpha (B.1.1.7) variants of concern: a cohort study. Lancet Infect Dis. 2022;22(1):35-42. Epub 20210827. doi: 10.1016/S1473-3099(21)00475-8. PubMed PMID: 34461056; PMCID: PMC8397301.

220. Levine-Tiefenbrun M, Yelin I, Alapi H, Katz R, Herzel E, Kuint J, Chodick G, Gazit S, Patalon T, Kishony R. Viral loads of Delta-variant SARS-CoV-2 breakthrough infections after vaccination and booster with BNT162b2. Nat Med. 2021;27(12):2108-10. Epub 20211102. doi: 10.1038/s41591-021-01575-4. PubMed PMID: 34728830.

221. WHO. Classification of Omicron (B.1.1.529): SARS-CoV-2 Variant of Concern 2021 [updated 11/26/2021; cited 2023 9/4]. Available from: https://www.who.int/news/item/26-11-2021-classification-of-omicron-(b.1.1.529)-sars-cov-2-variant-of-concern.

222. Vaughan A. Omicron emerges. New Sci. 2021;252(3363):7. Epub 20211203. doi: 10.1016/S0262-4079(21)02140-0. PubMed PMID: 34876769; PMCID: PMC8639363.

223. Viana R, Moyo S, Amoako DG, Tegally H, Scheepers C, Althaus CL, Anyaneji UJ, Bester PA, Boni MF, Chand M, Choga WT, Colquhoun R, Davids M, Deforche K, Doolabh D, du Plessis L, Engelbrecht S, Everatt J, Giandhari J, Giovanetti M, Hardie D, Hill V, Hsiao NY, Iranzadeh A, Ismail A, Joseph C, Joseph R, Koopile L, Kosakovsky Pond SL, Kraemer MUG, Kuate-Lere L, Laguda-Akingba O, Lesetedi-Mafoko O, Lessells RJ, Lockman S, Lucaci AG, Maharaj A, Mahlangu B, Maponga T, Mahlakwane K, Makatini Z, Marais G, Maruapula D, Masupu K, Matshaba M, Mayaphi S, Mbhele N, Mbulawa MB, Mendes A, Mlisana K, Mnguni A, Mohale T, Moir M, Moruisi K, Mosepele M, Motsatsi G, Motswaledi MS, Mphoyakgosi T, Msomi N, Mwangi PN, Naidoo Y, Ntuli N, Nyaga M,

Olubayo L, Pillay S, Radibe B, Ramphal Y, Ramphal U, San JE, Scott L, Shapiro R, Singh L, Smith-Lawrence P, Stevens W, Strydom A, Subramoney K, Tebeila N, Tshiabuila D, Tsui J, van Wyk S, Weaver S, Wibmer CK, Wilkinson E, Wolter N, Zarebski AE, Zuze B, Goedhals D, Preiser W, Treurnicht F, Venter M, Williamson C, Pybus OG, Bhiman J, Glass A, Martin DP, Rambaut A, Gaseitsiwe S, von Gottberg A, de Oliveira T. Rapid epidemic expansion of the SARS-CoV-2 Omicron variant in southern Africa. Nature. 2022;603(7902):679-86. Epub 20220107. doi: 10.1038/s41586-022-04411-y. PubMed PMID: 35042229; PMCID: PMC8942855.

224. Chen J, Wang R, Gilby NB, Wei GW. Omicron Variant (B.1.1.529): Infectivity, Vaccine Breakthrough, and Antibody Resistance. J Chem Inf Model. 2022;62(2):412-22. Epub 20220106. doi: 10.1021/acs.jcim.1c01451. PubMed PMID: 34989238; PMCID: PMC8751645.

225. Danielsson A, Nyhlin H, Suhr O. [SeHCAT--a gamma-radiating bile acid isotope for the diagnosis of dysfunction of the terminal ileum]. Lakartidningen. 1987;84(15):1266-70. PubMed PMID: 3586781.

226. Chatterjee S, Bhattacharya M, Nag S, Dhama K, Chakraborty C. A Detailed Overview of SARS-CoV-2 Omicron: Its Sub-Variants, Mutations and Pathophysiology, Clinical Characteristics, Immunological Landscape, Immune Escape, and Therapies. Viruses. 2023;15(1). Epub 20230105. doi: 10.3390/v15010167. PubMed PMID: 36680207; PMCID: PMC9866114.

227. WHO. EG.5 Initial Risk Evaluation, 9 August 2023 2023. Available from: https://www.who.int/docs/default-source/coronaviruse/09082023eg.5_ire_final.pdf?sfvrsn=2aa2daee_1.

228. Harris E. CDC Assesses Risk From BA.2.86, Highly Mutated COVID-19 Variant. JAMA. 2023. Epub 20230830. doi: 10.1001/jama.2023.16105. PubMed PMID: 37647093.

229. Callaway E. Why a highly mutated coronavirus variant has scientists on alert. Nature. 2023;620(7976):934. doi: 10.1038/d41586-023-02656-9. PubMed PMID: 37604863.

230. Janiaud P, Axfors C, Schmitt AM, Gloy V, Ebrahimi F, Hepprich M, Smith ER, Haber NA, Khanna N, Moher D, Goodman SN, Ioannidis JPA, Hemkens LG. Association of Convalescent Plasma Treatment With Clinical Outcomes in Patients With COVID-19: A Systematic Review and Meta-analysis. JAMA. 2021;325(12):1185-95. doi: 10.1001/jama.2021.2747. PubMed PMID: 33635310; PMCID: PMC7911095.

231. Begin P, Callum J, Jamula E, Cook R, Heddle NM, Tinmouth A, Zeller MP, Beaudoin-Bussieres G, Amorim L, Bazin R, Loftsgard KC, Carl R, Chasse M, Cushing MM, Daneman N, Devine DV, Dumaresq J, Fergusson DA, Gabe C, Glesby MJ, Li N, Liu Y, McGeer A, Robitaille N, Sachais BS, Scales DC, Schwartz L, Shehata N, Turgeon AF, Wood H, Zarychanski R, Finzi A, Group C-S, Arnold DM. Convalescent plasma for hospitalized patients with COVID-19: an open-label, randomized controlled trial. Nat Med.

2021;27(11):2012-24. Epub 20210909. doi: 10.1038/s41591-021-01488-2. PubMed PMID: 34504336; PMCID: PMC8604729.

232. Group RC. Convalescent plasma in patients admitted to hospital with COVID-19 (RECOVERY): a randomised controlled, open-label, platform trial. Lancet. 2021;397(10289):2049-59. Epub 20210514. doi: 10.1016/S0140-6736(21)00897-7. PubMed PMID: 34000257; PMCID: PMC8121538.

233. Writing Committee for the R-CAPI, Estcourt LJ, Turgeon AF, McQuilten ZK, McVerry BJ, Al-Beidh F, Annane D, Arabi YM, Arnold DM, Beane A, Begin P, van Bentum-Puijk W, Berry LR, Bhimani Z, Birchall JE, Bonten MJM, Bradbury CA, Brunkhorst FM, Buxton M, Callum JL, Chasse M, Cheng AC, Cove ME, Daly J, Derde L, Detry MA, De Jong M, Evans A, Fergusson DA, Fish M, Fitzgerald M, Foley C, Goossens H, Gordon AC, Gosbell IB, Green C, Haniffa R, Harvala H, Higgins AM, Hills TE, Hoad VC, Horvat C, Huang DT, Hudson CL, Ichihara N, Laing E, Lamikanra AA, Lamontagne F, Lawler PR, Linstrum K, Litton E, Lorenzi E, MacLennan S, Marshall J, McAuley DF, McDyer JF, McGlothlin A, McGuinness S, Miflin G, Montgomery S, Mouncey PR, Murthy S, Nichol A, Parke R, Parker JC, Priddee N, Purcell DFJ, Reyes LF, Richardson P, Robitaille N, Rowan KM, Rynne J, Saito H, Santos M, Saunders CT, Serpa Neto A, Seymour CW, Silversides JA, Tinmouth AA, Triulzi DJ, Turner AM, van de Veerdonk F, Walsh TS, Wood EM, Berry S, Lewis RJ, Menon DK, McArthur C, Zarychanski R, Angus DC, Webb SA, Roberts DJ, Shankar-Hari M. Effect of Convalescent Plasma on Organ Support-Free Days in Critically Ill Patients With COVID-19: A Randomized Clinical Trial. JAMA. 2021;326(17):1690-702. doi: 10.1001/jama.2021.18178. PubMed PMID: 34606578; PMCID: PMC8491132.

234. Millat-Martinez P, Gharbharan A, Alemany A, Rokx C, Geurtsvankessel C, Papageourgiou G, van Geloven N, Jordans C, Groeneveld G, Swaneveld F, van der Schoot E, Corbacho-Monne M, Ouchi D, Piccolo Ferreira F, Malchair P, Videla S, Garcia Garcia V, Ruiz-Comellas A, Ramirez-Morros A, Rodriguez Codina J, Amado Simon R, Grifols JR, Blanco J, Blanco I, Ara J, Bassat Q, Clotet B, Baro B, Troxel A, Zwaginga JJ, Mitja O, Rijnders BJA, Co VEsg, group CO-es. Prospective individual patient data meta-analysis of two randomized trials on convalescent plasma for COVID-19 outpatients. Nat Commun. 2022;13(1):2583. Epub 20220511. doi: 10.1038/s41467-022-29911-3. PubMed PMID: 35546145; PMCID: PMC9095637.

235. Dougan M, Azizad M, Mocherla B, Gottlieb RL, Chen P, Hebert C, Perry R, Boscia J, Heller B, Morris J, Crystal C, Igbinadolor A, Huhn G, Cardona J, Shawa I, Kumar P, Blomkalns A, Adams AC, Van Naarden J, Custer KL, Knorr J, Oakley G, Schade AE, Holzer TR, Ebert PJ, Higgs RE, Sabo J, Patel DR, Dabora MC, Williams M, Klekotka P, Shen L, Skovronsky DM, Nirula A. A Randomized, Placebo-Controlled Clinical Trial of Bamlanivimab and Etesevimab Together in High-Risk Ambulatory Patients With COVID-19 and Validation of the Prognostic Value of Persistently High Viral Load. Clin Infect Dis. 2022;75(1):e440-e9. doi: 10.1093/cid/ciab912. PubMed PMID: 34718468; PMCID: PMC9402688.

236. Gupta A, Gonzalez-Rojas Y, Juarez E, Crespo Casal M, Moya J, Rodrigues Falci D, Sarkis E, Solis J, Zheng H, Scott N, Cathcart AL, Parra S, Sager JE, Austin D, Peppercorn A, Alexander E, Yeh WW, Brinson C, Aldinger M, Shapiro AE, Investigators C-I. Effect of Sotrovimab on Hospitalization or Death Among High-risk Patients With Mild to Moderate COVID-19: A Randomized Clinical Trial. JAMA. 2022;327(13):1236-46. doi: 10.1001/jama.2022.2832. PubMed PMID: 35285853; PMCID: PMC8922199.

237. Weinreich DM, Sivapalasingam S, Norton T, Ali S, Gao H, Bhore R, Xiao J, Hooper AT, Hamilton JD, Musser BJ, Rofail D, Hussein M, Im J, Atmodjo DY, Perry C, Pan C, Mahmood A, Hosain R, Davis JD, Turner KC, Baum A, Kyratsous CA, Kim Y, Cook A, Kampman W, Roque-Guerrero L, Acloque G, Aazami H, Cannon K, Simon-Campos JA, Bocchini JA, Kowal B, DiCioccio AT, Soo Y, Geba GP, Stahl N, Lipsich L, Braunstein N, Herman G, Yancopoulos GD, Trial I. REGEN-COV Antibody Combination and Outcomes in Outpatients with Covid-19. N Engl J Med. 2021;385(23):e81. Epub 20210929. doi: 10.1056/NEJMoa2108163. PubMed PMID: 34587383; PMCID: PMC8522800.

238. NIH. Anti-SARS-CoV-2 Monoclonal Antibodies 2023 [updated 3/6/2023; cited 2023 9/4]. Available from: https://www.covid19treatmentguidelines.nih.gov/therapies/antivirals-including-antibody-products/anti-sars-cov-2-monoclonal-antibodies/.

239. FDA U. Coronavirus (COVID-19) | Drugs | FDA2023.

240. Mayence A, Vanden Eynde JJ. Baricitinib: A 2018 Novel FDA-Approved Small Molecule Inhibiting Janus Kinases. Pharmaceuticals (Basel). 2019;12(1). Epub 20190312. doi: 10.3390/ph12010037. PubMed PMID: 30871014; PMCID: PMC6469186.

241. Sheppard M, Laskou F, Stapleton PP, Hadavi S, Dasgupta B. Tocilizumab (Actemra). Hum Vaccin Immunother. 2017;13(9):1972-88. doi: 10.1080/21645515.2017.1316909. PubMed PMID: 28841363; PMCID: PMC5612212.

242. Stebbing J, Phelan A, Griffin I, Tucker C, Oechsle O, Smith D, Richardson P. COVID-19: combining antiviral and anti-inflammatory treatments. Lancet Infect Dis. 2020;20(4):400-2. Epub 20200227. doi: 10.1016/S1473-3099(20)30132-8. PubMed PMID: 32113509; PMCID: PMC7158903.

243. Richardson P, Griffin I, Tucker C, Smith D, Oechsle O, Phelan A, Rawling M, Savory E, Stebbing J. Baricitinib as potential treatment for 2019-nCoV acute respiratory disease. Lancet. 2020;395(10223):e30-e1. Epub 20200204. doi: 10.1016/S0140-6736(20)30304-4. PubMed PMID: 32032529; PMCID: PMC7137985.

244. Stebbing J, Krishnan V, de Bono S, Ottaviani S, Casalini G, Richardson PJ, Monteil V, Lauschke VM, Mirazimi A, Youhanna S, Tan YJ, Baldanti F, Sarasini A, Terres JAR, Nickoloff BJ, Higgs RE, Rocha G, Byers NL, Schlichting DE, Nirula A, Cardoso A, Corbellino M, Sacco Baricitinib Study G. Mechanism of baricitinib supports artificial intelligence-predicted testing in COVID-19 patients. EMBO Mol Med. 2020;12(8):e12697. Epub 20200624. doi: 10.15252/emmm.202012697. PubMed PMID: 32473600; PMCID: PMC7300657.

245. Kalil AC, Patterson TF, Mehta AK, Tomashek KM, Wolfe CR, Ghazaryan V, Marconi VC, Ruiz-Palacios GM, Hsieh L, Kline S, Tapson V, Iovine NM, Jain MK, Sweeney DA, El Sahly HM, Branche AR, Regalado Pineda J, Lye DC, Sandkovsky U, Luetkemeyer AF, Cohen SH, Finberg RW, Jackson PEH, Taiwo B, Paules CI, Arguinchona H, Erdmann N, Ahuja N, Frank M, Oh MD, Kim ES, Tan SY, Mularski RA, Nielsen H, Ponce PO, Taylor BS, Larson L, Rouphael NG, Saklawi Y, Cantos VD, Ko ER, Engemann JJ, Amin AN, Watanabe M, Billings J, Elie MC, Davey RT, Burgess TH, Ferreira J, Green M, Makowski M, Cardoso A, de Bono S, Bonnett T, Proschan M, Deye GA, Dempsey W, Nayak SU, Dodd LE, Beigel JH, Members A-SG. Baricitinib plus Remdesivir for Hospitalized Adults with Covid-19. N Engl J Med. 2021;384(9):795-807. Epub 2020/12/12. doi: 10.1056/NEJMoa2031994. PubMed PMID: 33306283; PMCID: PMC7745180.

246. Marconi VC, Ramanan AV, de Bono S, Kartman CE, Krishnan V, Liao R, Piruzeli MLB, Goldman JD, Alatorre-Alexander J, de Cassia Pellegrini R, Estrada V, Som M, Cardoso A, Chakladar S, Crowe B, Reis P, Zhang X, Adams DH, Ely EW, Group C-BS. Efficacy and safety of baricitinib for the treatment of hospitalised adults with COVID-19 (COV-BARRIER): a randomised, double-blind, parallel-group, placebo-controlled phase 3 trial. Lancet Respir Med. 2021;9(12):1407-18. Epub 20210901. doi: 10.1016/S2213-2600(21)00331-3. PubMed PMID: 34480861; PMCID: PMC8409066.

247. Company ELa. FDA Approves Lilly and Incyte's OLUMIANT® (baricitinib) for the Treatment of Certain Hospitalized Patients with COVID-19 | Eli Lilly and Company 2022 [cited 2023 9/4]. Available from: https://investor.lilly.com/news-releases/news-release-details/fda-approves-lilly-and-incytes-olumiantr-baricitinib-treatment.

248. Rubin R. Baricitinib Is First Approved COVID-19 Immunomodulatory Treatment. JAMA. 2023;327(23):2281-. doi: 10.1001/jama.2022.9846.

249. Gupta S, Wang W, Hayek SS, Chan L, Mathews KS, Melamed ML, Brenner SK, Leonberg-Yoo A, Schenck EJ, Radbel J, Reiser J, Bansal A, Srivastava A, Zhou Y, Finkel D, Green A, Mallappallil M, Faugno AJ, Zhang J, Velez JCQ, Shaefi S, Parikh CR, Charytan DM, Athavale AM, Friedman AN, Redfern RE, Short SAP, Correa S, Pokharel KK, Admon AJ, Donnelly JP, Gershengorn HB, Douin DJ, Semler MW, Hernan MA, Leaf DE, Investigators S-C. Association Between Early Treatment With Tocilizumab and Mortality Among Critically Ill Patients With COVID-19. JAMA Intern Med. 2021;181(1):41-51. doi: 10.1001/jamainternmed.2020.6252. PubMed PMID: 33080002; PMCID: PMC7577201.

250. Guaraldi G, Meschiari M, Cozzi-Lepri A, Milic J, Tonelli R, Menozzi M, Franceschini E, Cuomo G, Orlando G, Borghi V, Santoro A, Di Gaetano M, Puzzolante C, Carli F, Bedini A, Corradi L, Fantini R, Castaniere I, Tabbi L, Girardis M, Tedeschi S, Giannella M, Bartoletti M, Pascale R, Dolci G, Brugioni L, Pietrangelo A, Cossarizza A, Pea F, Clini E, Salvarani C, Massari M, Viale PL, Mussini C. Tocilizumab in patients with severe COVID-19: a retrospective cohort study. Lancet Rheumatol. 2020;2(8):e474-e84. Epub 20200624. doi: 10.1016/S2665-9913(20)30173-9. PubMed PMID: 32835257; PMCID: PMC7314456.

251. Investigators R-C, Gordon AC, Mouncey PR, Al-Beidh F, Rowan KM, Nichol AD, Arabi YM, Annane D, Beane A, van Bentum-Puijk W, Berry LR, Bhimani Z, Bonten MJM, Bradbury CA, Brunkhorst FM, Buzgau A, Cheng AC, Detry MA, Duffy EJ, Estcourt LJ, Fitzgerald M, Goossens H, Haniffa R, Higgins AM, Hills TE, Horvat CM, Lamontagne F, Lawler PR, Leavis HL, Linstrum KM, Litton E, Lorenzi E, Marshall JC, Mayr FB, McAuley DF, McGlothlin A, McGuinness SP, McVerry BJ, Montgomery SK, Morpeth SC, Murthy S, Orr K, Parke RL, Parker JC, Patanwala AE, Pettila V, Rademaker E, Santos MS, Saunders CT, Seymour CW, Shankar-Hari M, Sligl WI, Turgeon AF, Turner AM, van de Veerdonk FL, Zarychanski R, Green C, Lewis RJ, Angus DC, McArthur CJ, Berry S, Webb SA, Derde LPG. Interleukin-6 Receptor Antagonists in Critically Ill Patients with Covid-19. N Engl J Med. 2021;384(16):1491-502. Epub 20210225. doi: 10.1056/NEJMoa2100433. PubMed PMID: 33631065; PMCID: PMC7953461.

252. WHO. WHO recommends against the use of remdesivir in COVID-19 patients 2020 [cited 2023 9/4]. Available from: https://www.who.int/news-room/feature-stories/detail/who-recommends-against-the-use-of-remdesivir-in-covid-19-patients.

253. Warren TK, Jordan R, Lo MK, Ray AS, Mackman RL, Soloveva V, Siegel D, Perron M, Bannister R, Hui HC, Larson N, Strickley R, Wells J, Stuthman KS, Van Tongeren SA, Garza NL, Donnelly G, Shurtleff AC, Retterer CJ, Gharaibeh D, Zamani R, Kenny T, Eaton BP, Grimes E, Welch LS, Gomba L, Wilhelmsen CL, Nichols DK, Nuss JE, Nagle ER, Kugelman JR, Palacios G, Doerffler E, Neville S, Carra E, Clarke MO, Zhang L, Lew W, Ross B, Wang Q, Chun K, Wolfe L, Babusis D, Park Y, Stray KM, Trancheva I, Feng JY, Barauskas O, Xu Y, Wong P, Braun MR, Flint M, McMullan LK, Chen SS, Fearns R, Swaminathan S, Mayers DL, Spiropoulou CF, Lee WA, Nichol ST, Cihlar T, Bavari S. Therapeutic efficacy of the small molecule GS-5734 against Ebola virus in rhesus monkeys. Nature. 2016;531(7594):381-5. Epub 20160302. doi: 10.1038/nature17180. PubMed PMID: 26934220; PMCID: PMC5551389.

254. Lo MK, Jordan R, Arvey A, Sudhamsu J, Shrivastava-Ranjan P, Hotard AL, Flint M, McMullan LK, Siegel D, Clarke MO, Mackman RL, Hui HC, Perron M, Ray AS, Cihlar T, Nichol ST, Spiropoulou CF. GS-5734 and its parent nucleoside analog inhibit Filo-, Pneumo-, and Paramyxoviruses. Sci Rep. 2017;7:43395. Epub 20170306. doi: 10.1038/srep43395. PubMed PMID: 28262699; PMCID: PMC5338263.

255. Wang M, Cao R, Zhang L, Yang X, Liu J, Xu M, Shi Z, Hu Z, Zhong W, Xiao G. Remdesivir and chloroquine effectively inhibit the recently emerged novel coronavirus (2019-nCoV) in vitro. Cell Res. 2020;30(3):269-71. Epub 20200204. doi: 10.1038/s41422-020-0282-0. PubMed PMID: 32020029; PMCID: PMC7054408.

256. Consortium WHOST, Pan H, Peto R, Henao-Restrepo AM, Preziosi MP, Sathiyamoorthy V, Abdool Karim Q, Alejandria MM, Hernandez Garcia C, Kieny MP, Malekzadeh R, Murthy S, Reddy KS, Roses Periago M, Abi Hanna P, Ader F, Al-Bader AM, Alhasawi A, Allum E, Alotaibi A, Alvarez-Moreno CA, Appadoo S, Asiri A, Aukrust P, Barratt-Due A, Bellani S, Branca M, Cappel-Porter HBC, Cerrato N, Chow TS, Como N, Eustace J, Garcia PJ, Godbole S, Gotuzzo E, Griskevicius L, Hamra R, Hassan M, Hassany M, Hutton D, Irmansyah I, Jancoriene L, Kirwan J, Kumar S, Lennon P, Lopardo

G, Lydon P, Magrini N, Maguire T, Manevska S, Manuel O, McGinty S, Medina MT, Mesa Rubio ML, Miranda-Montoya MC, Nel J, Nunes EP, Perola M, Portoles A, Rasmin MR, Raza A, Rees H, Reges PPS, Rogers CA, Salami K, Salvadori MI, Sinani N, Sterne JAC, Stevanovikj M, Tacconelli E, Tikkinen KAO, Trelle S, Zaid H, Rottingen JA, Swaminathan S. Repurposed Antiviral Drugs for Covid-19 - Interim WHO Solidarity Trial Results. N Engl J Med. 2021;384(6):497-511. Epub 20201202. doi: 10.1056/NEJMoa2023184. PubMed PMID: 33264556; PMCID: PMC7727327.

257. Beigel JH, Tomashek KM, Dodd LE, Mehta AK, Zingman BS, Kalil AC, Hohmann E, Chu HY, Luetkemeyer A, Kline S, Lopez de Castilla D, Finberg RW, Dierberg K, Tapson V, Hsieh L, Patterson TF, Paredes R, Sweeney DA, Short WR, Touloumi G, Lye DC, Ohmagari N, Oh MD, Ruiz-Palacios GM, Benfield T, Fatkenheuer G, Kortepeter MG, Atmar RL, Creech CB, Lundgren J, Babiker AG, Pett S, Neaton JD, Burgess TH, Bonnett T, Green M, Makowski M, Osinusi A, Nayak S, Lane HC, Members A-SG. Remdesivir for the Treatment of Covid-19 - Final Report. N Engl J Med. 2020;383(19):1813-26. Epub 20201008. doi: 10.1056/NEJMoa2007764. PubMed PMID: 32445440; PMCID: PMC7262788.

258. Spinner CD, Gottlieb RL, Criner GJ, Arribas Lopez JR, Cattelan AM, Soriano Viladomiu A, Ogbuagu O, Malhotra P, Mullane KM, Castagna A, Chai LYA, Roestenberg M, Tsang OTY, Bernasconi E, Le Turnier P, Chang SC, SenGupta D, Hyland RH, Osinusi AO, Cao H, Blair C, Wang H, Gaggar A, Brainard DM, McPhail MJ, Bhagani S, Ahn MY, Sanyal AJ, Huhn G, Marty FM, Investigators G-U-. Effect of Remdesivir vs Standard Care on Clinical Status at 11 Days in Patients With Moderate COVID-19: A Randomized Clinical Trial. JAMA. 2020;324(11):1048-57. doi: 10.1001/jama.2020.16349. PubMed PMID: 32821939; PMCID: PMC7442954.

259. Wang Y, Zhang D, Du G, Du R, Zhao J, Jin Y, Fu S, Gao L, Cheng Z, Lu Q, Hu Y, Luo G, Wang K, Lu Y, Li H, Wang S, Ruan S, Yang C, Mei C, Wang Y, Ding D, Wu F, Tang X, Ye X, Ye Y, Liu B, Yang J, Yin W, Wang A, Fan G, Zhou F, Liu Z, Gu X, Xu J, Shang L, Zhang Y, Cao L, Guo T, Wan Y, Qin H, Jiang Y, Jaki T, Hayden FG, Horby PW, Cao B, Wang C. Remdesivir in adults with severe COVID-19: a randomised, double-blind, placebo-controlled, multicentre trial. Lancet. 2020;395(10236):1569-78. Epub 20200429. doi: 10.1016/S0140-6736(20)31022-9. PubMed PMID: 32423584; PMCID: PMC7190303.

260. Goldman JD, Lye DCB, Hui DS, Marks KM, Bruno R, Montejano R, Spinner CD, Galli M, Ahn MY, Nahass RG, Chen YS, SenGupta D, Hyland RH, Osinusi AO, Cao H, Blair C, Wei X, Gaggar A, Brainard DM, Towner WJ, Munoz J, Mullane KM, Marty FM, Tashima KT, Diaz G, Subramanian A, Investigators G-U-. Remdesivir for 5 or 10 Days in Patients with Severe Covid-19. N Engl J Med. 2020;383(19):1827-37. Epub 20200527. doi: 10.1056/NEJMoa2015301. PubMed PMID: 32459919; PMCID: PMC7377062.

261. Consortium WHOST. Remdesivir and three other drugs for hospitalised patients with COVID-19: final results of the WHO Solidarity randomised trial and updated meta-analyses. Lancet. 2022;399(10339):1941-53. Epub 20220502. doi: 10.1016/S0140-6736(22)00519-0. PubMed PMID: 35512728; PMCID: PMC9060606.

262. Gilead Sciences I. WHO Expands Recommendation for Veklury® (Remdesivir) to Patients With Severe Disease in Latest Update to COVID-19 Guideline2022.

263. Gottlieb RL, Vaca CE, Paredes R, Mera J, Webb BJ, Perez G, Oguchi G, Ryan P, Nielsen BU, Brown M, Hidalgo A, Sachdeva Y, Mittal S, Osiyemi O, Skarbinski J, Juneja K, Hyland RH, Osinusi A, Chen S, Camus G, Abdelghany M, Davies S, Behenna-Renton N, Duff F, Marty FM, Katz MJ, Ginde AA, Brown SM, Schiffer JT, Hill JA, Investigators G-U-. Early Remdesivir to Prevent Progression to Severe Covid-19 in Outpatients. N Engl J Med. 2022;386(4):305-15. Epub 20211222. doi: 10.1056/NEJMoa2116846. PubMed PMID: 34937145; PMCID: PMC8757570.

264. Who. Therapeutics and COVID-19: living guideline 2022. Available from: https://apps.who.int/iris/bitstream/handle/10665/359774/WHO-2019-nCoV-therapeutics-2022.4-eng.pdf.

265. FDA U. FDA Approves First Oral Antiviral for Treatment of COVID-19 in Adults | FDA2023.

266. Pillaiyar T, Manickam M, Namasivayam V, Hayashi Y, Jung SH. An Overview of Severe Acute Respiratory Syndrome-Coronavirus (SARS-CoV) 3CL Protease Inhibitors: Peptidomimetics and Small Molecule Chemotherapy. J Med Chem. 2016;59(14):6595-628. Epub 20160229. doi: 10.1021/acs.jmedchem.5b01461. PubMed PMID: 26878082; PMCID: PMC7075650.

267. Loos NHC, Beijnen JH, Schinkel AH. The Mechanism-Based Inactivation of CYP3A4 by Ritonavir: What Mechanism? Int J Mol Sci. 2022;23(17). Epub 20220830. doi: 10.3390/ijms23179866. PubMed PMID: 36077262; PMCID: PMC9456214.

268. Owen DR, Allerton CMN, Anderson AS, Aschenbrenner L, Avery M, Berritt S, Boras B, Cardin RD, Carlo A, Coffman KJ, Dantonio A, Di L, Eng H, Ferre R, Gajiwala KS, Gibson SA, Greasley SE, Hurst BL, Kadar EP, Kalgutkar AS, Lee JC, Lee J, Liu W, Mason SW, Noell S, Novak JJ, Obach RS, Ogilvie K, Patel NC, Pettersson M, Rai DK, Reese MR, Sammons MF, Sathish JG, Singh RSP, Steppan CM, Stewart AE, Tuttle JB, Updyke L, Verhoest PR, Wei L, Yang Q, Zhu Y. An oral SARS-CoV-2 M(pro) inhibitor clinical candidate for the treatment of COVID-19. Science. 2021;374(6575):1586-93. Epub 20211102. doi: 10.1126/science.abl4784. PubMed PMID: 34726479.

269. Hammond J, Leister-Tebbe H, Gardner A, Abreu P, Bao W, Wisemandle W, Baniecki M, Hendrick VM, Damle B, Simon-Campos A, Pypstra R, Rusnak JM, Investigators E-H. Oral Nirmatrelvir for High-Risk, Nonhospitalized Adults with Covid-19. N Engl J Med. 2022;386(15):1397-408. Epub 20220216. doi: 10.1056/NEJMoa2118542. PubMed PMID: 35172054; PMCID: PMC8908851.

270. Ganatra S, Dani SS, Ahmad J, Kumar A, Shah J, Abraham GM, McQuillen DP, Wachter RM, Sax PE. Oral Nirmatrelvir and Ritonavir in Nonhospitalized Vaccinated Patients With Coronavirus Disease 2019. Clin Infect Dis. 2023;76(4):563-72. doi: 10.1093/cid/ciac673. PubMed PMID: 35986628; PMCID: PMC9452095.

271. Toots M, Yoon JJ, Cox RM, Hart M, Sticher ZM, Makhsous N, Plesker R, Barrena AH, Reddy PG, Mitchell DG, Shean RC, Bluemling GR, Kolykhalov AA, Greninger AL, Natchus MG, Painter GR, Plemper RK. Characterization of orally efficacious influenza drug with high resistance barrier in ferrets and human airway epithelia. Sci Transl Med. 2019;11(515). doi: 10.1126/scitranslmed.aax5866. PubMed PMID: 31645453; PMCID: PMC6848974.

272. Reynard O, Nguyen XN, Alazard-Dany N, Barateau V, Cimarelli A, Volchkov VE. Identification of a New Ribonucleoside Inhibitor of Ebola Virus Replication. Viruses. 2015;7(12):6233-40. Epub 20151201. doi: 10.3390/v7122934. PubMed PMID: 26633464; PMCID: PMC4690858.

273. Urakova N, Kuznetsova V, Crossman DK, Sokratian A, Guthrie DB, Kolykhalov AA, Lockwood MA, Natchus MG, Crowley MR, Painter GR, Frolova EI, Frolov I. beta-d-N(4)-Hydroxycytidine Is a Potent Anti-alphavirus Compound That Induces a High Level of Mutations in the Viral Genome. J Virol. 2018;92(3). Epub 20180117. doi: 10.1128/JVI.01965-17. PubMed PMID: 29167335; PMCID: PMC5774879.

274. Sheahan TP, Sims AC, Zhou S, Graham RL, Pruijssers AJ, Agostini ML, Leist SR, Schafer A, Dinnon KH, 3rd, Stevens LJ, Chappell JD, Lu X, Hughes TM, George AS, Hill CS, Montgomery SA, Brown AJ, Bluemling GR, Natchus MG, Saindane M, Kolykhalov AA, Painter G, Harcourt J, Tamin A, Thornburg NJ, Swanstrom R, Denison MR, Baric RS. An orally bioavailable broad-spectrum antiviral inhibits SARS-CoV-2 in human airway epithelial cell cultures and multiple coronaviruses in mice. Sci Transl Med. 2020;12(541). Epub 20200406. doi: 10.1126/scitranslmed.abb5883. PubMed PMID: 32253226; PMCID: PMC7164393.

275. Jayk Bernal A, Gomes da Silva MM, Musungaie DB, Kovalchuk E, Gonzalez A, Delos Reyes V, Martin-Quiros A, Caraco Y, Williams-Diaz A, Brown ML, Du J, Pedley A, Assaid C, Strizki J, Grobler JA, Shamsuddin HH, Tipping R, Wan H, Paschke A, Butterton JR, Johnson MG, De Anda C, Group MO-OS. Molnupiravir for Oral Treatment of Covid-19 in Nonhospitalized Patients. N Engl J Med. 2022;386(6):509-20. Epub 20211216. doi: 10.1056/NEJMoa2116044. PubMed PMID: 34914868; PMCID: PMC8693688.

276. FDA U. Coronavirus (COVID-19) Update: FDA Authorizes Additional Oral Antiviral for Treatment of COVID-19 in Certain Adults | FDA2021.

277. Asmana Ningrum R. Human interferon alpha-2b: a therapeutic protein for cancer treatment. Scientifica (Cairo). 2014;2014:970315. Epub 20140310. doi: 10.1155/2014/970315. PubMed PMID: 24741445; PMCID: PMC3967813.

278. Gisslinger H, Klade C, Georgiev P, Krochmalczyk D, Gercheva-Kyuchukova L, Egyed M, Rossiev V, Dulicek P, Illes A, Pylypenko H, Sivcheva L, Mayer J, Yablokova V, Krejcy K, Grohmann-Izay B, Hasselbalch HC, Kralovics R, Kiladjian JJ, Group P-PS. Ropeginterferon alfa-2b versus standard therapy for polycythaemia vera (PROUD-PV and CONTINUATION-PV): a randomised, non-inferiority, phase 3 trial and its extension

study. Lancet Haematol. 2020;7(3):e196-e208. Epub 20200131. doi: 10.1016/S2352-3026(19)30236-4. PubMed PMID: 32014125.

279. Gisslinger H, Zagrijtschuk O, Buxhofer-Ausch V, Thaler J, Schloegl E, Gastl GA, Wolf D, Kralovics R, Gisslinger B, Strecker K, Egle A, Melchardt T, Burgstaller S, Willenbacher E, Schalling M, Them NC, Kadlecova P, Klade C, Greil R. Ropeginterferon alfa-2b, a novel IFNalpha-2b, induces high response rates with low toxicity in patients with polycythemia vera. Blood. 2015;126(15):1762-9. Epub 20150810. doi: 10.1182/blood-2015-04-637280. PubMed PMID: 26261238; PMCID: PMC4608390.

280. Filipi M, Jack S. Interferons in the Treatment of Multiple Sclerosis: A Clinical Efficacy, Safety, and Tolerability Update. Int J MS Care. 2020;22(4):165-72. Epub 20191030. doi: 10.7224/1537-2073.2018-063. PubMed PMID: 32863784; PMCID: PMC7446632.

281. Mesic A, Jackson EK, Lalika M, Koelle DM, Patel RC. Interferon-based agents for current and future viral respiratory infections: A scoping literature review of human studies. PLOS Glob Public Health. 2022;2(4):e0000231. Epub 20220406. doi: 10.1371/journal.pgph.0000231. PubMed PMID: 36962150; PMCID: PMC10022196.

282. Chen F, Chan KH, Jiang Y, Kao RY, Lu HT, Fan KW, Cheng VC, Tsui WH, Hung IF, Lee TS, Guan Y, Peiris JS, Yuen KY. In vitro susceptibility of 10 clinical isolates of SARS coronavirus to selected antiviral compounds. J Clin Virol. 2004;31(1):69-75. doi: 10.1016/j.jcv.2004.03.003. PubMed PMID: 15288617; PMCID: PMC7128415.

283. Morgenstern B, Michaelis M, Baer PC, Doerr HW, Cinatl J, Jr. Ribavirin and interferon-beta synergistically inhibit SARS-associated coronavirus replication in animal and human cell lines. Biochem Biophys Res Commun. 2005;326(4):905-8. doi: 10.1016/j.bbrc.2004.11.128. PubMed PMID: 15607755; PMCID: PMC7092851.

284. Stroher U, DiCaro A, Li Y, Strong JE, Aoki F, Plummer F, Jones SM, Feldmann H. Severe acute respiratory syndrome-related coronavirus is inhibited by interferon- alpha. J Infect Dis. 2004;189(7):1164-7. Epub 20040312. doi: 10.1086/382597. PubMed PMID: 15031783; PMCID: PMC7109643.

285. Tan EL, Ooi EE, Lin CY, Tan HC, Ling AE, Lim B, Stanton LW. Inhibition of SARS coronavirus infection in vitro with clinically approved antiviral drugs. Emerg Infect Dis. 2004;10(4):581-6. doi: 10.3201/eid1004.030458. PubMed PMID: 15200845; PMCID: PMC3323075.

286. Cinatl J, Morgenstern B, Bauer G, Chandra P, Rabenau H, Doerr HW. Treatment of SARS with human interferons. Lancet. 2003;362(9380):293-4. doi: 10.1016/s0140-6736(03)13973-6. PubMed PMID: 12892961; PMCID: PMC7112413.

287. Cinatl J, Morgenstern B, Bauer G, Chandra P, Rabenau H, Doerr HW. Glycyrrhizin, an active component of liquorice roots, and replication of SARS-associated coronavirus. Lancet. 2003;361(9374):2045-6. doi: 10.1016/s0140-6736(03)13615-x. PubMed PMID: 12814717; PMCID: PMC7112442.

288. Scagnolari C, Vicenzi E, Bellomi F, Stillitano MG, Pinna D, Poli G, Clementi M, Dianzani F, Antonelli G. Increased sensitivity of SARS-coronavirus to a combination of human type I and type II interferons. Antivir Ther. 2004;9(6):1003-11. PubMed PMID: 15651759.

289. Spiegel M, Pichlmair A, Muhlberger E, Haller O, Weber F. The antiviral effect of interferon-beta against SARS-coronavirus is not mediated by MxA protein. J Clin Virol. 2004;30(3):211-3. doi: 10.1016/j.jcv.2003.11.013. PubMed PMID: 15135736; PMCID: PMC7128634.

290. Zheng B, He ML, Wong KL, Lum CT, Poon LL, Peng Y, Guan Y, Lin MC, Kung HF. Potent inhibition of SARS-associated coronavirus (SCOV) infection and replication by type I interferons (IFN-alpha/beta) but not by type II interferon (IFN-gamma). J Interferon Cytokine Res. 2004;24(7):388-90. doi: 10.1089/1079990041535610. PubMed PMID: 15296649.

291. Hensley LE, Fritz LE, Jahrling PB, Karp CL, Huggins JW, Geisbert TW. Interferon-beta 1a and SARS coronavirus replication. Emerg Infect Dis. 2004;10(2):317-9. doi: 10.3201/eid1002.030482. PubMed PMID: 15030704; PMCID: PMC3322919.

292. Sainz B, Jr., Mossel EC, Peters CJ, Garry RF. Interferon-beta and interferon-gamma synergistically inhibit the replication of severe acute respiratory syndrome-associated coronavirus (SARS-CoV). Virology. 2004;329(1):11-7. doi: 10.1016/j.virol.2004.08.011. PubMed PMID: 15476870; PMCID: PMC7111895.

293. Falzarano D, de Wit E, Martellaro C, Callison J, Munster VJ, Feldmann H. Inhibition of novel beta coronavirus replication by a combination of interferon-alpha2b and ribavirin. Sci Rep. 2013;3:1686. doi: 10.1038/srep01686. PubMed PMID: 23594967; PMCID: PMC3629412.

294. Hart BJ, Dyall J, Postnikova E, Zhou H, Kindrachuk J, Johnson RF, Olinger GG, Frieman MB, Holbrook MR, Jahrling PB, Hensley L. Interferon-beta and mycophenolic acid are potent inhibitors of Middle East respiratory syndrome coronavirus in cell-based assays. J Gen Virol. 2014;95(Pt 3):571-7. Epub 20131209. doi: 10.1099/vir.0.061911-0. PubMed PMID: 24323636; PMCID: PMC3929173.

295. Haagmans BL, Kuiken T, Martina BE, Fouchier RA, Rimmelzwaan GF, van Amerongen G, van Riel D, de Jong T, Itamura S, Chan KH, Tashiro M, Osterhaus AD. Pegylated interferon-alpha protects type 1 pneumocytes against SARS coronavirus infection in macaques. Nat Med. 2004;10(3):290-3. Epub 20040222. doi: 10.1038/nm1001. PubMed PMID: 14981511; PMCID: PMC7095986.

296. Chan JF, Yao Y, Yeung ML, Deng W, Bao L, Jia L, Li F, Xiao C, Gao H, Yu P, Cai JP, Chu H, Zhou J, Chen H, Qin C, Yuen KY. Treatment With Lopinavir/Ritonavir or Interferon-beta1b Improves Outcome of MERS-CoV Infection in a Nonhuman Primate Model of Common Marmoset. J Infect Dis. 2015;212(12):1904-13. Epub 20150721. doi: 10.1093/infdis/jiv392. PubMed PMID: 26198719; PMCID: PMC7107395.

297. Loutfy MR, Blatt LM, Siminovitch KA, Ward S, Wolff B, Lho H, Pham DH, Deif H, LaMere EA, Chang M, Kain KC, Farcas GA, Ferguson P, Latchford M, Levy G, Dennis JW, Lai EK, Fish EN. Interferon alfacon-1 plus corticosteroids in severe acute respiratory syndrome: a preliminary study. JAMA. 2003;290(24):3222-8. doi: 10.1001/jama.290.24.3222. PubMed PMID: 14693875.

298. Zhao Z, Zhang F, Xu M, Huang K, Zhong W, Cai W, Yin Z, Huang S, Deng Z, Wei M, Xiong J, Hawkey PM. Description and clinical treatment of an early outbreak of severe acute respiratory syndrome (SARS) in Guangzhou, PR China. J Med Microbiol. 2003;52(Pt 8):715-20. doi: 10.1099/jmm.0.05320-0. PubMed PMID: 12867568.

299. Stockman LJ, Bellamy R, Garner P. SARS: systematic review of treatment effects. PLoS Med. 2006;3(9):e343. doi: 10.1371/journal.pmed.0030343. PubMed PMID: 16968120; PMCID: PMC1564166.

300. Saleki K, Yaribash S, Banazadeh M, Hajihosseinlou E, Gouravani M, Saghazadeh A, Rezaei N. Interferon therapy in patients with SARS, MERS, and COVID-19: A systematic review and meta-analysis of clinical studies. Eur J Pharmacol. 2021;906:174248. Epub 20210612. doi: 10.1016/j.ejphar.2021.174248. PubMed PMID: 34126092; PMCID: PMC8195694.

301. Morra ME, Van Thanh L, Kamel MG, Ghazy AA, Altibi AMA, Dat LM, Thy TNX, Vuong NL, Mostafa MR, Ahmed SI, Elabd SS, Fathima S, Le Huy Vu T, Omrani AS, Memish ZA, Hirayama K, Huy NT. Clinical outcomes of current medical approaches for Middle East respiratory syndrome: A systematic review and meta-analysis. Rev Med Virol. 2018;28(3):e1977. Epub 20180417. doi: 10.1002/rmv.1977. PubMed PMID: 29664167; PMCID: PMC7169085.

302. Momattin H, Al-Ali AY, Al-Tawfiq JA. A Systematic Review of therapeutic agents for the treatment of the Middle East Respiratory Syndrome Coronavirus (MERS-CoV). Travel Med Infect Dis. 2019;30:9-18. Epub 20190625. doi: 10.1016/j.tmaid.2019.06.012. PubMed PMID: 31252170; PMCID: PMC7110863.

303. Arabi YM, Asiri AY, Assiri AM, Balkhy HH, Al Bshabshe A, Al Jeraisy M, Mandourah Y, Azzam MHA, Bin Eshaq AM, Al Johani S, Al Harbi S, Jokhdar HAA, Deeb AM, Memish ZA, Jose J, Ghazal S, Al Faraj S, Al Mekhlafi GA, Sherbeeni NM, Elzein FE, Al-Hameed F, Al Saedi A, Alharbi NK, Fowler RA, Hayden FG, Al-Dawood A, Abdelzaher M, Bajhmom W, AlMutairi BM, Hussein MA, Alothman A, Saudi Critical Care Trials G. Interferon Beta-1b and Lopinavir-Ritonavir for Middle East Respiratory Syndrome. N Engl J Med. 2020;383(17):1645-56. Epub 20201007. doi: 10.1056/NEJMoa2015294. PubMed PMID: 33026741.

304. Ader F, Peiffer-Smadja N, Poissy J, Bouscambert-Duchamp M, Belhadi D, Diallo A, Delmas C, Saillard J, Dechanet A, Mercier N, Dupont A, Alfaiate T, Lescure FX, Raffi F, Goehringer F, Kimmoun A, Jaureguiberry S, Reignier J, Nseir S, Danion F, Clere-Jehl R, Bouiller K, Navellou JC, Tolsma V, Cabie A, Dubost C, Courjon J, Leroy S, Mootien J, Gaci R, Mourvillier B, Faure E, Pourcher V, Gallien S, Launay O, Lacombe K, Lanoix JP,

Makinson A, Martin-Blondel G, Bouadma L, Botelho-Nevers E, Gagneux-Brunon A, Epaulard O, Piroth L, Wallet F, Richard JC, Reuter J, Staub T, Lina B, Noret M, Andrejak C, Le MP, Peytavin G, Hites M, Costagliola D, Yazdanpanah Y, Burdet C, Mentre F, DisCoVeRy study g. An open-label randomized controlled trial of the effect of lopinavir/ritonavir, lopinavir/ritonavir plus IFN-beta-1a and hydroxychloroquine in hospitalized patients with COVID-19. Clin Microbiol Infect. 2021;27(12):1826-37. Epub 20210526. doi: 10.1016/j.cmi.2021.05.020. PubMed PMID: 34048876; PMCID: PMC8149166.

305. Kalil AC, Mehta AK, Patterson TF, Erdmann N, Gomez CA, Jain MK, Wolfe CR, Ruiz-Palacios GM, Kline S, Regalado Pineda J, Luetkemeyer AF, Harkins MS, Jackson PEH, Iovine NM, Tapson VF, Oh MD, Whitaker JA, Mularski RA, Paules CI, Ince D, Takasaki J, Sweeney DA, Sandkovsky U, Wyles DL, Hohmann E, Grimes KA, Grossberg R, Laguio-Vila M, Lambert AA, Lopez de Castilla D, Kim E, Larson L, Wan CR, Traenkner JJ, Ponce PO, Patterson JE, Goepfert PA, Sofarelli TA, Mocherla S, Ko ER, Ponce de Leon A, Doernberg SB, Atmar RL, Maves RC, Dangond F, Ferreira J, Green M, Makowski M, Bonnett T, Beresnev T, Ghazaryan V, Dempsey W, Nayak SU, Dodd L, Tomashek KM, Beigel JH. Efficacy of interferon beta-1a plus remdesivir compared with remdesivir alone in hospitalised adults with COVID-19: a double-bind, randomised, placebo-controlled, phase 3 trial. Lancet Respir Med. 2021;9(12):1365-76. Epub 20211018. doi: 10.1016/s2213-2600(21)00384-2. PubMed PMID: 34672949; PMCID: PMC8523116.

306. Hung IF, Lung KC, Tso EY, Liu R, Chung TW, Chu MY, Ng YY, Lo J, Chan J, Tam AR, Shum HP, Chan V, Wu AK, Sin KM, Leung WS, Law WL, Lung DC, Sin S, Yeung P, Yip CC, Zhang RR, Fung AY, Yan EY, Leung KH, Ip JD, Chu AW, Chan WM, Ng AC, Lee R, Fung K, Yeung A, Wu TC, Chan JW, Yan WW, Chan WM, Chan JF, Lie AK, Tsang OT, Cheng VC, Que TL, Lau CS, Chan KH, To KK, Yuen KY. Triple combination of interferon beta-1b, lopinavir-ritonavir, and ribavirin in the treatment of patients admitted to hospital with COVID-19: an open-label, randomised, phase 2 trial. Lancet. 2020;395(10238):1695-704. Epub 20200510. doi: 10.1016/S0140-6736(20)31042-4. PubMed PMID: 32401715; PMCID: PMC7211500.

307. Davoudi-Monfared E, Rahmani H, Khalili H, Hajiabdolbaghi M, Salehi M, Abbasian L, Kazemzadeh H, Yekaninejad MS. A Randomized Clinical Trial of the Efficacy and Safety of Interferon beta-1a in Treatment of Severe COVID-19. Antimicrob Agents Chemother. 2020;64(9). Epub 20200820. doi: 10.1128/AAC.01061-20. PubMed PMID: 32661006; PMCID: PMC7449227.

308. Rahmani H, Davoudi-Monfared E, Nourian A, Khalili H, Hajizadeh N, Jalalabadi NZ, Fazeli MR, Ghazaeian M, Yekaninejad MS. Interferon beta-1b in treatment of severe COVID-19: A randomized clinical trial. Int Immunopharmacol. 2020;88:106903. Epub 20200824. doi: 10.1016/j.intimp.2020.106903. PubMed PMID: 32862111; PMCID: PMC7445008.

309. Bhushan BLS, Wanve S, Koradia P, Bhomia V, Soni P, Chakraborty S, Khobragade A, Joshi S, Mendiratta SK, Kansagra KK, Parihar A, Sharma S, Patel J. Efficacy and safety of pegylated interferon-α2b in moderate COVID-19: a phase 3,

randomized, comparator-controlled, open-label study. Int J Infect Dis. 2021;111:281-7. Epub 20210821. doi: 10.1016/j.ijid.2021.08.044. PubMed PMID: 34428542; PMCID: PMC8379820.

310. Vanderheiden A, Ralfs P, Chirkova T, Upadhyay AA, Zimmerman MG, Bedoya S, Aoued H, Tharp GM, Pellegrini KL, Manfredi C, Sorscher E, Mainou B, Lobby JL, Kohlmeier JE, Lowen AC, Shi PY, Menachery VD, Anderson LJ, Grakoui A, Bosinger SE, Suthar MS. Type I and Type III Interferons Restrict SARS-CoV-2 Infection of Human Airway Epithelial Cultures. J Virol. 2020;94(19). Epub 20200915. doi: 10.1128/jvi.00985-20. PubMed PMID: 32699094; PMCID: PMC7495371.

311. Dinnon KH, 3rd, Leist SR, Schäfer A, Edwards CE, Martinez DR, Montgomery SA, West A, Yount BL, Jr., Hou YJ, Adams LE, Gully KL, Brown AJ, Huang E, Bryant MD, Choong IC, Glenn JS, Gralinski LE, Sheahan TP, Baric RS. A mouse-adapted model of SARS-CoV-2 to test COVID-19 countermeasures. Nature. 2020;586(7830):560-6. Epub 20200827. doi: 10.1038/s41586-020-2708-8. PubMed PMID: 32854108; PMCID: PMC8034761.

312. Feld JJ, Kandel C, Biondi MJ, Kozak RA, Zahoor MA, Lemieux C, Borgia SM, Boggild AK, Powis J, McCready J, Tan DHS, Chan T, Coburn B, Kumar D, Humar A, Chan A, O'Neil B, Noureldin S, Booth J, Hong R, Smookler D, Aleyadeh W, Patel A, Barber B, Casey J, Hiebert R, Mistry H, Choong I, Hislop C, Santer DM, Lorne Tyrrell D, Glenn JS, Gehring AJ, Janssen HLA, Hansen BE. Peginterferon lambda for the treatment of outpatients with COVID-19: a phase 2, placebo-controlled randomised trial. Lancet Respir Med. 2021;9(5):498-510. Epub 20210205. doi: 10.1016/S2213-2600(20)30566-X. PubMed PMID: 33556319; PMCID: PMC7906707.

313. Jagannathan P, Andrews JR, Bonilla H, Hedlin H, Jacobson KB, Balasubramanian V, Purington N, Kamble S, de Vries CR, Quintero O, Feng K, Ley C, Winslow D, Newberry J, Edwards K, Hislop C, Choong I, Maldonado Y, Glenn J, Bhatt A, Blish C, Wang T, Khosla C, Pinsky BA, Desai M, Parsonnet J, Singh U. Peginterferon Lambda-1a for treatment of outpatients with uncomplicated COVID-19: a randomized placebo-controlled trial. Nat Commun. 2021;12(1):1967. Epub 20210330. doi: 10.1038/s41467-021-22177-1. PubMed PMID: 33785743; PMCID: PMC8009873.

314. Wang H, Liu Q, Hu J, Zhou M, Yu MQ, Li KY, Xu D, Xiao Y, Yang JY, Lu YJ, Wang F, Yin P, Xu SY. Nasopharyngeal Swabs Are More Sensitive Than Oropharyngeal Swabs for COVID-19 Diagnosis and Monitoring the SARS-CoV-2 Load. Front Med (Lausanne). 2020;7:334. Epub 20200618. doi: 10.3389/fmed.2020.00334. PubMed PMID: 32626720; PMCID: PMC7314917.

315. Reis G, Moreira Silva EAS, Medeiros Silva DC, Thabane L, Campos VHS, Ferreira TS, Santos CVQ, Nogueira AMR, Almeida A, Savassi LCM, Figueiredo-Neto AD, Dias ACF, Freire Junior AM, Bitaraes C, Milagres AC, Callegari ED, Simplicio MIC, Ribeiro LB, Oliveira R, Harari O, Wilson LA, Forrest JI, Ruton H, Sprague S, McKay P, Guo CM, Limbrick-Oldfield EH, Kanters S, Guyatt GH, Rayner CR, Kandel C, Biondi MJ, Kozak R, Hansen B, Zahoor MA, Arora P, Hislop C, Choong I, Feld JJ, Mills EJ, Glenn JS,

Investigators T. Early Treatment with Pegylated Interferon Lambda for Covid-19. N Engl J Med. 2023;388(6):518-28. doi: 10.1056/NEJMoa2209760. PubMed PMID: 36780676; PMCID: PMC9933926.

316. CDC. End of the Federal COVID-19 Public Health Emergency (PHE) Declaration | CDC 2023 [updated 2023-07-13T12:49:48Z]. Available from: https://www.cdc.gov/coronavirus/2019-ncov/your-health/end-of-phe.html.

317. Baden LR, Sahly HME, Essink B, Kotloff K, Frey S, Novak R, Diemert D, Spector SA, Rouphael N, Creech CB, McGettigan J, Kehtan S, Segall N, Solis J, Brosz A, Fierro C, Schwartz H, Neuzil K, Corey L, Gilbert P, Janes H, Follmann D, Marovich M, Mascola J, Polakowski L, Ledgerwood J, Graham BS, Bennett H, Pajon R, Knightly C, Leav B, Deng W, Zhou H, Han S, Ivarsson M, Miller J, Zaks T. Efficacy and Safety of the mRNA-1273 SARS-CoV-2 Vaccine. New Engl J Med. 2020. doi: 10.1056/nejmoa2035389.

318. Mulligan MJ, Lyke KE, Kitchin N, Absalon J, Gurtman A, Lockhart S, Neuzil K, Raabe V, Bailey R, Swanson KA, Li P, Koury K, Kalina W, Cooper D, Fontes-Garfias C, Shi PY, Türeci Ö, Tompkins KR, Walsh EE, Frenck R, Falsey AR, Dormitzer PR, Gruber WC, Şahin U, Jansen KU. Phase I/II study of COVID-19 RNA vaccine BNT162b1 in adults. Nature. 2020;586(7830):589-93. Epub 2020/08/14. doi: 10.1038/s41586-020-2639-4. PubMed PMID: 32785213.

319. Polack FP, Thomas SJ, Kitchin N, Absalon J, Gurtman A, Lockhart S, Perez JL, Pérez Marc G, Moreira ED, Zerbini C, Bailey R, Swanson KA, Roychoudhury S, Koury K, Li P, Kalina WV, Cooper D, Frenck RW, Jr., Hammitt LL, Türeci Ö, Nell H, Schaefer A, Ünal S, Tresnan DB, Mather S, Dormitzer PR, Şahin U, Jansen KU, Gruber WC. Safety and Efficacy of the BNT162b2 mRNA Covid-19 Vaccine. N Engl J Med. 2020;383(27):2603-15. Epub 2020/12/11. doi: 10.1056/NEJMoa2034577. PubMed PMID: 33301246; PMCID: PMC7745181.

320. Carvalho T, Krammer F, Iwasaki A. The first 12 months of COVID-19: a timeline of immunological insights. Nat Rev Immunol. 2021;21(4):245-56. Epub 2021/03/17. doi: 10.1038/s41577-021-00522-1. PubMed PMID: 33723416; PMCID: PMC7958099 to SARS-CoV-2 serological assays and NDV-based SARS-CoV-2 vaccines, naming F.K. as co-inventor. The authors would also like to note the following, which could be perceived as a conflict of interest for F.K.: he has previously published work on influenza virus vaccines with S. Gilbert (University of Oxford), has consulted for Curevac, Merck and Pfizer (before 2020), is currently consulting for Avimex (Mexico) and Seqirus (Australia), his laboratory is collaborating with Pfizer on animal models of SARS-CoV-2, his laboratory is collaborating with N. Pardi at the University of Pennsylvania on mRNA vaccines against SARS-CoV-2, his laboratory was working in the past with GlaxoSmithKline on the development of influenza virus vaccines, and two of his mentees have recently joined Moderna. A.I. served as a consultant for Adaptive Biotechnologies. T.C. declares no competing interests.

321. Wichmann D, Sperhake JP, Lütgehetmann M, Steurer S, Edler C, Heinemann A, Heinrich F, Mushumba H, Kniep I, Schröder AS, Burdelski C, de Heer G, Nierhaus A,

Frings D, Pfefferle S, Becker H, Bredereke-Wiedling H, de Weerth A, Paschen HR, Sheikhzadeh-Eggers S, Stang A, Schmiedel S, Bokemeyer C, Addo MM, Aepfelbacher M, Püschel K, Kluge S. Autopsy Findings and Venous Thromboembolism in Patients With COVID-19: A Prospective Cohort Study. Ann Intern Med. 2020;173(4):268-77. Epub 2020/05/07. doi: 10.7326/m20-2003. PubMed PMID: 32374815; PMCID: PMC7240772.

322. Silvin A, Chapuis N, Dunsmore G, Goubet A-G, Dubuisson A, Derosa L, Almire C, Hénon C, Kosmider O, Droin N, Rameau P, Catelain C, Alfaro A, Dussiau C, Friedrich C, Sourdeau E, Marin N, Szwebel T-A, Cantin D, Mouthon L, Borderie D, Deloger M, Bredel D, Mouraud S, Drubay D, Andrieu M, Lhonneur A-S, Saada V, Stoclin A, Willekens C, Pommeret F, Griscelli F, Ng LG, Zhang Z, Bost P, Amit I, Barlesi F, Marabelle A, Pène F, Gachot B, André F, Zitvogel L, Ginhoux F, Fontenay M, Solary E. Elevated calprotectin and abnormal myeloid cell subsets discriminate severe from mild COVID-19. Cell. 2020. doi: 10.1016/j.cell.2020.08.002.

323. Moore JB, June CH. Cytokine release syndrome in severe COVID-19. Science. 2020;368(6490):473-4. Epub 2020/04/19. doi: 10.1126/science.abb8925. PubMed PMID: 32303591.

324. Muñoz-Fontela C, Dowling WE, Funnell SGP, Gsell PS, Riveros-Balta AX, Albrecht RA, Andersen H, Baric RS, Carroll MW, Cavaleri M, Qin C, Crozier I, Dallmeier K, de Waal L, de Wit E, Delang L, Dohm E, Duprex WP, Falzarano D, Finch CL, Frieman MB, Graham BS, Gralinski LE, Guilfoyle K, Haagmans BL, Hamilton GA, Hartman AL, Herfst S, Kaptein SJF, Klimstra WB, Knezevic I, Krause PR, Kuhn JH, Le Grand R, Lewis MG, Liu WC, Maisonnasse P, McElroy AK, Munster V, Oreshkova N, Rasmussen AL, Rocha-Pereira J, Rockx B, Rodríguez E, Rogers TF, Salguero FJ, Schotsaert M, Stittelaar KJ, Thibaut HJ, Tseng CT, Vergara-Alert J, Beer M, Brasel T, Chan JFW, García-Sastre A, Neyts J, Perlman S, Reed DS, Richt JA, Roy CJ, Segalés J, Vasan SS, Henao-Restrepo AM, Barouch DH. Animal models for COVID-19. Nature. 2020;586(7830):509-15. Epub 2020/09/24. doi: 10.1038/s41586-020-2787-6. PubMed PMID: 32967005.

325. Routhu NK, Cheedarla N, Gangadhara S, Bollimpelli VS, Boddapati AK, Shiferaw A, Rahman SA, Sahoo A, Edara V, Lai L, Floyd K, Wang S, Fischinger S, Atyeo C, Shin SA, Gumber S, Kirejczyk S, Cohen J, Jean SM, Wood JS, Connor-Stroud F, Stammen RL, Upadhyay AA, Pellegrini K, Montefiori D, Shi P-Y, Menachery VD, Alter G, Vanderford TH, Bosinger SE, Suthar MS, Amara RR. Modified Vaccinia Ankara Vector-Based Vaccine Protects Macaques from SARS-CoV-2 Infection, Immune Pathology and Dysfunction in the Lung. Immunity. 2021. doi: 10.1016/j.immuni.2021.02.001.

326. Williamson BN, Feldmann F, Schwarz B, Meade-White K, Porter DP, Schulz J, Doremalen Nv, Leighton I, Yinda CK, Pérez-Pérez L, Okumura A, Lovaglio J, Hanley PW, Saturday G, Bosio CM, Anzick S, Barbian K, Cihlar T, Martens C, Scott DP, Munster VJ, Wit Ed. Clinical benefit of remdesivir in rhesus macaques infected with SARS-CoV-2. Nature. 2020;585(7824):273-6. doi: 10.1038/s41586-020-2423-5 PMID - 32516797.

327. Singh DK, Singh B, Ganatra SR, Gazi M, Cole J, Thippeshappa R, Alfson KJ, Clemmons E, Gonzalez O, Escobedo R, Lee T-H, Chatterjee A, Goez-Gazi Y, Sharan R,

Gough M, Alvarez C, Blakley A, Ferdin J, Bartley C, Staples H, Parodi L, Callery J, Mannino A, Klaffke B, Escareno P, Platt RN, Hodara V, Scordo J, Gautam S, Vilanova AG, Olmo-Fontanez A, Schami A, Oyejide A, Ajithdoss DK, Copin R, Baum A, Kyratsous C, Alvarez X, Ahmed M, Rosa B, Goodroe A, Dutton J, Hall-Ursone S, Frost PA, Voges AK, Ross CN, Sayers K, Chen C, Hallam C, Khader SA, Mitreva M, Anderson TJC, Martinez-Sobrido L, Patterson JL, Turner J, Torrelles JB, Dick EJ, Brasky K, Schlesinger LS, Giavedoni LD, Carrion R, Kaushal D. Responses to acute infection with SARS-CoV-2 in the lungs of rhesus macaques, baboons and marmosets. Nat Microbiol. 2021;6(1):73-86. doi: 10.1038/s41564-020-00841-4 PMID - 33340034.

328. Fahlberg MD, Blair RV, Doyle-Meyers LA, Midkiff CC, Zenere G, Russell-Lodrigue KE, Monjure CJ, Haupt EH, Penney TP, Lehmicke G, Threeton BM, Golden N, Datta PK, Roy CJ, Bohm RP, Maness NJ, Fischer T, Rappaport J, Vaccari M. Cellular events of acute, resolving or progressive COVID-19 in SARS-CoV-2 infected non-human primates. Nat Commun. 2020;11(1):6078. doi: 10.1038/s41467-020-19967-4 PMID - 33247138.

329. Hoang TN, Viox EG, Upadhyay AA, Strongin Z, Tharp GK, Pino M, Nchioua R, Hirschenberger M, Gagne M, Nguyen K, Harper JL, Marciano S, Boddapati AK, Pellegrini KL, Tisoncik-Go J, Whitmore LS, Karunakaran KA, Roy M, Kirejczyk S, Curran EH, Wallace C, Wood JS, Connor-Stroud F, Kasturi SP, Levit RD, Gale M, Vanderford TH, Silvestri G, Busman-Sahay K, Estes JD, Vaccari M, Douek DC, Sparrer KMJ, Kirchhoff F, Johnson RP, Schreiber G, Bosinger SE, Paiardini M. Modulation of type I interferon responses potently inhibits SARS-CoV-2 replication and inflammation in rhesus macaques. bioRxiv. 2022:2022.10.21.512606. doi: 10.1101/2022.10.21.512606.

330. Schultze JL, Aschenbrenner AC. COVID-19 and the human innate immune system. Cell. 2021. doi: 10.1016/j.cell.2021.02.029.

331. Aran D, Looney AP, Liu L, Wu E, Fong V, Hsu A, Chak S, Naikawadi RP, Wolters PJ, Abate AR, Butte AJ, Bhattacharya M. Reference-based analysis of lung single-cell sequencing reveals a transitional profibrotic macrophage. Nat Immunol. 2019;20(2):163-72. Epub 20190114. doi: 10.1038/s41590-018-0276-y. PubMed PMID: 30643263; PMCID: PMC6340744.

332. Gibbings SL, Thomas SM, Atif SM, McCubbrey AL, Desch AN, Danhorn T, Leach SM, Bratton DL, Henson PM, Janssen WJ, Jakubzick CV. Three Unique Interstitial Macrophages in the Murine Lung at Steady State. Am J Respir Cell Mol Biol. 2017;57(1):66-76. Epub 2017/03/04. doi: 10.1165/rcmb.2016-0361OC. PubMed PMID: 28257233; PMCID: PMC5516280.

333. Chakarov S, Lim HY, Tan L, Lim SY, See P, Lum J, Zhang XM, Foo S, Nakamizo S, Duan K, Kong WT, Gentek R, Balachander A, Carbajo D, Bleriot C, Malleret B, Tam JKC, Baig S, Shabeer M, Toh SES, Schlitzer A, Larbi A, Marichal T, Malissen B, Chen J, Poidinger M, Kabashima K, Bajenoff M, Ng LG, Angeli V, Ginhoux F. Two distinct interstitial macrophage populations coexist across tissues in specific subtissular niches. Science. 2019;363(6432). Epub 2019/03/16. doi: 10.1126/science.aau0964. PubMed PMID: 30872492.

334. Ural BB, Yeung ST, Damani-Yokota P, Devlin JC, de Vries M, Vera-Licona P, Samji T, Sawai CM, Jang G, Perez OA, Pham Q, Maher L, Loke P, Dittmann M, Reizis B, Khanna KM. Identification of a nerve-associated, lung-resident interstitial macrophage subset with distinct localization and immunoregulatory properties. Sci Immunol. 2020;5(45). Epub 2020/03/30. doi: 10.1126/sciimmunol.aax8756. PubMed PMID: 32220976; PMCID: PMC7717505.

335. Schyns J, Bai Q, Ruscitti C, Radermecker C, De Schepper S, Chakarov S, Farnir F, Pirottin D, Ginhoux F, Boeckxstaens G, Bureau F, Marichal T. Non-classical tissue monocytes and two functionally distinct populations of interstitial macrophages populate the mouse lung. Nat Commun. 2019;10(1):3964. Epub 2019/09/05. doi: 10.1038/s41467-019-11843-0. PubMed PMID: 31481690; PMCID: PMC6722135.

336. Esaulova E, Das S, Singh DK, Choreno-Parra JA, Swain A, Arthur L, Rangel-Moreno J, Ahmed M, Singh B, Gupta A, Fernandez-Lopez LA, de la Luz Garcia-Hernandez M, Bucsan A, Moodley C, Mehra S, Garcia-Latorre E, Zuniga J, Atkinson J, Kaushal D, Artyomov MN, Khader SA. The immune landscape in tuberculosis reveals populations linked to disease and latency. Cell Host Microbe. 2021;29(2):165-78 e8. Epub 20201218. doi: 10.1016/j.chom.2020.11.013. PubMed PMID: 33340449; PMCID: PMC7878437.

337. Hao Y, Hao S, Andersen-Nissen E, Mauck WM, Zheng S, Butler A, Lee MJ, Wilk AJ, Darby C, Zagar M. Integrated analysis of multimodal single-cell data. bioRxiv. 2020.

338. Corry J, Kettenburg G, Upadhyay AA, Wallace M, Marti MM, Wonderlich ER, Bissel SJ, Goss K, Sturgeon TJ, Watkins SC, Reed DS, Bosinger SE, Barratt-Boyes SM. Infiltration of inflammatory macrophages and neutrophils and widespread pyroptosis in lung drive influenza lethality in nonhuman primates. PLoS Pathog. 2022;18(3):e1010395. Epub 2022/03/11. doi: 10.1371/journal.ppat.1010395. PubMed PMID: 35271686; PMCID: PMC8939778.

339. Cai Y, Sugimoto C, Arainga M, Alvarez X, Didier ES, Kuroda MJ. In vivo characterization of alveolar and interstitial lung macrophages in rhesus macaques: implications for understanding lung disease in humans. J Immunol. 2014;192(6):2821-9. Epub 2014/02/19. doi: 10.4049/jimmunol.1302269. PubMed PMID: 24534529; PMCID: PMC3959879.

340. Kumagai T, Fan S, Smith AM. ADAMDEC1 and its role in inflammatory disease and cancer. Metalloproteinases In Medicine. 2020;7:15-28.

341. Coillard A, Segura E. In vivo Differentiation of Human Monocytes. Front Immunol. 2019;10:1907. Epub 2019/08/29. doi: 10.3389/fimmu.2019.01907. PubMed PMID: 31456804; PMCID: PMC6700358.

342. Vanderheiden A, Thomas J, Soung AL, Davis-Gardner ME, Floyd K, Jin F, Cowan DA, Pellegrini K, Creanga A, Pegu A, Derrien-Colemyn A, Shi P-Y, Grakoui A, Klein RS, Bosinger SE, Kohlmeier JE, Menachery VD, Suthar MS. CCR2-dependent monocyte-

derived cells restrict SARS-CoV-2 infection. bioRxiv. 2021:2021.05.03.442538. doi: 10.1101/2021.05.03.442538.

343. Habermann AC, Gutierrez AJ, Bui LT, Yahn SL, Winters NI, Calvi CL, Peter L, Chung MI, Taylor CJ, Jetter C, Raju L, Roberson J, Ding G, Wood L, Sucre JMS, Richmond BW, Serezani AP, McDonnell WJ, Mallal SB, Bacchetta MJ, Loyd JE, Shaver CM, Ware LB, Bremner R, Walia R, Blackwell TS, Banovich NE, Kropski JA. Single-cell RNA sequencing reveals profibrotic roles of distinct epithelial and mesenchymal lineages in pulmonary fibrosis. Sci Adv. 2020;6(28):eaba1972. Epub 2020/08/25. doi: 10.1126/sciadv.aba1972. PubMed PMID: 32832598; PMCID: PMC7439444.

344. Morse C, Tabib T, Sembrat J, Buschur KL, Bittar HT, Valenzi E, Jiang Y, Kass DJ, Gibson K, Chen W, Mora A, Benos PV, Rojas M, Lafyatis R. Proliferating SPP1/MERTK-expressing macrophages in idiopathic pulmonary fibrosis. Eur Respir J. 2019;54(2). Epub 2019/06/22. doi: 10.1183/13993003.02441-2018. PubMed PMID: 31221805; PMCID: PMC8025672.

345. Rubin R. Baricitinib Is First Approved COVID-19 Immunomodulatory Treatment. Jama. 2022;327(23):2281. doi: 10.1001/jama.2022.9846. PubMed PMID: 35727290.

346. Bronte V, Ugel S, Tinazzi E, Vella A, Sanctis FD, Canè S, Batani V, Trovato R, Fiore A, Petrova V, Hofer F, Barouni RM, Musiu C, Caligola S, Pinton L, Torroni L, Polati E, Donadello K, Friso S, Pizzolo F, Iezzi M, Facciotti F, Pelicci PG, Righetti D, Bazzoni P, Rampudda M, Comel AC, Mosaner W, Lunardi C, Olivieri O. Baricitinib restrains the immune dysregulation in severe COVID-19 patients. J Clin Invest. 2020. doi: 10.1172/jci141772.

347. Ren X, Wen W, Fan X, Hou W, Su B, Cai P, Li J, Liu Y, Tang F, Zhang F, Yang Y, He J, Ma W, He J, Wang P, Cao Q, Chen F, Chen Y, Cheng X, Deng G, Deng X, Ding W, Feng Y, Gan R, Guo C, Guo W, He S, Jiang C, Liang J, Li YM, Lin J, Ling Y, Liu H, Liu J, Liu N, Liu SQ, Luo M, Ma Q, Song Q, Sun W, Wang G, Wang F, Wang Y, Wen X, Wu Q, Xu G, Xie X, Xiong X, Xing X, Xu H, Yin C, Yu D, Yu K, Yuan J, Zhang B, Zhang P, Zhang T, Zhao J, Zhao P, Zhou J, Zhou W, Zhong S, Zhong X, Zhang S, Zhu L, Zhu P, Zou B, Zou J, Zuo Z, Bai F, Huang X, Zhou P, Jiang Q, Huang Z, Bei JX, Wei L, Bian XW, Liu X, Cheng T, Li X, Zhao P, Wang FS, Wang H, Su B, Zhang Z, Qu K, Wang X, Chen J, Jin R, Zhang Z. COVID-19 immune features revealed by a large-scale single-cell transcriptome atlas. Cell. 2021;184(7):1895-913 e19. Epub 2021/03/04. doi: 10.1016/j.cell.2021.01.053. PubMed PMID: 33657410; PMCID: PMC7857060.

348. Liegeois M, Legrand C, Desmet CJ, Marichal T, Bureau F. The interstitial macrophage: A long-neglected piece in the puzzle of lung immunity. Cell Immunol. 2018;330:91-6. Epub 2018/02/21. doi: 10.1016/j.cellimm.2018.02.001. PubMed PMID: 29458975.

349. Hoppstädter J, Diesel B, Zarbock R, Breinig T, Monz D, Koch M, Meyerhans A, Gortner L, Lehr CM, Huwer H, Kiemer AK. Differential cell reaction upon Toll-like receptor 4 and 9 activation in human alveolar and lung interstitial macrophages. Respir Res.

2010;11(1):124. Epub 2010/09/17. doi: 10.1186/1465-9921-11-124. PubMed PMID: 20843333; PMCID: PMC2949727.

350. Blanco-Melo D, Nilsson-Payant BE, Liu WC, Uhl S, Hoagland D, Moller R, Jordan TX, Oishi K, Panis M, Sachs D, Wang TT, Schwartz RE, Lim JK, Albrecht RA, tenOever BR. Imbalanced Host Response to SARS-CoV-2 Drives Development of COVID-19. Cell. 2020;181(5):1036-45 e9. Epub 2020/05/18. doi: 10.1016/j.cell.2020.04.026. PubMed PMID: 32416070; PMCID: PMC7227586.

351. Asano T, Boisson B, Onodi F, Matuozzo D, Moncada-Velez M, Maglorius Renkilaraj MRL, Zhang P, Meertens L, Bolze A, Materna M, Korniotis S, Gervais A, Talouarn E, Bigio B, Seeleuthner Y, Bilguvar K, Zhang Y, Neehus AL, Ogishi M, Pelham SJ, Le Voyer T, Rosain J, Philippot Q, Soler-Palacin P, Colobran R, Martin-Nalda A, Riviere JG, Tandjaoui-Lambiotte Y, Chaibi K, Shahrooei M, Darazam IA, Olyaei NA, Mansouri D, Hatipoglu N, Palabiyik F, Ozcelik T, Novelli G, Novelli A, Casari G, Aiuti A, Carrera P, Bondesan S, Barzaghi F, Rovere-Querini P, Tresoldi C, Franco JL, Rojas J, Reyes LF, Bustos IG, Arias AA, Morelle G, Christele K, Troya J, Planas-Serra L, Schluter A, Gut M, Pujol A, Allende LM, Rodriguez-Gallego C, Flores C, Cabrera-Marante O, Pleguezuelo DE, de Diego RP, Keles S, Aytekin G, Akcan OM, Bryceson YT, Bergman P, Brodin P, Smole D, Smith CIE, Norlin AC, Campbell TM, Covill LE, Hammarstrom L, Pan-Hammarstrom Q, Abolhassani H, Mane S, Marr N, Ata M, Al Ali F, Khan T, Spaan AN, Dalgard CL, Bonfanti P, Biondi A, Tubiana S, Burdet C, Nussbaum R, Kahn-Kirby A, Snow AL, Effort CHG, Clinicians C-S, Clinicians C, Imagine CG, French CCSG, Co VCC, Amsterdam UMCC, Biobank, Group N-UCS, Bustamante J, Puel A, Boisson-Dupuis S, Zhang SY, Beziat V, Lifton RP, Bastard P, Notarangelo LD, Abel L, Su HC, Jouanguy E, Amara A, Soumelis V, Cobat A, Zhang Q, Casanova JL. X-linked recessive TLR7 deficiency in ~1% of men under 60 years old with life-threatening COVID-19. Sci Immunol. 2021;6(62). Epub 2021/08/21. doi: 10.1126/sciimmunol.abl4348. PubMed PMID: 34413140.

352. Bastard P, Gervais A, Le Voyer T, Rosain J, Philippot Q, Manry J, Michailidis E, Hoffmann HH, Eto S, Garcia-Prat M, Bizien L, Parra-Martinez A, Yang R, Haljasmagi L, Migaud M, Sarekannu K, Maslovskaja J, de Prost N, Tandjaoui-Lambiotte Y, Luyt CE, Amador-Borrero B, Gaudet A, Poissy J, Morel P, Richard P, Cognasse F, Troya J, Trouillet-Assant S, Belot A, Saker K, Garcon P, Riviere JG, Lagier JC, Gentile S, Rosen LB, Shaw E, Morio T, Tanaka J, Dalmau D, Tharaux PL, Sene D, Stepanian A, Megarbane B, Triantafyllia V, Fekkar A, Heath JR, Franco JL, Anaya JM, Sole-Violan J, Imberti L, Biondi A, Bonfanti P, Castagnoli R, Delmonte OM, Zhang Y, Snow AL, Holland SM, Biggs C, Moncada-Velez M, Arias AA, Lorenzo L, Boucherit S, Coulibaly B, Anglicheau D, Planas AM, Haerynck F, Duvlis S, Nussbaum RL, Ozcelik T, Keles S, Bousfiha AA, El Bakkouri J, Ramirez-Santana C, Paul S, Pan-Hammarstrom Q, Hammarstrom L, Dupont A, Kurolap A, Metz CN, Aiuti A, Casari G, Lampasona V, Ciceri F, Barreiros LA, Dominguez-Garrido E, Vidigal M, Zatz M, van de Beek D, Sahanic S, Tancevski I, Stepanovskyy Y, Boyarchuk O, Nukui Y, Tsumura M, Vidaur L, Tangye SG, Burrel S, Duffy D, Quintana-Murci L, Klocperk A, Kann NY, Shcherbina A, Lau YL, Leung D, Coulongeat M, Marlet J, Koning R, Reyes LF, Chauvineau-Grenier A, Venet F, Monneret G, Nussenzweig MC, Arrestier R, Boudhabhay I, Baris-Feldman H, Hagin D,

Wauters J, Meyts I, Dyer AH, Kennelly SP, Bourke NM, Halwani R, Sharif-Askari NS, Dorgham K, Sallette J, Sedkaoui SM, AlKhater S, Rigo-Bonnin R, Morandeira F, Roussel L, Vinh DC, Ostrowski SR, Condino-Neto A, Prando C, Bonradenko A, Spaan AN, Gilardin L, Fellay J, Lyonnet S, Bilguvar K, Lifton RP, Mane S, Lab H, Clinicians C, Clinicians C-S, Group NIRtC, Group N-CS, Danish C, Danish Blood Donor S, St. James's H, group SCI, French CCSG, Imagine C-G, Milieu Interieur C, Co VCC, Amsterdam UMCC, Biobank I, Effort CHG, cohort C, Study CD, Cerba H-C, Etablissement du Sang study g, Anderson MS, Boisson B, Beziat V, Zhang SY, Vandreakos E, Hermine O, Pujol A, Peterson P, Mogensen TH, Rowen L, Mond J, Debette S, de Lamballerie X, Duval X, Mentre F, Zins M, Soler-Palacin P, Colobran R, Gorochov G, Solanich X, Susen S, Martinez-Picado J, Raoult D, Vasse M, Gregersen PK, Piemonti L, Rodriguez-Gallego C, Notarangelo LD, Su HC, Kisand K, Okada S, Puel A, Jouanguy E, Rice CM, Tiberghien P, Zhang Q, Cobat A, Abel L, Casanova JL. Autoantibodies neutralizing type I IFNs are present in ~4% of uninfected individuals over 70 years old and account for ~20% of COVID-19 deaths. Sci Immunol. 2021;6(62). Epub 2021/08/21. doi: 10.1126/sciimmunol.abl4340. PubMed PMID: 34413139.

353. Bastard P, Orlova E, Sozaeva L, Levy R, James A, Schmitt MM, Ochoa S, Kareva M, Rodina Y, Gervais A, Le Voyer T, Rosain J, Philippot Q, Neehus AL, Shaw E, Migaud M, Bizien L, Ekwall O, Berg S, Beccuti G, Ghizzoni L, Thiriez G, Pavot A, Goujard C, Fremond ML, Carter E, Rothenbuhler A, Linglart A, Mignot B, Comte A, Cheikh N, Hermine O, Breivik L, Husebye ES, Humbert S, Rohrlich P, Coaquette A, Vuoto F, Faure K, Mahlaoui N, Kotnik P, Battelino T, Trebusak Podkrajsek K, Kisand K, Ferre EMN, DiMaggio T, Rosen LB, Burbelo PD, McIntyre M, Kann NY, Shcherbina A, Pavlova M, Kolodkina A, Holland SM, Zhang SY, Crow YJ, Notarangelo LD, Su HC, Abel L, Anderson MS, Jouanguy E, Neven B, Puel A, Casanova JL, Lionakis MS. Preexisting autoantibodies to type I IFNs underlie critical COVID-19 pneumonia in patients with APS-1. J Exp Med. 2021;218(7). Epub 2021/04/24. doi: 10.1084/jem.20210554. PubMed PMID: 33890986; PMCID: PMC8077172 reported a patent to 63/055,155 pending and a patent to 63/141,669 pending. No other disclosures were reported.

354. Bastard P, Rosen LB, Zhang Q, Michailidis E, Hoffmann HH, Zhang Y, Dorgham K, Philippot Q, Rosain J, Beziat V, Manry J, Shaw E, Haljasmagi L, Peterson P, Lorenzo L, Bizien L, Trouillet-Assant S, Dobbs K, de Jesus AA, Belot A, Kallaste A, Catherinot E, Tandjaoui-Lambiotte Y, Le Pen J, Kerner G, Bigio B, Seeleuthner Y, Yang R, Bolze A, Spaan AN, Delmonte OM, Abers MS, Aiuti A, Casari G, Lampasona V, Piemonti L, Ciceri F, Bilguvar K, Lifton RP, Vasse M, Smadja DM, Migaud M, Hadjadj J, Terrier B, Duffy D, Quintana-Murci L, van de Beek D, Roussel L, Vinh DC, Tangye SG, Haerynck F, Dalmau D, Martinez-Picado J, Brodin P, Nussenzweig MC, Boisson-Dupuis S, Rodriguez-Gallego C, Vogt G, Mogensen TH, Oler AJ, Gu J, Burbelo PD, Cohen JI, Biondi A, Bettini LR, D'Angio M, Bonfanti P, Rossignol P, Mayaux J, Rieux-Laucat F, Husebye ES, Fusco F, Ursini MV, Imberti L, Sottini A, Paghera S, Quiros-Roldan E, Rossi C, Castagnoli R, Montagna D, Licari A, Marseglia GL, Duval X, Ghosn J, Lab H, Group N-UIRtC, Clinicians C, Clinicians C-S, Imagine CG, French CCSG, Milieu Interieur C, Co VCC, Amsterdam UMCC-B, Effort CHG, Tsang JS, Goldbach-Mansky R, Kisand K, Lionakis MS, Puel A, Zhang SY, Holland SM, Gorochov G, Jouanguy E, Rice CM, Cobat A, Notarangelo LD, Abel L, Su HC, Casanova JL. Autoantibodies against type I IFNs in patients with life-

threatening COVID-19. Science. 2020;370(6515). Epub 2020/09/26. doi: 10.1126/science.abd4585. PubMed PMID: 32972996; PMCID: PMC7857397.

355. Lopez J, Mommert M, Mouton W, Pizzorno A, Brengel-Pesce K, Mezidi M, Villard M, Lina B, Richard JC, Fassier JB, Cheynet V, Padey B, Duliere V, Julien T, Paul S, Bastard P, Belot A, Bal A, Casanova JL, Rosa-Calatrava M, Morfin F, Walzer T, Trouillet-Assant S. Early nasal type I IFN immunity against SARS-CoV-2 is compromised in patients with autoantibodies against type I IFNs. J Exp Med. 2021;218(10). Epub 20210806. doi: 10.1084/jem.20211211. PubMed PMID: 34357402; PMCID: PMC8352718.

356. Solanich X, Rigo-Bonnin R, Gumucio VD, Bastard P, Rosain J, Philippot Q, Perez-Fernandez XL, Fuset-Cabanes MP, Gordillo-Benitez MA, Suarez-Cuartin G, Boza-Hernandez E, Riera-Mestre A, Parra-Martinez A, Colobran R, Antoli A, Navarro S, Rocamora-Blanch G, Framil M, Calatayud L, Corbella X, Casanova JL, Morandeira F, Sabater-Riera J. Pre-existing Autoantibodies Neutralizing High Concentrations of Type I Interferons in Almost 10% of COVID-19 Patients Admitted to Intensive Care in Barcelona. J Clin Immunol. 2021. Epub 2021/09/28. doi: 10.1007/s10875-021-01136-x. PubMed PMID: 34570326; PMCID: PMC8475877.

357. van der Wijst MGP, Vazquez SE, Hartoularos GC, Bastard P, Grant T, Bueno R, Lee DS, Greenland JR, Sun Y, Perez R, Ogorodnikov A, Ward A, Mann SA, Lynch KL, Yun C, Havlir DV, Chamie G, Marquez C, Greenhouse B, Lionakis MS, Norris PJ, Dumont LJ, Kelly K, Zhang P, Zhang Q, Gervais A, Le Voyer T, Whatley A, Si Y, Byrne A, Combes AJ, Rao AA, Song YS, Fragiadakis GK, Kangelaris K, Calfee CS, Erle DJ, Hendrickson C, Krummel MF, Woodruff PG, Langelier CR, Casanova JL, Derisi JL, Anderson MS, Ye CJ, consortium UC. Type I interferon autoantibodies are associated with systemic immune alterations in patients with COVID-19. Sci Transl Med. 2021;13(612):eabh2624. Epub 2021/08/26. doi: 10.1126/scitranslmed.abh2624. PubMed PMID: 34429372.

358. Zhang Q, Bastard P, Liu Z, Le Pen J, Moncada-Velez M, Chen J, Ogishi M, Sabli IKD, Hodeib S, Korol C, Rosain J, Bilguvar K, Ye J, Bolze A, Bigio B, Yang R, Arias AA, Zhou Q, Zhang Y, Onodi F, Korniotis S, Karpf L, Philippot Q, Chbihi M, Bonnet-Madin L, Dorgham K, Smith N, Schneider WM, Razooky BS, Hoffmann HH, Michailidis E, Moens L, Han JE, Lorenzo L, Bizien L, Meade P, Neehus AL, Ugurbil AC, Corneau A, Kerner G, Zhang P, Rapaport F, Seeleuthner Y, Manry J, Masson C, Schmitt Y, Schluter A, Le Voyer T, Khan T, Li J, Fellay J, Roussel L, Shahrooei M, Alosaimi MF, Mansouri D, Al-Saud H, Al-Mulla F, Almourfi F, Al-Muhsen SZ, Alsohime F, Al Turki S, Hasanato R, van de Beek D, Biondi A, Bettini LR, D'Angio M, Bonfanti P, Imberti L, Sottini A, Paghera S, Quiros-Roldan E, Rossi C, Oler AJ, Tompkins MF, Alba C, Vandernoot I, Goffard JC, Smits G, Migeotte I, Haerynck F, Soler-Palacin P, Martin-Nalda A, Colobran R, Morange PE, Keles S, Colkesen F, Ozcelik T, Yasar KK, Senoglu S, Karabela SN, Rodriguez-Gallego C, Novelli G, Hraiech S, Tandjaoui-Lambiotte Y, Duval X, Laouenan C, Clinicians C-S, Clinicians C, Imagine CG, French CCSG, Co VCC, Amsterdam UMCC-B, Effort CHG, Group N-UTCI, Snow AL, Dalgard CL, Milner JD, Vinh DC, Mogensen TH, Marr N, Spaan AN, Boisson B, Boisson-Dupuis S, Bustamante J, Puel A, Ciancanelli MJ, Meyts I, Maniatis T, Soumelis V, Amara A, Nussenzweig M, Garcia-Sastre A, Krammer F, Pujol

A, Duffy D, Lifton RP, Zhang SY, Gorochov G, Beziat V, Jouanguy E, Sancho-Shimizu V, Rice CM, Abel L, Notarangelo LD, Cobat A, Su HC, Casanova JL. Inborn errors of type I IFN immunity in patients with life-threatening COVID-19. Science. 2020;370(6515). Epub 2020/09/26. doi: 10.1126/science.abd4570. PubMed PMID: 32972995; PMCID: PMC7857407.

359. Arunachalam PS, Wimmers F, Mok CKP, Perera RAPM, Scott M, Hagan T, Sigal N, Feng Y, Bristow L, Tsang OT-Y, Wagh D, Coller J, Pellegrini KL, Kazmin D, Alaaeddine G, Leung WS, Chan JMC, Chik TSH, Choi CYC, Huerta C, McCullough MP, Lv H, Anderson E, Edupuganti S, Upadhyay AA, Bosinger SE, Maecker HT, Khatri P, Rouphael N, Peiris M, Pulendran B. Systems biological assessment of immunity to mild versus severe COVID-19 infection in humans. Science. 2020:eabc6261. doi: 10.1126/science.abc6261 PMID - 32788292.

360. Liu C, Martins AJ, Lau WW, Rachmaninoff N, Chen J, Imberti L, Mostaghimi D, Fink DL, Burbelo PD, Dobbs K, Delmonte OM, Bansal N, Failla L, Sottini A, Quiros-Roldan E, Han KL, Sellers BA, Cheung F, Sparks R, Chun TW, Moir S, Lionakis MS, Consortium NC, Clinicians C, Rossi C, Su HC, Kuhns DB, Cohen JI, Notarangelo LD, Tsang JS. Time-resolved systems immunology reveals a late juncture linked to fatal COVID-19. Cell. 2021;184(7):1836-57 e22. Epub 2021/03/14. doi: 10.1016/j.cell.2021.02.018. PubMed PMID: 33713619; PMCID: PMC7874909.

361. Shebl FM, Pinto LA, García-Piñeres A, Lempicki R, Williams M, Harro C, Hildesheim A. Comparison of mRNA and protein measures of cytokines following vaccination with human papillomavirus-16 L1 virus-like particles. Cancer Epidemiol Biomarkers Prev. 2010;19(4):978-81. Epub 20100323. doi: 10.1158/1055-9965.Epi-10-0064. PubMed PMID: 20332253; PMCID: PMC2852493.

362. Waggoner JJ, Stittleburg V, Pond R, Saklawi Y, Sahoo MK, Babiker A, Hussaini L, Kraft CS, Pinsky BA, Anderson EJ, Rouphael N. Triplex Real-Time RT-PCR for Severe Acute Respiratory Syndrome Coronavirus 2. Emerg Infect Dis. 2020;26(7):1633-5. Epub 20200621. doi: 10.3201/eid2607.201285. PubMed PMID: 32294051; PMCID: PMC7323516.

363. Wolfel R, Corman VM, Guggemos W, Seilmaier M, Zange S, Muller MA, Niemeyer D, Jones TC, Vollmar P, Rothe C, Hoelscher M, Bleicker T, Brunink S, Schneider J, Ehmann R, Zwirglmaier K, Drosten C, Wendtner C. Virological assessment of hospitalized patients with COVID-2019. Nature. 2020;581(7809):465-9. Epub 20200401. doi: 10.1038/s41586-020-2196-x. PubMed PMID: 32235945.

364. McGary CS, Deleage C, Harper J, Micci L, Ribeiro SP, Paganini S, Kuri-Cervantes L, Benne C, Ryan ES, Balderas R, Jean S, Easley K, Marconi V, Silvestri G, Estes JD, Sekaly RP, Paiardini M. CTLA-4(+)PD-1(-) Memory CD4(+) T Cells Critically Contribute to Viral Persistence in Antiretroviral Therapy-Suppressed, SIV-Infected Rhesus Macaques. Immunity. 2017;47(4):776-88 e5. doi: 10.1016/j.immuni.2017.09.018. PubMed PMID: 29045906; PMCID: PMC5679306.

365. Micci L, Ryan ES, Fromentin R, Bosinger SE, Harper JL, He T, Paganini S, Easley KA, Chahroudi A, Benne C, Gumber S, McGary CS, Rogers KA, Deleage C, Lucero C, Byrareddy SN, Apetrei C, Estes JD, Lifson JD, Piatak M, Jr., Chomont N, Villinger F, Silvestri G, Brenchley JM, Paiardini M. Interleukin-21 combined with ART reduces inflammation and viral reservoir in SIV-infected macaques. J Clin Invest. 2015;125(12):4497-513. Epub 20151109. doi: 10.1172/jci81400. PubMed PMID: 26551680; PMCID: PMC4665780.

366. Love MI, Huber W, Anders S. Moderated estimation of fold change and dispersion for RNA-seq data with DESeq2. Genome Biol. 2014;15(12):550. doi: 10.1186/s13059-014-0550-8. PubMed PMID: 25516281; PMCID: PMC4302049.

367. Subramanian A, Tamayo P, Mootha VK, Mukherjee S, Ebert BL, Gillette MA, Paulovich A, Pomeroy SL, Golub TR, Lander ES, Mesirov JP. Gene set enrichment analysis: a knowledge-based approach for interpreting genome-wide expression profiles. Proc Natl Acad Sci U S A. 2005;102(43):15545-50. Epub 20050930. doi: 10.1073/pnas.0506580102. PubMed PMID: 16199517; PMCID: PMC1239896.

368. Sandler NG, Bosinger SE, Estes JD, Zhu RT, Tharp GK, Boritz E, Levin D, Wijeyesinghe S, Makamdop KN, del Prete GQ, Hill BJ, Timmer JK, Reiss E, Yarden G, Darko S, Contijoch E, Todd JP, Silvestri G, Nason M, Norgren RB, Jr., Keele BF, Rao S, Langer JA, Lifson JD, Schreiber G, Douek DC. Type I interferon responses in rhesus macaques prevent SIV infection and slow disease progression. Nature. 2014;511(7511):601-5. Epub 20140709. doi: 10.1038/nature13554. PubMed PMID: 25043006; PMCID: PMC4418221.

369. Blighe K, Rana S, Lewis M. EnhancedVolcano: Publication-ready volcano plots with enhanced colouring and labeling. https://github.com/kevinblighe/EnhancedVolcano. https://github.com/kevinblighe/EnhancedVolcano(2020.

370. Gu Z, Eils R, Schlesner M. Complex heatmaps reveal patterns and correlations in multidimensional genomic data. Bioinformatics. 2016;32(18):2847-9. Epub 20160520. doi: 10.1093/bioinformatics/btw313. PubMed PMID: 27207943.

371. Butler A, Hoffman P, Smibert P, Papalexi E, Satija R. Integrating single-cell transcriptomic data across different conditions, technologies, and species. Nat Biotechnol. 2018;36(5):411-20. Epub 20180402. doi: 10.1038/nbt.4096. PubMed PMID: 29608179; PMCID: PMC6700744.

372. Tang-Huau TL, Gueguen P, Goudot C, Durand M, Bohec M, Baulande S, Pasquier B, Amigorena S, Segura E. Human in vivo-generated monocyte-derived dendritic cells and macrophages cross-present antigens through a vacuolar pathway. Nat Commun. 2018;9(1):2570. Epub 20180702. doi: 10.1038/s41467-018-04985-0. PubMed PMID: 29967419; PMCID: PMC6028641.

373. Finak G, McDavid A, Yajima M, Deng J, Gersuk V, Shalek AK, Slichter CK, Miller HW, McElrath MJ, Prlic M, Linsley PS, Gottardo R. MAST: a flexible statistical framework for assessing transcriptional changes and characterizing heterogeneity in single-cell RNA

sequencing data. Genome Biol. 2015;16:278. Epub 20151210. doi: 10.1186/s13059-015-0844-5. PubMed PMID: 26653891; PMCID: PMC4676162.

374. Andreatta M, Carmona SJ. UCell: Robust and scalable single-cell gene signature scoring. Comput Struct Biotechnol J. 2021;19:3796-8. Epub 20210630. doi: 10.1016/j.csbj.2021.06.043. PubMed PMID: 34285779; PMCID: PMC8271111.

375. A. UA, K. TG. TREM2+ and interstitial-like macrophages orchestrate airway inflammation in SARS-CoV-2 infection in rhesus macaques, NHP_COVID-19_2 https://github.com/BosingerLab/NHP_COVID-19_2 DOI: 10.5281/zenodo.7626608)(2023.

376. Tan W, Zhao X, Ma X, Wang W, Niu P, Xu W, Gao GF, Wu G. A Novel Coronavirus Genome Identified in a Cluster of Pneumonia Cases - Wuhan, China 2019-2020. China CDC Wkly. 2020;2(4):61-2. PubMed PMID: 34594763; PMCID: PMC8393069.

377. WHO. 2023. Available from: https://covid19.who.int/.

378. Fensterl V, Chattopadhyay S, Sen GC. No Love Lost Between Viruses and Interferons. Annu Rev Virol. 2015;2(1):549-72. Epub 20150925. doi: 10.1146/annurev-virology-100114-055249. PubMed PMID: 26958928.

379. Schoggins JW. Interferon-Stimulated Genes: What Do They All Do? Annu Rev Virol. 2019;6(1):567-84. Epub 20190705. doi: 10.1146/annurev-virology-092818-015756. PubMed PMID: 31283436.

380. Combes AJ, Courau T, Kuhn NF, Hu KH, Ray A, Chen WS, Chew NW, Cleary SJ, Kushnoor D, Reeder GC, Shen A, Tsui J, Hiam-Galvez KJ, Muñoz-Sandoval P, Zhu WS, Lee DS, Sun Y, You R, Magnen M, Rodriguez L, Im KW, Serwas NK, Leligdowicz A, Zamecnik CR, Loudermilk RP, Wilson MR, Ye CJ, Fragiadakis GK, Looney MR, Chan V, Ward A, Carrillo S, Matthay M, Erle DJ, Woodruff PG, Langelier C, Kangelaris K, Hendrickson CM, Calfee C, Rao AA, Krummel MF. Global absence and targeting of protective immune states in severe COVID-19. Nature. 2021;591(7848):124-30. Epub 20210125. doi: 10.1038/s41586-021-03234-7. PubMed PMID: 33494096; PMCID: PMC8567458.

381. Wang EY, Mao T, Klein J, Dai Y, Huck JD, Jaycox JR, Liu F, Zhou T, Israelow B, Wong P, Coppi A, Lucas C, Silva J, Oh JE, Song E, Perotti ES, Zheng NS, Fischer S, Campbell M, Fournier JB, Wyllie AL, Vogels CBF, Ott IM, Kalinich CC, Petrone ME, Watkins AE, Dela Cruz C, Farhadian SF, Schulz WL, Ma S, Grubaugh ND, Ko AI, Iwasaki A, Ring AM. Diverse functional autoantibodies in patients with COVID-19. Nature. 2021;595(7866):283-8. Epub 20210519. doi: 10.1038/s41586-021-03631-y. PubMed PMID: 34010947.

382. Pairo-Castineira E, Clohisey S, Klaric L, Bretherick AD, Rawlik K, Pasko D, Walker S, Parkinson N, Fourman MH, Russell CD, Furniss J, Richmond A, Gountouna E, Wrobel N, Harrison D, Wang B, Wu Y, Meynert A, Griffiths F, Oosthuyzen W, Kousathanas A, Moutsianas L, Yang Z, Zhai R, Zheng C, Grimes G, Beale R, Millar J, Shih B, Keating S,

Zechner M, Haley C, Porteous DJ, Hayward C, Yang J, Knight J, Summers C, Shankar-Hari M, Klenerman P, Turtle L, Ho A, Moore SC, Hinds C, Horby P, Nichol A, Maslove D, Ling L, McAuley D, Montgomery H, Walsh T, Pereira AC, Renieri A, Shen X, Ponting CP, Fawkes A, Tenesa A, Caulfield M, Scott R, Rowan K, Murphy L, Openshaw PJM, Semple MG, Law A, Vitart V, Wilson JF, Baillie JK. Genetic mechanisms of critical illness in COVID-19. Nature. 2021;591(7848):92-8. Epub 20201211. doi: 10.1038/s41586-020-03065-y. PubMed PMID: 33307546.

383. Ziegler CGK, Miao VN, Owings AH, Navia AW, Tang Y, Bromley JD, Lotfy P, Sloan M, Laird H, Williams HB, George M, Drake RS, Christian T, Parker A, Sindel CB, Burger MW, Pride Y, Hasan M, Abraham GE, 3rd, Senitko M, Robinson TO, Shalek AK, Glover SC, Horwitz BH, Ordovas-Montanes J. Impaired local intrinsic immunity to SARS-CoV-2 infection in severe COVID-19. Cell. 2021;184(18):4713-33.e22. Epub 20210723. doi: 10.1016/j.cell.2021.07.023. PubMed PMID: 34352228; PMCID: PMC8299217.

384. Kousathanas A, Pairo-Castineira E, Rawlik K, Stuckey A, Odhams CA, Walker S, Russell CD, Malinauskas T, Wu Y, Millar J, Shen X, Elliott KS, Griffiths F, Oosthuyzen W, Morrice K, Keating S, Wang B, Rhodes D, Klaric L, Zechner M, Parkinson N, Siddiq A, Goddard P, Donovan S, Maslove D, Nichol A, Semple MG, Zainy T, Maleady-Crowe F, Todd L, Salehi S, Knight J, Elgar G, Chan G, Arumugam P, Patch C, Rendon A, Bentley D, Kingsley C, Kosmicki JA, Horowitz JE, Baras A, Abecasis GR, Ferreira MAR, Justice A, Mirshahi T, Oetjens M, Rader DJ, Ritchie MD, Verma A, Fowler TA, Shankar-Hari M, Summers C, Hinds C, Horby P, Ling L, McAuley D, Montgomery H, Openshaw PJM, Elliott P, Walsh T, Tenesa A, Fawkes A, Murphy L, Rowan K, Ponting CP, Vitart V, Wilson JF, Yang J, Bretherick AD, Scott RH, Hendry SC, Moutsianas L, Law A, Caulfield MJ, Baillie JK. Whole-genome sequencing reveals host factors underlying critical COVID-19. Nature. 2022. Epub 20220307. doi: 10.1038/s41586-022-04576-6. PubMed PMID: 35255492.

385. Povysil G, Butler-Laporte G, Shang N, Wang C, Khan A, Alaamery M, Nakanishi T, Zhou S, Forgetta V, Eveleigh RJ, Bourgey M, Aziz N, Jones SJ, Knoppers B, Scherer SW, Strug LJ, Lepage P, Ragoussis J, Bourque G, Alghamdi J, Aljawini N, Albes N, Al-Afghani HM, Alghamdi B, Almutairi MS, Mahmoud ES, Abu-Safieh L, El Bardisy H, Harthi FSA, Alshareef A, Suliman BA, Alqahtani SA, Almalik A, Alrashed MM, Massadeh S, Mooser V, Lathrop M, Fawzy M, Arabi YM, Mbarek H, Saad C, Al-Muftah W, Jung J, Mangul S, Badji R, Thani AA, Ismail SI, Gharavi AG, Abedalthagafi MS, Richards JB, Goldstein DB, Kiryluk K. Rare loss-of-function variants in type I IFN immunity genes are not associated with severe COVID-19. J Clin Invest. 2021;131(14). doi: 10.1172/jci147834. PubMed PMID: 34043590; PMCID: PMC8279578.

386. Lee JS, Park S, Jeong HW, Ahn JY, Choi SJ, Lee H, Choi B, Nam SK, Sa M, Kwon JS, Jeong SJ, Lee HK, Park SH, Park SH, Choi JY, Kim SH, Jung I, Shin EC. Immunophenotyping of COVID-19 and influenza highlights the role of type I interferons in development of severe COVID-19. Sci Immunol. 2020;5(49). doi: 10.1126/sciimmunol.abd1554. PubMed PMID: 32651212; PMCID: PMC7402635.

387. Blanco-Melo D, Nilsson-Payant BE, Liu W-C, Uhl S, Hoagland D, Møller R, Jordan TX, Oishi K, Panis M, Sachs D, Wang TT, Schwartz RE, Lim JK, Albrecht RA, tenOever BR. Imbalanced Host Response to SARS-CoV-2 Drives Development of COVID-19. Cell. 2020;181(5):1036-45.e9. doi: 10.1016/j.cell.2020.04.026.

388. Major J, Crotta S, Llorian M, McCabe TM, Gad HH, Priestnall SL, Hartmann R, Wack A. Type I and III interferons disrupt lung epithelial repair during recovery from viral infection. Science. 2020;369(6504):712-7. Epub 20200611. doi: 10.1126/science.abc2061. PubMed PMID: 32527928; PMCID: PMC7292500.

389. Sefik E, Qu R, Junqueira C, Kaffe E, Mirza H, Zhao J, Brewer JR, Han A, Steach HR, Israelow B, Blackburn HN, Velazquez SE, Chen YG, Halene S, Iwasaki A, Meffre E, Nussenzweig M, Lieberman J, Wilen CB, Kluger Y, Flavell RA. Inflammasome activation in infected macrophages drives COVID-19 pathology. Nature. 2022;606(7914):585-93. Epub 20220428. doi: 10.1038/s41586-022-04802-1. PubMed PMID: 35483404.

390. Laurent P, Yang C, Rendeiro AF, Nilsson-Payant BE, Carrau L, Chandar V, Bram Y, tenOever BR, Elemento O, Ivashkiv LB, Schwartz RE, Barrat FJ. Sensing of SARS-CoV-2 by pDCs and their subsequent production of IFN-I contribute to macrophage-induced cytokine storm during COVID-19. Sci Immunol. 2022;7(75):eadd4906. Epub 20220909. doi: 10.1126/sciimmunol.add4906. PubMed PMID: 36083891; PMCID: PMC9853436.

391. Prelli Bozzo C, Nchioua R, Volcic M, Koepke L, Krüger J, Schütz D, Heller S, Stürzel CM, Kmiec D, Conzelmann C, Müller J, Zech F, Braun E, Groß R, Wettstein L, Weil T, Weiß J, Diofano F, Rodríguez Alfonso AA, Wiese S, Sauter D, Münch J, Goffinet C, Catanese A, Schön M, Boeckers TM, Stenger S, Sato K, Just S, Kleger A, Sparrer KMJ, Kirchhoff F. IFITM proteins promote SARS-CoV-2 infection and are targets for virus inhibition in vitro. Nat Commun. 2021;12(1):4584. Epub 20210728. doi: 10.1038/s41467-021-24817-y. PubMed PMID: 34321474; PMCID: PMC8319209.

392. Nchioua R, Kmiec D, Muller JA, Conzelmann C, Gross R, Swanson CM, Neil SJD, Stenger S, Sauter D, Munch J, Sparrer KMJ, Kirchhoff F. SARS-CoV-2 Is Restricted by Zinc Finger Antiviral Protein despite Preadaptation to the Low-CpG Environment in Humans. mBio. 2020;11(5). Epub 20201016. doi: 10.1128/mBio.01930-20. PubMed PMID: 33067384; PMCID: PMC7569149.

393. Singh DK, Aladyeva E, Das S, Singh B, Esaulova E, Swain A, Ahmed M, Cole J, Moodley C, Mehra S, Schlesinger LS, Artyomov MN, Khader SA, Kaushal D. Myeloid cell interferon responses correlate with clearance of SARS-CoV-2. Nat Commun. 2022;13(1):679. Epub 20220203. doi: 10.1038/s41467-022-28315-7. PubMed PMID: 35115549; PMCID: PMC8814034.

394. Nelson CE, Namasivayam S, Foreman TW, Kauffman KD, Sakai S, Dorosky DE, Lora NE, Brooks K, Potter EL, Garza NL, Lafont BAP, Johnson RF, Roederer M, Sher A, Weiskopf D, Sette A, de Wit E, Hickman HD, Brenchley JM, Via LE, Barber DL, Abdi A, Dayao EK, Fleegle JD, Gomez F, Piazza MK, Repoli KM, Sloan BY, Butler AL, Walker

AM, Weiner DM, Woodcock MJ, Vatthauer A. Mild SARS-CoV-2 infection in rhesus macaques is associated with viral control prior to antigen-specific T cell responses in tissues. Sci Immunol. 2022:eabo0535. Epub 20220310. doi: 10.1126/sciimmunol.abo0535. PubMed PMID: 35271298; PMCID: PMC8995035.

395. Levin D, Schneider WM, Hoffmann HH, Yarden G, Busetto AG, Manor O, Sharma N, Rice CM, Schreiber G. Multifaceted activities of type I interferon are revealed by a receptor antagonist. Sci Signal. 2014;7(327):ra50. Epub 20140527. doi: 10.1126/scisignal.2004998. PubMed PMID: 24866020; PMCID: PMC4311876.

396. Urin V, Levin D, Sharma N, Harari D, Schreiber G. Fine Tuning of a Type 1 Interferon Antagonist. PLoS One. 2015;10(7):e0130797. Epub 20150709. doi: 10.1371/journal.pone.0130797. PubMed PMID: 26158644; PMCID: PMC4497658.

397. Nganou-Makamdop K, Billingsley JM, Yaffe Z, O'Connor G, Tharp GK, Ransier A, Laboune F, Matus-Nicodemos R, Lerner A, Gharu L, Robertson JM, Ford ML, Schlapschy M, Kuhn N, Lensch A, Lifson J, Nason M, Skerra A, Schreiber G, Bosinger SE, Douek DC. Type I IFN signaling blockade by a PASylated antagonist during chronic SIV infection suppresses specific inflammatory pathways but does not alter T cell activation or virus replication. PLoS Pathog. 2018;14(8):e1007246. Epub 20180824. doi: 10.1371/journal.ppat.1007246. PubMed PMID: 30142226; PMCID: PMC6126880.

398. Forero A, Ozarkar S, Li H, Lee CH, Hemann EA, Nadjsombati MS, Hendricks MR, So L, Green R, Roy CN, Sarkar SN, von Moltke J, Anderson SK, Gale M, Jr., Savan R. Differential Activation of the Transcription Factor IRF1 Underlies the Distinct Immune Responses Elicited by Type I and Type III Interferons. Immunity. 2019;51(3):451-64 e6. Epub 20190827. doi: 10.1016/j.immuni.2019.07.007. PubMed PMID: 31471108; PMCID: PMC7447158.

399. Gagne M, Corbett KS, Flynn BJ, Foulds KE, Wagner DA, Andrew SF, Todd JM, Honeycutt CC, McCormick L, Nurmukhambetova ST, Davis-Gardner ME, Pessaint L, Bock KW, Nagata BM, Minai M, Werner AP, Moliva JI, Tucker C, Lorang CG, Zhao B, McCarthy E, Cook A, Dodson A, Teng IT, Mudvari P, Roberts-Torres J, Laboune F, Wang L, Goode A, Kar S, Boyoglu-Barnum S, Yang ES, Shi W, Ploquin A, Doria-Rose N, Carfi A, Mascola JR, Boritz EA, Edwards DK, Andersen H, Lewis MG, Suthar MS, Graham BS, Roederer M, Moore IN, Nason MC, Sullivan NJ, Douek DC, Seder RA. Protection from SARS-CoV-2 Delta one year after mRNA-1273 vaccination in rhesus macaques coincides with anamnestic antibody response in the lung. Cell. 2022;185(1):113-30.e15. Epub 20211203. doi: 10.1016/j.cell.2021.12.002. PubMed PMID: 34921774; PMCID: PMC8639396.

400. Gagne M, Moliva JI, Foulds KE, Andrew SF, Flynn BJ, Werner AP, Wagner DA, Teng IT, Lin BC, Moore C, Jean-Baptiste N, Carroll R, Foster SL, Patel M, Ellis M, Edara VV, Maldonado NV, Minai M, McCormick L, Honeycutt CC, Nagata BM, Bock KW, Dulan CNM, Cordon J, Flebbe DR, Todd JM, McCarthy E, Pessaint L, Van Ry A, Narvaez B, Valentin D, Cook A, Dodson A, Steingrebe K, Nurmukhambetova ST, Godbole S, Henry AR, Laboune F, Roberts-Torres J, Lorang CG, Amin S, Trost J, Naisan M, Basappa M,

Willis J, Wang L, Shi W, Doria-Rose NA, Zhang Y, Yang ES, Leung K, O'Dell S, Schmidt SD, Olia AS, Liu C, Harris DR, Chuang GY, Stewart-Jones G, Renzi I, Lai YT, Malinowski A, Wu K, Mascola JR, Carfi A, Kwong PD, Edwards DK, Lewis MG, Andersen H, Corbett KS, Nason MC, McDermott AB, Suthar MS, Moore IN, Roederer M, Sullivan NJ, Douek DC, Seder RA. mRNA-1273 or mRNA-Omicron boost in vaccinated macaques elicits similar B cell expansion, neutralizing responses, and protection from Omicron. Cell. 2022;185(9):1556-71.e18. Epub 20220325. doi: 10.1016/j.cell.2022.03.038. PubMed PMID: 35447072; PMCID: PMC8947944.

401. Szabo PA, Dogra P, Gray JI, Wells SB, Connors TJ, Weisberg SP, Krupska I, Matsumoto R, Poon MML, Idzikowski E, Morris SE, Pasin C, Yates AJ, Ku A, Chait M, Davis-Porada J, Guo XV, Zhou J, Steinle M, Mackay S, Saqi A, Baldwin MR, Sims PA, Farber DL. Longitudinal profiling of respiratory and systemic immune responses reveals myeloid cell-driven lung inflammation in severe COVID-19. Immunity. 2021;54(4):797-814.e6. Epub 20210311. doi: 10.1016/j.immuni.2021.03.005. PubMed PMID: 33765436; PMCID: PMC7951561.

402. Silvin A, Chapuis N, Dunsmore G, Goubet AG, Dubuisson A, Derosa L, Almire C, Henon C, Kosmider O, Droin N, Rameau P, Catelain C, Alfaro A, Dussiau C, Friedrich C, Sourdeau E, Marin N, Szwebel TA, Cantin D, Mouthon L, Borderie D, Deloger M, Bredel D, Mouraud S, Drubay D, Andrieu M, Lhonneur AS, Saada V, Stoclin A, Willekens C, Pommeret F, Griscelli F, Ng LG, Zhang Z, Bost P, Amit I, Barlesi F, Marabelle A, Pene F, Gachot B, Andre F, Zitvogel L, Ginhoux F, Fontenay M, Solary E. Elevated Calprotectin and Abnormal Myeloid Cell Subsets Discriminate Severe from Mild COVID-19. Cell. 2020;182(6):1401-18 e18. Epub 20200805. doi: 10.1016/j.cell.2020.08.002. PubMed PMID: 32810439; PMCID: PMC7405878.

403. Schulte-Schrepping J, Reusch N, Paclik D, Bassler K, Schlickeiser S, Zhang B, Kramer B, Krammer T, Brumhard S, Bonaguro L, De Domenico E, Wendisch D, Grasshoff M, Kapellos TS, Beckstette M, Pecht T, Saglam A, Dietrich O, Mei HE, Schulz AR, Conrad C, Kunkel D, Vafadarnejad E, Xu CJ, Horne A, Herbert M, Drews A, Thibeault C, Pfeiffer M, Hippenstiel S, Hocke A, Muller-Redetzky H, Heim KM, Machleidt F, Uhrig A, Bosquillon de Jarcy L, Jurgens L, Stegemann M, Glosenkamp CR, Volk HD, Goffinet C, Landthaler M, Wyler E, Georg P, Schneider M, Dang-Heine C, Neuwinger N, Kappert K, Tauber R, Corman V, Raabe J, Kaiser KM, Vinh MT, Rieke G, Meisel C, Ulas T, Becker M, Geffers R, Witzenrath M, Drosten C, Suttorp N, von Kalle C, Kurth F, Handler K, Schultze JL, Aschenbrenner AC, Li Y, Nattermann J, Sawitzki B, Saliba AE, Sander LE, Deutsche C-OI. Severe COVID-19 Is Marked by a Dysregulated Myeloid Cell Compartment. Cell. 2020;182(6):1419-40 e23. Epub 20200805. doi: 10.1016/j.cell.2020.08.001. PubMed PMID: 32810438; PMCID: PMC7405822.

404. Doehn JM, Tabeling C, Biesen R, Saccomanno J, Madlung E, Pappe E, Gabriel F, Kurth F, Meisel C, Corman VM, Hanitsch LG, Treskatsch S, Heim K, Stegemann MS, Ruwwe-Glösenkamp C, Müller-Redetzky HC, Uhrig A, Somasundaram R, Spies C, von Bernuth H, Hofmann J, Drosten C, Suttorp N, Witzenrath M, Sander LE, Hübner RH. CD169/SIGLEC1 is expressed on circulating monocytes in COVID-19 and expression levels are associated with disease severity. Infection. 2021;49(4):757-62. Epub

20210406. doi: 10.1007/s15010-021-01606-9. PubMed PMID: 33825125; PMCID: PMC8023546.

405. Pino M, Abid T, Pereira Ribeiro S, Edara VV, Floyd K, Smith JC, Latif MB, Pacheco-Sanchez G, Dutta D, Wang S, Gumber S, Kirejczyk S, Cohen J, Stammen RL, Jean SM, Wood JS, Connor-Stroud F, Pollet J, Chen WH, Wei J, Zhan B, Lee J, Liu Z, Strych U, Shenvi N, Easley K, Weiskopf D, Sette A, Pollara J, Mielke D, Gao H, Eisel N, LaBranche CC, Shen X, Ferrari G, Tomaras GD, Montefiori DC, Sekaly RP, Vanderford TH, Tomai MA, Fox CB, Suthar MS, Kozlowski PA, Hotez PJ, Paiardini M, Bottazzi ME, Kasturi SP. A yeast expressed RBD-based SARS-CoV-2 vaccine formulated with 3M-052-alum adjuvant promotes protective efficacy in non-human primates. Sci Immunol. 2021;6(61). doi: 10.1126/sciimmunol.abh3634. PubMed PMID: 34266981; PMCID: PMC9119307.

406. Aceti A, Margarucci LM, Scaramucci E, Orsini M, Salerno G, Di Sante G, Gianfranceschi G, Di Liddo R, Valeriani F, Ria F, Simmaco M, Parnigotto PP, Vitali M, Romano Spica V, Michetti F. Serum S100B protein as a marker of severity in Covid-19 patients. Sci Rep. 2020;10(1):18665. Epub 20201029. doi: 10.1038/s41598-020-75618-0. PubMed PMID: 33122776; PMCID: PMC7596559.

407. Chen L, Long X, Xu Q, Tan J, Wang G, Cao Y, Wei J, Luo H, Zhu H, Huang L, Meng F, Huang L, Wang N, Zhou X, Zhao L, Chen X, Mao Z, Chen C, Li Z, Sun Z, Zhao J, Wang D, Huang G, Wang W, Zhou J. Elevated serum levels of S100A8/A9 and HMGB1 at hospital admission are correlated with inferior clinical outcomes in COVID-19 patients. Cell Mol Immunol. 2020;17(9):992-4. Epub 20200703. doi: 10.1038/s41423-020-0492-x. PubMed PMID: 32620787; PMCID: PMC7332851.

408. Guo Q, Zhao Y, Li J, Liu J, Yang X, Guo X, Kuang M, Xia H, Zhang Z, Cao L, Luo Y, Bao L, Wang X, Wei X, Deng W, Wang N, Chen L, Chen J, Zhu H, Gao R, Qin C, Wang X, You F. Induction of alarmin S100A8/A9 mediates activation of aberrant neutrophils in the pathogenesis of COVID-19. Cell Host Microbe. 2021;29(2):222-35 e4. Epub 20201226. doi: 10.1016/j.chom.2020.12.016. PubMed PMID: 33388094; PMCID: PMC7762710.

409. Swanson KV, Deng M, Ting JP. The NLRP3 inflammasome: molecular activation and regulation to therapeutics. Nat Rev Immunol. 2019;19(8):477-89. doi: 10.1038/s41577-019-0165-0. PubMed PMID: 31036962; PMCID: PMC7807242.

410. Upadhyay AA, Viox EG, Hoang TN, Boddapati AK, Pino M, Lee MY, Corry J, Strongin Z, Cowan DA, Beagle EN, Horton TR, Hamilton S, Aoued H, Harper JL, Edwards CT, Nguyen K, Pellegrini KL, Tharp GK, Piantadosi A, Levit RD, Amara RR, Barratt-Boyes SM, Ribeiro SP, Sekaly RP, Vanderford TH, Schinazi RF, Paiardini M, Bosinger SE. TREM2(+) and interstitial-like macrophages orchestrate airway inflammation in SARS-CoV-2 infection in rhesus macaques. Nat Commun. 2023;14(1):1914. Epub 20230406. doi: 10.1038/s41467-023-37425-9. PubMed PMID: 37024448; PMCID: PMC10078029.

411. Singh DK, Singh B, Ganatra SR, Gazi M, Cole J, Thippeshappa R, Alfson KJ, Clemmons E, Gonzalez O, Escobedo R, Lee TH, Chatterjee A, Goez-Gazi Y, Sharan R, Gough M, Alvarez C, Blakley A, Ferdin J, Bartley C, Staples H, Parodi L, Callery J, Mannino A, Klaffke B, Escareno P, Platt RN, 2nd, Hodara V, Scordo J, Gautam S, Vilanova AG, Olmo-Fontanez A, Schami A, Oyejide A, Ajithdoss DK, Copin R, Baum A, Kyratsous C, Alvarez X, Ahmed M, Rosa B, Goodroe A, Dutton J, Hall-Ursone S, Frost PA, Voges AK, Ross CN, Sayers K, Chen C, Hallam C, Khader SA, Mitreva M, Anderson TJC, Martinez-Sobrido L, Patterson JL, Turner J, Torrelles JB, Dick EJ, Jr., Brasky K, Schlesinger LS, Giavedoni LD, Carrion R, Jr., Kaushal D. Responses to acute infection with SARS-CoV-2 in the lungs of rhesus macaques, baboons and marmosets. Nat Microbiol. 2021;6(1):73-86. Epub 20201218. doi: 10.1038/s41564-020-00841-4. PubMed PMID: 33340034; PMCID: PMC7890948.

412. Rendeiro AF, Ravichandran H, Bram Y, Chandar V, Kim J, Meydan C, Park J, Foox J, Hether T, Warren S, Kim Y, Reeves J, Salvatore S, Mason CE, Swanson EC, Borczuk AC, Elemento O, Schwartz RE. The spatial landscape of lung pathology during COVID-19 progression. Nature. 2021;593(7860):564-9. Epub 20210329. doi: 10.1038/s41586-021-03475-6. PubMed PMID: 33780969; PMCID: PMC8204801.

413. Travaglini KJ, Nabhan AN, Penland L, Sinha R, Gillich A, Sit RV, Chang S, Conley SD, Mori Y, Seita J, Berry GJ, Shrager JB, Metzger RJ, Kuo CS, Neff N, Weissman IL, Quake SR, Krasnow MA. A molecular cell atlas of the human lung from single-cell RNA sequencing. Nature. 2020;587(7835):619-25. Epub 20201118. doi: 10.1038/s41586-020-2922-4. PubMed PMID: 33208946; PMCID: PMC7704697.

414. Kelley N, Jeltema D, Duan Y, He Y. The NLRP3 Inflammasome: An Overview of Mechanisms of Activation and Regulation. Int J Mol Sci. 2019;20(13). Epub 20190706. doi: 10.3390/ijms20133328. PubMed PMID: 31284572; PMCID: PMC6651423.

415. Knoll R, Schultze JL, Schulte-Schrepping J. Monocytes and Macrophages in COVID-19. Front Immunol. 2021;12:720109. Epub 20210721. doi: 10.3389/fimmu.2021.720109. PubMed PMID: 34367190; PMCID: PMC8335157.

416. Vanderheiden A, Thomas J, Soung AL, Davis-Gardner ME, Floyd K, Jin F, Cowan DA, Pellegrini K, Shi PY, Grakoui A, Klein RS, Bosinger SE, Kohlmeier JE, Menachery VD, Suthar MS. CCR2 Signaling Restricts SARS-CoV-2 Infection. mBio. 2021;12(6):e0274921. Epub 20211109. doi: 10.1128/mBio.02749-21. PubMed PMID: 34749524; PMCID: PMC8576528.

417. Chen ST, Park MD, Del Valle DM, Buckup M, Tabachnikova A, Simons NW, Mouskas K, Lee B, Geanon D, D'Souza D, Dawson T, Marvin R, Nie K, Thompson RC, Zhao Z, LeBerichel J, Chang C, Jamal H, Chaddha U, Mathews K, Acquah S, Brown SA, Reiss M, Harkin T, Feldmann M, Powell CA, Hook JL, Kim-Schulze S, Rahman AH, Brown BD, Beckmann ND, Gnjatic S, Kenigsberg E, Charney AW, Merad M. Shift of lung macrophage composition is associated with COVID-19 disease severity and recovery. bioRxiv. 2022. Epub 20220112. doi: 10.1101/2022.01.11.475918. PubMed PMID: 35043110; PMCID: PMC8764718.

418. Melms JC, Biermann J, Huang H, Wang Y, Nair A, Tagore S, Katsyv I, Rendeiro AF, Amin AD, Schapiro D, Frangieh CJ, Luoma AM, Filliol A, Fang Y, Ravichandran H, Clausi MG, Alba GA, Rogava M, Chen SW, Ho P, Montoro DT, Kornberg AE, Han AS, Bakhoum MF, Anandasabapathy N, Suárez-Fariñas M, Bakhoum SF, Bram Y, Borczuk A, Guo XV, Lefkowitch JH, Marboe C, Lagana SM, Del Portillo A, Tsai EJ, Zorn E, Markowitz GS, Schwabe RF, Schwartz RE, Elemento O, Saqi A, Hibshoosh H, Que J, Izar B. A molecular single-cell lung atlas of lethal COVID-19. Nature. 2021;595(7865):114-9. Epub 20210429. doi: 10.1038/s41586-021-03569-1. PubMed PMID: 33915568; PMCID: PMC8814825.

419. Xiang Q, Feng Z, Diao B, Tu C, Qiao Q, Yang H, Zhang Y, Wang G, Wang H, Wang C, Liu L, Wang C, Liu L, Chen R, Wu Y, Chen Y. SARS-CoV-2 Induces Lymphocytopenia by Promoting Inflammation and Decimates Secondary Lymphoid Organs. Front Immunol. 2021;12:661052. Epub 20210428. doi: 10.3389/fimmu.2021.661052. PubMed PMID: 33995382; PMCID: PMC8113960.

420. Grant RA, Morales-Nebreda L, Markov NS, Swaminathan S, Querrey M, Guzman ER, Abbott DA, Donnelly HK, Donayre A, Goldberg IA, Klug ZM, Borkowski N, Lu Z, Kihshen H, Politanska Y, Sichizya L, Kang M, Shilatifard A, Qi C, Lomasney JW, Argento AC, Kruser JM, Malsin ES, Pickens CO, Smith SB, Walter JM, Pawlowski AE, Schneider D, Nannapaneni P, Abdala-Valencia H, Bharat A, Gottardi CJ, Budinger GRS, Misharin AV, Singer BD, Wunderink RG. Circuits between infected macrophages and T cells in SARS-CoV-2 pneumonia. Nature. 2021;590(7847):635-41. Epub 20210111. doi: 10.1038/s41586-020-03148-w. PubMed PMID: 33429418; PMCID: PMC7987233.

421. Pan M, Kalie E, Scaglione BJ, Raveche ES, Schreiber G, Langer JA. Mutation of the IFNAR-1 receptor binding site of human IFN-alpha2 generates type I IFN competitive antagonists. Biochemistry. 2008;47(46):12018-27. Epub 20081021. doi: 10.1021/bi801588g. PubMed PMID: 18937499.

422. Frey S, Gorlich D. A new set of highly efficient, tag-cleaving proteases for purifying recombinant proteins. J Chromatogr A. 2014;1337:95-105. Epub 20140219. doi: 10.1016/j.chroma.2014.02.029. PubMed PMID: 24636565.

423. Francica JR, Flynn BJ, Foulds KE, Noe AT, Werner AP, Moore IN, Gagne M, Johnston TS, Tucker C, Davis RL, Flach B, O'Connell S, Andrew SF, Lamb E, Flebbe DR, Nurmukhambetova ST, Donaldson MM, Todd JM, Zhu AL, Atyeo C, Fischinger S, Gorman MJ, Shin S, Edara VV, Floyd K, Lai L, Boyoglu-Barnum S, Van De Wetering R, Tylor A, McCarthy E, Lecouturier V, Ruiz S, Berry C, Tibbitts T, Andersen H, Cook A, Dodson A, Pessaint L, Van Ry A, Koutsoukos M, Gutzeit C, Teng IT, Zhou T, Li D, Haynes BF, Kwong PD, McDermott A, Lewis MG, Fu TM, Chicz R, van der Most R, Corbett KS, Suthar MS, Alter G, Roederer M, Sullivan NJ, Douek DC, Graham BS, Casimiro D, Seder RA. Protective antibodies elicited by SARS-CoV-2 spike protein vaccination are boosted in the lung after challenge in nonhuman primates. Sci Transl Med. 2021;13(607). Epub 20210727. doi: 10.1126/scitranslmed.abi4547. PubMed PMID: 34315825.

424. Corbett KS, Nason MC, Flach B, Gagne M, O'Connell S, Johnston TS, Shah SN, Edara VV, Floyd K, Lai L, McDanal C, Francica JR, Flynn B, Wu K, Choi A, Koch M, Abiona OM, Werner AP, Moliva JI, Andrew SF, Donaldson MM, Fintzi J, Flebbe DR, Lamb E, Noe AT, Nurmukhambetova ST, Provost SJ, Cook A, Dodson A, Faudree A, Greenhouse J, Kar S, Pessaint L, Porto M, Steingrebe K, Valentin D, Zouantcha S, Bock KW, Minai M, Nagata BM, van de Wetering R, Boyoglu-Barnum S, Leung K, Shi W, Yang ES, Zhang Y, Todd JM, Wang L, Alvarado GS, Andersen H, Foulds KE, Edwards DK, Mascola JR, Moore IN, Lewis MG, Carfi A, Montefiori D, Suthar MS, McDermott A, Roederer M, Sullivan NJ, Douek DC, Graham BS, Seder RA. Immune correlates of protection by mRNA-1273 vaccine against SARS-CoV-2 in nonhuman primates. Science. 2021;373(6561):eabj0299. Epub 20210917. doi: 10.1126/science.abj0299. PubMed PMID: 34529476; PMCID: PMC8449013.

425. Dobin A, Davis CA, Schlesinger F, Drenkow J, Zaleski C, Jha S, Batut P, Chaisson M, Gingeras TR. STAR: ultrafast universal RNA-seq aligner. Bioinformatics. 2013;29(1):15-21. Epub 2012/10/30. doi: 10.1093/bioinformatics/bts635. PubMed PMID: 23104886; PMCID: PMC3530905.

426. Anders S, Pyl PT, Huber W. HTSeq--a Python framework to work with high-throughput sequencing data. Bioinformatics. 2015;31(2):166-9. Epub 2014/09/28. doi: 10.1093/bioinformatics/btu638. PubMed PMID: 25260700; PMCID: PMC4287950.

427. Hao Y, Hao S, Andersen-Nissen E, Mauck WM, 3rd, Zheng S, Butler A, Lee MJ, Wilk AJ, Darby C, Zager M, Hoffman P, Stoeckius M, Papalexi E, Mimitou EP, Jain J, Srivastava A, Stuart T, Fleming LM, Yeung B, Rogers AJ, McElrath JM, Blish CA, Gottardo R, Smibert P, Satija R. Integrated analysis of multimodal single-cell data. Cell. 2021;184(13):3573-87.e29. Epub 20210531. doi: 10.1016/j.cell.2021.04.048. PubMed PMID: 34062119; PMCID: PMC8238499.

428. Harper J, Gordon S, Chan CN, Wang H, Lindemuth E, Galardi C, Falcinelli SD, Raines SLM, Read JL, Nguyen K, McGary CS, Nekorchuk M, Busman-Sahay K, Schawalder J, King C, Pino M, Micci L, Cervasi B, Jean S, Sanderson A, Johns B, Koblansky AA, Amrine-Madsen H, Lifson J, Margolis DM, Silvestri G, Bar KJ, Favre D, Estes JD, Paiardini M. CTLA-4 and PD-1 dual blockade induces SIV reactivation without control of rebound after antiretroviral therapy interruption. Nat Med. 2020;26(4):519-28. Epub 20200316. doi: 10.1038/s41591-020-0782-y. PubMed PMID: 32284611; PMCID: PMC7790171.

429. Pino M, Paganini S, Deleage C, Padhan K, Harper JL, King CT, Micci L, Cervasi B, Mudd JC, Gill KP, Jean SM, Easley K, Silvestri G, Estes JD, Petrovas C, Lederman MM, Paiardini M. Fingolimod retains cytolytic T cells and limits T follicular helper cell infection in lymphoid sites of SIV persistence. PLoS Pathog. 2019;15(10):e1008081. Epub 20191018. doi: 10.1371/journal.ppat.1008081. PubMed PMID: 31626660; PMCID: PMC6834281.

430. Kasturi SP, Rasheed MAU, Havenar-Daughton C, Pham M, Legere T, Sher ZJ, Kovalenkov Y, Gumber S, Huang JY, Gottardo R, Fulp W, Sato A, Sawant S, Stanfield-

Oakley S, Yates N, LaBranche C, Alam SM, Tomaras G, Ferrari G, Montefiori D, Wrammert J, Villinger F, Tomai M, Vasilakos J, Fox CB, Reed SG, Haynes BF, Crotty S, Ahmed R, Pulendran B. 3M-052, a synthetic TLR-7/8 agonist, induces durable HIV-1 envelope-specific plasma cells and humoral immunity in nonhuman primates. Sci Immunol. 2020;5(48). doi: 10.1126/sciimmunol.abb1025. PubMed PMID: 32561559; PMCID: PMC8109745.

431. Crawford KHD, Eguia R, Dingens AS, Loes AN, Malone KD, Wolf CR, Chu HY, Tortorici MA, Veesler D, Murphy M, Pettie D, King NP, Balazs AB, Bloom JD. Protocol and Reagents for Pseudotyping Lentiviral Particles with SARS-CoV-2 Spike Protein for Neutralization Assays. Viruses. 2020;12(5). Epub 20200506. doi: 10.3390/v12050513. PubMed PMID: 32384820; PMCID: PMC7291041.

432. Voigt EA, Gerhardt A, Hanson D, Jennewein MF, Battisti P, Reed S, Singh J, Mohamath R, Bakken J, Beaver S, Press C, Soon-Shiong P, Paddon CJ, Fox CB, Casper C. A self-amplifying RNA vaccine against COVID-19 with long-term room-temperature stability. NPJ Vaccines. 2022;7(1):136. Epub 20221102. doi: 10.1038/s41541-022-00549-y. PubMed PMID: 36323666; PMCID: PMC9628444.

433. Esaulova E, Das S, Singh DK, Choreño-Parra JA, Swain A, Arthur L, Rangel-Moreno J, Ahmed M, Singh B, Gupta A, Fernández-López LA, de la Luz Garcia-Hernandez M, Bucsan A, Moodley C, Mehra S, García-Latorre E, Zuniga J, Atkinson J, Kaushal D, Artyomov MN, Khader SA. The immune landscape in tuberculosis reveals populations linked to disease and latency. Cell Host Microbe. 2021;29(2):165-78.e8. Epub 20201218. doi: 10.1016/j.chom.2020.11.013. PubMed PMID: 33340449; PMCID: PMC7878437.

434. Zheng GX, Terry JM, Belgrader P, Ryvkin P, Bent ZW, Wilson R, Ziraldo SB, Wheeler TD, McDermott GP, Zhu J, Gregory MT, Shuga J, Montesclaros L, Underwood JG, Masquelier DA, Nishimura SY, Schnall-Levin M, Wyatt PW, Hindson CM, Bharadwaj R, Wong A, Ness KD, Beppu LW, Deeg HJ, McFarland C, Loeb KR, Valente WJ, Ericson NG, Stevens EA, Radich JP, Mikkelsen TS, Hindson BJ, Bielas JH. Massively parallel digital transcriptional profiling of single cells. Nat Commun. 2017;8:14049. Epub 20170116. doi: 10.1038/ncomms14049. PubMed PMID: 28091601; PMCID: PMC5241818.

435. Langmead B, Salzberg SL. Fast gapped-read alignment with Bowtie 2. Nat Methods. 2012;9(4):357-9. Epub 20120304. doi: 10.1038/nmeth.1923. PubMed PMID: 22388286; PMCID: PMC3322381.

436. Robinson MD, Oshlack A. A scaling normalization method for differential expression analysis of RNA-seq data. Genome Biol. 2010;11(3):R25. Epub 20100302. doi: 10.1186/gb-2010-11-3-r25. PubMed PMID: 20196867; PMCID: PMC2864565.

437. Robinson MD, McCarthy DJ, Smyth GK. edgeR: a Bioconductor package for differential expression analysis of digital gene expression data. Bioinformatics.

2010;26(1):139-40. Epub 20091111. doi: 10.1093/bioinformatics/btp616. PubMed PMID: 19910308; PMCID: PMC2796818.

438. Law CW, Chen Y, Shi W, Smyth GK. voom: Precision weights unlock linear model analysis tools for RNA-seq read counts. Genome Biol. 2014;15(2):R29. Epub 20140203. doi: 10.1186/gb-2014-15-2-r29. PubMed PMID: 24485249; PMCID: PMC4053721.

439. Simillion C, Liechti R, Lischer HE, Ioannidis V, Bruggmann R. Avoiding the pitfalls of gene set enrichment analysis with SetRank. BMC Bioinformatics. 2017;18(1):151. Epub 20170304. doi: 10.1186/s12859-017-1571-6. PubMed PMID: 28259142; PMCID: PMC5336655.

440. Hafemeister C, Satija R. Normalization and variance stabilization of single-cell RNA-seq data using regularized negative binomial regression. Genome Biol. 2019;20(1):296. Epub 20191223. doi: 10.1186/s13059-019-1874-1. PubMed PMID: 31870423; PMCID: PMC6927181.

441. Stuart T, Butler A, Hoffman P, Hafemeister C, Papalexi E, Mauck WM, 3rd, Hao Y, Stoeckius M, Smibert P, Satija R. Comprehensive Integration of Single-Cell Data. Cell. 2019;177(7):1888-902.e21. Epub 20190606. doi: 10.1016/j.cell.2019.05.031. PubMed PMID: 31178118; PMCID: PMC6687398.

442. Wu T, Hu E, Xu S, Chen M, Guo P, Dai Z, Feng T, Zhou L, Tang W, Zhan L, Fu X, Liu S, Bo X, Yu G. clusterProfiler 4.0: A universal enrichment tool for interpreting omics data. Innovation (Camb). 2021;2(3):100141. Epub 20210701. doi: 10.1016/j.xinn.2021.100141. PubMed PMID: 34557778; PMCID: PMC8454663.

443. Liberzon A, Subramanian A, Pinchback R, Thorvaldsdóttir H, Tamayo P, Mesirov JP. Molecular signatures database (MSigDB) 3.0. Bioinformatics. 2011;27(12):1739-40. Epub 20110505. doi: 10.1093/bioinformatics/btr260. PubMed PMID: 21546393; PMCID: PMC3106198.

444. Liberzon A, Birger C, Thorvaldsdóttir H, Ghandi M, Mesirov JP, Tamayo P. The Molecular Signatures Database (MSigDB) hallmark gene set collection. Cell Syst. 2015;1(6):417-25. doi: 10.1016/j.cels.2015.12.004. PubMed PMID: 26771021; PMCID: PMC4707969.

445. Kuri-Cervantes L, Pampena MB, Meng W, Rosenfeld AM, Ittner CAG, Weisman AR, Agyekum RS, Mathew D, Baxter AE, Vella LA, Kuthuru O, Apostolidis SA, Bershaw L, Dougherty J, Greenplate AR, Pattekar A, Kim J, Han N, Gouma S, Weirick ME, Arevalo CP, Bolton MJ, Goodwin EC, Anderson EM, Hensley SE, Jones TK, Mangalmurti NS, Luning Prak ET, Wherry EJ, Meyer NJ, Betts MR. Comprehensive mapping of immune perturbations associated with severe COVID-19. Sci Immunol. 2020;5(49). Epub 2020/07/17. doi: 10.1126/sciimmunol.abd7114. PubMed PMID: 32669287.

446. Abbasi J. What to Know About EG.5, the Latest SARS-CoV-2 “Variant of Interest”. JAMA. 2023. Epub 8/18/2023. doi: 10.1001/jama.2023.16498.

447. Kale A, Shelke V, Dagar N, Anders HJ, Gaikwad AB. How to use COVID-19 antiviral drugs in patients with chronic kidney disease. Front Pharmacol. 2023;14:1053814. Epub 20230209. doi: 10.3389/fphar.2023.1053814. PubMed PMID: 36843922; PMCID: PMC9947246.

448. Hu Y, Lewandowski EM, Tan H, Zhang X, Morgan RT, Zhang X, Jacobs LMC, Butler SG, Gongora MV, Choy J, Deng X, Chen Y, Wang J. Naturally Occurring Mutations of SARS-CoV-2 Main Protease Confer Drug Resistance to Nirmatrelvir. ACS Cent Sci. 2023;9(8):1658-69. Epub 20230724. doi: 10.1021/acscentsci.3c00538. PubMed PMID: 37637734; PMCID: PMC10451032.

449. Mehta P, Titanji BK. Baricitinib in COVID-19: a coming-of-age from artificial intelligence to reducing mortality. Lancet. 2022;400(10349):338-9. doi: 10.1016/S0140-6736(22)01295-8. PubMed PMID: 35908561; PMCID: PMC9333997.

450. Davis HE, McCorkell L, Vogel JM, Topol EJ. Long COVID: major findings, mechanisms and recommendations. Nat Rev Microbiol. 2023;21(3):133-46. Epub 20230113. doi: 10.1038/s41579-022-00846-2. PubMed PMID: 36639608; PMCID: PMC9839201.

451. FDA U. FDA announces Evusheld is not currently authorized for emergency use in the U.S. | FDA2023.